

AFOSR TR. 89-1510

CORROSION FATIGUE AND  
FATIGUE CRACK GROWTH  
IN AIRCRAFT STRUCTURAL  
MATERIALS

by

DAVID W. HOEPPNER, PH.D., P.E.  
COCKBURN PROFESSOR OF ENGINEERING DESIGN  
FACULTY OF APPLIED SCIENCE AND ENGINEERING  
UNIVERSITY OF TORONTO

PREPARED FOR  
AIR FORCE OFFICE OF SCIENTIFIC RESEARCH  
BOLLING AIR FORCE BASE, D.C. 20332

JUNE 1979

Contract No. AFOSR 77-3178

AFOSR TECHNICAL MONITORS  
DR. CHARLES HAYS  
DR. WILLIAM WALKER  
LT. COL. J. MORGAN

Best Available Copy

AD-A215 019

PHOTOGRAPH THIS SHEET

AD-A215 019

DTIC ACCESSION NUMBER

LEVEL

INVENTORY

AFOSR TR 89-1510

DOCUMENT IDENTIFICATION

JUNE 1979

DTIC FILE COPY

DISTRIBUTION STATEMENT A

Approved for public release; Distribution Unlimited

DISTRIBUTION STATEMENT

ACCESSION FOR	
NTIS	GRA&I <input checked="" type="checkbox"/>
DTIC	TAB <input type="checkbox"/>
UNANNOUNCED	<input type="checkbox"/>
JUSTIFICATION	
BY	
DISTRIBUTION / AVAILABILITY CODES	
DIST	AVAIL AND/OR SPECIAL
A-1	

DISTRIBUTION STAMP



S DTIC ELECTE D  
DEC 04 1989  
E

DATE ACCESSIONED

DATE RETURNED

REGISTERED OR CERTIFIED NO.

89 11 20 104

DATE RECEIVED IN DTIC

PHOTOGRAPH THIS SHEET AND RETURN TO DTIC-PDAC

## REPORT DOCUMENTATION PAGE

Form Approved  
OMB No. 0704-0188

1a. REPORT SECURITY CLASSIFICATION		1b. RESTRICTIVE MARKINGS		
2a. SECURITY CLASSIFICATION AUTHORITY		3. DISTRIBUTION / AVAILABILITY OF REPORT Approved for public release; distribution unlimited.		
2b. DECLASSIFICATION / DOWNGRADING SCHEDULE				
4. PERFORMING ORGANIZATION REPORT NUMBER(S)		5. MONITORING ORGANIZATION REPORT NUMBER(S) <del>AFOSR</del> - LR - 89 - 1510		
6a. NAME OF PERFORMING ORGANIZATION University of Missouri College of Engineering	6b. OFFICE SYMBOL (if applicable)	7a. NAME OF MONITORING ORGANIZATION AFOSR		
6c. ADDRESS (City, State, and ZIP Code) Columbia, Missouri		7b. ADDRESS (City, State, and ZIP Code) BLDG 410 BAFB DC 20332-6448		
8a. NAME OF FUNDING / SPONSORING ORGANIZATION AFOSR	8b. OFFICE SYMBOL (if applicable)	9. PROCUREMENT INSTRUMENT IDENTIFICATION NUMBER AFOSR 77-3178		
8c. ADDRESS (City, State, and ZIP Code) BLDG 410 BAFB DC 20332-6448		10. SOURCE OF FUNDING NUMBERS		
		PROGRAM ELEMENT NO. 61102F	PROJECT NO. 2307	TASK NO. B2
11. TITLE (Include Security Classification) CORROSION FATIGUE AND FATIGUE CRACK GROWTH IN AIRCRAFT STRUCTURAL MATERIALS				
12. PERSONAL AUTHOR(S) David W. Hoepfner				
13a. TYPE OF REPORT Final	13b. TIME COVERED FROM Nov 76 TO Nov 78	14. DATE OF REPORT (Year, Month, Day) June 1979	15. PAGE COUNT 264	
16. SUPPLEMENTARY NOTATION				
17. COSATI CODES		18. SUBJECT TERMS (Continue on reverse if necessary and identify by block number)		
FIELD	GROUP			SUB-GROUP
19. ABSTRACT (Continue on reverse if necessary and identify by block number)				
20. DISTRIBUTION / AVAILABILITY OF ABSTRACT <input checked="" type="checkbox"/> UNCLASSIFIED/UNLIMITED <input type="checkbox"/> SAME AS RPT <input type="checkbox"/> DTIC USERS		21. ABSTRACT SECURITY CLASSIFICATION unclassified		
22a. NAME OF RESPONSIBLE INDIVIDUAL		22b. TELEPHONE (Include Area Code) 767-4987	22c. OFFICE SYMBOL NA	

## INTRODUCTION:

This report is the final technical report for the subject contract. It is a summary of work accomplished during the period October 1976 - September 1978. During this period the author was Professor of Engineering at the University of Missouri - Columbia (UM-C). In late summer 1978 the author moved to the University of Toronto to assume the Cockburn Chair of Engineering Design and several students concluded work at UM-C under direction of the author. The last student completed his work in May, 1979. Sponsorship of the research effort from October 1978 to May 1979 was assisted by the University of Missouri-Columbia, Engineering Experiment Station and Department of Mechanical Engineering. In addition, the University of Toronto supported travel, time supplies reproduction costs and various items during the conclusion of this effort. The author is grateful to all of these organizations for helping in support of the research.

The following sections provide

- 1) A list of theses supported fully or partially by the subject contract.
- 2) A list of publications (with copies enclosed) prepared for the open literature under this contract.
- 3) A copy of the thesis of Mr. James Cox.
- 4) A concluding statement related to the research.
- 5) An acknowledgement section.

1) Theses supported under contract AFOSR 77-3178

1. Author: Michael E. Mayfield  
Title: Corrosion Assisted Fatigue in 2024-T851 Aluminum Alloy.  
A Thesis submitted in partial Fulfillment of the Requirement of the Degree of Master of Science, University of Missouri-Columbia. May, 1978.  
Full Support.
2. Author: Eugene R. Nickel  
Title: Fatigue and Fretting Fatigue of Polycrystalline Copper  
A Thesis submitted in partial Fulfillment of the Requirement of the Degree of Master of Science, University of Missouri-Columbia, May, 1978.  
Full Support.
3. Author: James Michael Cox  
Title: Pitting and Fatigue Crack Initiation of 2124-T851 Aluminum in 3.5% NaCl solution.  
A thesis submitted in partial fulfillment of the requirements for the Degree of Master of Science, University of Missouri-Columbia, May 1979.  
Full Support.
4. Author: Dale Alan Wilson  
Title: A Statistically Based Investigation of Microstructural Effects on the Fatigue Properties of Titanium and Titanium Alloys.  
A Thesis submitted in Partial Fulfillment of the Requirement of the Degree of Doctor of Philosophy, University of Missouri, December, 1978.  
Partial Support.
5. Author: Cheung Jarm Poon  
Title: Environmental Effects on the Mechanism of Fretting Fatigue in 7075-T6 Aluminum.  
A Thesis submitted in Partial Fulfillment of the Requirement of the Degree of Doctor of Philosophy University of Missouri-Columbia. December, 1978.  
Partial Support

2) LIST OF PUBLICATIONS PREPARED UNDER CONTRACT AFOSR 77-3178

(Copies attached as Appendix A.)

1. David W. Hoepfner, "A Fractographic Analysis of Flaw Growth in a High Strength Titanium Alloy", Metallography, Vol. 11, pp 129-154 (1978).
2. D.W. Hoepfner, "Effect of Microstructure on Fatigue-Crack Growth Behavior in Forged Materials", Forging and Properties of Aerospace Materials, The Metals Society, London, England, (1978) pp 103-142.
3. Cheung Poon and David W. Hoepfner, "The Effect of Temperature and R Ratio on Fatigue Crack Growth in A612 Grade B Steel", ENGN. Fracture Mech, to be published.
4. G.C. Salivar and D.W. Hoepfner, "A Weibull Analysis of Fatigue-Crack Propagation Data from a Nuclear Pressure Vessel Steel", ENGN. Fracture Mech, to be published.
5. David W. Hoepfner, "Model for Prediction of Fatigue Lives Based Upon A Pitting Corrosion Fatigue Process", to be published - ASTM presented @ International Conference on Mechanism of Fatigue, May 1978, K.C., Mo., ASTM.

- 3) Copy of thesis of Mr. James Cox completed May, 1979. This is enclosed because it represents a summary of pitting results, presents several models, and is viewed as potentially significant work in this area.

A Concluding Statement related to the Research:

- 4) This research provided significant progress related to modelling the corrosion pitting fatigue process in aluminum alloys. It will undoubtedly provide the basis for extensive work in this area as time progresses.

5) Acknowledgement Section:

The author would like to personally acknowledge the contributions of the students to this effort. In addition, I would like to acknowledge the direct contributions of the following people to the aid of the conduct of this effort in one way or another:

University of Missouri-Columbia:

Dr. Paul Braisted

Dr. Jack Lysen

Dean W. kimel

Professors D. Creighton, C. Oran, J. Seydel, J. Baldwin,  
S. Loyalka, R. Duffield, R. Warder.

Mr. Larry Clark, Mr. Tony Lampe, Mr. R. Jenkins,

Mr. Arthur Brown, Mrs. Lois Fowler, Mrs. Dev. Mayclin,

Mrs. Dianne Robinson, Mrs. Rosie Jamieson, Mrs. Christine Best.

University of Toronto: Miss Janet Lambert.

Part 2

Appendix A

Copies of Papers  
Prepared Under  
Contract AFOSR 773178

## A Fractographic Analysis of Flaw Growth in a High Strength Titanium Alloy

DAVID HOEPPNER

*Professor, College of Engineering, University of Missouri, Columbia, Missouri 65201  
U.S.A.*

*EDITOR'S NOTE: If you were educated in the fifties or earlier, you are probably unaware of a modern design method based on the defect tolerance approach. In the old days, metallurgical designs were based on the simple parameters of ultimate tensile strength, hardness and/or fatigue strength. As many of us recall, these parameters were always determined through the use of unflawed and highly-polished test specimens. Performance characterization tests of today are seldom done with anything except flawed specimens and realistic surfaces as exposed to typical environs of stress, temperature, frequency and corrosives. The design concept of today poses the question, "Given a certain distribution of defects, how long can a specific structure endure known conditions?" On this basis, the modern designer considers defect tolerance as his prime criterion. In so doing, the approach involves certain assumptions for weaknesses, not strengths; e.g.,*

- *Fracture cannot always be avoided so it must be understood.*
- *Fracture is a terminal event that is preceded by initiation and propagation of defects.*
- *Fracture cannot always be halted but it can be effectively retarded.*

*This is to say that today's technology is vitally concerned with fracture and the mechanics of fracture through fractography.*

*Of the many metallurgists that work the problem of understanding fracture, one such outstanding individual is the internationally-renown Dr. David W. Hoepfner, Professor of Engineering at the University of Missouri-Columbia. Dr. Hoepfner has pioneered the field of fracture mechanics in areas that concern the effect of microstructure. He has been directly involved in scientific researches for crack-retardant materials in airplane engines, pressure vessels and nuclear reactors. For reasons that should now be obvious, David W. Hoepfner has become a recognized expert in this specialized field of study and a highly-regarded consultant for the United States Air Force, the Electric Power Research Institute, Rolls Royce Limited, the Lockheed Company and others too numerous to mention.*

*On a daily basis, Professor Hoepfner administers regular dosages of new knowledge on fracture mechanics to his students in Mechanical and Aerospace Engineering at Columbia, Missouri. He and his students are enthusiastically dedicated to the development of a new discipline called the Structural Integrity Engineering Program.*

*The Editorial Staff of METALLOGRAPHY is pleased to feature a sampling of Dr. Hoepfner's work as an invited paper. This article is another of the series that attempts to*

*profile professionals in action. Dr. Hoepfner was asked to submit an invited paper that best describes some of his technical interests and/or problems. Hoepfner's selected response is this detailed fractographic evaluation of a titanium alloy—IMI 685. This unpublished work is technologically significant and, historically, most important. IMI 685 is a titanium alloy that is expected to "fly" on airplane engines of the 1980 era—as improved by silicon additions with isothermal forging. METALLOGRAPHY is proud to offer an example of fractographic analyses from the laboratories of Dr. David W. Hoepfner, one of America's finest metallurgists.*

---

### Introduction

Several service failures of forged discs made from a high strength titanium alloy prompted an investigation of the alloy in an attempt to understand the mechanism of failure. Mechanical tests on the alloy of interest were conducted and the results were reported earlier [1]. Selected specimens from these tests were examined fractographically in an attempt to develop additional insight into the complex relationship between environment, loading mode, and microstructure. Much of this work was originally accomplished during the first six months of 1973 while the author was at Lockheed Rye Canyon Advanced Design and Research Laboratory. Mr. Gary Goss and Mr. Walter Fitze aided in performing the scanning and transmission electron microscopy.

### Background

Engineering materials exhibit many different and sometimes complex mechanisms of fracture. Titanium alloy systems, depending upon composition, manufacturing method, thermomechanical treatment, loading spectrum and environmental conditions, may fracture by several mechanisms. Dimpled rupture, fatigue striations, intergranular cracking, delamination and cleavage are several of the fracture surface appearances that are encountered in fractographic analyses of titanium. The significance of each surface and corresponding fracture mechanism is very important in that each fracture mode correlates to a corresponding energy of fracture and resistance to crack extension.

IMI 685, an alpha-beta structured titanium alloy, would be expected to exhibit dimpled rupture, fatigue striations and under the proper environmental and stress conditions, cleavage. Dimpled rupture, a high energy absorbing fracture mode can occur under static loading conditions, as in a tensile test, or dynamic loading conditions, as in the stable tear portion

of a crack growth test or due to orientation effects in cyclic loading. In either case the energy absorbed, due to the high degree of plasticity, is very high—a desirable fracture mechanism.

Fatigue striations are produced by dynamic loading conditions, and are an indication that a fracture surface was produced by other than one cycle (static) failure. A fatigue striation is usually produced by a single load cycle and the morphology of the striations vary according to the applied stress, microstructure, frequency, temperature, chemical environment, and radiation environment.

The energy relationships of fatigue mechanisms are not understood. The important fact is that the amount of energy utilized in producing a striated fracture surface is usually much higher than that for other fracture mechanisms described below.

Intergranular fracture occurs in titanium alloys when a foreign or contaminating species atom such as hydrogen, chlorine, etc. concentrates at the grain boundaries and weakens the cohesive force between adjacent grains. In alpha-beta titanium alloys intergranular fracture usually occurs at prior beta boundaries, as well as along primary alpha boundaries. At high magnifications the intergranular fracture has a so-called "rock candy" appearance, with a high degree of secondary cracking present. Because of the loss of grain boundary cohesive strength the energy absorbed to separate the grains is very low and there is little, if any, plastic flow involved in the process.

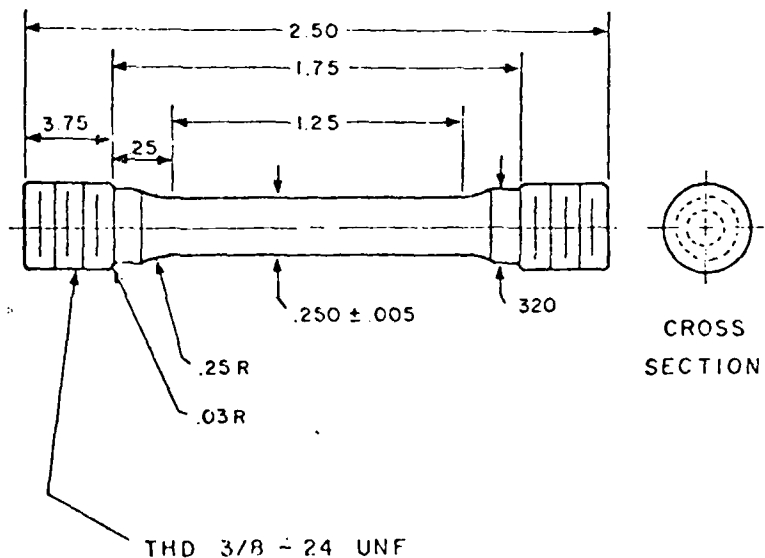
Cleavage is the last fracture mode of interest in the fracture analysis of titanium alloys. All of the above processes, with the exception of fatigue striation formation, have no direct relationship to the crystallography of the material. Cleavage, on the other hand, is directly related to the crystallography of the microstructure and usually occurs on the basal (0001) plane. Although cleavage and fatigue striations are related to crystallography they behave much differently with regards to slip and plastic deformation. Striation formation is entirely a consequence of slip, while the cleavage process in the pure sense is totally devoid of slip (although cleavage can be induced by plastic strain incompatibility). Pure cleavage is the separation of the atomic bonds with virtually no plastic deformation occurring. The fracture surface of a cleaved material is very flat with "river markings" that are produced when the crack front changes atomic layers due to imperfections within the crystal lattice. The energy required to propagate the crack once initiated is very low; or indeed energy is released and the crack propagates very rapidly. The total energy to failure is thus very low, relative to plastic flow processes. All of these fracture modes can be encountered in fracture of titanium.

This report covers the results of an SEM fractographic analysis of IMI 685 Titanium. It covers analysis of static tensile specimens with and without environment, and cracks induced in the structure during service that were opened for study of fractographic features of service induced cracks.

### Results and Discussion

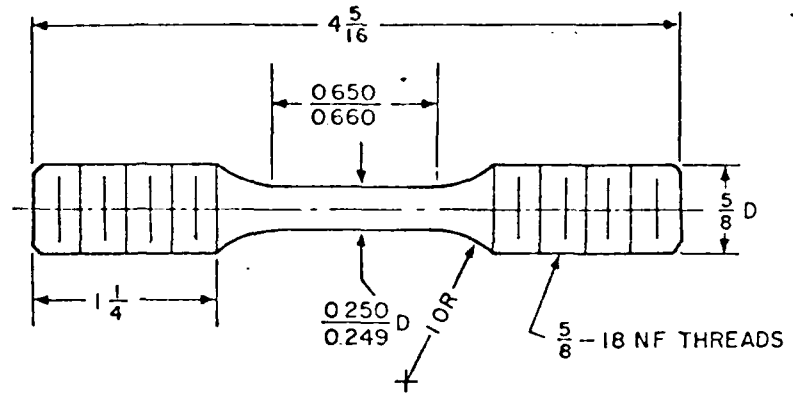
Table 1 is a listing of the specimens examined, their type and history. Figures 1 and 2 describe the geometry of each type of specimen. The test results of each specimen listed, with the exception of the hub cracks, have been presented in an earlier report [1] covering the test program.

The discussion section is divided into separate sub-sections covering: (a) tensile specimen, (b) strain control fatigue specimen, (c) WOL type crack growth specimens with and without environment, and (d) opened cracks from a region of the structure.



ALL DIMENSIONS IN INCHES

FIG. 1(a). Tensile specimen geometry.

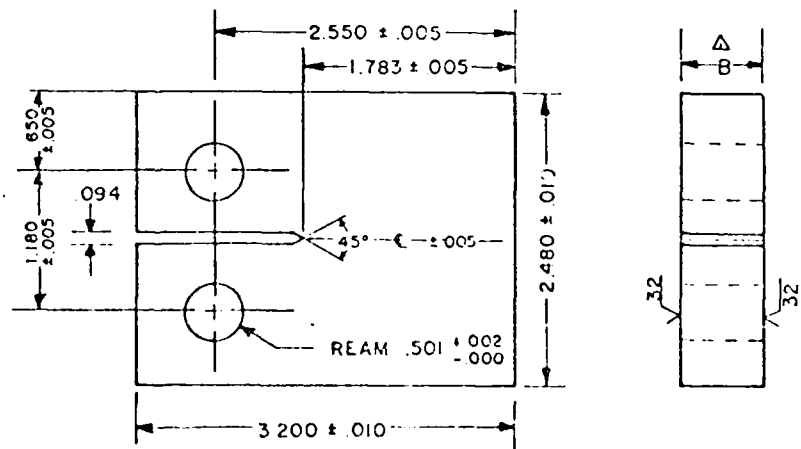


ALL DIMENSIONS IN INCHES

FIG. 1(b). Strain controlled low cycle fatigue specimen geometry.

Tensile Specimen

Figures 3 and 4 are macro and microphotographs of the fracture surface of tensile specimen A-HF1-1. The overall macro (3A) illustrates the coarseness of the fracture surface. The high dependence of the fracture morphology on microstructure can be seen quite clearly in



ALL DIMENSIONS IN INCHES

FIG. 2. WOL specimen geometry.

TABLE 1  
Specimens Utilized in SEM Fractographic Analysis

Specimen Type	Yield Strength	Ultimate Strength	Elongation (%)	Reduction of Area	Temperature
A-HPT-1 Tensile	131 KSI	131.4 KSI	10%	16%	RT
Specimen Type	Geometry	Strain Amplitude $\epsilon/2$	Strain Ratio min/max	Cycles to Failure	Temperature
A-HPT-1 Strain Control Fatigue	$K_t = 1.0$	0.005 in/in	-1.0	4,887	RT
Specimen Type	Stress Ratio (min/max)	Stress Intensity Range	Environmental Conditions	Temperature	
F-8 WOL <sup>2</sup>	0	48.16 Ksi $\sqrt{\text{in}}$ .	180 min hold, DI H <sub>2</sub> O	RT	

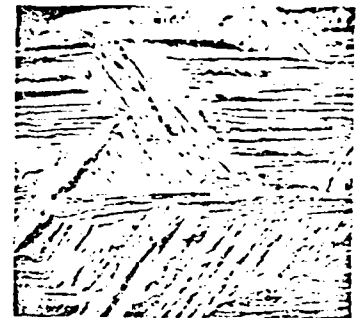
Specimen Type	Stress Ratio ( $\sigma_{\min}/\sigma_{\max}$ )	Stress Intensity Range	Environmental Conditions	Temperature
E-9 WOL	+0.1	17-53 Ksi $\sqrt{\text{in.}}$	10 Hz, Air	RT
Specimen Type	Stress Ratio	Stress Intensity Range	Environmental Conditions	Temperature
E-25 WOL	0	44-53 Ksi $\sqrt{\text{in.}}$	5 min loaded/5 min unloaded, Air	RT
Service Crack BB-A		Crack from hairpin radius region that was subsequently opened		
Service Crack BB-3		Crack from hairpin radius region that was subsequently opened		
Service Crack BB-4		Crack from hairpin radius region that was subsequently opened		

<sup>a</sup> HPT—Hairpin region-tangential.

<sup>b</sup> WOL—Wedge Opening Load



(a) Macro view of fracture surface, 10 $\times$ .



(b) View showing dependence of fracture on microstructure, 150 $\times$ .



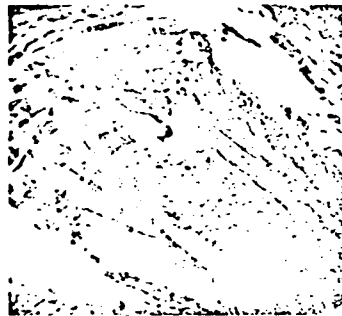
(c) Dimpled rupture showing microstructural effect, 1000 $\times$ .



(d) Equiaxed and shear dimples near specimen surface, 500 $\times$ .

FIG. 3. Static tensile specimen A-HPT-1.

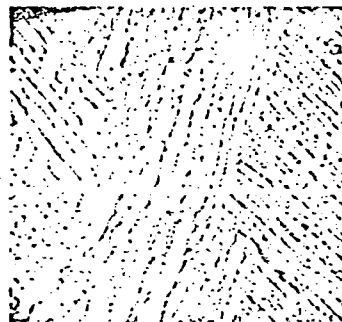
Figures 3(b), 3(c), and 4(c). Figures 3(b) and 3(c) show dimpled structures that are related to the alpha-beta lamellar platelet structure and are composed of elongated dimples. Figures 4(c) and 4(d) exhibit microstructural dependence but at higher magnification equiaxed dimples very much smaller than the dimples of Figure 3(c) are resolved. Much larger equiaxed dimples containing microvoids typical of many static fractures are illustrated in Figure 3(d). Secondary cracking and large flat dimpled areas can be seen in Figs. 4(a) and 4(b). The large flat fracture regions are the result of a high degree of microstructural dependence of the fracture mechanism and a large prior  $\beta$  grain size.



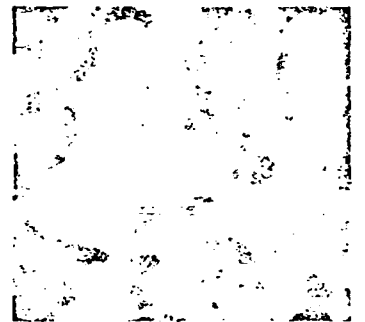
(a) View showing secondary cracking. 300 $\times$ .



(b) Microphoto showing large flat fracture surface facets. 200 $\times$ .



(c) Higher magnification view showing microstructural dependence. 1000 $\times$ .



(d) View showing extremely fine dimples. 12,500 $\times$ .

FIG. 4. Static tensile specimen A-HPT-1.

The results of the fractographic analysis verify the results of the mechanical properties as listed for the tensile specimen in Table 1. Even though there is a high dependence on microstructure, the primary fracture mode—dimpled rupture—results in high yield and ultimate strengths with good ductility.

#### Strain Control Fatigue Specimen

Figures 5, 6, and 7 are macro and microphotographic views of the origin area of strain control or low cycle fatigue specimen A-HPT-1.

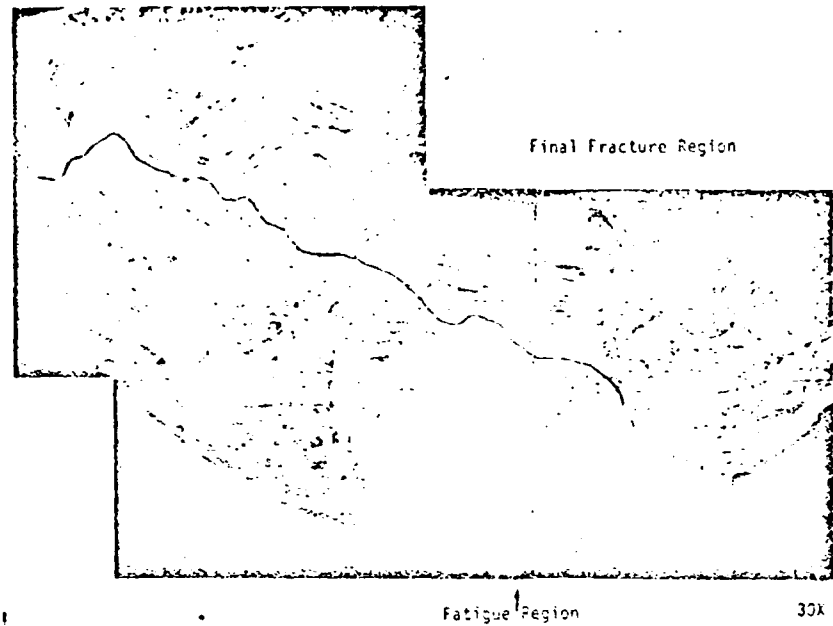


FIG. 5. Low cycle fatigue specimen A-HPT-1.

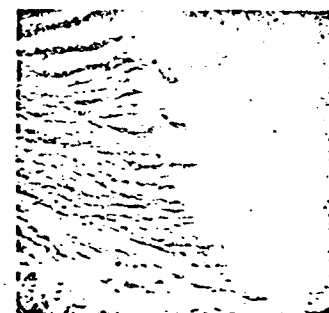
Figures 6 and 7 illustrate the modes of fracture encountered in the origin area. The origin area is not composed entirely of fatigue striations but rather a mixture of striations and a quasicleavage type of fracture. Figure 6(a) demonstrates this mixture well. In Fig. 6(b) the fracture mode changes from a quasicleavage microstructural dependent case to fatigue striations which are independent of the alpha-beta structure. The linear transition suggests a grain boundary that demonstrates the dependence of fracture mode on grain orientation. A transition from fatigue striations to dimpled rupture in Fig. 6(c) illustrates the region near the crack front at final failure. Fatigue striations exhibiting secondary cracking are seen in Fig. 6(d). The field is located near the surface of the specimen and environmental and/or stress effects may have caused the secondary cracking. Figure 7 shows examples of fatigue striated fields in the interior of the specimen. Many areas such as 7(b) and 7(c) exhibit uniformly spaced linear striations, while others such as 7(a) give a confusing appearance. In Fig. 7(a), the crack is propagating from bottom to top and apparently changes direction by  $90^\circ$  midway. Actually, at that point the microstructure exerts a strong influence on the

crack morphology and the alpha-beta microstructure is seen in the striation topography. Caution must be used so that alpha-beta lamellar fields are not mistaken for striation fields.

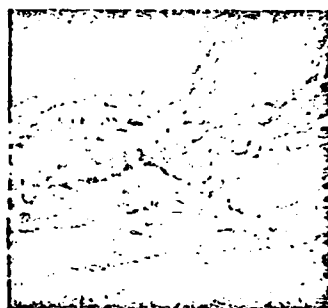
A strain control fatigue specimen fracture surface exhibits many fracture modes and appearances and care must be taken lest erroneous interpretations and conclusions be made. It is important to note here that the mixed fracture modes apparent on a fatigue specimen could yield marked changes in crack growth rates at either "microstructural" or "macrostructural" levels.



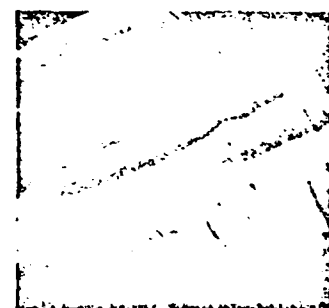
(a) Origin area showing fracture flow patterns, 220 $\times$ .



(b) Change of fracture mode, 1250 $\times$ .



(c) Change of fracture mode, 1600 $\times$ .

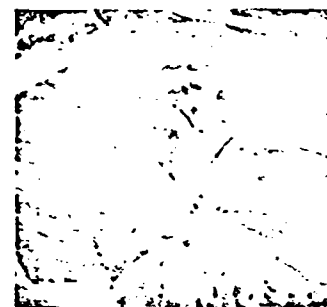


(d) Fatigue striations exhibiting secondary cracking, 3000 $\times$ .

FIG. 6. Low cycle fatigue specimen A-HPT-1.



(a) Fatigue striated area exhibiting microstructural dependence. 2100 $\times$ .



(b) Striated area with grain boundary and secondary cracks. 2100 $\times$ .



(c) Well defined striations. 2100 $\times$ .

FIG. 7. Low cycle fatigue specimen A-HPT-1.

### WOL Type Crack Growth Specimens

Three crack growth specimens were examined. They were selected to evaluate baseline (10 HZ, room temperature, dry air) fracture behavior, sustained load (5 min. loaded/5 min. unloaded, room temperature, dry air) behavior and environmental (180 min. hold, deionized water, room temperature) behavior. They are labeled E-9, E-25, and E-8 respectively.

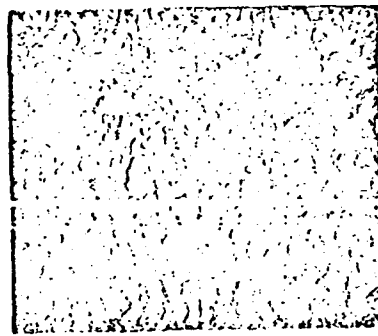
Figure 8 presents the macro and micro fracture surface appearance of specimen E-9. Much of the surface shown in 8(b) is composed of large flat regions that show little evidence of ductile rupture or fatigue

striations. At higher magnification as in 8(c) the flat regions resemble the quasicleavage as seen in the strain control fatigue specimen A-HPT-1. As the crack propagated further into the specimen and attained higher  $\Delta K$  values, the large flat regions diminish in size and number. Evidence of a change in morphology can be seen in 8d-f. Well defined fatigue striations are evident in 8(d) as well as 8(e) while debris covers the fracture surface in 8(f).

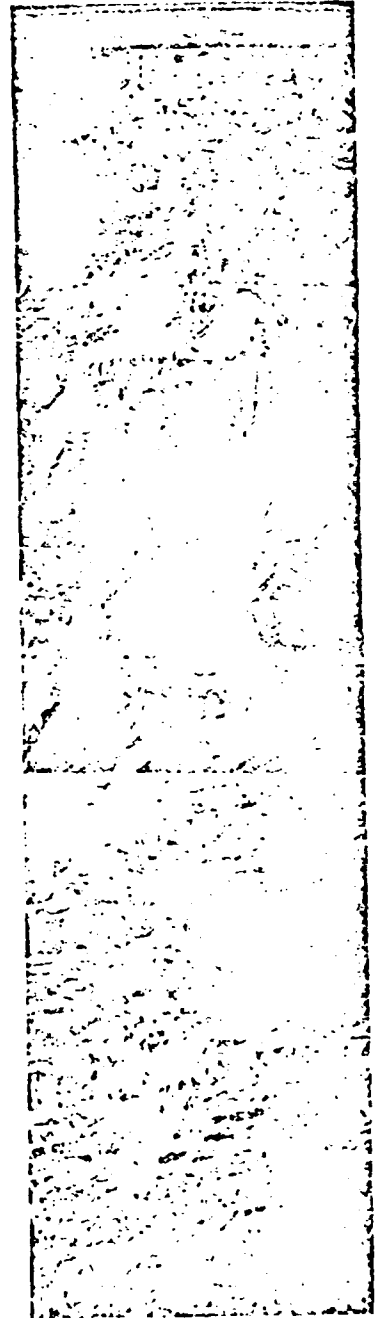
The fracture surface is not composed of evenly distributed striated areas but a mixed mode of quasicleavage regions and striated fields that make it difficult or impossible to assess crack growth rate by striation spacing measurement. Growth rates are more properly evaluated by surface crack measurement techniques.

The sustained load specimen E-25, Fig. 9, demonstrates a dramatic change in fracture surface morphology at the transition from precrack to test. The precrack region exhibits much the same appearance as the baseline specimen E-9, Fig. 8. That is, fields of quasicleavage and striations as seen at higher magnification in Figs. 9(c) and 9(d). Figure 9(d) shows the transition from precrack to test. The precrack striations propagate from the left in a uniform field and abruptly change to more widely spaced microstructurally affected striations on the right. The test area in Fig. 9(b) is very coarse with many secondary cracks present. The sustained load appears to have the same effect on crack morphology as environmental attack in many other materials, and crack propagation rates are virtually impossible to determine because of this effect. Some fields of fatigue or cyclic loading striations are present in the test region as seen in Fig. 9(e), but the major portion is composed of quasicleavage as seen in Fig. 9(f). Sustained load then has the effect of coarsening the surface topography and lessening the probability of striation formation. A comparison of Figs. 9(f) and 8(e) demonstrates this effect. Thus, a change in the micromechanics of crack growth obviously is occurring with sustained load.

The effects of sustained load in combination with an environment of deionized water on WOL Specimen E-8 are seen in Fig. 10. A comparison of Figs. 10(b) and 9(b) and 8(b) illustrates the dramatic change in fracture morphology when the wet environment is imposed. In Fig. 10(b) the precrack region is on the left with the crack propagating from left to right. The precrack region is very similar to the two previous specimen precrack regions. In the test region the topography is very blocky with a high degree of secondary cracking in evidence. Figure 10(c) is a precrack to test transition region where the crack propagating in a flat non-striated, non dimpled mode after the transition is seen to propagate in a brittle quasi-cleavage mode. Figure 10(e) presents the transition area

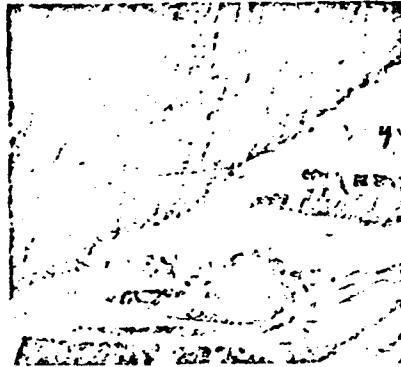


(a)

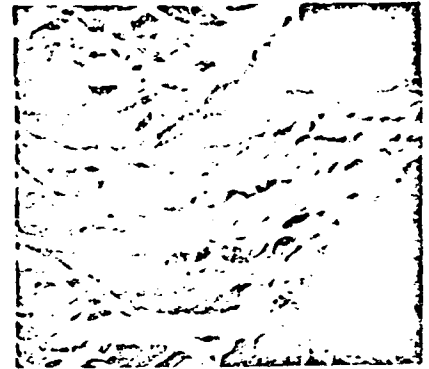


(b)

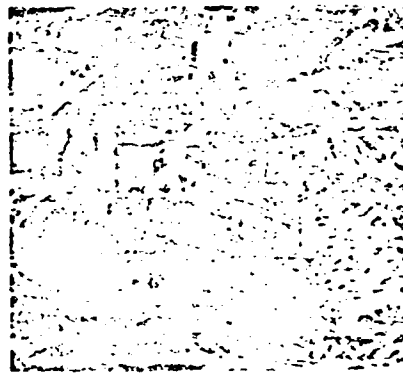
FIG. 8. WOI. Specimen L-9 baseline 10HZ, room temperature, dry air. (a) Macro surface, 1.6x. (b) Crack propagation morphology, 50x.



(c) Transition in fracture mode probably at a grain boundary. 1000 $\times$ .



(d) Fatigue striated field. 1750 $\times$ .



(e) Mixed mode striations and dimpled rupture. 500 $\times$ .



(f) Debris caused by repeated contacts of the fracture surface during testing. 1500 $\times$ .

where the crack front had been propagating by fatigue and changed to a mixed mode ductile rupture and quasicleavage. Figure 10(f) is representative of most of the test area being composed of blocky quasicleavage with secondary cracking. This is the form of crack extension with very little resistance to propagation. Specimen E-8 failed after four load applications indicating the high crack propagation rate. Deionized water



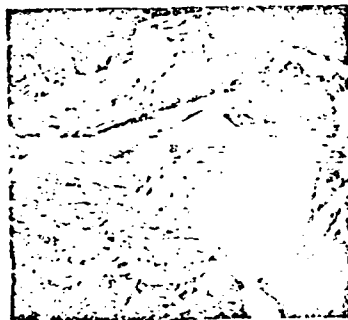
FIG. 9. WOI. Specimen E-25. 5 min. loaded/5 min. loaded. Room temperature, dry air.



(c) Precrack region, 300x.



(d) Precrack to test transition, 1000x.



(e) Isolated striated field test region, 250x.

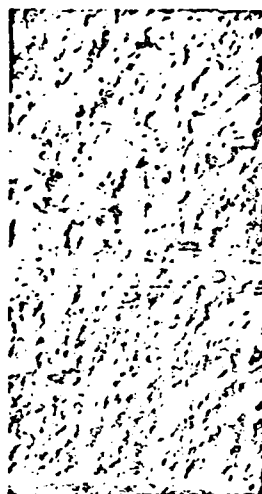


(f) Fracture morphology in test region, 300x.

had the most severe effect on the crack propagation rate which is corroborated by the fracture appearance of Fig. 10.

#### Service Induced Cracks

A structural component was found to contain at least twenty-nine cracks induced during service and was removed from service. A section of that disc in the "hairpin" radius region containing several crack indications was removed for analysis. The cracks were opened carefully by mechanical means and examined by SEM Analysis. Three of the



(a) Macro surface.



(b) Precrack to test region, 50x.

Precrack region

Test region

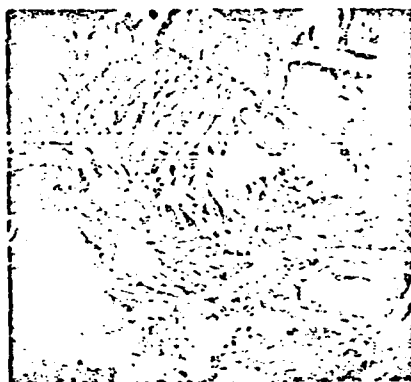
FIG. 10. WOI, Specimen 1-8, 3-hour hold detionized water room temperature



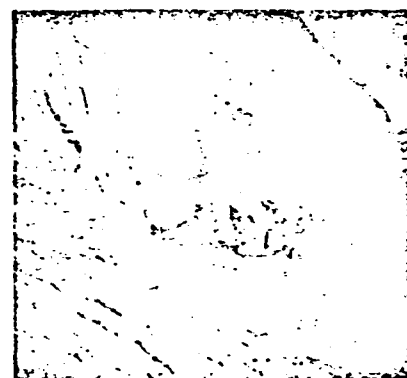
(c) Flat fracture mode in precrack to test transition region, 300x.



(d) Precrack region, 300x.



(e) Precrack—Test transition region, 250x.



(f) Test region, 300x.

fracture surfaces are shown in Figs. 11-15. The fracture surface of Specimen B-A as seen in Fig. 11 exhibits many of the fracture modes encountered in previous test specimens. Quasicleavage areas are seen in Figs. 11(b) and 11(d) while fatigue striated areas are evident in Figs. 11(c), 11(e), and 11(f) is a view of the probable origin area and is seen in greater detail in Fig. 12. The darker fan-shaped area is the suspected origin because all fracture flow lines originate or propagate from this region. Figs. 12(b) and 12(c) detail the left portion of the region shown in

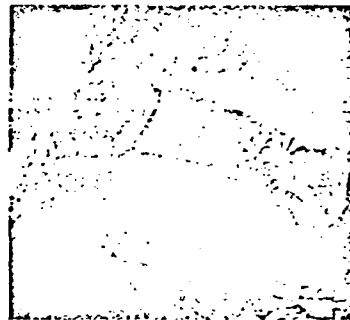
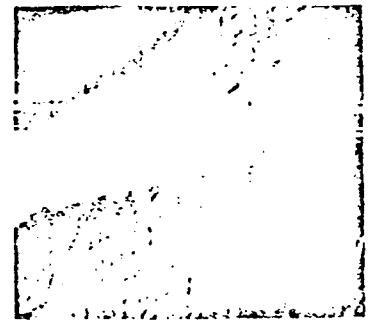
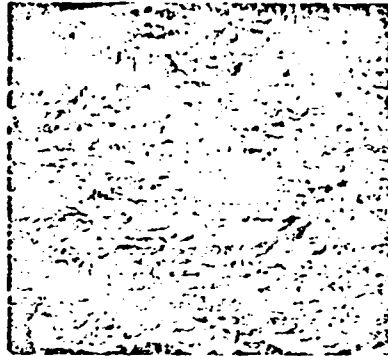
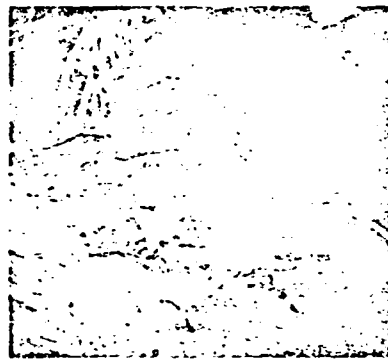
(a) Macro surface. 30 $\times$ .(b) Quasicleavage appearance. 200 $\times$ .(c) Fatigue striations. 1500 $\times$ .

FIG. 11. Disc crack B-A.

Fig. 12(a). The surface is composed of small fissures and covered with particles. Earlier reports [2, 3] have shown the existence of precipitate  $(Ti, Zr)_3Si_2$  particles in this alloy and have indicated a correspondence with fracture origins.

A second opened service crack, Specimen BB-4, is shown in Fig. 13. The surface is very similar to the previous example, but the existence of a field of fatigue striations at the furthest extension of the crack tip before opening is seen in Fig. 13(b).

(d) Quasicleavage appearance, 750 $\times$ .(e) Striations near surface, 100 $\times$ .(f) Origin area, 100 $\times$ .(g) Fatigue striations, 2500 $\times$ .

Higher magnification views are seen in Figs. 13(c) and 13(d). This proves conclusively that after the crack initiated by cleavage the propagation of the crack involved fatigue. An origin site could not be identified but that did not preclude a site at the extension of a secondary crack subsurface to the fracture surface and the major fracture surface being at some angle to the fracture surface. On this surface as with the previous fracture a large percentage of the crack extension was by a cleavage like propagation mode.

Figures 14 and 15 are views of a third opened hub crack Specimen BB-3. On examination a probable origin site was located and is shown at higher magnification in Figs. 14(b) and 14(c). All fracture flowlines emanate from the void in the center of Fig. 14(c).

(a) Fan shaped origin area, 150 $\times$ .(b) Void near probable origin, 1000 $\times$ .(c) Particles near probable origin, 1500 $\times$ .

FIG. 12. Origin area of specimen B-A.

To determine if there is any chemical peculiarity associated with the void and surrounding area an EDAX (Energy Dispersive Analysis of X-rays) analysis was performed. Figure 15 presents the results of that analysis. Figures 15(a) and 15(b) show the region of the void on both fracture surfaces. It is interesting to note the presence of particles surrounding the void on one surface and a corresponding depression or hole on the opposite surface. Figures 15(c) and 15(d) are the EDAX readouts for the fractures indicated in 15(a) and 15(b) respectively. In Figure 15(c) the bars represent the base metal showing aluminum, a small amount of silicon, zirconium and titanium. The dots represent the

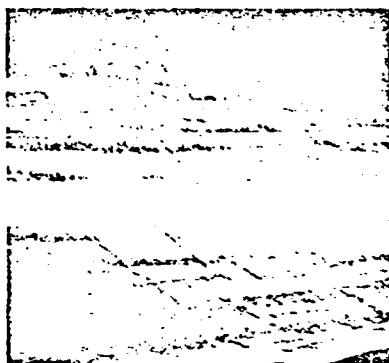
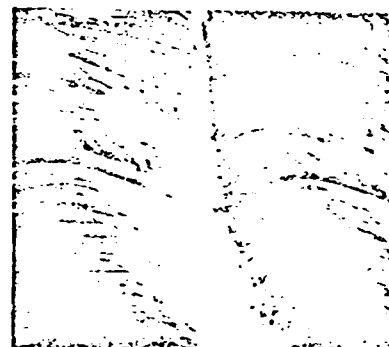
(a) Macro surface, 10 $\times$ .(b) Fatigue region, 100 $\times$ .(c) Fatigue region, 1250 $\times$ .(d) Fatigue region, 750 $\times$ .

FIG. 13. Hub crack specimen BB-4.

chemistry of the particle at the edge of the void. They show a higher than normal (when compared with the bars representing the base material) reading for silicon. This is strong evidence in support of the assumption that the particle is a precipitate of the chemical composition described earlier  $(Ti, Zr)_2Si_3$ . The precipitate appears to have a strong influence on the initiation of the crack; however, the cleavage burst initiation could occur at other sites as well. For example, under the



extension  
of crack  
in service

(a) Macro surface. 10 $\times$ .



(b) Origin area. 90 $\times$ .



(c) Void at origin. 500 $\times$ .

FIG. 14. Hub crack specimen BB-3.

proper strain field, strain values, local chemistry and, microstructure, and texture other local discontinuities such as voids or grain boundary triple points could also initiate the failure. A higher than normal level of silicon was indicated around the void as seen in Fig. 15(d). This is in agreement with the results presented in reference [2].

### Conclusions

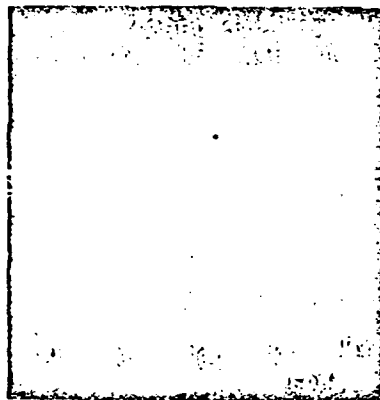
The titanium alloy studied herein, IMI 685, behaves much the same as other titanium alloys in static tensile properties. That is, the strength and



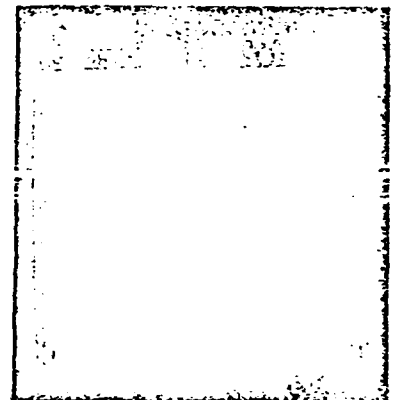
(a) Bars—away from the hole; dots—on particle. 2000 $\times$ .



(b) Bars—away from hole; dots—at edge of hole. 2000 $\times$ .



(c) EDAX composition determination of surface in Fig. 15(a).



(d) EDAX composition determination of surface in Fig. 15(b).

FIG. 15.

ductility are within specified limits. The fracture surface is composed of highly ductile fracture modes, while the fracture morphology exhibits a strong dependence on microstructure.

The strain controlled fatigue behavior exhibited well defined fatigue striations mixed with a quasicleavage appearance in the origin area. The fracture mode tended to be dependent on grain orientation, often

changing modes upon encountering a grain boundary. Again the fracture appearance was typical for a titanium strain controlled fatigue specimen.

Specimens E-25 and E-8, hold time and hold time with deionized water, respectively, propagated almost entirely by quasicleavage which corroborates the accelerated growth rates for the specimens with respect to the baseline specimen E-9. The kinetics of this process and mechanics will undoubtedly be rigorously explored in the future.

The hub crack specimens probably initiated in regions containing silicate precipitates but more importantly propagated by a quasicleavage mode that led to accelerated observed crack growth rates under given stress conditions. The inservice cracks propagated due to alternating loads, as indicated by the presence of the striations. The presence of large amounts of cleavage facets and delamination leads to the conclusion that the hold-time during service loading also was a factor in the accelerated crack growth that was observed.

*The author is grateful to numerous colleagues for interaction and encouragement. These brief reflections were put together in the hopes that any insights gained during the 1972-73 period may aid our understanding of these most interesting phenomena. I owe an extreme debt of gratitude to many colleagues at Lockheed California Co., Rolls Royce (1971) Limited (Derby), Naval Ship Engineering Center, and the University of Missouri. I am especially grateful to Chris Best and Rosie Jamieson for their patience in typing and layout of the manuscript. In addition, I want to express a debt of gratitude to Dr. Paul Braisted, Chairman of the MAE Department at UMC, for providing the opportunity to sift and winnow in a free fashion.*

#### References

1. J. T. Ryder, D. E. Pettit, W. E. Krupp, and D. W. Hoepfner. Evaluation of Mechanical Property Characteristics of IMI 685. *Lockheed Fracture Laboratory Final Report* (October, 1973).
2. E. C. Burke. Summary Progress Report on RB.211 Engine Fan Disc Materials Studies. April, 1973, Lockheed Private Data.
3. J. B. Rittenhouse. Private communication.

*Received May, 1977*

# FORGING AND PROPERTIES OF AEROSPACE MATERIALS

Proceedings of an international conference  
organized by Activity Group Committee 2  
(Applied Metallurgy and Metals Technology)  
of The Metals Society, in association with  
the Leeds and Bradford Metallurgical Societies.  
The conference was held in the Houldsworth  
School of Applied Science, University of Leeds,  
on 5 - 7 January 1977.

THE METALS SOCIETY

BOOK 189: PUBLISHED 1978 BY

THE METALS SOCIETY,  
1 CARLTON HOUSE TERRACE,  
LONDON SW1Y 5DB.

© 1978 THE METALS SOCIETY

all rights reserved

ISBN 0 904357 12 0

PRINTED BY  
THE CHAMELEON PRESS  
LONDON

## EFFECT OF MICROSTRUCTURE ON FATIGUE CRACK GROWTH BEHAVIOR IN FORGED MATERIALS

D. Hoepfner

The effect of microstructure on fatigue-crack growth of a model structural material is investigated. It is shown that fatigue-crack growth in this model material is strongly dependent on local microstructure. A number of crack growth experiments are presented that dramatize the potential role of microstructure. It is suggested that the current two parameter approach to fatigue-crack growth study in vogue is not adequate to assess the role of microstructure in the fatigue process. Rather, a more physically based and mathematically rational curve fitting procedure is suggested. Use of a better curve fitting approach will permit the examination of the role of microstructure in fatigue-crack growth in a more realistic way.

From the results of this study, it is concluded that optimum fatigue-crack growth resistance can be developed by alloy tailoring through chemistry and process manipulation.

Professor of Engineering  
College of Engineering, University of Missouri  
Columbia, Missouri U. S. A.

1. INTRODUCTION. Ever since "scientific" research into factors that affect fatigue behavior has been underway there has been considerable effort expended toward developing insight into the role of microstructure in fatigue. It appears that after some years, and a large number of publications that have been directed toward resolution of differences related to the role of microstructure, a great deal of confusion still exists. The advent of "modern fracture mechanics" has not helped to clear things up either. This conference is entitled Forging and Properties of Aerospace Materials. It seems to me that there is an implication in the title that forging practice can modify the properties of a material. Indeed, many of the papers at the conference illustrate this point. In this brief paper it is my intention to once again attempt to show that microstructure is a major factor in the fatigue-crack growth behavior of materials.

This concept certainly is not new. Alan Griffith<sup>1</sup> pointed the way for us in

his classic treatise on flow and fracture. Let us take a brief look at some of the statements that Dr. Griffith made regarding the potential for modifying the mechanical properties of a structural material. "From the engineering standpoint the chief interest of the foregoing work centres round the suggestion that enormous improvement is possible in the properties of structural materials. Of secondary, but still considerable, importance is the demonstration that the methods of strength estimation in common use may lead in some cases to serious error."<sup>1</sup>, p. 193 "In the case of ductile metals, the effect of scratches is important only under alternating or repeated stresses. On the theory advanced in the preceding section, fatigue failure under such stresses is determined by phenomena which occur at the intercrystalline boundaries."<sup>1</sup> p. 193.

"The most obvious means of making the theoretical molecular tenacity available for technical purposes is to break up the molecular sheet-formation and so eliminate the "flaws." In the case of crystalline material this has the further advantage of eliminating yield and probably also fatigue failure." ..... "These considerations suggest that if a piece of metal were rendered completely amorphous by cold working, and then suitably heat-treated, its molecules might take up the stable strong configuration already described. The theory indicates, however, that over-straining tends to set up tensile stresses in the unchanged parts of the crystals which may start cracks long before decrystallization is complete. Such cracking could be prevented if the over-straining were carried out under a sufficiently great hydrostatic pressure, and this line of research seems to be well worth following up." ..... "The problem may be attacked in another way. As has been seen, the theory suggests that the drop in stress at the initiation of yield is due to the surface energy of the intercrystal boundaries. Thus, the yield point may be raised by "refining" the metal, i.e., so heat-treating it as to reduce the size of the crystals. The limit of refinement is, doubtless, reached when each "crystal" contains but a single molecule and the material is then in the strong stable state already described."

"Refining is also of great value in connection with resistance to fatigue failure. Suppose, in accordance with the foregoing theory of fatigue, that one crystal has been fractured, then the general criterion of rupture shows that the crack cannot spread unless the material is subjected to a certain minimum stress, which is greater the smaller the crack. Thus, reducing the size of the crystals increases the stress necessary to cause the initial crack to extend."<sup>1</sup>, p. 194-195.

Thus, Dr. Griffith suggests that a minimum energy threshold for crack growth exists and that the threshold and subsequent rate of growth of the crack is influenced by "molecular attraction," grain size and texture. Certainly, since the time Dr. Griffith put forth his classic ideas which served as the formalized beginning of energy concepts applied to fracture and led to fracture mechanics, we have added to our reservoir of knowledge regarding the growth of cracks. Actually, even though methods of modifying the "strength" of a solid were suggested by Griffith, there still is some confusion in the technical community as to whether modifying the microstructure can modify the fatigue-crack growth behavior. (Even though many of us in attendance at this conference generally agree that microstructure is a major factor influencing the "strength" of solids.) Let me dramatize this point by quoting from a recent paper presented in a U.S. journal of wide "popular" distribution.<sup>2</sup>, p.17

"The fact that the inert-environment fatigue crack growth properties of different alloys within a given metal system are similar indicates that fatigue crack growth rate behavior is essentially independent of the alloy's conventional mechanical and metallurgical properties. This observation further

indicates by conventional apparent in material p.243, states for shows that benign env properties as to what things, us

As a result elements of greater in brief effort of microstr many of my major intr growth bene as the crys include ori may not be convenient example of tize the in material se tion).

Currently, University, paper provi

2. CURRENT vehicles and material sp assure reli had been su strength sp tensile str controls to

Early aircr yield streng fatigue desi concepts, a fatigue-crack metodologie

- Impro
- Devel
- inspe
- Estab
- Setti
- Comp

look at some  
for modifying  
engineering  
and suggest-  
structural  
the demonstra-  
lead in some  
is, the effect  
resses. On the  
r such stresses  
boundaries."

acity available  
tion and so  
s has the fur-  
ailure." .....  
dered completely  
molecules might  
theory indi-  
esses in the  
pre decrystal-  
over-straining  
e, and this  
The problem may  
sts that the  
energy of the  
"refining"  
e crystals.  
" contains  
ble state

to fine  
tigs that  
apture shows  
a certain  
reducing the  
initial crack

crack growth  
he crack is  
ertainly,  
rved as the  
led to fracture  
the growth  
ngth" of a  
in the tech-  
scify the  
dence at this  
influencing  
ng from a  
tribution. 2, p.17

ties of differ-  
t fatigue  
y's conven-  
further

indicates that such fatigue crack growth rate behavior cannot be controlled by conventional alloy development or heat treating techniques. Thus, it is apparent that this fatigue crack growth behavior is not a pertinent factor<sup>3</sup> in materials selection considerations." A recent book on "Fracture Control" p.243, states "...the use of a single equation to predict fatigue-crack-growth rates for these steels may be justified." ..... "The preceding discussion shows that the region II fatigue-crack-growth rate behavior of steels in a benign environment is essentially independent of mechanical and metallurgical properties of the material." These latter references might raise some question as to whether we'd want to take Dr. Griffith's suggestion and, among other things, use forging to modify the fatigue-crack growth behavior of a solid.

As a result of certain exciting events of 1973, among other things, various elements of the technical community are now directing effort toward developing greater insight into the role of microstructure in fatigue-crack growth. This brief effort was in part directed toward adding further insight into the role of microstructure in crack growth. The hypothesis of this work, as with so many of my own researches in the past, is that microstructure is one of the major intrinsic characteristics of a solid that determines its fatigue-crack growth behavior. Obviously, the basic alloy chemistry is a factor, as well as the crystallographic texture. For the purposes of this paper, I choose to include orientation (texture) effects as part of the microstructure (this may not be convention but in the manner that the work shall unfold it is not convenient herein to separate the local orientation effects). Following the example of Dr. Griffith ( and others ) a model material is selected to dramatize the importance that microstructure plays in fatigue-crack growth. The material selected is a titanium alloy (Ti-6Al-5Zr-0.5 Mo -- nominal composition).

Currently, a rather extensive effort on this subject is underway at the University of Missouri. A list of theses and dissertations appended to this paper provides much more detail than that included herein.

2. CURRENT DESIGN CONCEPTS. As the service requirements for aerospace vehicles and engines have become more demanding, the design procedures and material specifications have of necessity become more stringent in order to assure reliable and safe operational performance of the structure. Initially it had been sufficient to procure materials with concern only for the tensile strength specification. As demands on materials increased the upward push of tensile strength level necessitated improvements in process and inspection controls to assure proper reliability.

Early aircraft and engine designs were based, in the main, on ultimate and yield strength criteria. The design methodology then evolved to include fatigue design methodology (stress cycling S-N concepts), strain cycling concepts, and more recently linear elastic fracture mechanics procedures, and fatigue-crack growth concepts. The development of each of these design methodologies has provided another tool to aid the designer in:

- Improving structural reliability
- Developing viable material, process, raw material, and inspections and controls
- Establishing the design life
- Setting operating stress or strain allowables
- Component sizing and configuring

Each of these methodologies is somewhat different but all are directed at the five stated objectives. This paper deals with the concept of fatigue-crack growth, as stated.

The development of fatigue-crack growth design procedures have evolved rapidly in the past 20 years<sup>4</sup>. The procedure involves an evaluation of a rate equation from an initial flaw size to a critical flaw size. The rate equation is typically of the form:

$$da/dN = f(S, a, \phi) \quad (1)$$

where  $da/dN$  is the fatigue-crack growth rate, in./cycle,  $f(S, a, \phi)$  is a functional relationship between the gross stress ( $S$ ), crack length ( $a$ ) and part geometry,  $\phi$ .

One of the common empirical descriptions of the crack growth rate is the equation,

$$da/dN = C (\Delta K)^n \quad (2)$$

where  $\Delta K$  is the stress intensity range ( $K_{max} - K_{min}$ ) and  $C$  and  $n$  are empirical constants. However, this equation is not generally valid over the full range of  $da/dN$  values. Unfortunately, many papers related to fatigue-crack growth have dealt only with the limited range of applicability of the above equation to the fatigue crack extension process.

Even though fracture toughness ( $K_{IC}$  or  $K_Q$ ), initial flaw size, and stress all have a role in life prediction analysis, it has frequently been found that microstructural influences, environment, load ratio, wave form, frequency (or time), and spectrum can have an overriding influence on the fatigue-crack rate and related life prediction analysis.

Equation 2 is usually evaluated by conducting fatigue-crack growth tests utilizing "standard" test variables. The data then are plotted in the form of Figure 1. The curve is comprised of three major line segments, indicated on the figure as segments 1, 2, 3. Segments 2 and 3 are the segments that have received the greatest amount of study (equation 2 normally being applied to segment 2). Very little attention has been given to the area in or near the threshold - segment 1. In addition, many of the studies carried out on segments 2 and 3 have not considered microstructural variables and rarely has the range of external variables such as environment, wave-form, frequency, load ratio, and spectrum been systematically studied in an evaluation program. This has often resulted in the development of laboratory data which is of limited applicability to the analysis of actual service conditions.

If any equation of the form of Equation 2 is to provide a reliable methodology for fatigue life prediction, the contributions of the variables microstructure, environment, waveform, frequency, load ratio, and spectrum, must be considered in detail. These variables could have major effects in segment 1, and could have significant effects in segments 2 and 3. Note that the low  $\Delta K$  region (segment 1) where microstructural effects may be greatest is the region where the majority of the allowable fatigue life frequently is expended.

It is for the reasons stated above that the authors quoted earlier concluded that alloy development and process development have no effect on fatigue crack growth. It is asserted here that that statement is not a correct interpretation of the data that result from fatigue-crack growth tests.

FATIGUE CRACK  
GROWTH RATE  
 $\Delta a / \Delta N$ ,  
INCH / CYCLE  
(LOG SCALE)

Figure

2. THE ES  
process for  
cracking, v  
scopically  
has tradit

- \* Init
- \* Prop
- \* Fine

The importa  
process has

Many resear  
crack prop  
when compar  
conflicting  
considerati  
propagation

Total Fatig  
has a signi  
strength fo  
primary alp  
that workin  
while forgi  
prior beta

directed at  
of fatigue-

evolved  
valuation of a  
p. The rate

(1)

$\phi$ ) is a func-  
(a) and part

te is the

(2)

n are empirical  
the full range  
-crack growth  
above equation

and stress all  
four distinct  
frequency  
fatigue-crack

th tests  
in the form of  
indicated on  
ts that have  
applied to  
or near the  
out on seg-  
rarely has  
frequency,  
ation program.  
ich is of

le methodology  
microstructure,  
be considered  
, and could  
AK region  
region where

r concluded  
fatigue crack  
interpreta-

FATIGUE CRACK  
GROWTH RATE,  
 $\Delta a/\Delta N$ ,  
INCH/CYCLE  
(LOG SCALE)

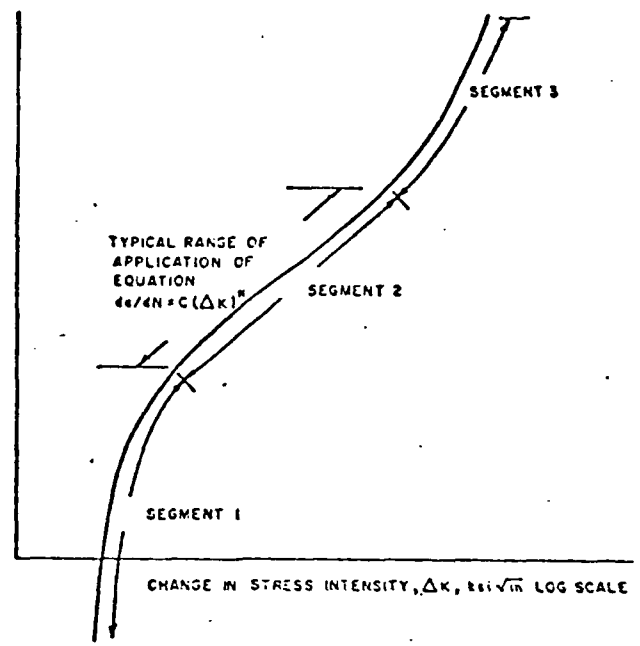


Figure 1. Typical plot of fatigue-crack growth results using linear elastic fracture mechanics correlation.

3. THE EFFECT OF TITANIUM MICROSTRUCTURE ON DYNAMIC BEHAVIOR. The fatigue process begins with dislocation motion generating slip bands that lead to cracking, with the subsequent growth of the crack normally described macroscopically in terms of the laws of continuum mechanics. The fatigue process has traditionally been divided into three stages, namely

- \* Initiation
- \* Propagation
- \* Final Fracture

The importance that metallurgical factors play in each stage of the fatigue process has been discussed by Hoepfner.<sup>5</sup>

Many research programs have been performed to study the mechanisms of fatigue-crack propagation and initiation in Ti alloys. However, some conflict exists when comparing results from different programs. Some resolution of the conflicting data and identification of trends can be accomplished by separate consideration of total fatigue life (S-N), time for crack nucleation, and crack propagation rates.

Total Fatigue Life - Several research programs have indicated microstructure has a significant effect on fatigue life. Bartlo<sup>6</sup> reported increased fatigue strength for thermal treatments that produced fine grained alpha-beta or fine primary alpha and alpha prime. Lucas<sup>7</sup> examined high cycle fatigue and found that working at 1775°F produced 40-50 percent increases in fatigue strength while forging just above the beta transus produced 60 percent increases, prior beta grain size had little influence, but finer alpha grain sizes

increased fatigue strength. For low cycle fatigue, Satlar et al.<sup>8</sup> found little difference in lives of three separate structures containing 10 percent primary alpha, 50 percent primary alpha and transformed beta. In contrast, Sprague et al.<sup>9</sup> found that a coarsened alpha phase had poor low-cycle fatigue life and that high temperature thermal mechanical working to produce a fine alpha-beta substructure increased fatigue life. Bowen and Stubbington<sup>10</sup> found that alpha-beta working improved low-cycle fatigue strength. They ascribed the improvement to a decrease in the mean free slip path caused by a reduction in prior beta grain size, refinement of alpha grain size, and introduction of averaged alpha prime martensites. Sparks<sup>11</sup> found that refinement of prior beta grain size increased fatigue life and eliminated directionality.

Differences in fatigue strength between small rolled bar and thick forged bar were ascribed to differences in microstructure by Stubbington and Bowen<sup>12</sup>. The small bar, which showed 50 percent better fatigue strength, had received large alpha-beta reductions to produce complete recrystallization and a finer grain size. In contrast the large bars were only partially recrystallized and some of the prior beta grain structure remained.

For the most part, these results all indicate that a fine grained alpha material will have improved S-N fatigue life over a large grained alpha structure. The fatigue life may be altered by either strong alpha or beta texturing. The fatigue lives of fine grained beta materials also appear to be quite good. Thus, the earlier statements of A. Griffith<sup>1</sup> are being verified.

Crack Nucleation - Low cycle fatigue-crack initiation in Ti-6Al-4V(STA) was studied by Wells and Sullivan<sup>13</sup>. Fatigue cracks initiated primarily in slip bands within the alpha phase particles with some cracks forming at the interface between the alpha and transformed beta phases. Fatigue-crack initiation in Ti-6Al-4V(MA) was investigated by Benson et al.<sup>14</sup> who found that under conditions of low stress at room temperature, cracks initiated at the alpha-beta phase interface. For high stress at room temperature, high and low stresses at 600°F, cracks were initiated in slip-bands within the alpha phase. No relation could be found between crack initiation and deformation twins, as previously noted for alpha titanium<sup>15</sup>.

During low-cycle fatigue of Ti-6Al-4V, Sprague et al.<sup>9</sup> noted crack initiation at primary alpha phase interfaces, and that finer alpha particle size increased resistance to crack initiation. Other work also noted that crack initiation at low stresses occurs more readily for structures containing coarse alpha, either acicular or equiaxed.

Work by Stubbington and Bowen<sup>12</sup> related low fatigue strength to early initiation and growth of Stage I cracks caused by localized plastic strain in large prior beta grains. For this case texture of the forged bars limited the number of active slip systems and restricted the slip to a few properly oriented beta grains (inhomogeneous slip). Alpha-beta working of the beta annealed bars improved the crack initiation resistance, both by a refinement of prior beta and alpha grain sizes (smaller mean free slip paths reduce the magnitude of localized plastic strain) and a modification of the texture (more homogeneous slip distribution).

A recent study used a computer imaging approach to quantify the microstructure characteristics. A variety of geometric parameters appeared to correlate with crack initiation and cycles to a 1/32-inch crack length. While some technical difficulties still exist the potential usefulness of the approach was demonstrated for tensile and fracture toughness estimations.

As might  
are simil  
alpha gra  
again may  
tures may

The Effect  
for fatig  
the role  
that "...  
plastic b  
cycled ca  
nature of

Robinson  
cially pu  
identifie  
orientati  
sensitive  
and Birkb  
grain exe

Robinson  
on grain  
the grain  
ture on f

Fatigue-c  
found tha  
the linki  
applied s  
at 600°F,  
Stage I g  
accompani  
Yuen and  
formation  
and Bowen  
ΔK = 1200  
ascribed  
tip. The  
grain size

A signific  
of Ti-6Al-  
containing  
with the a  
highest fa  
treated ar  
due to cra

Farrigan  
processing  
fatigue-cr  
contents,  
and beta a  
(MA) and s  
improverer

As might be expected, the general trends observed for fatigue crack nucleation are similar to those noted for S-N fatigue life in that smaller primary alpha grain sizes increase the time for crack nucleation. Texture effects again may reduce the cycles to nucleate a crack and transformed beta structures may show relatively short crack nucleation times.

The Effect of Microstructure on Fatigue Crack Propagation - As was the case for fatigue life and crack initiation, some disagreement exists concerning the role of microstructure in fatigue-crack propagation. Laird<sup>15</sup> maintained that "...there was only one general mechanism of fatigue-crack growth, that of plastic blunting, so that the microstructure of the material being fatigue cycled can change only the kinetics of crack propagation, not the general nature of the process."

Robinson and Beevers<sup>16</sup> performed fatigue-crack propagation tests on commercially pure alpha-titanium alloys and two distinct modes of crack growth were identified. At low-growth rates the crack path was highly dependent on the orientation of the grain the crack was traversing. This microstructurally sensitive Stage II crack growth has also been noted by Hoepfner for copper<sup>17</sup> and Birkbeck et al.<sup>18</sup> for low carbon steel. At high-crack growth rates the grain exerted little influence on the crack path.

Robinson and Beevers<sup>16</sup> have suggested that the extent of crack path dependence on grain orientation was greatest when crack tip plasticity was less than the grain size. This would indicate that the major influence of microstructure on fatigue-crack growth would be most pronounced at low  $\Delta K$  and  $K_{max}$  values.

Fatigue-crack propagation in Ti-6Al-4V(MA) was studied by Benson et al.<sup>14</sup> who found that for low stress at room temperature, Stage I cracking started with the linking of alpha-beta interface cracks growing at 45° angles to the applied stress. At higher stresses at room temperature and for all stresses at 600°F, Stage I cracking proceeded by the linking of slip-band cracks. All Stage I growth was transgranular, as was all Stage II growth. Profuse twinning accompanied crack growth but did not appear to affect crack growth rates. Yuen and Leverant<sup>19</sup> showed that a transition from cleavage to striation formation occurred at a  $\Delta K = 12000 \text{ psi } \sqrt{\text{in.}}$  for Ti-6Al-4V(MA). Stubbington and Bowen<sup>12</sup> found a transition between Stage I and Stage II cracking at a  $\Delta K = 12000 \text{ psi } \sqrt{\text{in.}}$  for Ti-6Al-4V. The transition for both phenomena was ascribed to a change from single slip to multiple slip systems at the crack tip. The same investigators<sup>10,12</sup> also found that a refinement of prior beta grain size increased resistance to Stage I crack growth.

A significant dependence of fatigue-crack growth rates on the microstructure of Ti-6Al-6V-2Sn was shown by Amateau et al.<sup>20</sup> Mill annealed material containing equiaxed primary alpha had the lowest crack propagation resistance, with the acicular alpha structure resulting from beta annealing showing the highest fatigue-crack growth resistance by a factor of four. The solution treated and aged structure also displayed high fatigue-crack growth resistance due to crack branching and deviation around primary alpha particles.

Harrigan et al.<sup>21</sup> examined the effect of aluminum plus oxygen content and processing parameters on fatigue-crack growth in Ti-6Al-4V. Improvements in fatigue-crack growth rates were obtained by decreasing oxygen and aluminum contents, especially for the RW orientation. The recrystallized anneal (RA) and beta anneal products showed lower crack growth rates than the annealed (MA) and solution-treated-overaged (S/OA) products. For the RA material, the improvement was due to full recrystallization and an equiaxed, fine-grained

alpha-beta structure. For the beta material, the improvement was due to refinement in prior beta grain size and a fine acicular alpha structure.

Bowen<sup>22</sup> examined the role of texture in the growth of fatigue cracks in Ti-6Al-4V bar. Crack growth was controlled by the texture in the alpha phase and the relevant slip systems for an orientation. Crack growth at low rates was totally crystallographic. Rapid-crack growth was associated with cleavage or ductile tear modes of crack advance. Harrigan et al.<sup>23</sup> found basal plane textures control the fatigue crack growth rate in Ti-6Al-2Sn-4Zr-6Mo.

The preceding discussion stresses a general conclusion of all of the papers reviewed: the more tortuous the crack path, the slower will be the crystallographic cracking, as long as cleavage and ductile tear are not caused.

Amateau et al.<sup>20</sup> also showed that no existing crack-growth model<sup>4</sup> could be used to describe the ranking of microstructure or the magnitude of crack-growth rates.

Additional work on the role of microstructure by this author and his colleagues has added further verification to Dr. Griffith's earlier observation<sup>24-26</sup>. Further reference to the effect of microstructure on fatigue is provided in references 27-35. From the extensive literature available it now appears possible to state in conceptual energy terms the physical process of fatigue crack growth. It is possible to cross an energy threshold that will produce fatigue crack growth. When observation techniques permit, that growth can be quantified in crack growth rate ( $da/dN$ ) terms. After this energy threshold is crossed, "the crack" propagates under continued fluctuations of load. On a time interval basis it should be clear that the rate of crack extension is related to the resistance it encounters from the surrounding material. This resistance can be presented as surface energy requirements for crack extension, plastic work terms, heat dissipation and other thermodynamic factors. As Griffith stated, and as most of the literature cited dramatizes, the microstructure is one of the principal factors that determines the energy requirement for crack extension. We may not be able to formulate all the mathematical expressions just yet but we are beginning to understand the phenomena reasonably well. A material was selected for this study that would dramatize the role of microstructure in fatigue-crack growth. Furthermore, it has been this author's contention for some time that the effect of microstructure on the fatigue cracking process can be observed on one specimen if one pays attention to detail, watches the crack, does not smooth out real data indiscriminately and does not attempt to overextend the real meaning of a fatigue crack growth rate ( $da/dN$ ) versus change in stress intensity ( $\Delta K$ ) plot. Thus, this brief study concentrates on observing, with some attention to detail, the crack growth process as affected by microstructure. Several studies are underway at other laboratories, as well as some at UM-C, which produce a wide range in microstructures and then conduct tests on each of the microstructures.

4. MATERIAL. The material used in this study had a chemical composition as listed in Table 1. Typical microstructures of the material are shown in Figure 2a-d. Figure 2a and 2b are photomicrographs at 20X (original mag.). Figures 2c and 2d are photomicrographs at 500X (original mag.). The material was forged and heat treated such that a prior  $\beta$  grain size of 0.100 - 0.200 inch resulted. As will be seen in the next section, this prior  $\beta$  grain size was frequently larger than the specimen thickness. The specimens for this study were sectioned for actual forgings of compressor discs. Thus, this model material also is a real structural material.

5. SPECIMEN  
3. Figure 4  
Fatigue precrack length  
growth tests  
load was initiated  
each specimen  
made and the  
and number of  
readings were  
large prior  
given specimen  
deal. However  
test technique  
followed. T

Constit

Aluminum  
Zirconium  
Molybdenum  
Silicon  
Iron (Fe)  
Hydrogen

\*Commercial  
Nominal

6. RESULTS  
(N) plot and  
intensity ( $\Delta K$ )  
the same two  
plotted is a  
dure may intr  
due to microstr  
may average.  
produce a bul  
to show that  
a single spec  
2.00 mm., 2.2  
being generated  
to the case w  
thickness. C

During each test  
predetermined  
would either  
in Figures 5a  
in the plots,  
affect the total  
the instantaneous  
occurs yearly  
These changes

was due to  
stress  
cracks in  
the alpha  
growth at low  
associated with  
al.23 found  
Ti-6Al-2Sn-

of the papers  
be the crystal-  
not caused.

el<sup>4</sup> could be  
of crack-growth

nd his collea-  
observation<sup>24-26</sup>.  
s provided in  
now appears  
ess of fatigue  
t will produce  
t growth can be  
ry threshold is  
load. On a  
extension is  
aterial. This  
crack extension  
ectory. As  
s, micro-  
energy require-  
the mathematical  
phenomena reason-  
rationalize the  
t has been  
structure on  
one pays  
l data indis-  
of a fatigue  
) plot. Thus,  
to detail, the  
udies are  
produce a  
the microstruc-

composition  
are shown in  
ginal fig.).  
The material  
000 - 0.200  
β grain size  
s for this  
us, this model

5. SPECIMEN. The specimen geometry used for this study is shown in Figure 3. Figure 4 is a photograph of one of the specimens used in the study. Fatigue precracking was conducted in closed loop load control and the final precrack length was nearly identical in all specimens. The fatigue crack growth tests were conducted in closed loop equipment under load control. The load was initially set so that the initial calculated K level was the same in each specimens. Observations related to the crack growth were continually made and the raw data resulting from the experiments was crack length (a) and number of cycles of sinusoidally reversed load at 20 Hz. Crack length readings were made on the front and back face of the specimen. Because of the large prior β grain size and the variation in microstructure possible in a given specimen the front and back face readings frequently differed a great deal. However, this difference is attributed to the microstructure - not to test technique. All of the best fatigue-crack growth test practices were followed. The results from the tests follow.

TABLE 1 Chemical Composition\*

Constituent	Percent of Constituent
Aluminum (Al)	5.7 - 6.3
Zirconium (Zr)	4.0 - 6.0
Molybdenum (Mo)	0.25 - 0.75
Silicon (Si)	0.10 - 0.40
Iron (Fe)	0.2 max
Hydrogen (H <sub>2</sub> )	0.006

\*Commercial designation IMI 695  
Nominal composition from IMI Brochure

6. RESULTS. Figure 5a and 5b present the crack length (a) versus cycles (N) plot and the fatigue-crack growth rate (da/dN) versus change in stress intensity (ΔK) plot for one of the specimens. Figures 6 to 14 then present the same two respective plots for nine (9) additional tests. The crack length plotted is a linear average of the front and back face readings. This procedure may introduce some error because of the difference sometimes observed due to microstructure. Given, however, that the microstructure is random this may average. It is not my intention to either overkill the point or to produce a bulky paper. The reason I have presented the large amount of data is to show that the discontinuities in the fatigue crack growth process are not a single specimen anomaly. Data are presented herein for four thicknesses, viz. 2.00 mm., 2.25 mm., 3.00 mm., 3.99 mm. Data on thicknesses 12 mm and 25 mm are being generated at the current time. These data being generated are important to the case where the prior β grain size is less than the specimen (structural) thickness. Clearly, a continuum problem!

During each test, the observer would take readings of crack length at a predetermined number of cycles. It was frequently observed that the crack would either decelerate markedly or stop for some period. This is evidenced in Figures 5a - 14a by changes in slope of the a vs. N plot. As will be noted in the plots, frequent horizontal "arrests" occur. These "arrests" markedly affect the total cycles to failure of a given specimen and obviously affect the instantaneous crack growth rate. It will be noted that if an "arrest" occurs early in the crack growth process a large extension of life results. These changes in slope and "arrests" are the direct result of local

microstructural changes. In addition to the deceleration or arrest of the crack it frequently was observed that cracks would burst (accelerate rapidly) at times. This also is related to microstructure. Preferential orientation for cleavage or grain boundary decohesion results in acceleration of the crack. As originally suggested by Dr. Griffith, and elaborated on by this author on many occasions, this type of behavior is the result of the localized crack size, local crystallographic orientation, prior grain size, localized modulus (compliance), & type (acicular, equiaxed, etc)\*. It is not the intent of this paper to go into the detailed mechanisms of crack growth but to dramatize that the microstructure has an effect.

The da/dN vs ΔK plots presented in Figs 5b to 14b, exhibit a dispersion of data. These plots result from the a-N plots. Some investigators would take the a-N plots presented herein and smooth them out "by hand" or with a "smoothing function."

In this study, we let the data speak for itself! A point-by-point (a) incremental method was used to obtain the da/dN values. The ΔK value was calculated at the central point. Use of the point-by-point method provides some assessment of the variation in da/dN that results from the microstructural variation.

7. DISCUSSION OF RESULTS. The variation in a-N behavior and dispersion of da/dN data suggest a large variation that can be attributed to localized microstructural variation. It has been known that the fatigue-crack growth rate is a functional relationship of the following form:

$$\frac{da}{dN} = f(a, \sigma, \epsilon, env., T, \omega, P(l)) \quad (1)$$

- a - CRACK SIZE
- σ - STRESS
- ε - STRAIN
- env - ENVIRONMENT
- T - TEMPERATURE
- ω - FREQUENCY
- P(l) - CARRIER FUNCTION

The factors listed in equation 1 are extrinsic in the main. [The stress (strain) must include consideration of internal stresses]. The manner in which these parameters are combined is directly related to the intrinsic material character. Intrinsic factors that are believed to relate to the fatigue crack growth behavior are:

- material chemistry
- microstructure (crystallographic texture)
- working texture

\* A factor being neglected in this current discussion is the residual stress. It is believed that the residual stress is a significant factor in fatigue-crack growth. We have efforts underway to study this variable in more detail (see M. S. thesis of Ms. Cole on attached list).

Obviously related to "initial" has been distributions depending

Frequently data that Figures 5b to "fit" c

As indicated frequently the equation initial fit allowables

As pointed even though package for quite misl of a plot how one would that

A) line ΔK→

B) line ΔK→

Thus, the equation. Frequently fit the data shown below

arrest of the  
 (propagate rapidly)  
 (initial orientation  
 of the crack,  
 this author on  
 localized  $\Delta\sigma$  packet  
 localized modulus  
 intent of this  
 to dramatize that

dispersion of  
 factors would take  
 into account

point (a)  
 K value was  
 method provides  
 the microstructural

dispersion of  
 localized  
 crack growth

(1)

the stress  
 pattern in  
 intrinsic  
 due to the

residual stress,  
 in fatigue-  
 detail

Obviously the way these factors contribute to crack growth will be directly related to the processing. The combination of factors thus will yield in "initial" statistical distribution of fatigue crack growth parameters. It has been demonstrated that the above factors can relate to statistical distributions whose central tendencies and dispersion may change in service -- depending on carrier function, environment, etc.

Frequently, it is common to attempt to fit a straight line to  $da/dN$  vs.  $\Delta K$  data that are plotted on a log-log basis. Note that the  $da/dN$  vs.  $\Delta K$  plots in Figures 5b to 14b are plotted on a log-linear basis. The common equation used to "fit" crack growth data is

$$\begin{aligned} &\text{CRACK GROWTH} \\ &\frac{da}{dN} = C (\Delta K)^n \quad (2) \\ &N = \int_{a_1}^{a_2} \frac{C}{(C \Delta K)^n} da \end{aligned}$$

INTEGRATE FOR LIFE

As indicated, after the parameters (incorrectly called constants all too frequently) C and n are evaluated by experiment, it is possible to integrate the equation to determine residual fatigue life for a given distribution of initial flaw sizes (either assumed or determined from flaw size design allowables).<sup>4</sup>

As pointed out by this author and Professor Freudenthal<sup>36</sup> on many occasions, even though this approach may be simplistic and provides a nice conceptual package for introducing fatigue-crack growth to life prediction, it may be quite misleading. Equation 2 is of course the equation of a straight line of a plot of  $da/dN$  vs.  $\Delta K$  on a log-log basis. It is now appropriate to ask how one would "fit" a straight line to the data of this study. Furthermore, the utilization of equation 2 does not fit the physical boundary conditions that

$$A) \lim_{\Delta K \rightarrow K_{Ib}} \left( \frac{da}{dN} \right) \rightarrow \infty \quad (\text{or some fraction of the acoustic wave velocity as proposed})$$

$K_{Ib}$  - instability value

$$B) \lim_{\Delta K \rightarrow K_{th}} \left( \frac{da}{dN} \right) \rightarrow 0$$

$K_{th}$  - threshold stress intensity, ksi  $\sqrt{\text{in}}$   
 [level of K below which a crack will not propagate - see quote from Dr. Griffith in introduction].

Thus, the fatigue crack growth data becomes an asymptotic distribution function. Freudenthal<sup>36</sup> proposed a form of exponential that more realistically fit the data. However, Bowie and Hoepfner<sup>37</sup> proposed a fitting function as shown below.

CRACK GROWTH

$$\frac{da}{dN} = C \cdot (\Delta K)^v \cdot \left[ -A \cdot \ln \left( 1 - \frac{\Delta K}{K_b} \right) \right]^{1/k} \quad (3)$$

CHARACTERISTIC VALUE  
 $\Delta K \text{ where } \frac{da}{dN} \rightarrow \text{INSTABILITY}$   
 SHAPE PARAMETER  
 THRESHOLD PARAMETER  
 CRACK GROWTH RATE

This equation has not been fitted to the data of this study- that effort is underway. However, Equation 3 has been found to fit fatigue-crack growth data and to provide a physical rationale for changes in the fitting function that result from changes in microstructure. The above equation is basically a four parameter approach. The parameters are  $v$ ,  $k$ ,  $A$ , and  $K_b$ . It has been found that changes in microstructure result in changes of all four parameters. Furthermore, it is not usually realistic in formulating a fatigue life prediction to truncate the lower and upper portion of the curves. These portions of the curve influence the fit a great deal as demonstrated in (38,39). Further research is underway at UI-C to complete the curve fits for different microstructures of titanium.

Figure 15 is a composite a-N plot for the ten specimens. The dispersion of results is accentuated and the discontinuities in the lower portion of the curve are more apparent. It is suggested that development of the curves at even lower rates would accentuate the microstructural differences. It also is apparent in the composite a-N plot that after a length of crack of about 0.95 inch is attained there is no apparent difference in the curves. In other words they could be superimposed. It is apparent here that the continuum strain field is now dominant and microstructure does not have a discernible influence. It is, of course, known that microstructure does influence the instability parameter.

Upon detailed examination of the  $da/dN$  vs.  $\Delta K$  plots it is observed that a rather extensive dispersion of the data exists. This dispersion is extremely useful to the curve fitting techniques described and thus gives a good indication of the scatter in data for a given microstructure. It is suggested, and as reviewed in the introduction, that a different microstructure will have a different distribution and this will be evidenced in the four parameters. If, however, one were to view the data at higher crack growth rates and plot on log-log paper it would be possible to conclude that microstructural changes introduced by processing and alloying produce no effect on fatigue-crack growth. However, it is asserted that such a conclusion is not valid for many materials.

**8. CONCLUDING REMARK.** It is shown that within a given titanium alloy the local variations in microstructure produce gross changes in the fatigue crack growth behavior. The potential for alloy tailoring to optimize fatigue crack growth resistance appears very good. This observation has already been exploited in many applications as it was suggested by Dr. Griffith. It is hoped that as we move toward inclusion of fatigue-crack growth as a primary design consideration we utilize data transformation and presentation procedures that more realistically represent the physics of the cracking process.

ACKNOWLEDGMENT  
 and friends  
 thanks is  
 the financ  
 the confere  
 ence at the  
 of the mate  
 growth spec  
 continuing  
 Mr. D. Pete  
 Kondas, Mr.  
 a student a  
 He coordinat  
 University)  
 Special tha  
 these perso  
 we have und  
 structural

REFERENCES

1. A. Grif  
Philosophic
2. W. G. C  
Affect Mate  
August 1974
3. S. Rolf  
Application  
N. J. (1977)
4. Hoeppe  
of Fatigue-C
5. Hoeppe  
AMS 1971 WES
6. Bartlo,  
Ti-6Al-4V Ba  
Philadelphia
7. Lucas, J  
Journal of A
8. Saltar,  
"Low Cycle F  
08-24.4, Oct
9. Sprague,  
Structure on  
and Technolo
10. Bowen,  
Fatigue and

ACKNOWLEDGEMENTS - The author is grateful to many organizations, colleagues, and friends for encouragement, interaction, and financial support. A special thanks is expressed to the U. S. Air Force Office of Scientific Research for the financial support (Grant No. 77 3178) that made it possible to attend the conference. Dr. C. Hays of AFOSR has been most supportive of my attendance at the meeting. I am indebted to Rolls Royce (1971) Ltd. for provision of the material and to Lockheed California Co. for preparation of the crack growth specimens. The following persons provided much stimulation for continuing work: Mr. R. Jeal, Mr. D. Alexander - Rolls Royce, Dr. G. Bowie, Mr. D. Pettit, Dr. J. Ryder, Mr. W. Krupp - Lockheed California Co., Dr. K. Kondas, Mr. W. Baumann, Mr. A. People, P. Clarkin - U. S. Navy. Mr. Gene Nickel, a student at University of Missouri, aided in the performance of the tests. He coordinated the efforts of Mr. M. Weinstein (now a freshman at Washington University), Mr. E. Breummer, Mr. T. Hanley, Mr. C. Baggett, Mr. V. Shah. Special thanks is extended to Mr. A. Braun for continued efforts. All of these persons and their respective organizations have supported the researches we have underway at the University of Missouri - Columbia related to micro-structural effects in crack growth, as well as other areas.

#### REFERENCES

1. A. Griffith, "The Phenomena of Rupture and Flow in Solids", Philosophical Transactions of the Royal Society, vol. 221A (1920) pp 163-198
2. W. G. Clark, Jr., "How Fatigue Crack Initiation and Growth Properties Affect Material Selection and Design Criteria", Metals Engineering Quarterly, August 1974, pp 16-22
3. S. Rolfe, J. Barson, Fracture and Fatigue Control in Structures - Application of Fracture Mechanics, Prentice Hall, Inc. Englewood Cliffs, N. J. (1977)
4. Hoepfner, D. W., Krupp, W. E., "Prediction of Component Life by Application of Fatigue-Crack Growth Knowledge," Engineering Fracture Mechanics, 1974
5. Hoepfner, D. W., "Metallurgical Aspects of Fatigue," paper presented at AMS 1971 WESTEC, Los Angeles, California, March 1971.
6. Bartlo, L. J., "The Effect of Microstructure on the Fatigue Properties of Ti-6Al-4V Bar," ASTM STP 459, American Society for Testing and Materials, Philadelphia, Pa., 1970, p. 144
7. Lucas, J. J., "Fatigue Strength Improvements in Ti-6Al-4V Forgings," Journal of American Helicopter Society, July 1972, p. 20
8. Saltar, S. A., Oberle, H. J., Kellogg, D. H., and Greene, B. N., "Low Cycle Fatigue in 6Al-4V Titanium Alloy," ASME Report Systems Paper DS-24.4, October 1968.
9. Sprague, R. A., Ruckle, D. L., and Smith, M.P., "The Effect of Micro-Structure on the Low Cycle Fatigue Behavior of Ti-6Al-4V," Titanium Science and Technology, Volume 3, Plenum Press, London, 1973, p. 2069
10. Bowen, A. W., and Stubbington, C. A., "The Effect of  $\alpha$ - $\beta$  Working on the Fatigue and Tensile Properties of Ti-6Al-4V Bars," ibid, p. 2097.

11. Sparks, R. B., "The Effect of Macro (Prior Beta) Grain Size on the Fatigue of Ti-6Al-4V Forgings," TMS Paper No. S6902, May, 1969
12. Stubbington, C. A., and Bowen, A. W., "Effect of Section Size on the Fatigue Properties of Ti-6Al-4V Bars," Titanium Science and Technology, Volume 2, Plenum Press, London, 1973, p. 1283.
13. Wells, C. H., and Sullivan, C. P., "Low-Cycle Fatigue Crack Initiation in Ti-6Al-4V," Transactions of the ASM, Volume 62, 1969, p. 263.
14. Benson, D. K., Grosskreutz, J. C., and Shaw, G. G., "Mechanisms of Fatigue in Mill-Annealed Ti-6Al-4V at Room Temperature and 600° F," AFML-TR-71-81, WPAFB, Ohio, April 1971.
15. Laird, C., "The Influence of Metallurgical Structure on the Mechanisms of Fatigue Crack Propagation," ASTM STP 415, American Society of Testing and Materials, Philadelphia, Pa., 1967, p. 131.
16. Robinson, J. L., and Beevers, C. J., "Some Observations on Fatigue Crack Growth in Alpha-Titanium," Titanium Science and Technology, Plenum Press, London, 1973, p. 1245.
17. Hoepfner, D. W., "The Effect of Grain Size on Fatigue Crack Propagation in Copper," ASTM STP 415, American Society for Testing and Materials, Philadelphia, Pa., 1967, p. 486.
18. Birkbeck, G. Hinkle, A. E., and Waldron, G. W. J., "Aspects of Stage II Fatigue Crack Propagation in Low Carbon Steel," Journal of Material Science, Volume 6, 1971, p. 319.
19. Yuen, A., and Leverant, G. R., "Correlations Between Fracture Surface Appearance and Fracture Mechanics Parameters for Stage II Fatigue Crack Propagation in Ti-6Al-4V," Report 73-603, Pratt & Whitney Aircraft, East Hartford, Connecticut.
20. Amateau, M. F., Hanna, W. D., and Kendall, E. G., "The Effect of Microstructure on Fatigue Crack Propagation in Ti-6Al-6V-2Sn Alloy," Mechanical Behavior on Materials, Volume 2, The Society of Material Science, Japan, 1972, p. 77.
21. Harrigan, M. J., Kaplan, M.P., and Sommer, A. W., "Effects of Chemistry and Heat Treatment on the Fracture Mechanics Properties of Ti-6Al-4V Alloy," NA-72-235, North American Rockwell, Los Angeles, California, March 1972.
22. Bowen, A. W., Royal Aircraft Establishment, Farnborough, Hants, United Kingdom, private communication.
23. Harrigan, M.J., Sommer, A. W., Reimers, P. G., and Alers, G.A., "The Effect of Rolling Texture on the Fracture Mechanics Properties of Ti-6Al-2Sn-4Zr-6Mo Alloy," Titanium Science and Technology, Plenum Press, London, 1973, p. 1297.
24. D. E. Pettit, D. Ryder, W. Krupp, D. Hoepfner, "Investigation of the Effects of Stress and Chemical Environments on the Prediction of Fracture of Aircraft Structural Materials," AFML-TR-74-183, Volume 1, 2, December 1974.

25. J. R. IMIGOS,
26. D. W. Strength
27. C. R. Orientati Internal
28. J. L. Content, Titanium" Birmingham
29. N. L. Microstruc April 197
30. K. Hi H. G. T.
31. G. S. Fatigue C AG/RD.
32. E. Ho A Y-Fe-Ni-
33. G. G. Aluminum A
34. J. R. Properties Fractogr pp. 99-138
35. A. B. Crack Grow (1975) p.
36. A.M. Mechanics,
37. G. E. Propagatio on Compute part 2 (19
38. K. Ko Fatigue - Ph.D. Dis
39. P. Pe Ph. D. Dis

Size on the  
69.

n Size on the  
Technology.

ack Initiation  
63.

hanisms of  
0° F,

the Mechanisms  
of Testing

on Fatigue  
logy,

ck Propagation  
erials,

cts of Stage  
Material Science.

ture Surface  
e Crack  
raft,

ect of Micro-  
Mechanical  
e, Japan,

of Chemistry  
Al-4V Alloy,"  
rch 1972.

ants, United

G.A., "The  
of Ti-6Al-2Sn-4Zr-  
on, 1973,

on of the  
fracture of  
ember

25. J. Ryder, W. Krupp, D. Pettit, D. Hoepfner, "The Mechanical Properties of IM1685," Lockheed Report, 1973 (Copy available on request)

26. D. W. Hoepfner, "A Fractographic Analysis of Flaw Growth in a High Strength Titanium Alloy", University of Missouri report, August 1975.

27. C. Romero, D. Hoepfner, "The Effect of Microstructure and Preferred Orientation on the Mechanical Behavior of Titanium Alloy Forgings", Lockheed Internal Report., December 1970.

28. J. L. Robinson, C. J. Beevers, "The Effects of Load Ratio, Interstitial Content, and Grain Size on Low-Stress Fatigue - Crack Propagation in  $\alpha$ -Titanium", Metal Science Journal, vol. 7 (1973) p. 153 [Also University of Birmingham Research Report, May 1973].

29. N. L. Richards, "The Relationship Between Fracture Toughness and Microstructure in Titanium Alloys", Ph. D. Thesis, University of Aston, April 1972.

30. K Hill, "The Crack Propagation Characteristics of Some Titanium Alloys", N. G. T. E. Note No: NT 819, April 1971

31. G. Sertmour, C. Bathias, "Influence of Microstructure on the Growth of Fatigue Cracks", presented at 37th Panel of Structures and Materials Panel - AGARD.

32. E. Hornbogen, K. Zum Gahr, "Microstructure and Fatigue Crack Growth in A Y-Fe-Ni-Al Alloy", Acta Metallurgica, vol. 24 (1976) pp. 581-592.

33. G. G. Garrett, J. Knott, "Crystallographic Fatigue-Crack Growth in Aluminum Alloys", Acta Metallurgica, vol. 23 (1975) pp. 841-848.

34. J. Chesnutt, C. Rhodes, J. Williams, "Relationship Between Mechanical Properties, Microstructure, and Fracture Topography in ( $\alpha$  &  $\beta$ ) Titanium Alloys", Fractography - Microscopic Cracking Processes, ASTM STP 600, ASTM (1976) pp. 99-138

35. A. Bowen, "The Influence of Crystallographic Orientation on Fatigue-Crack Growth in Strongly Textured Ti-6Al-4V", Acta Metallurgica, vol. 23 (1975) p. 1401-1409.

36. A.M. Freudenthal, "Fatigue and Fracture Mechanics", Engineering Fracture Mechanics, vol. 5 (1973) pp. 403-414

37. G. E. Bowie, D. W. Hoepfner, "Numerical Modeling of Fatigue and Crack Propagation Test Results", Proceedings of the 1976 International Conference on Computer Simulation for Materials Applications, Nuclear Metallurgy, vol. 20 part 2 (1976) pp. 1171-1178

38. K. Kondas, "Influence of Microstructural and Load Wave Form Control on Fatigue - Crack Growth Behavior of Precipitation Hardening Stainless Steels", Ph.D. Dissertation, University of Missouri - Columbia, July, 1976.

39. R. Reeves, "Microstructural and Environmental Effects in Fretting Fatigue" Ph. D. Dissertation, University of Missouri - Columbia, In preparation.

## ATTACHMENT

The following theses and dissertations provide additional information on the effects of microstructure and internal stresses on fatigue-crack growth. A limited number of copies are available upon request to D. Hoepfner.

Jerry Alan Wear, THE EFFECT OF MICROSTRUCTURE ON THE FATIGUE PROPERTIES OF OF A .40/ .50 CARBON STEEL, December, 1975, M. S. Thesis

Dale Alan Wilson, THE EFFECTS OF MICROSTRUCTURE ON THE FATIGUE LIFE OF TITANIUM, December, 1975, M. S. Thesis

Sharon Langenbeck Cole, THE EFFECT OF MEAN STRESS AND R RATIO ON THE FATIGUE BEHAVIOR OF TURBINE ALLOYS, May, 1976, M. S. Thesis

Vidyet P. Shah, THE RESIDUAL FATIGUE LIFE OF 1020 STEEL AND 7070-T6 ALUMINUM AS A FUNCTION OF INITIAL FLAW SIZE, M. S. Thesis

Cheung Jarm Poon, THE EFFECT OF ENVIRONMENT AND FREQUENCY ON THE FATIGUE BEHAVIOR OF WELDED PRESSURE VESSEL STEEL, July, 1976, M. S. Thesis

Kevin Richard Kondas, INFLUENCE OF MICROSTRUCTURAL AND LOAD WAVE FORM CONTROL ON FATIGUE-CRACK GROWTH BEHAVIOR OF PRECIPITATION HARDENING STAINLESS STEEL, July, 1976, Ph.D. dissertation

John Adrian Panhuise III, THE EFFECT OF A FREQUENCY ENVIRONMENT SYNERGISM ON THE FATIGUE-CRACK GROWTH OF SA533B-1; A NUCLEAR PRESSURE VESSEL STEEL, August, 1976, M. S. Thesis

Gary Charles Salivar, THE EFFECT OF CRYSTALLOGRAPHIC ORIENTATION ON FATIGUE AND FRETTING OF COPPER SINGLE CRYSTALS, August 1, 1976, M. S. Thesis

Andrew Wushung Tsai, THE EVALUATION OF FATIGUE CRACK GROWTH IN A NUCLEAR PRESSURE VESSEL STEEL, to be published December, 1976, Ph.D. dissertation

Roger Reeves, MICROSTRUCTURAL AND ENVIRONMENTAL INFLUENCES IN FRETTING FATIGUE, to be published, February 1977, Ph.D. dissertation

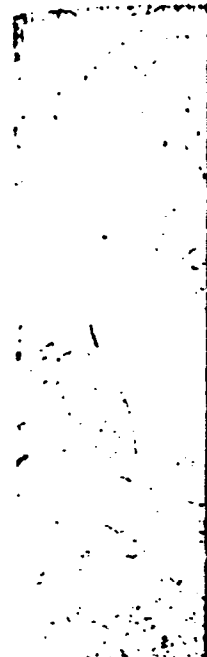


Figure 2



Figure 2

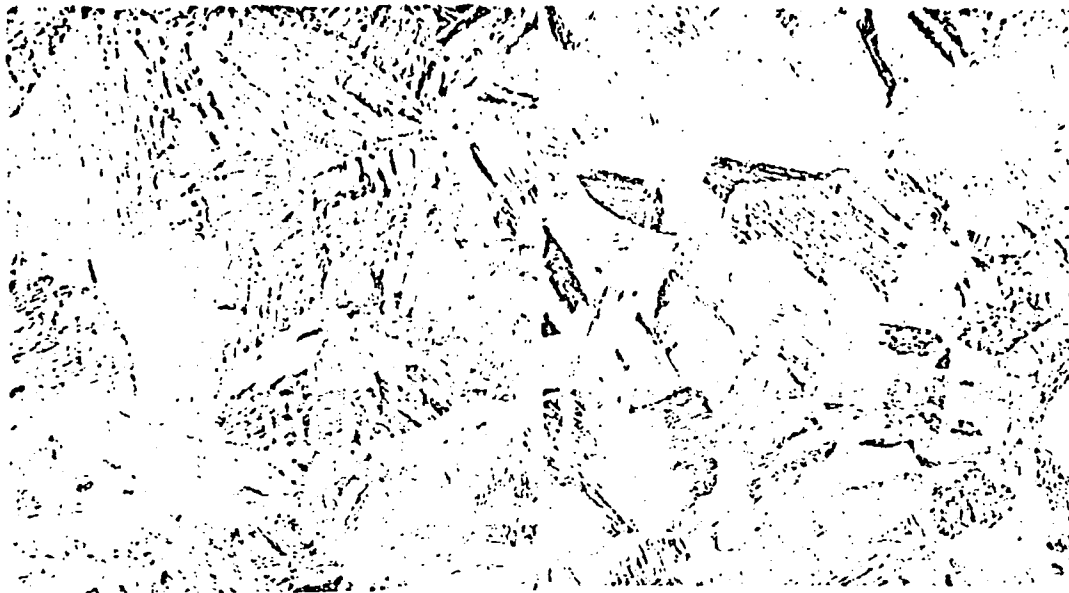


Figure 2 A x 17

Figure 2b x 17

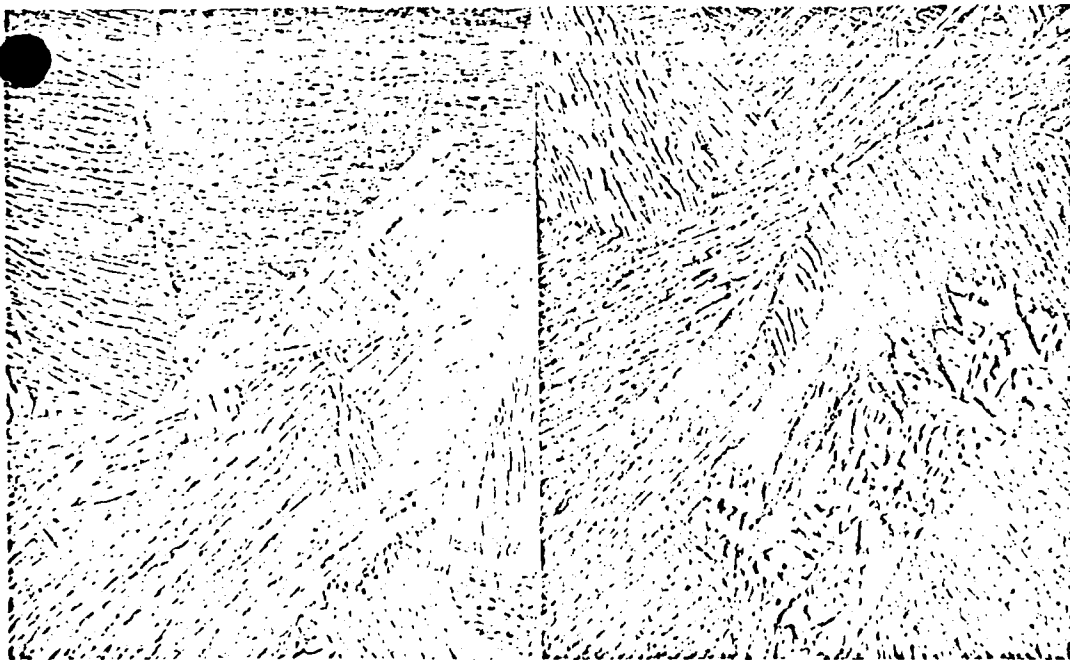


Figure 2 C x 420

Figure 2 D x 420

Figure 2. Typical photomicrographs showing the microstructure of the material used in this study.

COMPACT TENSION SPECIMEN

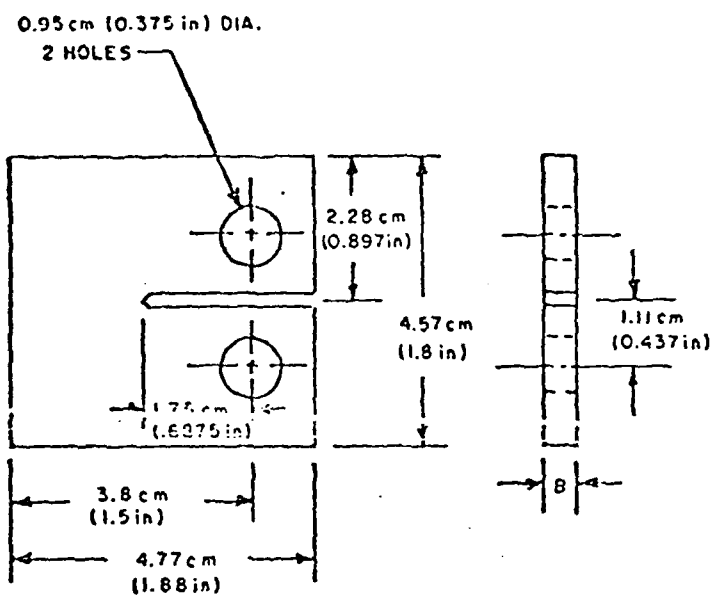


Figure 3 - Specimen Geometry

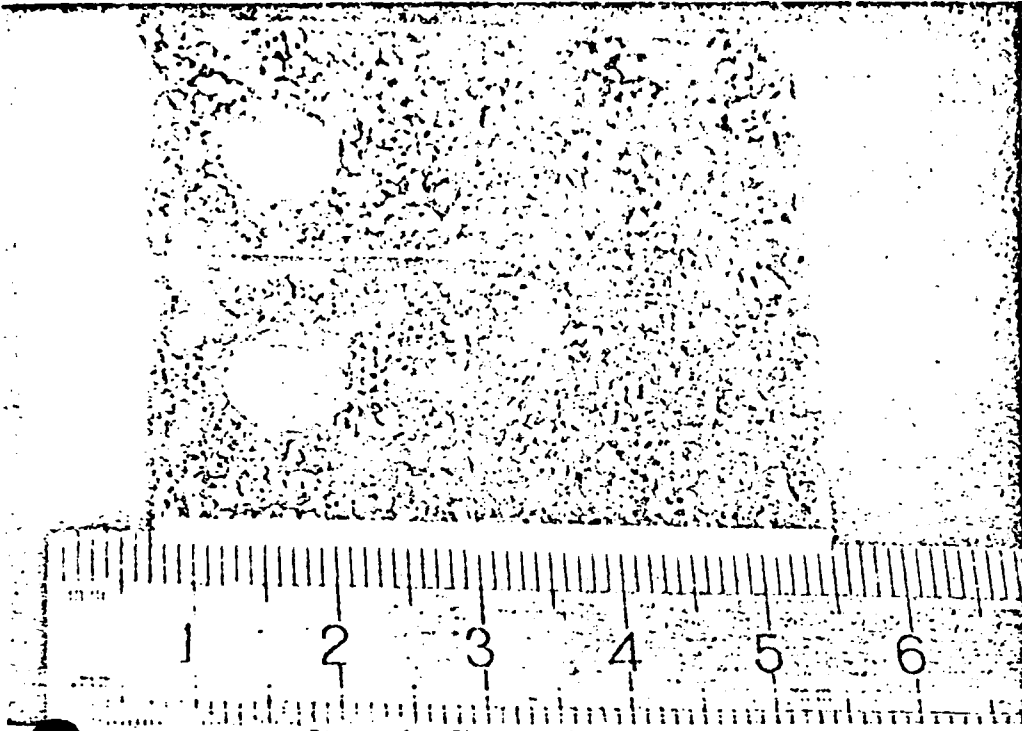


Figure 4 - Photograph of modified WOL  
Specimen used in the study

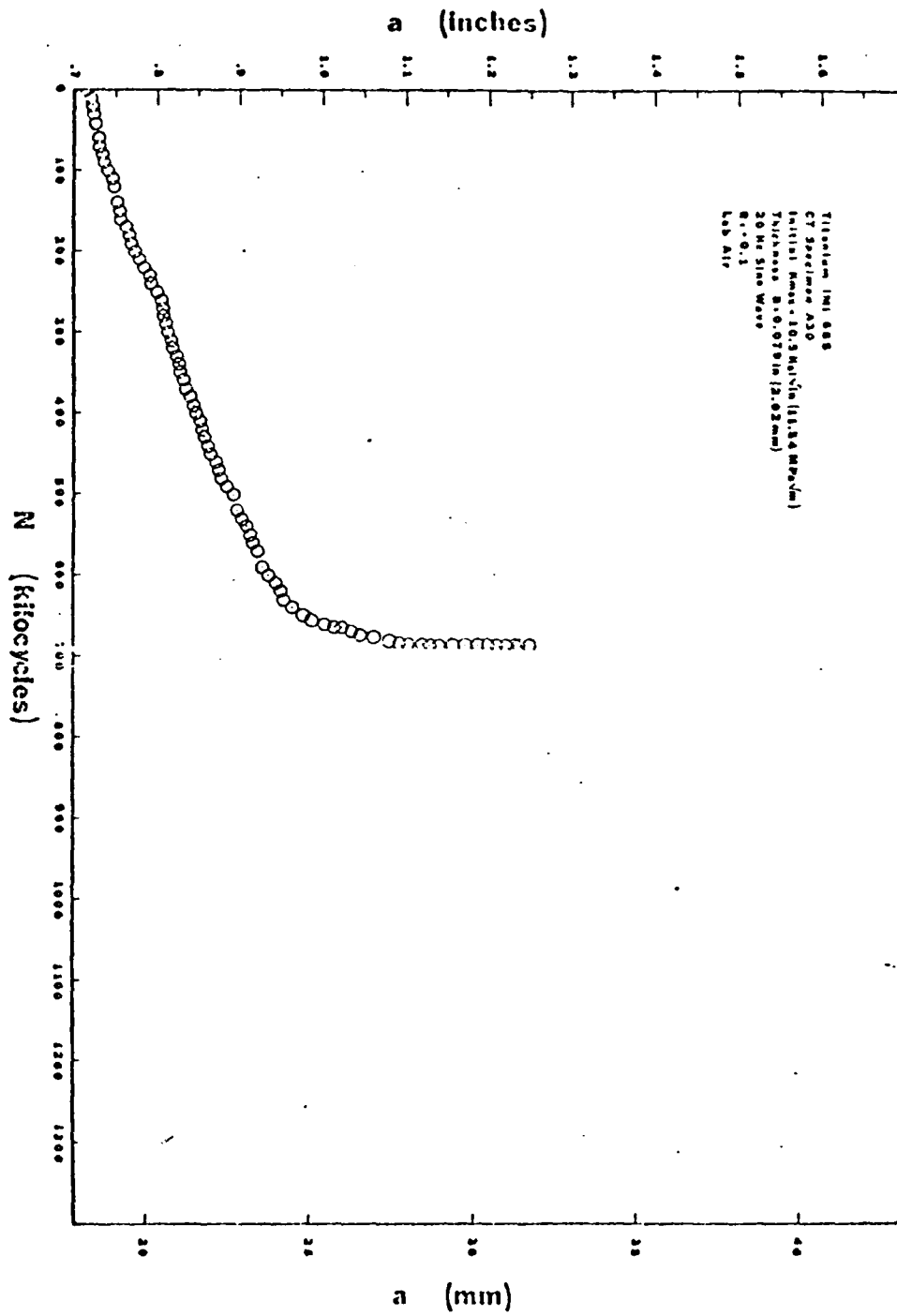


Fig.5a Plots of crack length (a) versus cycles (N); Specimen A30

DELTA K MPa√m

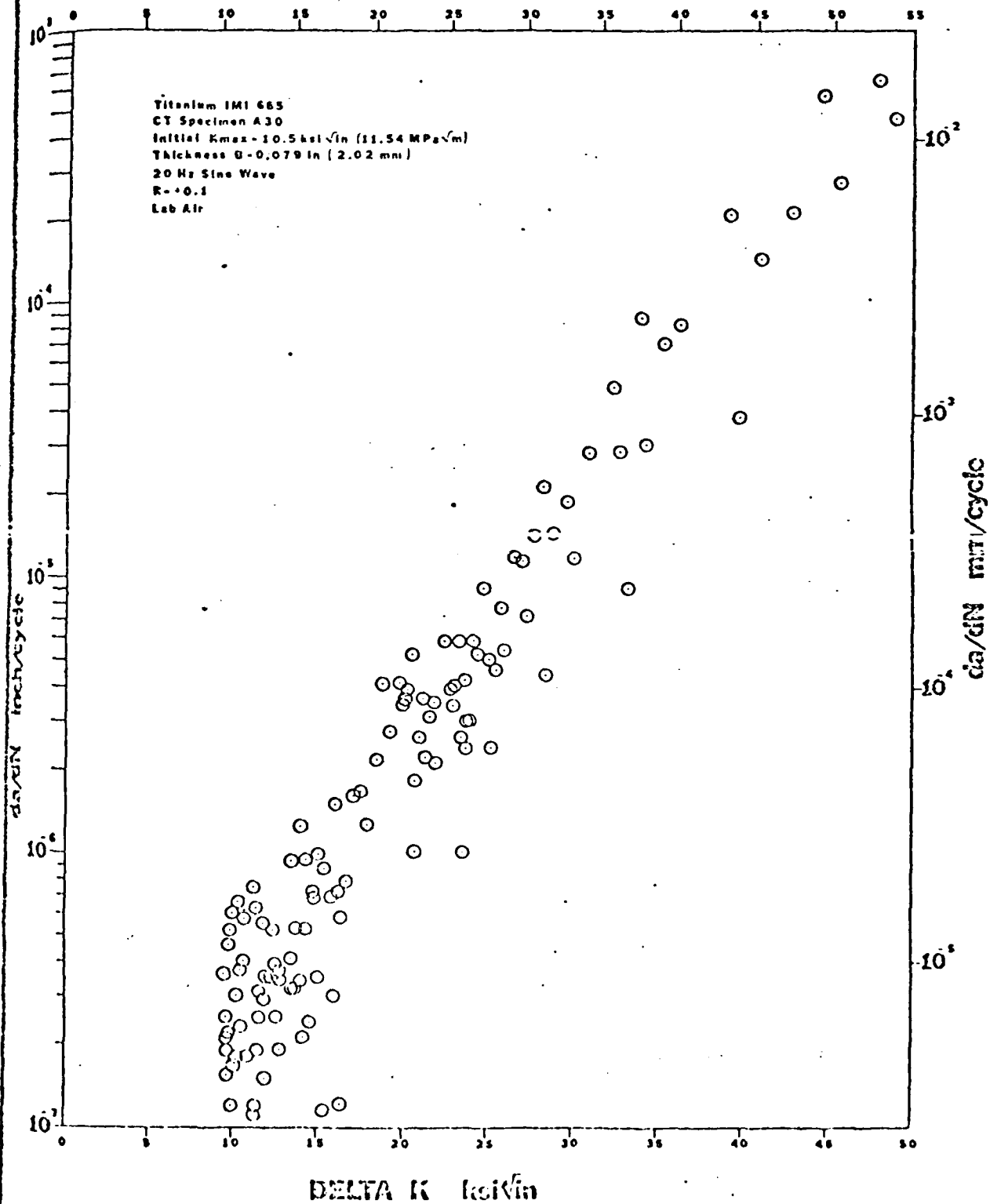


Fig. 5b Plot of fatigue crack growth rate (da/dN) versus change in stress intensity ( $\Delta k$ ); Specimen A30

Titanium IMI 665  
 CT Specimen A30  
 Initial Kmax = 10.5 ksi√in (11.54 MPa√m)  
 Thickness B = 0.079 in (2.02 mm)

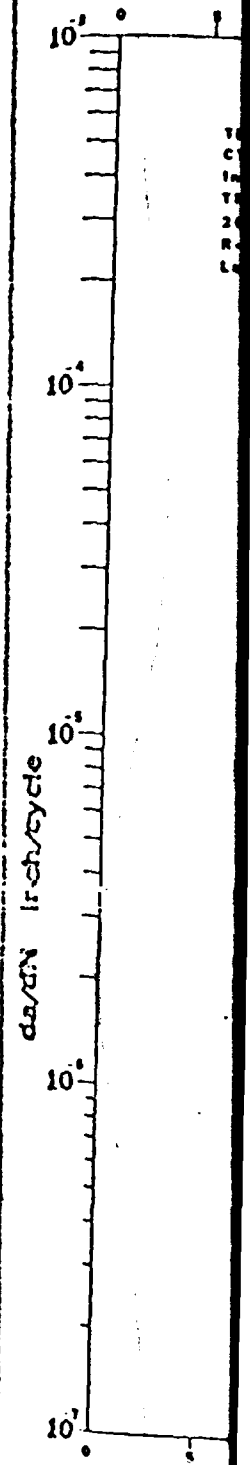
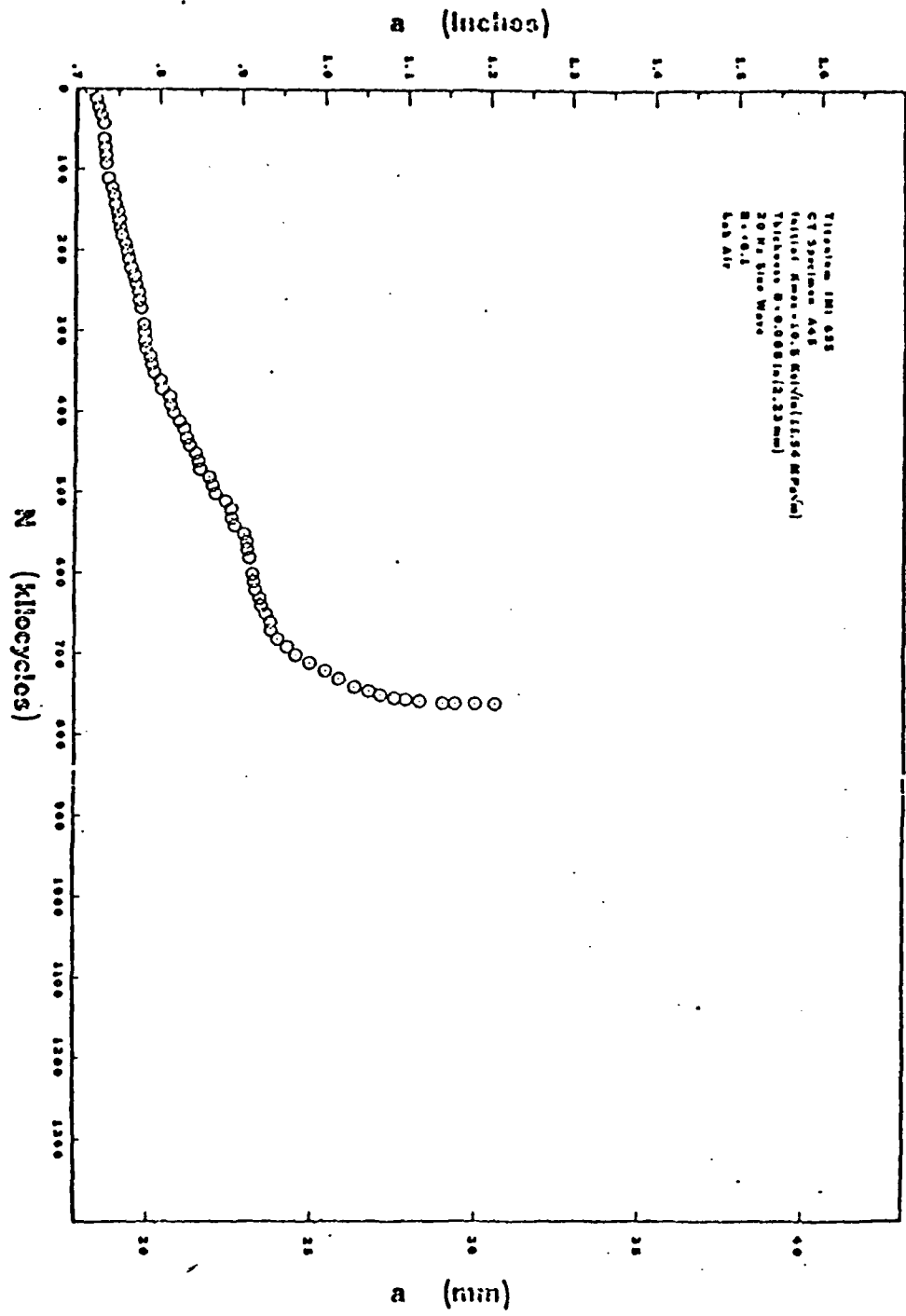


Fig. 6a Plots of a versus N ; Specimen A45

Titanium IMI 685  
 CT Specimen A45  
 Initial Kmax = 10.5 ksi√in (11.54 MPa√m)  
 Thickness B = 0.088 in (2.23 mm)  
 20 Hz Sine Wave  
 R = 0.1  
 Lab Afr

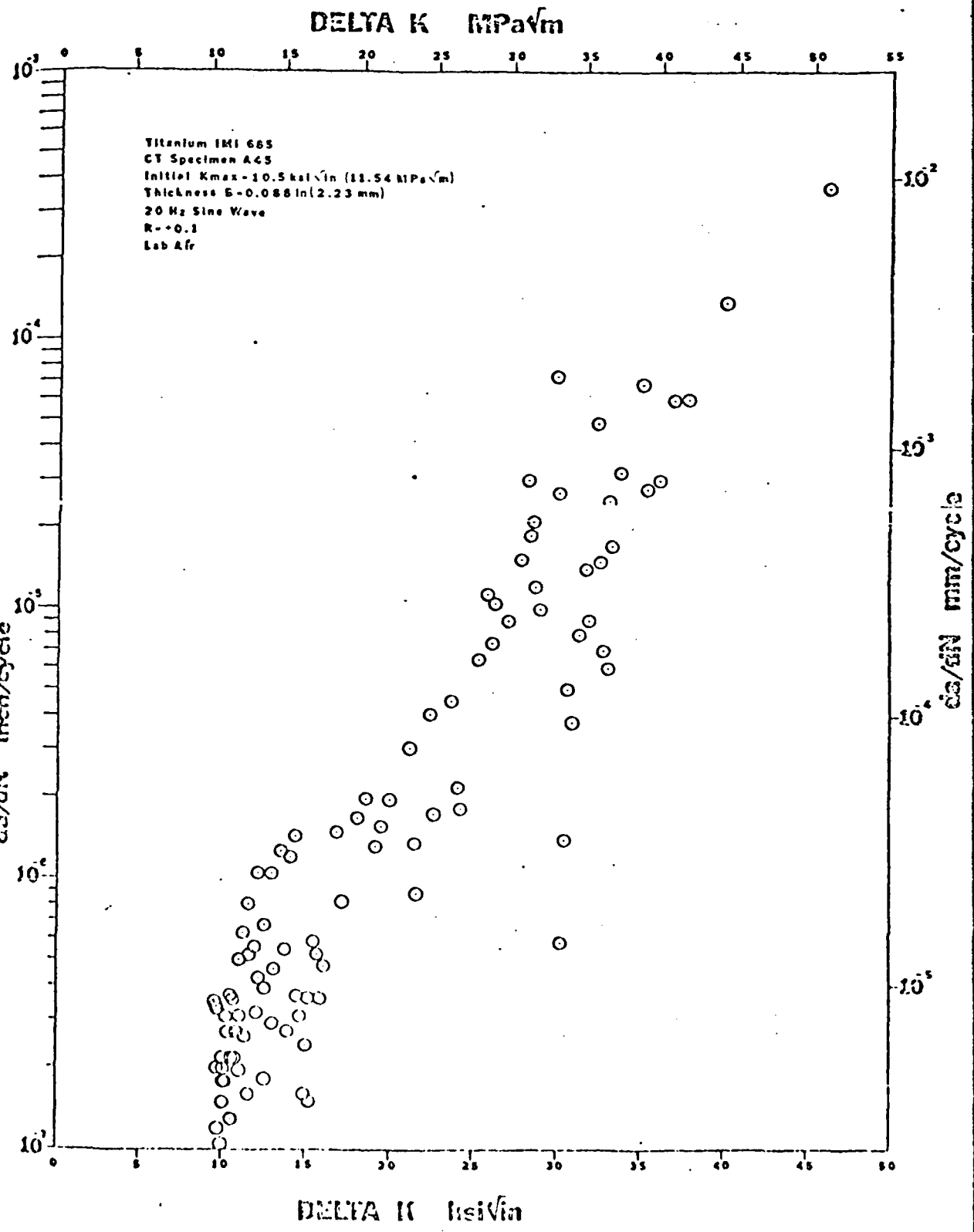


Fig. 6b Plots of da/dN versus Δk; Specimen A45

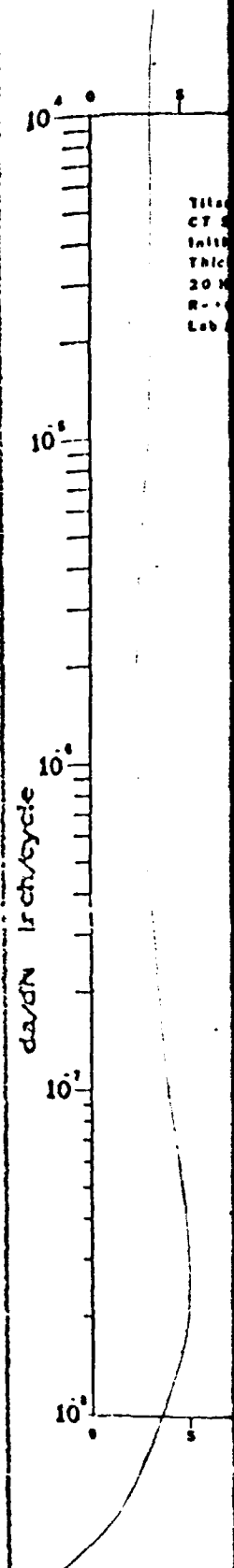
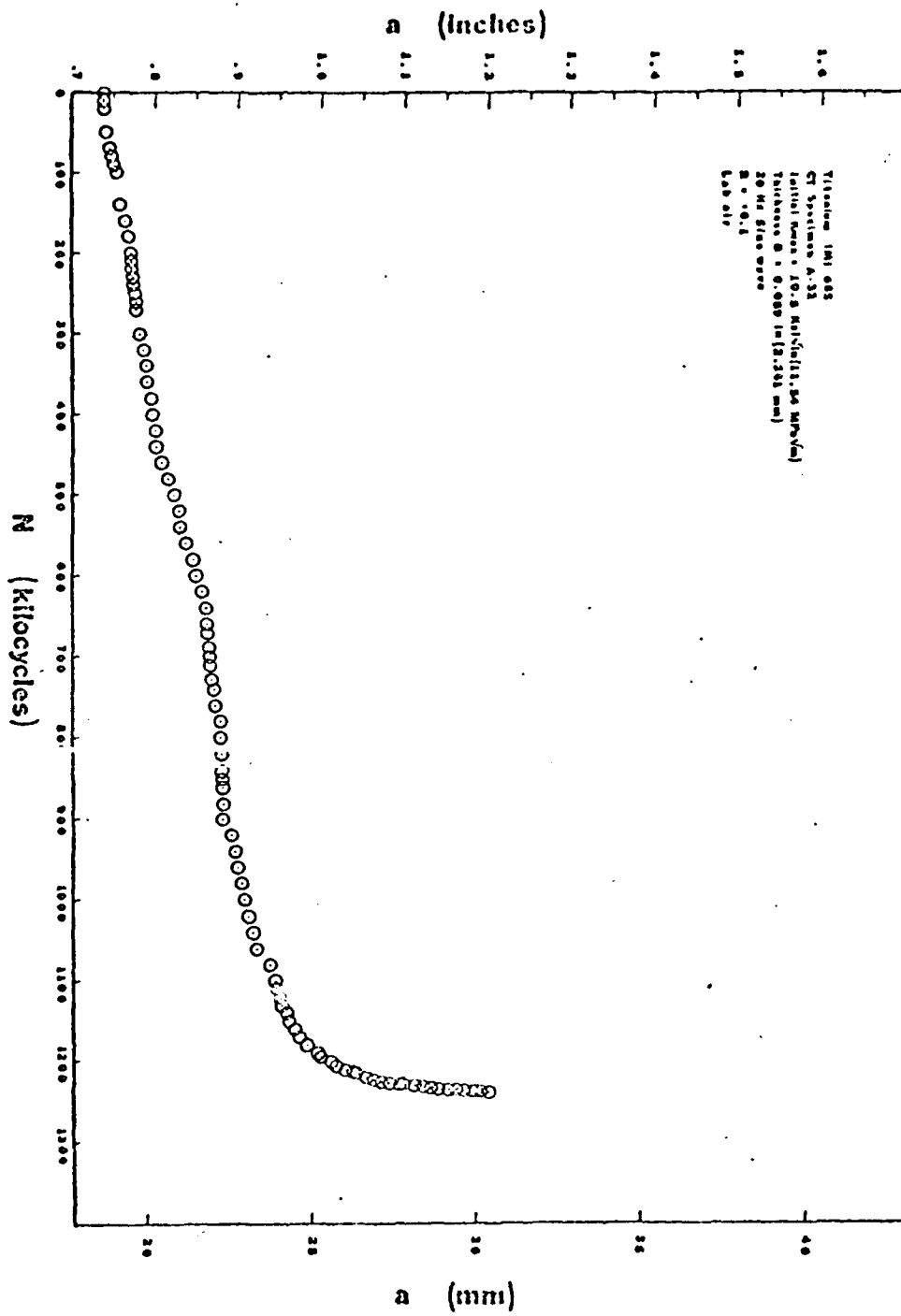


Fig.7a Plots of a versus N; Specimen A-32

1.0  
 Titanium IMI 685  
 CT Specimen A-32  
 Initial  $K_{max}$  - 10.5 ksi $\sqrt{in}$  (11.54 MPa $\sqrt{m}$ )  
 Thickness B - 0.089 in (2.261 mm)  
 20 Hz Sine Wave  
 R = 0.1  
 Lab Air

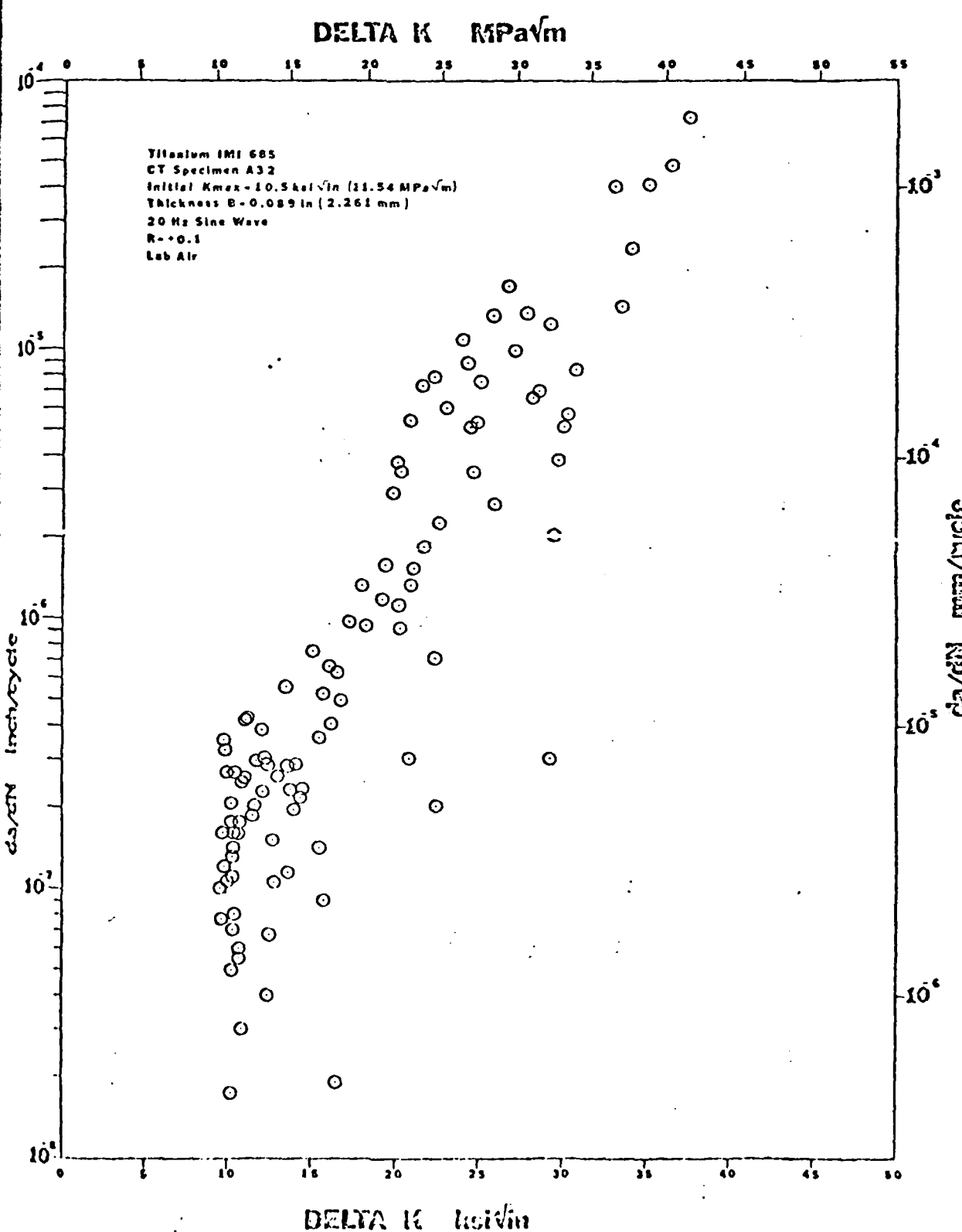


Fig. 2b Plots of da/dN versus  $\Delta K$  (Specimen A-32)

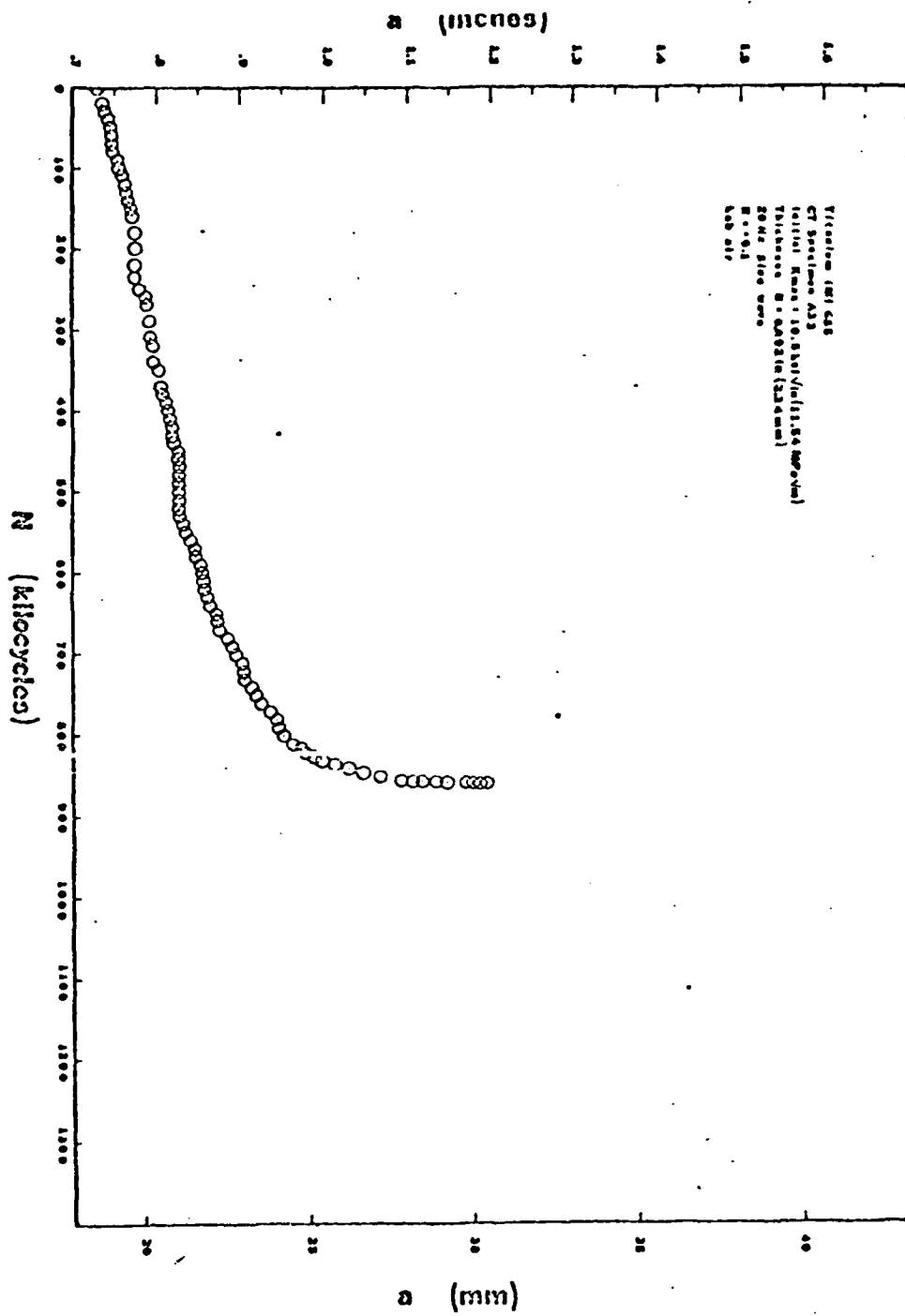


Fig. 8a Plots of a versus N; Specimen a-33

Titanium IMI 685  
 CT Specimen A33  
 Initial Kmax = 10.5 ksi√in (11.54 MPa√m)  
 Thickness B = 0.092 in (2.34 mm)  
 20 Hz Sine Wave  
 R = 0.1  
 Lab Air

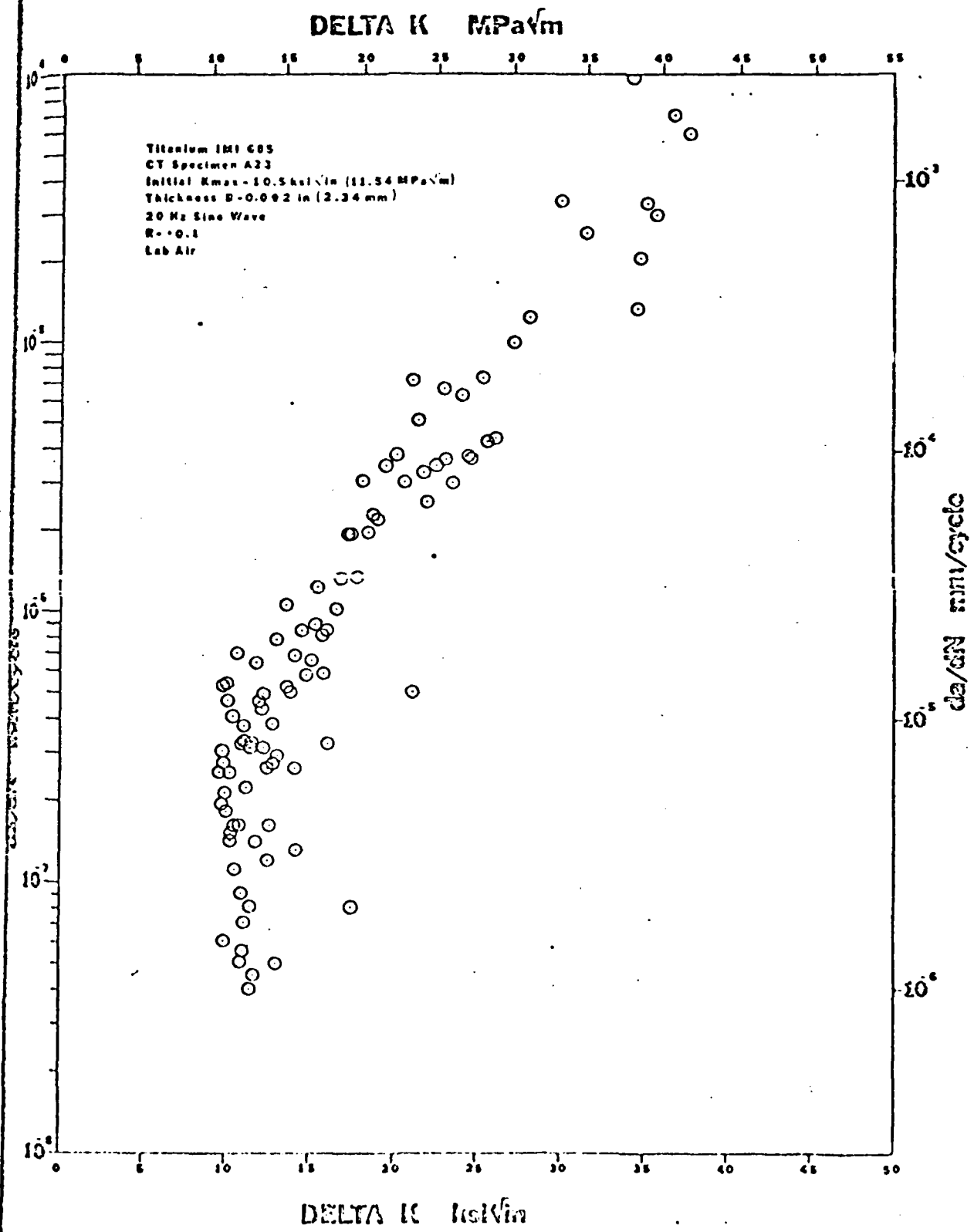


Fig. 8b Plots of da/dN versus ΔK; Specimen A-33

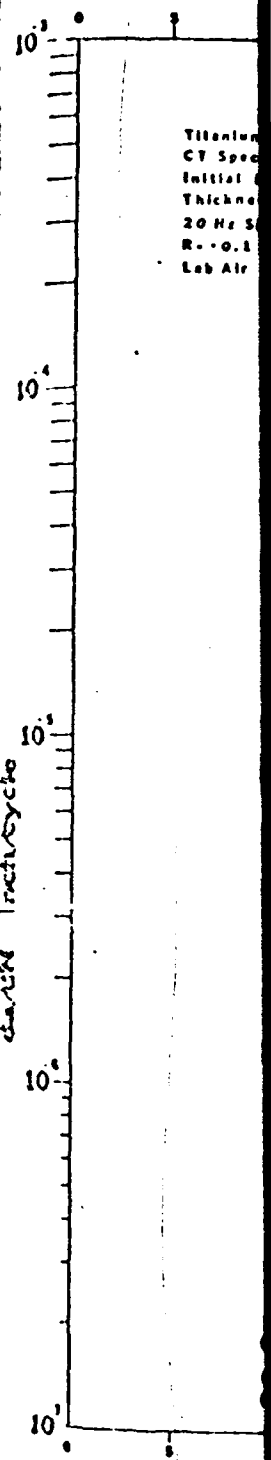
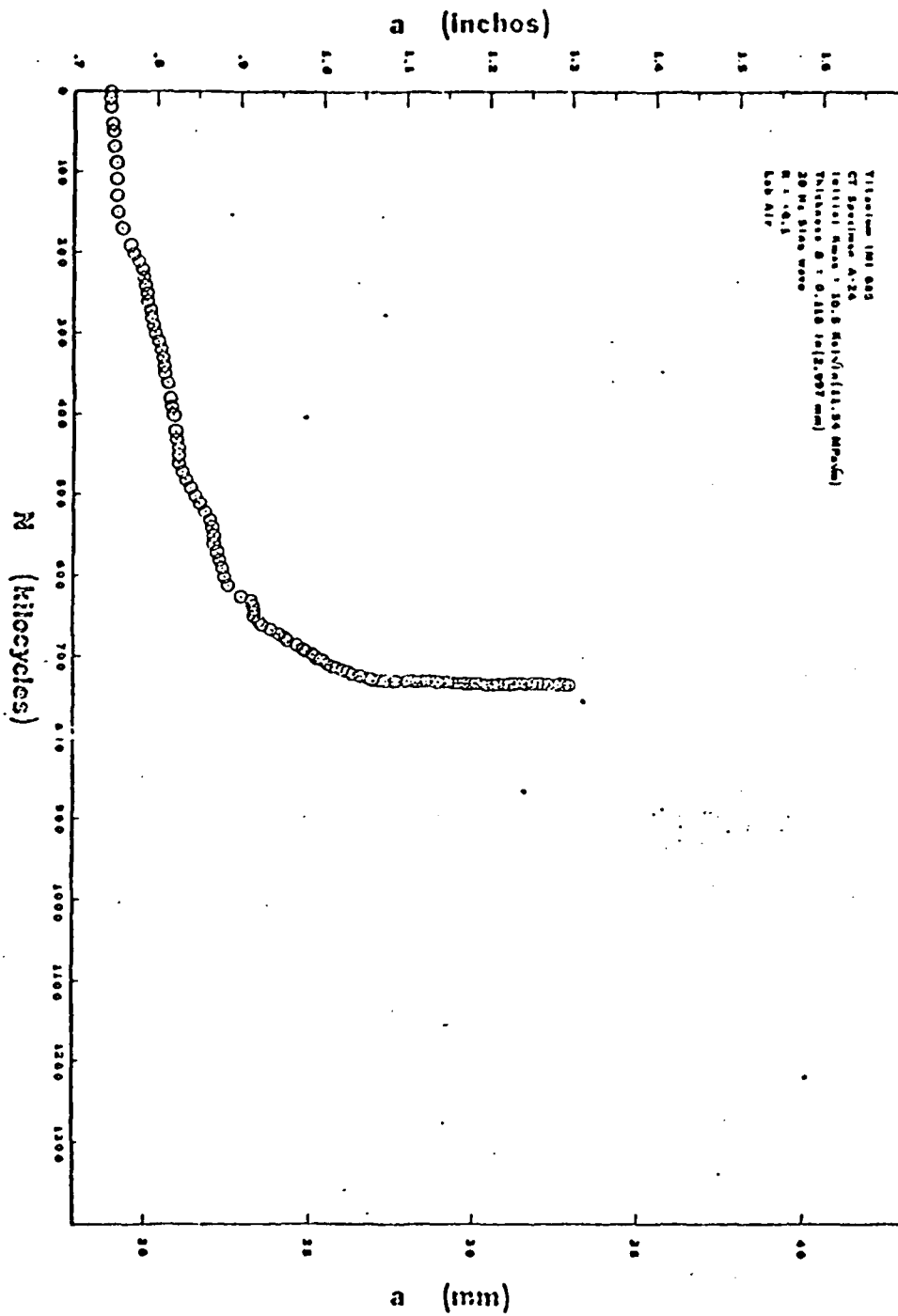


Fig. 9a Plots of a versus N; Specimen A-24

1.5  
 1.0  
 Titanium IMI 685  
 CT Specimen A24  
 Initial Kmax = 10.5 ksi√in (11.54 MPa√m)  
 Thickness B = 0.118 in (2.997 mm)  
 20 Hz Sine Wave  
 R = +0.1  
 Lab Air

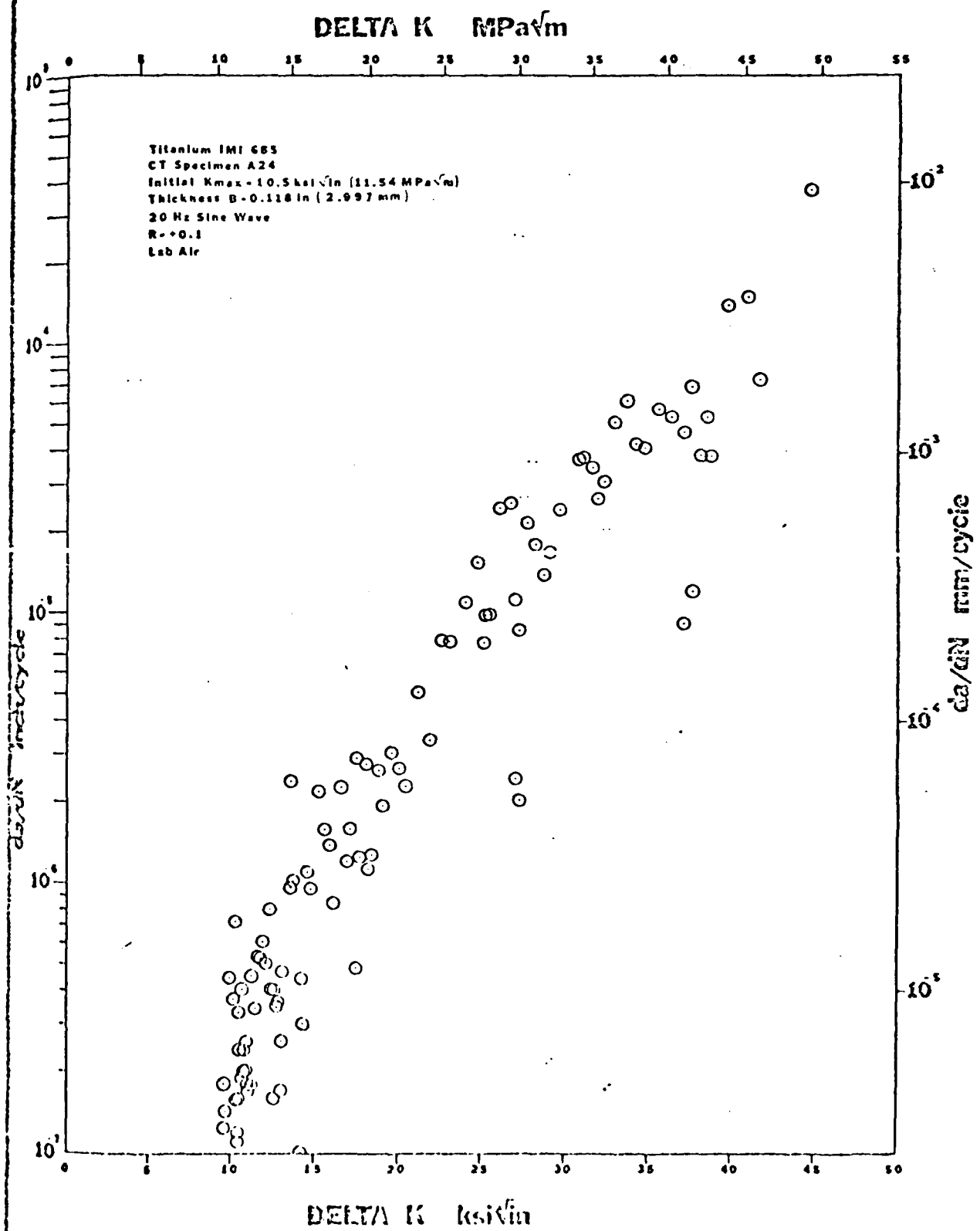


Fig. 9b Plots of da/dN versus  $\Delta k$ ; Specimen A-24

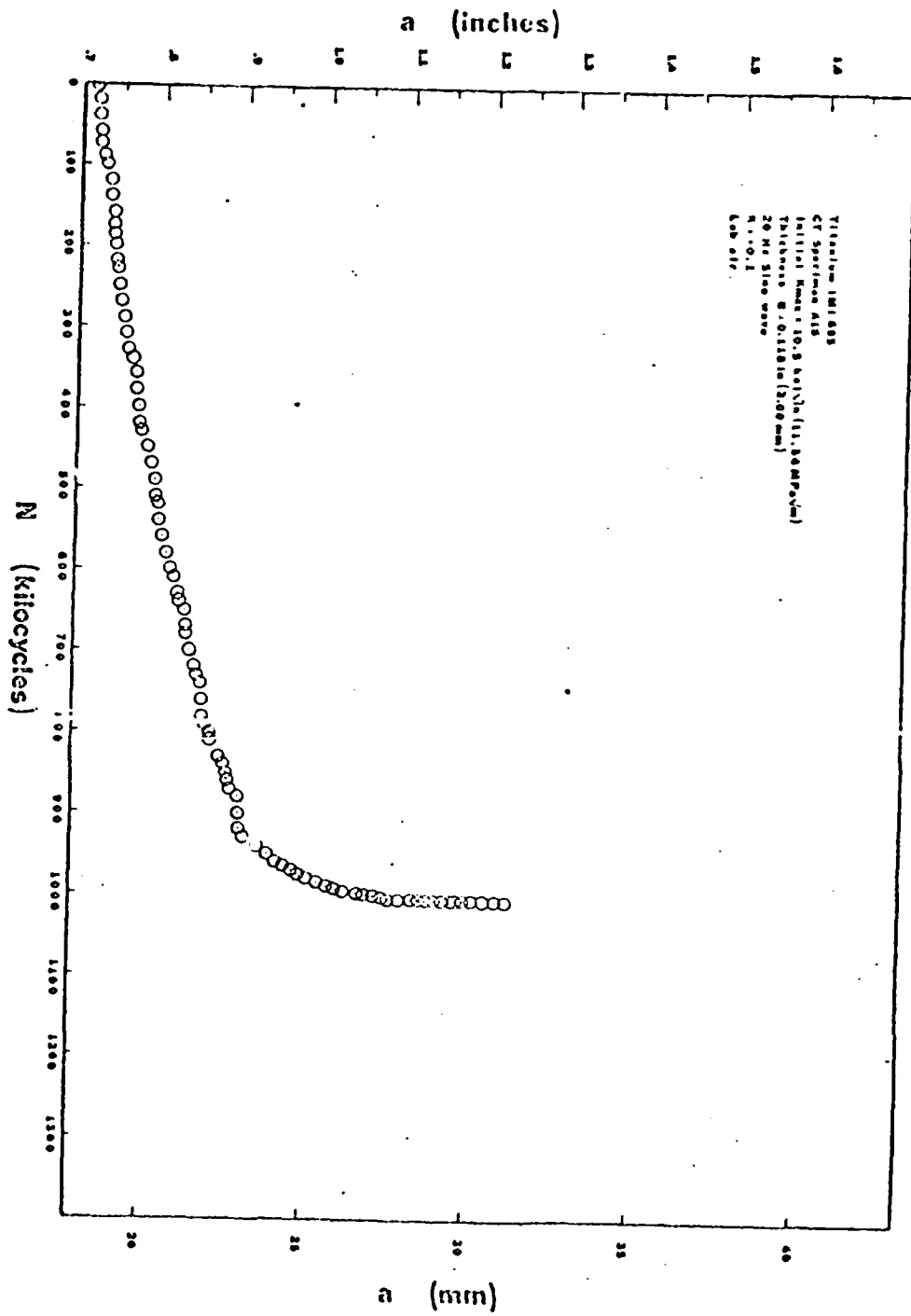
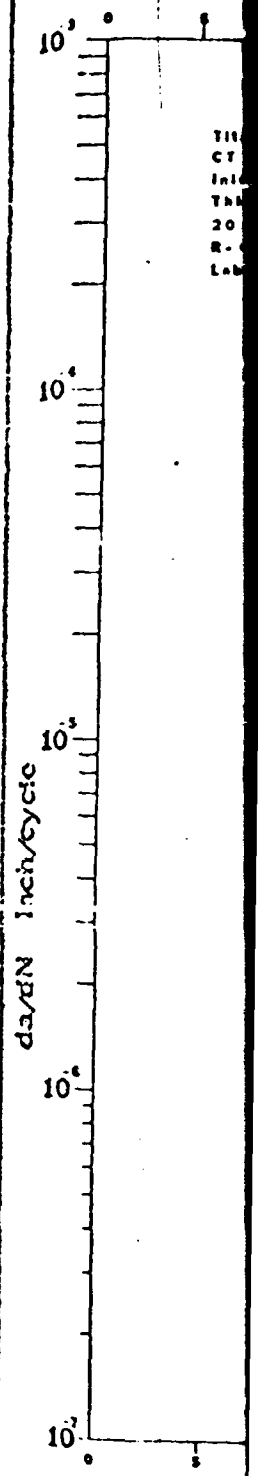
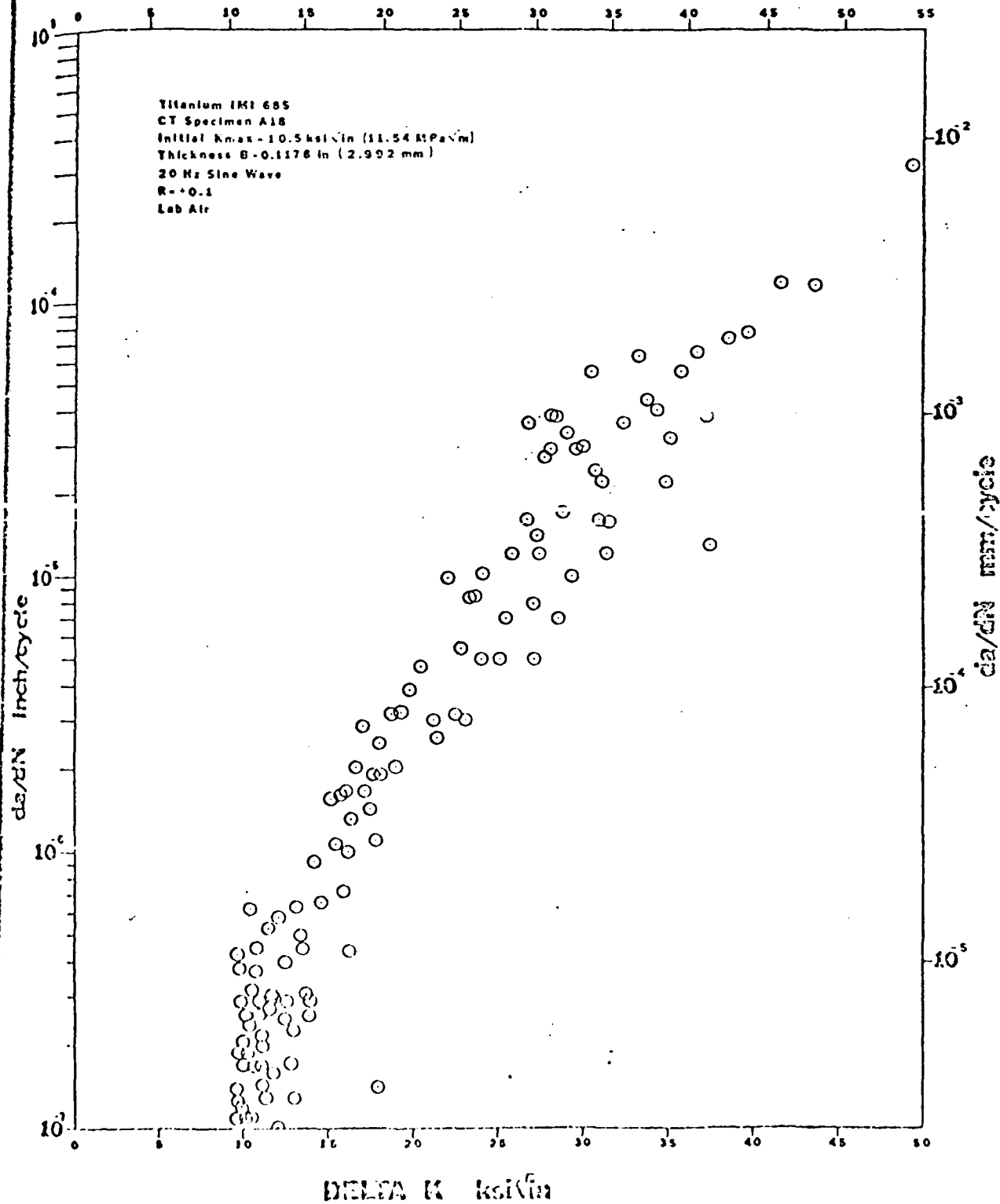


Fig. 10a Plots of a versus N; Specimen A-18

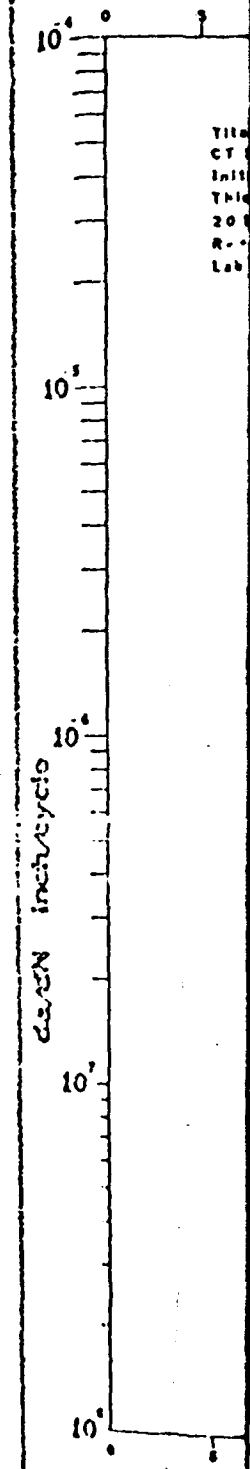
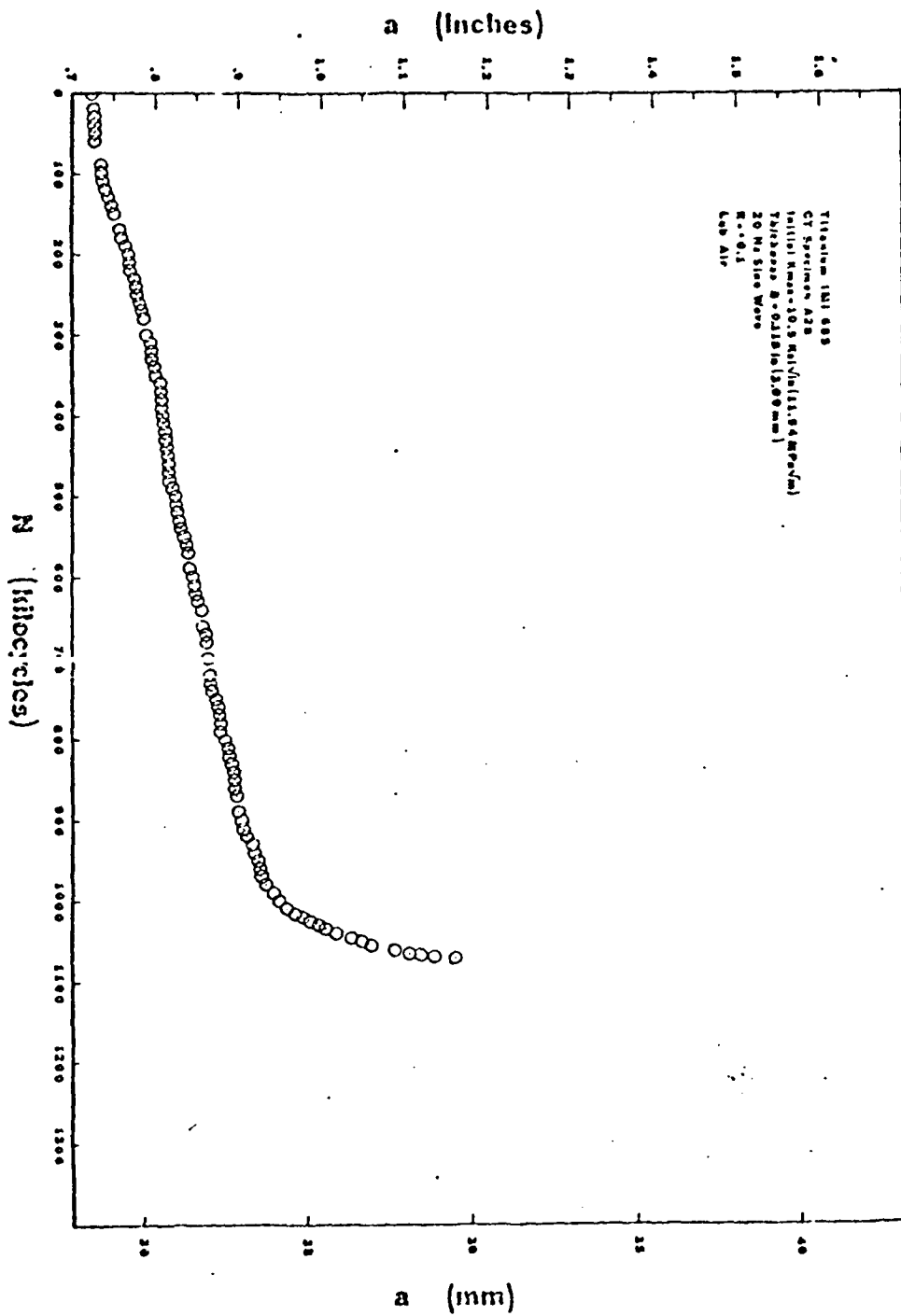


DELTA K MPa√m



Titanium IMI 685  
 CT Specimen A18  
 Initial Kmax = 10.5 ksi√in (11.54 MPa√m)  
 Thickness B = 0.1178 in (2.992 mm)  
 20 Hz Sine Wave  
 R = -0.1  
 Lab Air

Fig. 10b. Plots of da/dN versus ΔK; Specimen A-18



Title  
 CT  
 Initial  
 Thickness  
 20 Hz  
 R =  
 Lab

Fig. 11a Plots of a versus N ; Specimen A28

Titanium IMI 685  
 CT Specimen A28  
 Initial Kmax = 10.5 ksi√in (11.54 MPa√m)  
 Thickness B = 0.1183 in (3.01mm)

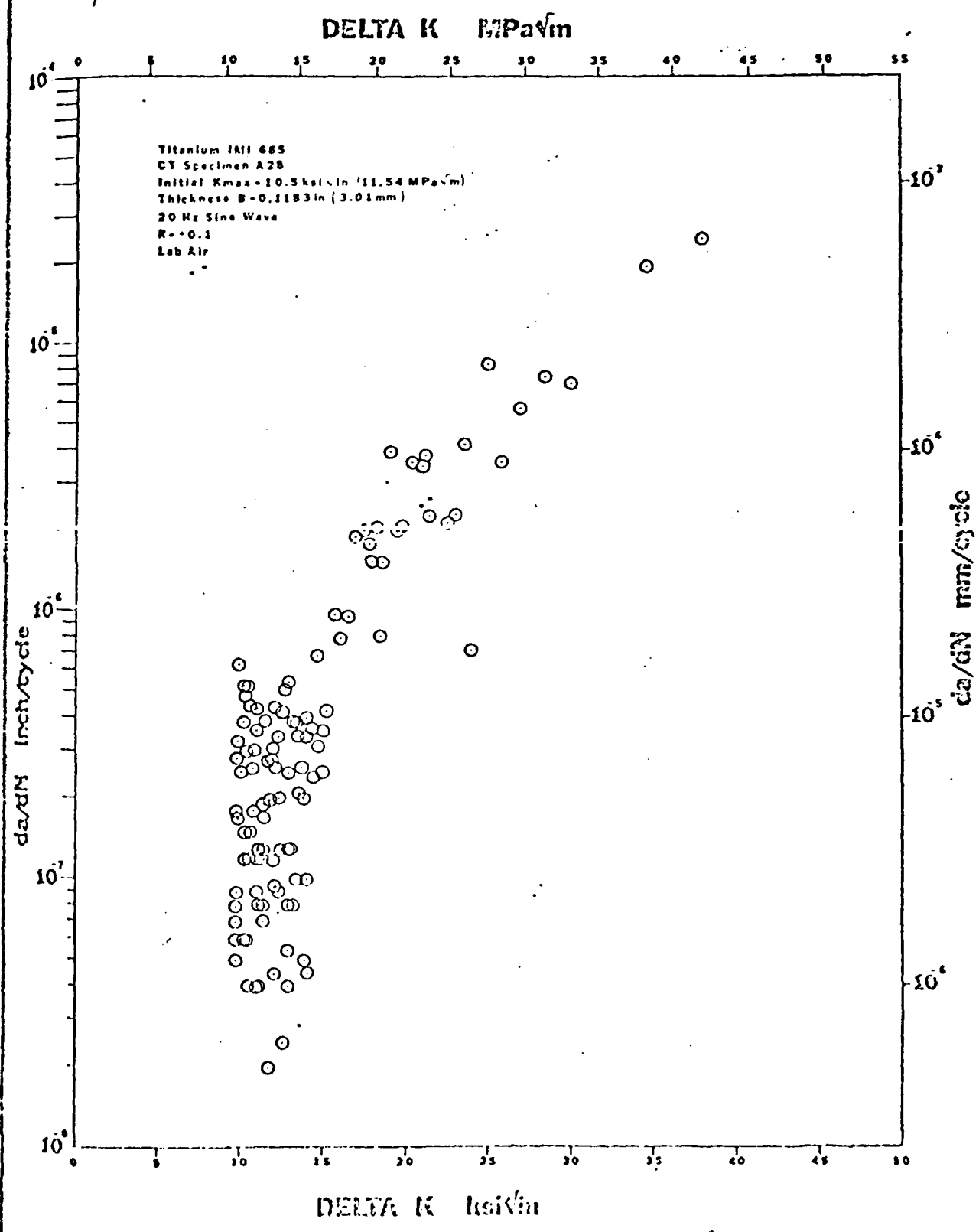


Fig. 11b Plot of da/dN versus Δk; Specimen A28

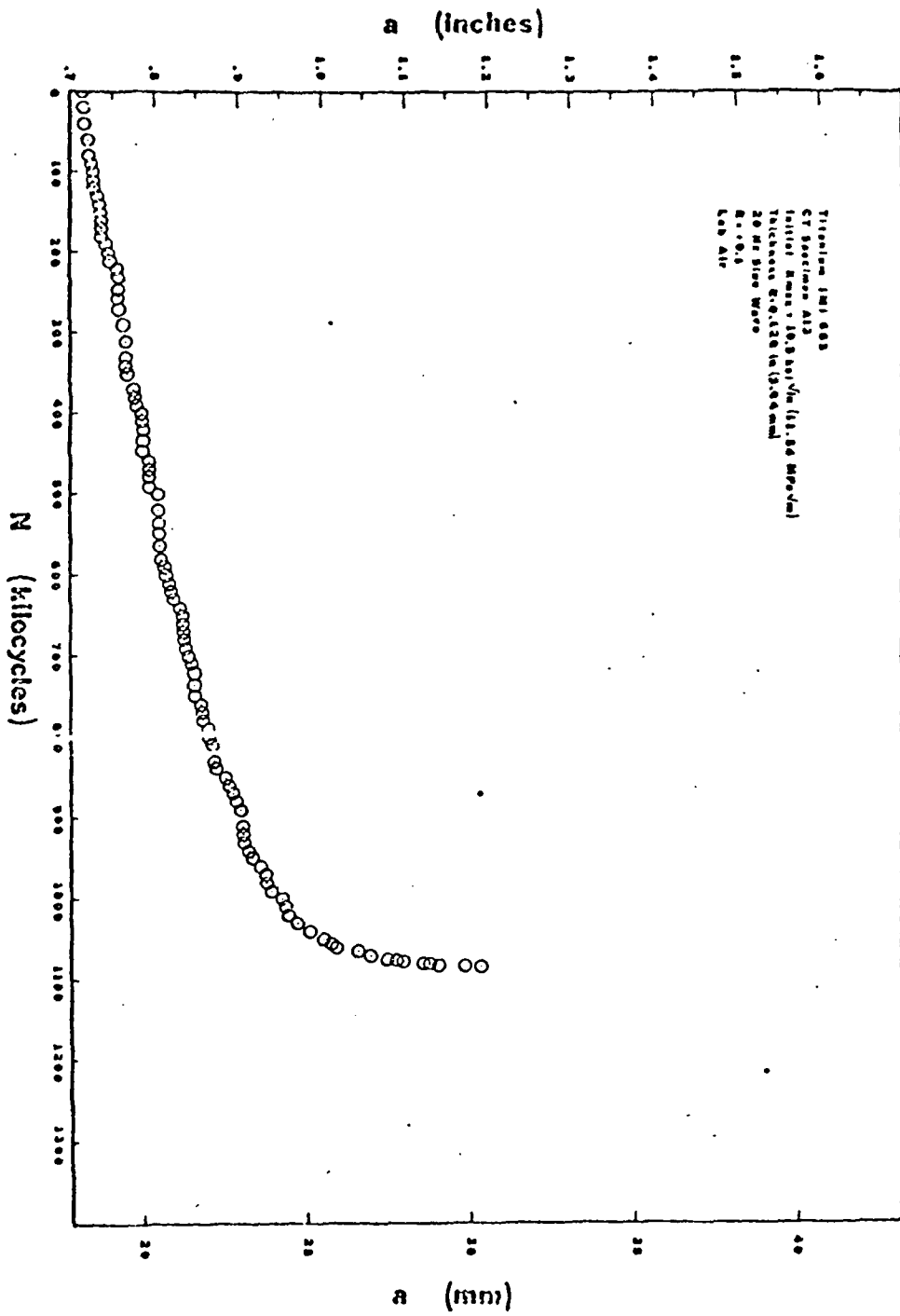


Fig. 12a Plots of a versus N; Specimen A-13

1.8  
 1.0  
 Titanium IM1 685  
 CT Specimen A13  
 Initial K<sub>max</sub> = 10.5 ksi√in (11.54 MPa√m)  
 Thickness B = 0.120 in (3.04 mm)  
 20 Hz Sine Wave  
 R = -0.1  
 Lab Air  
 A-13

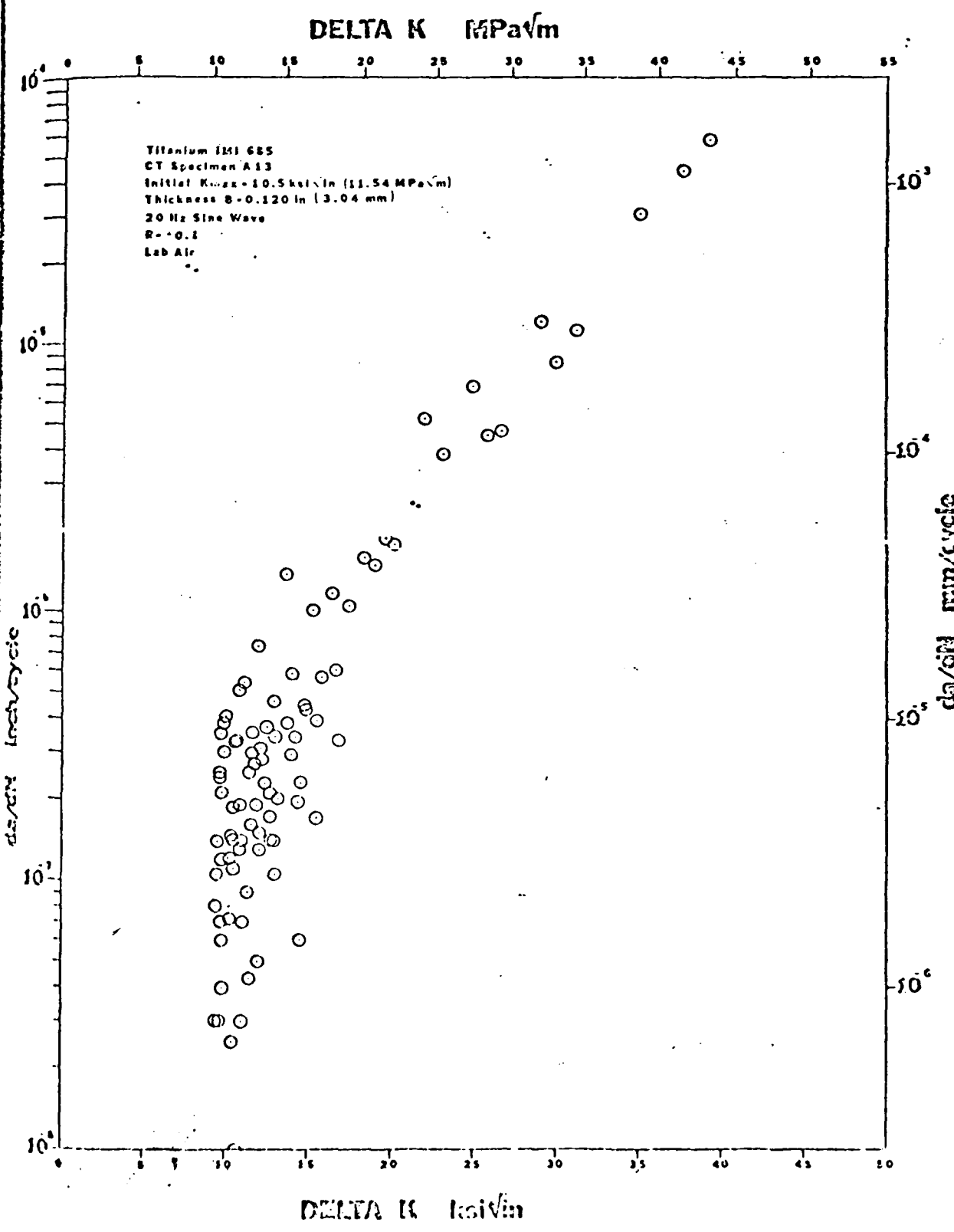


Fig. 12b Plots of  $da/dN$  versus  $\Delta K$ ; Specimen A-13

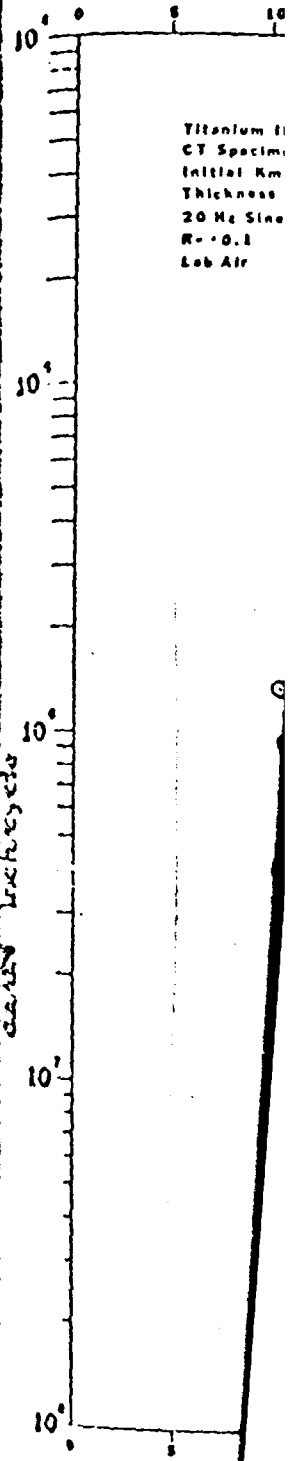
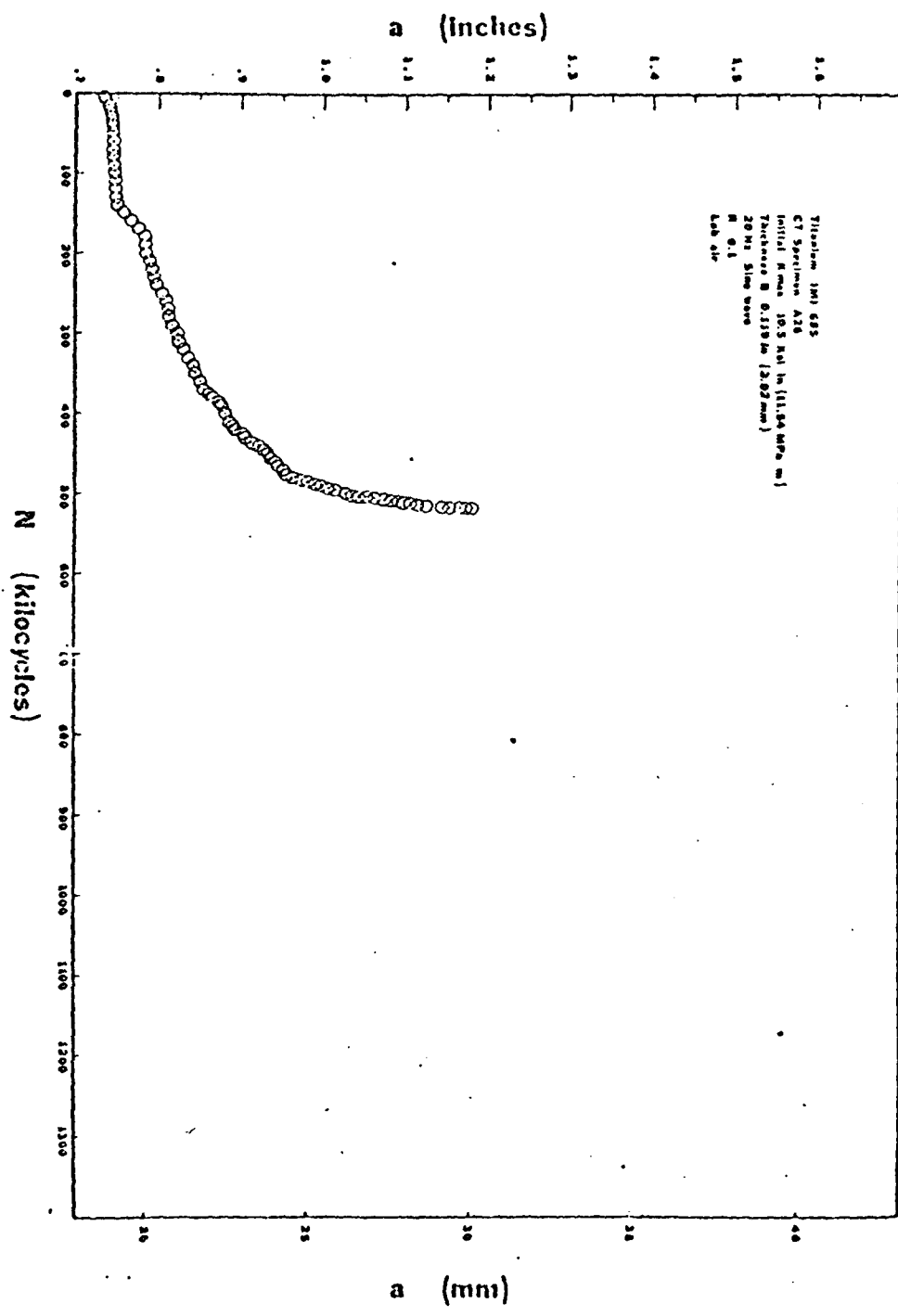


Fig. 13a Plots of a versus N; Specimen A-26

Titanium IMI 685  
 CT Specimen A26  
 Initial Kmax - 10.5 ksi/in (11.54 MPa√m)  
 Thickness B - 0.119 in (3.028 mm)  
 20 Hz Sine Wave

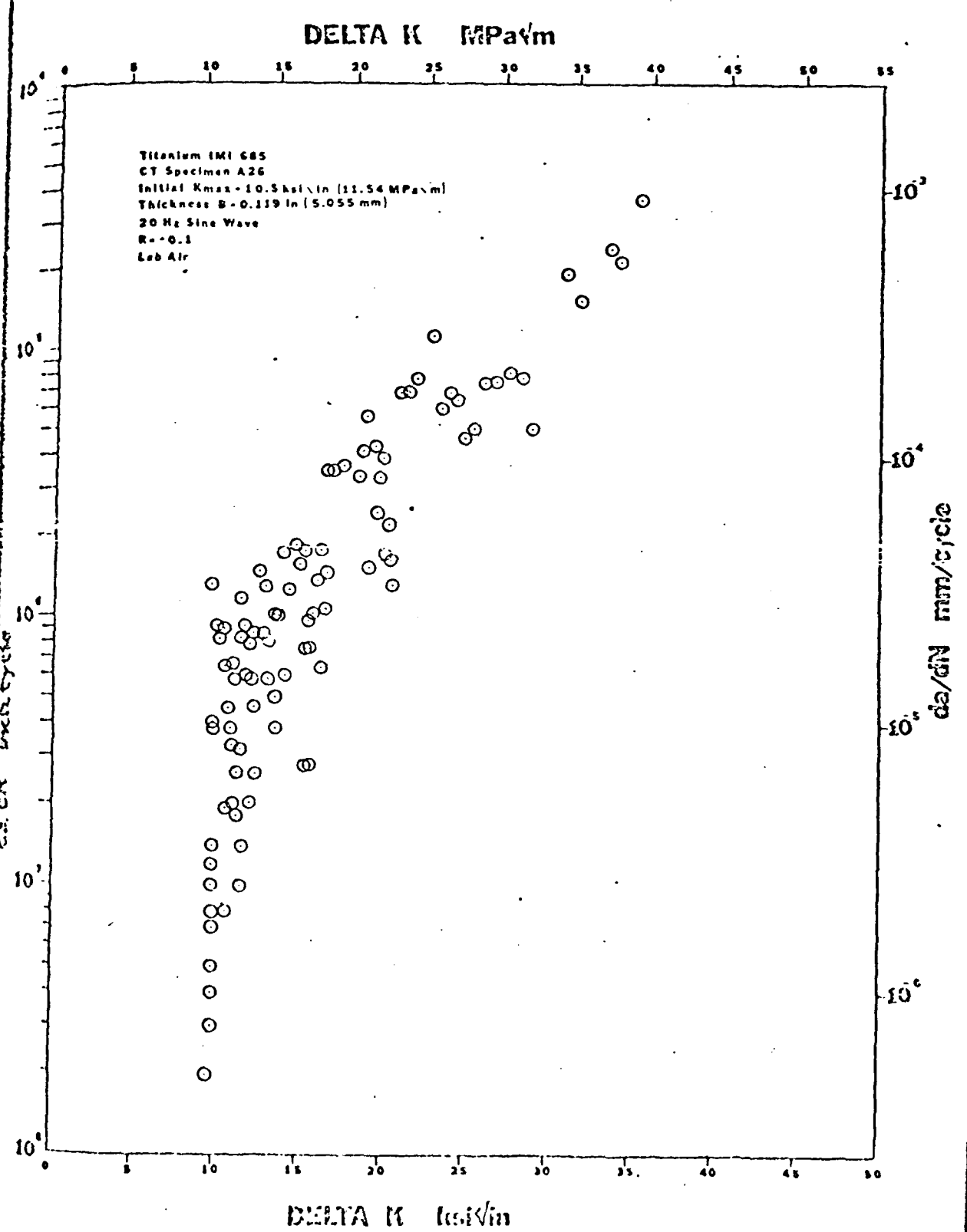
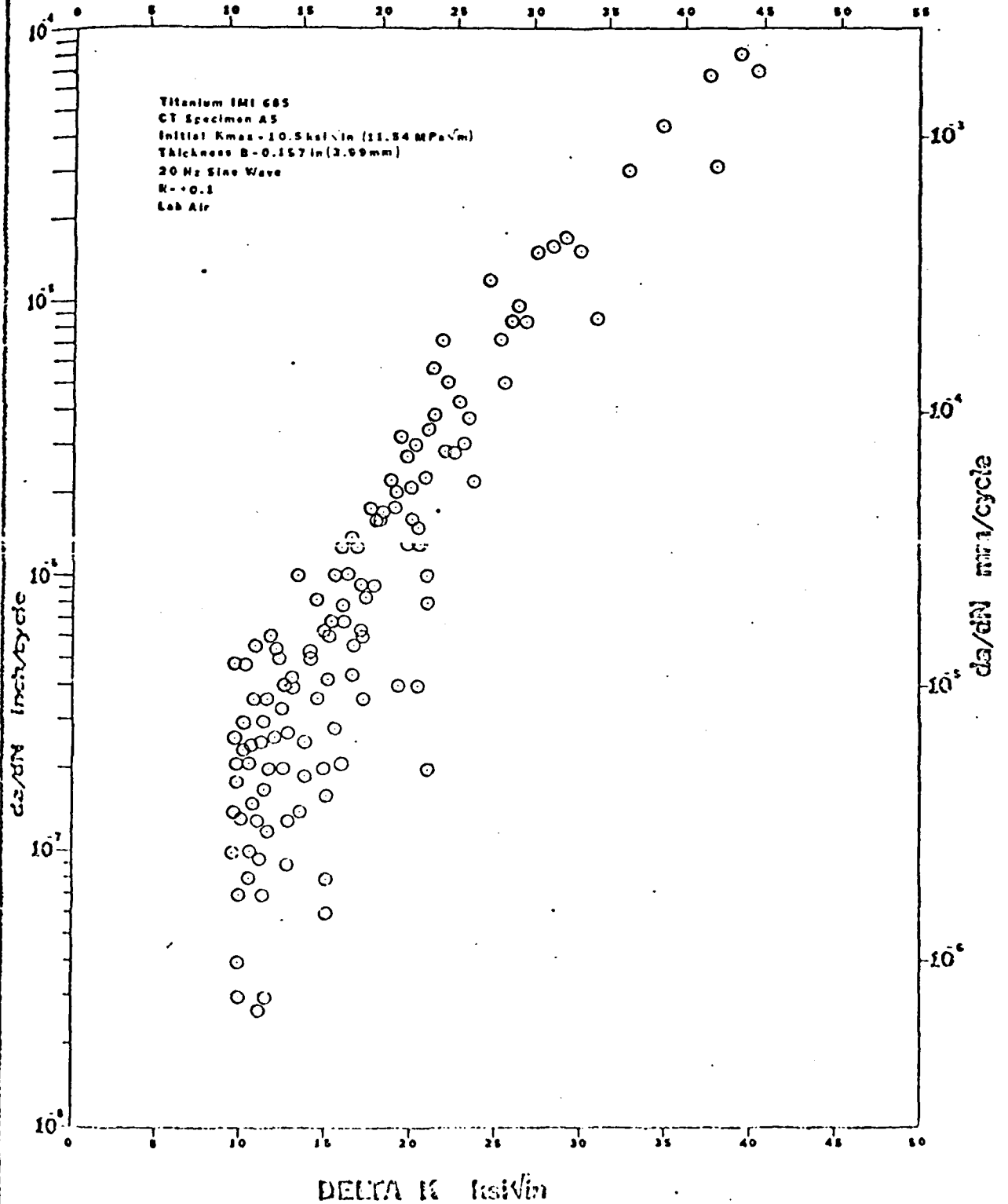


Fig. 13b Plot of da/dN versus Δk: Specimen A-26



DELTA K MPa√m



Titanium IMI 685  
 CT Specimen A5  
 Initial Kmax = 10.5 ksi√in (11.54 MPa√m)

Fig. 14b Plots of da/dN versus ΔK; Specimen A-5

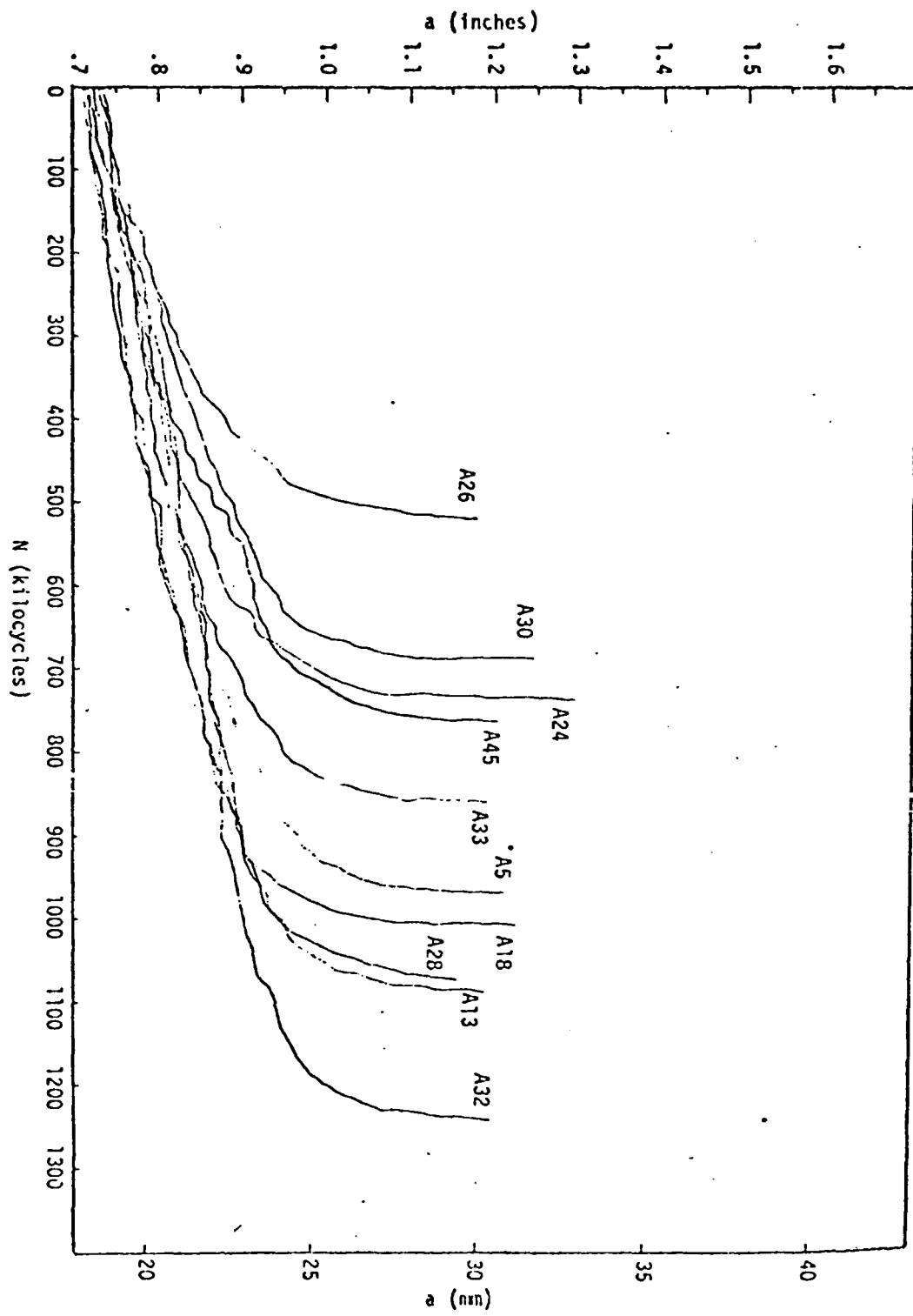


Figure 15. Composite plot of a-N results for all specimens.

F. H. Froes\*  
J. P. Hirth\*

The mechanical line for aero efficiency ad applications ness and adequ titanium alloy goals using the properties she of the importa ties, specific ade to define ture. With th the metastable phase particle ratio of prima range of micro dependence on it controls yi

\*Colt Industri  
Carnegie Mello  
European Offic  
The Ohio State

Titanium and ti of the weight s of the weight s number of heat strength-to-wei however, have n first, the com alloy, the w ortion size in strength-critic deep hardening of the heat tre all flaws need techniques can

## THE EFFECT OF TEMPERATURE AND $R$ RATIO ON FATIGUE CRACK GROWTH IN A612 GRADE B STEEL

CHEUNG POON

University of Missouri, College of Engineering, Columbia, MO 65201, U.S.A.

and

DAVID W. HOEPPNER

University of Toronto, Department of Mechanical Engineering, Toronto, Ontario, Canada M5S 1A4

**Abstract**—Fatigue-crack propagation rates in ASTM A612 Grade B steel were investigated at room temperature and  $-100^{\circ}\text{F}$  ( $-73^{\circ}\text{C}$ ) with  $R$  ratio =  $-0.1$  and  $+0.67$ . The data were evaluated in terms of the crack propagation rates ( $da/dN$ ) as a function of the alternating stress intensity ( $\Delta K$ ), according to  $da/dN = c + (r - c)(- \ln(1 - \Delta K/K_0))^{1/m}$ . It was found that crack growth rates were increased due to increasing  $R$  ratio. Also the dependence of crack growth rates on  $R$  ratio is strongest at the lowest crack growth rates where a  $\Delta K$  fatigue threshold is established. Crack growth rates were decreased due to decreasing test temperature in the slow crack growth region. However, it was found that crack growth rates were increased due to decreasing test temperature in the fast crack growth region near the upper instability asymptote. Decreased test temperature and increased  $R$  ratio interact synergistically to increase crack growth rates for the entire range of  $\Delta K$ .

### INTRODUCTION

MOST ENGINEERING structures, when subjected to alternating types of loading, will fail by fatigue which is a progressive process involving initiation, propagation and instability of a fatigue crack. Fatigue-crack growth has been known to be affected by many external and internal variables, but test temperature and  $R$  ratio are among the most important external variables. Fracture toughness of most ferritic and martensitic steels decreases markedly with decreasing test or operating temperature. Clark and Trout, in their studies on the effect of test temperature in the range from  $70^{\circ}\text{F}$  ( $21^{\circ}\text{C}$ ) to  $-100^{\circ}\text{F}$  ( $-73^{\circ}\text{C}$ ) on fatigue-crack growth rates in a forging grade Ni-Nb-V steel, found that the crack growth rate for a given alternating stress intensity decreased as the test temperature decreased[1]. Andreassen and Vitovec investigated the effects of temperature on fatigue crack propagation in an A.P.I. 5L Grade B steel in the range from  $+70^{\circ}\text{C}$  to  $-60^{\circ}\text{C}$  and concluded that fatigue-crack propagation rate at a fixed stress intensity has a maximum at room temperature[2]. Rolfe and Munse found for mild steel that as the test temperature decreased from  $70^{\circ}\text{F}$  ( $21^{\circ}\text{C}$ ) to  $-40^{\circ}\text{F}$  ( $-40^{\circ}\text{C}$ ), the fatigue-crack growth rate decreased[3].

The effects of  $R$  ratio on fatigue-crack growth has been studied by many investigators in many different materials[4-7]. Generally,  $R$  ratio is found to influence fatigue-crack growth rates, with increased  $R$  ratio was most influential at the lowest crack growth rates where a  $\Delta K$  fatigue threshold is established.

The Paris relation  $da/dN = D(\Delta K)^m$  has limited usage in fitting a curve to the entire range of fatigue-crack growth rate data. There is no term in this simple relation to account for the  $R$  ratio effects, the temperature effects and the combined effects. Because these external parameters can modify the response of the material to the cyclic loads the empirical parameters from any fitting function must be such that they reflect these effects. There are other potential fitting functions that more accurately reflect changes in external parameters. The Paris relation has been modified by many investigators[8-11] but none of these proposed models can account for the combined effects satisfactorily. Bowie and Hoepfner proposed a relation based on the Four Parameter Weibull Survivorship Function to fit a median curve to crack growth rate data[12]. Many investigators have used this relation and concluded that it accurately fits  $da/dN$  vs  $\Delta K$  over the entire[13-16]. The four parameters of the curve fitting relation, which can be determined analytically, account for the effects of test variables on fatigue-crack growth rates.

## EXPERIMENTAL PROCEDURE

The material used in this investigation was ASTM A612 Grade B steel. The chemical composition and mechanical properties are listed in Table I.

Four Wedge-Open Loading (WOL) specimens were machined according to the dimensions shown in Fig. 1. The surface of the specimen was polished by 400 Grit Silicon Carbide paper. The direction of polishing was perpendicular to the direction of crack growth. The specimen was mounted in a servo-controlled electrohydraulic fatigue machine and was subjected to a sinusoidal cyclic load for precracking. During precracking, the total crack growth was approximately 0.1 in. (0.254 cm). The final 0.025 in. (0.063 cm) of the crack growth was accomplished by a reduced load such that the alternating stress intensity at the end of precracking did not exceed that at the beginning of the fatigue crack growth test which was performed immediately after precracking.

Fatigue-crack growth tests were performed at room temperature (about 70°F/21°C) and at -100°C (-73°C) with an *R* ratio (ratio of minimum load to maximum load) equal to +0.1 and +0.67. A sinusoidal loading waveform at a frequency of 10 Hz was used for the tests. The specimen was cycled to failure. The crack length was measured periodically during the test at a predetermined number of load cycles by a forty-power (40×) travelling microscope.

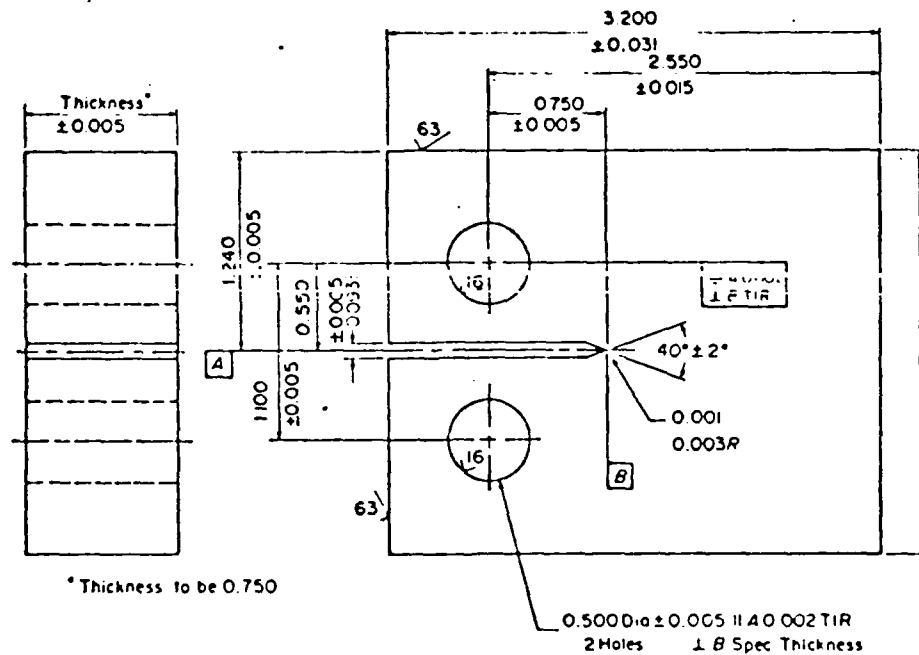


Fig. 1. Dimensioned wedge-open loading specimen used in fatigue-crack growth testing.

Table I. Chemical composition and material properties of the test material

Element	Weight Percent
Carbon	0.25
Manganese	1.29
Phosphorus	.013
Sulfur	.027
Silicon	.30
Copper	.27
Nickel	.21
Chromium	.20
Molybdenum	.060

## Material Properties.

Yield Stress	65000 psi (474.411 N/mm <sup>2</sup> )
Ultimate Tensile Strength	95000 psi (690.411 N/mm <sup>2</sup> )
Elongation	12%

## The effect of temperature and R ratio on fatigue crack growth in A612 grade B steel

A stainless steel cooling tank with a transparent viewing side was constructed for low temperature testing. A mixture of freon and dry ice was used as a cooling medium in which the specimen was submerged. The test temperature was monitored by a thermocouple located close to the crack tip of the specimen.

## PRESENTATION AND DISCUSSION OF TEST RESULTS

The raw data obtained in this investigation consisted of pairs of crack length,  $a$ , vs the number of load cycles,  $N$ . The pairs of  $a-N$  values were further reduced to crack growth rate,  $da/dN$ , vs alternating stress intensity,  $\Delta K$ , values. The raw data and the reduced data were shown in the appendix. The methods of the calculations were given in Ref.[17].

Pairs of  $da/dN$  vs  $\Delta K$  values were plotted on a log-linear basis as shown in Figs.2-5. A curve fitting relation based on the Four Parameter Weibull Survivorship Function was used to fit a median curve to the data. This curve fitting relation is given in eqn(1), below:

$$da/dN = e + (v - e) (-\ln(1 - \Delta K/K_b))^{1/k} \quad (1)$$

where  $k$ ,  $e$  and  $v$  are parameters related to the intrinsic material parameters and the extrinsic test parameters.  $K_b$  is the alternating stress intensity which has the following characteristic:

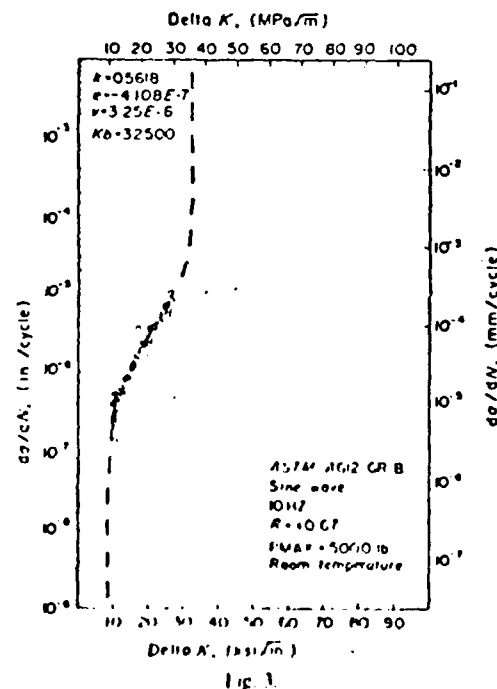
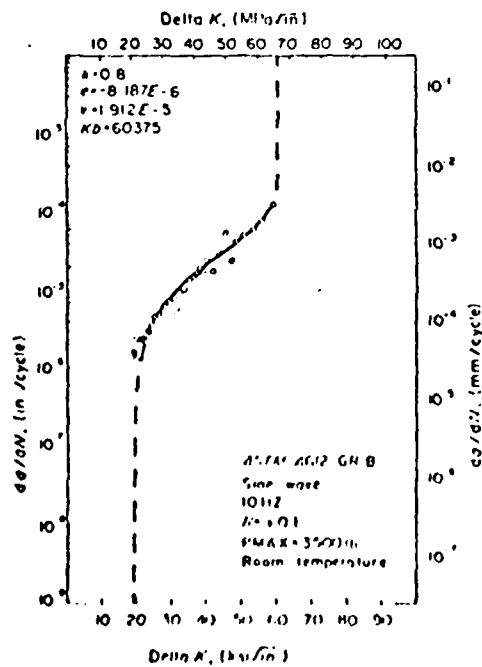
$$\lim_{(\Delta K \rightarrow K_b)} (da/dN) \rightarrow \text{infinity} \quad (2)$$

These four parameters were computed using regression techniques. The results were shown in Table 2. A comparison of the curve fitting relation used in this investigation with other relations can be found in Ref.[13]. A discussion of the theory of the analytical procedure is given in Refs.[13-15].

Rearranging eqn(1),  $\Delta K$  can be solved for in terms of  $da/dN$ :

$$\Delta K = K_b (1 - \exp(-(da/dN - e)/(v - e)))^k \quad (3)$$

The lower asymptotic condition of the  $da/dN$  vs  $\Delta K$  curve can be solved for by substituting



Figs. 2 and 3. Log linear graph of  $da/dN$  vs  $\Delta K$  fitted with a Weibull curve.

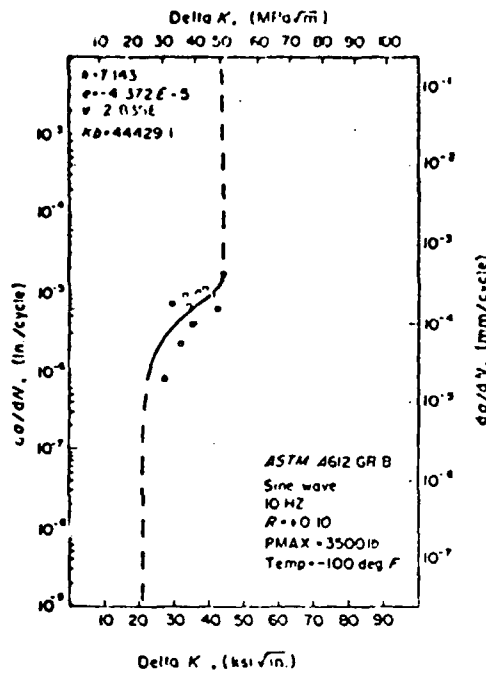


Fig. 4.

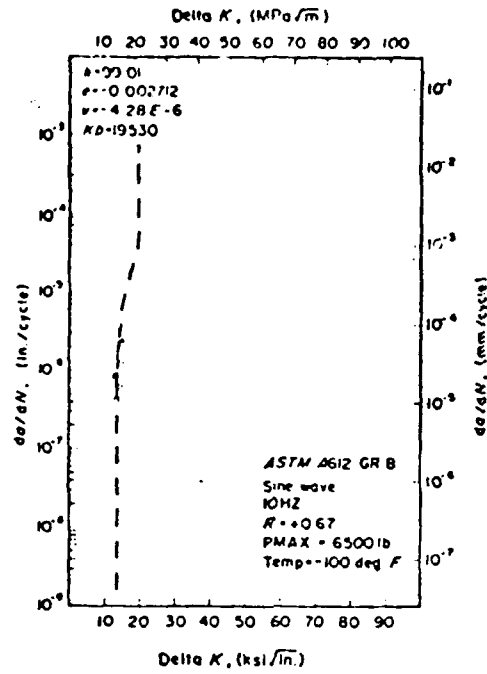


Fig. 5.

Figs. 4 and 5. Log-linear graph of  $da/dN$  vs  $\Delta K$  fitted with a Weibull curve.

Table 2. Results of the calculations for the values of the four Weibull parameters and the lower threshold

Seriation number and description of test conditions	Upper instability parameter, $K_u$ $\text{ksi}\sqrt{\text{in.}}$ ( $\text{MPa}\sqrt{\text{m}}$ )	Shape parameter $k$	Threshold parameter, $c$ in/cycle ( $\text{mm}/\text{cycle}$ )	Characteristic value, $v$ in/cycle ( $\text{mm}/\text{cycle}$ )	Lower threshold, $K_{th}$ $\text{ksi}\sqrt{\text{in.}}$ ( $\text{MPa}\sqrt{\text{m}}$ )
HP-1 R=+.10 Room Temperature	60.37 (65.33)	0.80	$-8.19 \times 10^{-6}$ ( $-2.07 \times 10^{-4}$ )	$1.91 \times 10^{-5}$ ( $4.85 \times 10^{-4}$ )	19.15 (21.04)
HP-2 R=+.67 Room Temperature	32.5 (35.71)	0.56	$-4.11 \times 10^{-7}$ ( $-1.04 \times 10^{-5}$ )	$3.25 \times 10^{-6}$ ( $8.25 \times 10^{-5}$ )	8.24 (9.05)
HP-3 R=+.10 -103°F (-73°C)	44.43 (48.81)	7.14	$-4.37 \times 10^{-5}$ ( $-1.11 \times 10^{-3}$ )	$2.83 \times 10^{-6}$ ( $7.2 \times 10^{-5}$ )	20.96 (23.03)
HP-4 R=+.67 -105°F (-73°C)	19.53 (21.46)	99.01	$-2.71 \times 10^{-3}$ ( $-6.89 \times 10^{-2}$ )	$-4.28 \times 10^{-6}$ ( $-1.09 \times 10^{-4}$ )	12.37 (14.71)

$da/dN = 0$  into eqn(3). Let  $K_{th} = \Delta K$  when  $da/dN = 0$ , eqn(3) can be written as:

$$k_{th} = K_u (1 - \exp(-(-c)/(v - c)))^k \quad (4)$$

The values of the lower threshold  $K_{th}$  were calculated by using eqn(4) and were shown in Table 2. A composite plot of  $da/dN$  vs  $\Delta K$  values and median curves for comparison of temperature and R ratio effects is given in Fig. 6.

By increasing the values of the variable R ratio from +0.1 to +0.67, the following effects were observed under both temperature conditions. The crack growth rate curve was shifted to the left; the upper instability parameter,  $K_u$ , and the lower threshold parameter,  $K_{th}$ , were both reduced to lower  $\Delta K$  values; the size of the interval of  $\Delta K$  between the upper and the lower asymptotes was compressed; and the slope of the median curve between the two asymptotes

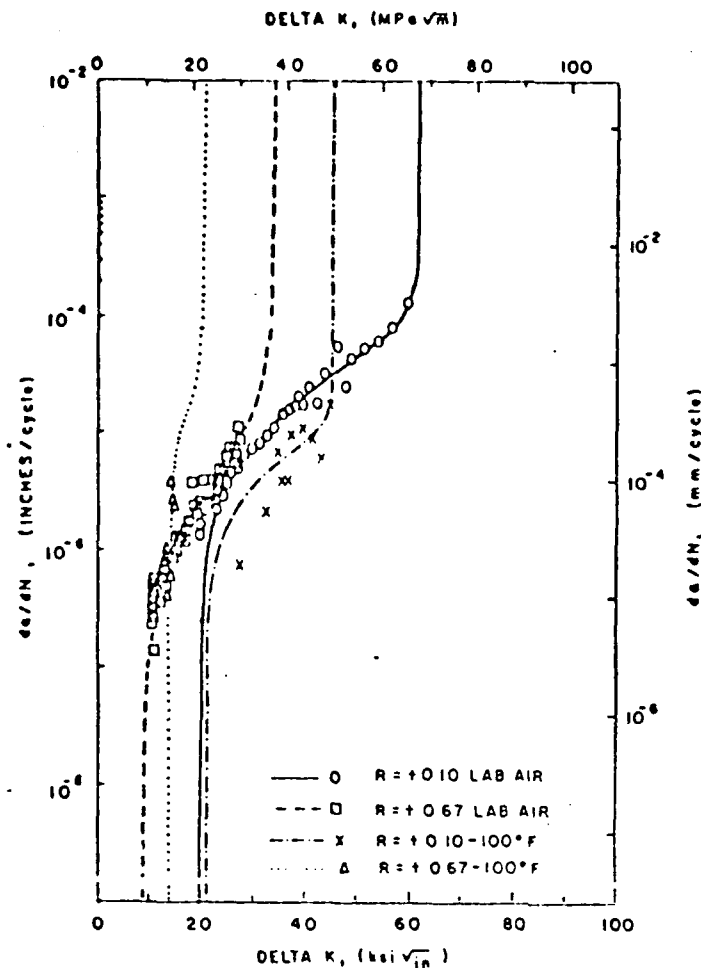


Fig. 6. Composite log-linear plot of  $da/dN$  vs  $\Delta K$  used to compare temperature and  $R$  ratio.

was increased. Thus, at higher  $R$  ratio, fatigue crack can be initiated from a smaller critical flaw dimension. These results were in agreement with those of other investigators.

At  $R = +0.1$ , decreasing the test temperature from room temperature to  $-100^\circ\text{F}$  ( $-73^\circ\text{C}$ ) reduced the value of  $K_{th}$  from  $60.37 \text{ ksi}\sqrt{\text{in}}$  ( $66.33 \text{ MPa}\sqrt{\text{m}}$ ) to  $44.43 \text{ ksi}\sqrt{\text{in}}$  ( $48.81 \text{ MPa}\sqrt{\text{m}}$ ). However, the value to  $K_{th}$  was increased slightly from  $19.15 \text{ ksi}\sqrt{\text{in}}$  ( $21.04 \text{ MPa}\sqrt{\text{m}}$ ) to  $20.96 \text{ ksi}\sqrt{\text{in}}$  ( $23.03 \text{ MPa}\sqrt{\text{m}}$ ). The median curve for low temperature remained below that for room temperature until at  $\Delta K = 45 \text{ ksi}\sqrt{\text{in}}$  ( $49.44 \text{ MPa}\sqrt{\text{m}}$ ), it then crossed over the other curve and remained above it. The size of the interval of  $\Delta K$  between the two asymptotes was reduced from  $41.23 \text{ ksi}\sqrt{\text{in}}$  ( $45.3 \text{ MPa}\sqrt{\text{m}}$ ) to  $23.7 \text{ ksi}\sqrt{\text{in}}$  ( $26.04 \text{ MPa}\sqrt{\text{m}}$ ) when the test temperature was lowered. Note that the value of  $K_{th}$  of  $20.96 \text{ ksi}\sqrt{\text{in}}$  reported herein was high when compared with the threshold stress intensity for low alloy steels reported in the literature. The discrepancy may be caused by extrapolating the limited amount of data points in the threshold regime available in this study to the limit of zero crack growth rate.

At  $R = +0.67$ , decreasing the test temperature reduced  $K_{th}$  from  $32.5 \text{ ksi}\sqrt{\text{in}}$  ( $35.71 \text{ MPa}\sqrt{\text{m}}$ ) to  $19.53 \text{ ksi}\sqrt{\text{in}}$  ( $21.46 \text{ MPa}\sqrt{\text{m}}$ ).  $K_{th}$  was increased from  $8.24 \text{ ksi}\sqrt{\text{in}}$  ( $9.05 \text{ MPa}\sqrt{\text{m}}$ ) to  $13.39 \text{ ksi}\sqrt{\text{in}}$  ( $14.71 \text{ MPa}\sqrt{\text{m}}$ ). The median curve for low temperature remained below the median curve for room temperature from  $K_{th}$  to  $\Delta K = 16 \text{ ksi}\sqrt{\text{in}}$  ( $17.58 \text{ MPa}\sqrt{\text{m}}$ ), then it crossed over the other curve and remained above it. The size of the interval of  $\Delta K$  between the two asymptotes was compressed from  $24.26 \text{ ksi}\sqrt{\text{in}}$  ( $26.65 \text{ MPa}\sqrt{\text{m}}$ ) to  $14 \text{ ksi}\sqrt{\text{in}}$  ( $15.25 \text{ MPa}\sqrt{\text{m}}$ ).

Investigators examining the low temperature effects of fatigue crack growth rates reported that the crack growth rate was decreased for a given value of  $\Delta K$  when the test temperature was reduced. The results of this experiment showed that the crack growth rate was decreased for a given value  $\Delta K$  between  $K_{th}$  and some higher  $\Delta K$  value in the slow crack growth region.

Higher crack growth rates were obtained when  $\Delta K$  was in the fast crack growth region near the upper instability asymptotic value.

Low temperature and high  $R$  ratio apparently interact to produce higher fatigue-crack growth rates in the entire interval of  $\Delta K$  between the two asymptotes (compare the median curves for  $R = +0.1$ , room temperature and  $R = +0.67$ ,  $-100^\circ\text{F}$  in Fig. 6). The upper instability parameter,  $K_{th}$ , was reduced to a greater extent because lower test temperature tended to increase the value of  $K_{th}$  while higher  $R$  ratio tended to reduce it. The results indicate that the  $R$  ratio variable produced a stronger effect in reducing the threshold than the test temperature in increasing it.

Although further data are desirable to define the variability of the data and obtain a better fit median curve, the effects of temperature and  $R$  ratio are clear. However, it is emphasized again that fatigue-crack growth data over the entire range of interest, from  $K_{th}$  to  $K_b$ , are needed. Also, enough points are needed to allow a numerical optimization of the fit.

Variation in fracture appearance of the specimen with test temperature is shown in Fig. 7. The crystalline facets found on the flat fracture surface of the specimen tested at  $-100^\circ\text{F}$  clearly indicated a cleavage mode of fracture which was different from the ductile mode exhibited by the massive plastic tearing found on the fracture surface of the specimen tested at room temperature. This contrast in fracture surface appearance is quite evident in Figs. 7(a-d) for the conditions cited in the figure caption. Note that the size of the region of stable crack growth was reduced when the test temperature was decreased.

The fracture surface was examined at higher magnifications by using a Bausch and Lomb SEM II scanning electron microscope and the fractographs obtained are shown in Fig. 8. Details of the SEM specimen layout for fractographic studies are presented in Table 3. In Figs. 8(a) and (b), the fracture surface of the specimen tested at  $-100^\circ\text{F}$  with  $R = +0.67$  exhibits cleavage facets and short intergranular cracks which are typical features of cleavage fracture. In Figs. 8(c) and (d), exhibits dimples and fibrous regions which are typical features of ductile fracture. It is clear from these fractographs that the fatigue-crack growth process below the transition temperature involves a different mechanism of crack growth than above the transition temperature.

### CONCLUSIONS

Crack growth behavior of ASTM A612 Grade B steel was examined at room temperature and at  $-100^\circ\text{F}$  ( $-73^\circ\text{C}$ ) with  $R$  ratio =  $+0.1$  and  $+0.67$ . The results lead to the following conclusions.

(1) A curve fitting relation based on the Four Parameter Weibull Survivorship Function provided a much more adequate curve fit for crack growth rate data than other proposed relations. The effects as well as the synergistic interaction of test variables can be accounted for by the four parameters which can be analytically determined. Also, once the four parameters have been obtained, inference can be made on the threshold,  $K_{th}$ .

(2) The effects of increasing the  $R$  ratio were to cause an increase in the crack growth rates, a decrease in the values of  $K_b$  and  $K_{th}$ , and a compression of the range of  $\Delta K$  between the upper and the lower asymptotes.

(3) Lowering the test temperature from room temperature to  $-100^\circ\text{F}$  decreased the crack growth rates in the slow crack growth region between  $K_{th}$  and some higher  $\Delta K$  value. However, the crack growth rates in the fast crack growth region near  $K_b$  were increased. In addition, lowering the test temperature increased  $K_b$ . The range of  $\Delta K$  between the two asymptotes was also compressed.

(4) The combined effects of decreased test temperature and increased  $R$  ratio produced an increase in crack growth rates in the entire range of  $\Delta K$ . Also  $K_b$  was reduced to a greater extent.

(5) Fractographic analysis indicated that the fracture mechanism changed from ductile fracture to cleavage fracture when the test temperature was lowered from room temperature to  $-100^\circ\text{F}$  ( $-73^\circ\text{C}$ ).

It is to be emphasized that very limited data are available in this study and the literature concerning the effect of temperature and  $R$  ratio. Furthermore, because more data are needed

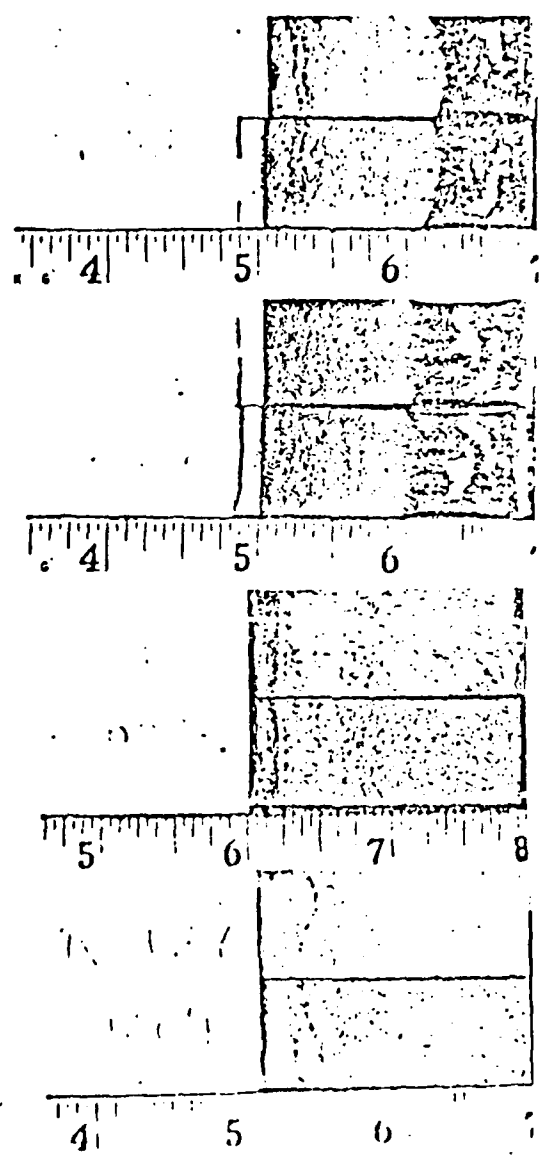


Fig. 7. Fracture surfaces of test specimens.

+

+



(a)



(c)



(b)



(d)

Fig 8(a). Scanning electron Micrograph of fracture surface of specimen tested at  $-100 \text{ F} (-73 \text{ C})$  with  $R = 10.67$ ; cleavage facets and short intergranular cracks are found on the fracture surface ( $800 \times$  magnification); (b) a magnified view of a cleavage facet on the fracture surface is shown ( $1500 \times$  magnification); (c) dimples and fibrous regions are found on the fracture surface ( $800 \times$  magnification); (d) dimples and microcracks are shown ( $1500 \times$  magnification).

Table 3. SEM specimen layout for four topographic studies

Test Conditions	Average Distance of the Specimen from the Notch Tip, in (mm)	Average $da/dN$ $\times 10^{-5}$ , in/cycle	Average $K$ , ksi $\sqrt{in}$ (MPa $\sqrt{m}$ )
-100°F, $R = +0.67$	0.25 (6.35)	3.65 (92.71)	14.4 (15.8)
Room Temp., $R = +0.67$	0.85 (21.59)	5.49 (13.94)	23.7 (26.0)

to adequately fit the Weibull Survivorship function the results presented herein should be viewed as tentative until satisfactorily planned experiments can be conducted and also until more data can be generated in the threshold and instability regimes.

**Acknowledgments**—This work was sponsored by the Office of Naval Research. The authors wish to acknowledge the encouragements and interests of Dr. Phillip Clarkin for continuous progress. We are grateful to Mr. Arthur Braun and Mr. Bill Watts for their assistance in conducting the experiments. We are also grateful to Mr. Larry Mueller for preparing the computer programs for data analysis. The authors wish to express sincere thanks to Dr. G. Bowie, Mr. R. Jeal, Sue Hoepfner and Winnie Ho who provided inspiration constantly.

### REFERENCES

- [1] W. G. Clark, Jr. and H. E. Trout, Jr., Influence of temperature and section size on fatigue crack growth behavior in Ni-Mo-V alloy steel. *Engng Fracture Mech.* 2, 107-123 (1970).
- [2] D. H. Andreassen and F. H. Vitovec, The effects of temperature on fatigue crack propagation in limepipe steel. *Metallurgical Transactions* 5, 1779-1783 (1974).
- [3] S. T. Rolfe and W. H. Munse, Fatigue crack propagation in notched mild steel plates. *Welding J. Res. Supplement* 42, 252s-260s (1963).
- [4] A. Braun, The effect of  $R$  ratio on fatigue crack growth of SA533-B1 steel in air and distilled water. Masters thesis, University of Missouri-Columbia (1977).
- [5] S. L. Cole, The effect of mean stress and  $R$  ratio on fatigue behavior of turbine alloys. Masters Thesis, University of Missouri-Columbia (1976).
- [6] M. Katcher and M. Kaplan, Effects of  $R$ -Factor and crack closure on fatigue crack growth for aluminum and titanium alloys. *Fracture Toughness and Slow Stable Cracking*, ASTM STP 660, Am. Soc. for Testing and Materials, pp. 261-292 (1974).
- [7] P. C. Paris, R. J. Bucci, E. T. Wessel, W. G. Clark and T. R. Mager, Extensive study of low fatigue crack growth rates in A533 and A508 steels. Stress Analysis and Growth of Cracks. *Proc. 1971 Nat. Sym. Fracture Mech. Part I*, ASTM STP 513, Am. Soc. Testing and Materials, pp. 141-176 (1972).
- [8] R. G. Forman, V. E. Kearny and R. M. Engle, Numerical analysis of crack propagation in cyclic-loaded structures. *J. Basic Engng.* 459-464 (1976).
- [9] F. K. Walker, The effects of environment and complex loading history on fatigue life. *ASTM STP 621*, Am. Soc. Testing and Materials, pp. 1-14 (1970).
- [10] W. Elber, Fatigue crack closure under cyclic tension. *Engng Fracture Mech.* 2, 37-45 (1970).
- [11] W. Elber, Damage tolerance in aircraft structures. *ASTM STP 486*, Am. Soc. Testing and Materials, pp. 230-242 (1971).
- [12] G. E. Bowie and D. W. Hoepfner, Numerical modeling of fatigue and crack propagation test results. *Proc. Conf. Computer Simulation for Materials Applications*, National Bureau of Standards, Gaithersburg, Maryland (1976).
- [13] L. N. Mueller, The statistical analysis and presentation of fatigue crack growth rate data. Masters Thesis, University of Missouri-Columbia (1978).
- [14] K. R. Kondas, Influence of microstructural and load wave form control on fatigue crack growth behavior of precipitation hardening stainless steels. Doctoral Dissertation, University of Missouri-Columbia (1976).
- [15] R. K. Reeves, Microstructural and environmental effects on fretting fatigue. Doctoral Dissertation, University of Missouri-Columbia (1977).
- [16] R. K. Reeves and D. W. Hoepfner, A Weibull analysis of center cracked panel crack growth data of a 0.40/0.50 carbon steel. *Engng Fracture Mech.* 10(4), 571-581 (1978).
- [17] D. W. Hoepfner and A. Braun, The effect of  $R$  ratio on fatigue crack growth of SA 533-B1 Steel in air and distilled water. University of Missouri-Columbia Tech. Rep. UMC-SIMS-1-PR1-V (1977) *Engng Fracture Mech.* submitted for publication.

(Received 9 June 1978, received for publication 4 September 1978)

## A WEIBULL ANALYSIS OF FATIGUE-CRACK PROPAGATION DATA FROM A NUCLEAR PRESSURE VESSEL STEEL

G. C. SALIVAR and D. W. HOEPPNER

*Graduate Student  
University of Missouri  
Columbia Mo 65201*

**Abstract**—Techniques of curve fitting, based upon an equation in the form of the four parameter Weibull Survivorship Function, are presented for the reduction of fatigue crack propagation rate data obtained from a nuclear pressure vessel steel. The importance of data in the near threshold and the high crack propagation rate regions of the DA/DN vs  $\Delta K$  curve, as it relates to the curve fit, is demonstrated with respect to a change in the four parameters of the Weibull function.

*Cockburn Professor  
APSE  
University of  
Toronto  
Toronto Ontario  
M5S 1A4*

### INTRODUCTION

CURVE FITTING techniques are essential to a life prediction utilizing the fatigue-crack propagation characteristics of a material. An equation in the form of the four parameter Weibull Survivorship Function is used in this work and applied to the data obtained from three compact tension specimens of ASTM 533B-1 nuclear pressure vessel steel. The specimens are subjected to three distinct environments while under a constant sinusoidal type loading. The Weibull function is used to determine the variation in the fatigue-crack propagation data as a function of environment, based upon the four parameters of the curve fit. The effects of the lack of near threshold and high crack propagation rate data, as indicated by a comparison of the curve fits of the three data sets, will be discussed.

### DATA ANALYSIS TECHNIQUES

An equation in the form of the Weibull Survivorship Function [1-3] is used to determine the relationship between DA/DN vs  $\Delta K$  data:

$$1 - \frac{\Delta K}{K_b} = \exp \left( - \left( \frac{DA/DN - e}{v - e} \right)^k \right) \quad (1)$$

This represents a four parameter equation in which  $e$  = the threshold parameter;  $v$  = the characteristic value;  $k$  = the shaping parameter;  $K_b$  = the value of  $\Delta K$  at the point of unstable fracture ( $DA/DN \rightarrow \infty$ ).

Equation (1) may be rearranged as

$$\left[ -\ln \left( 1 - \frac{\Delta K}{K_b} \right) \right]^{1/k} = \frac{DA/DN - e}{v - e} \quad (2)$$

which is in the form of the equation of a straight line

$$y = mx + b \quad (3)$$

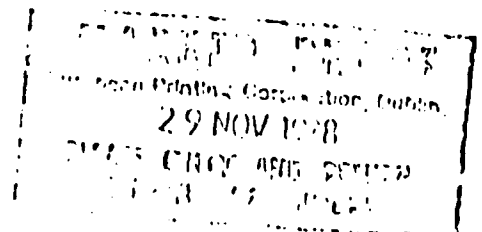
where

$$y = \left[ -\ln \left( 1 - \frac{\Delta K}{K_b} \right) \right]^{1/k}$$

$$m = \frac{1}{v - e}$$

$$x = DA/DN$$

$$b = \frac{e}{v - e}$$



Arranging the equation in this form allows a linear regression analysis to be performed by incrementing  $K_b$  and the shaping parameter  $k$ . The sample correlation coefficient ( $R$ ) is then determined by

$$R = \frac{n\sum xy - \sum x \sum y}{((n\sum x^2 - (\sum x)^2) - (n\sum y^2 - (\sum y)^2))^{1/2}}$$

The maximum value of  $R$  ( $R \rightarrow 1$ ) will provide the best linear fit to the data and will determine the  $K_b$  and  $k$  values. Using the slope ( $m$ ) and the intercept ( $b$ ) of this line, the values of  $e$  and  $v$  can be calculated.

The purpose of using an equation of the form of the four parameter Weibull function is that it takes into account both asymptotes of the sigmoidal curve shape to which  $DA/DN$  vs  $\Delta K$  data correspond. It allows the four parameters of the function to be determined by a linear regression analysis rather than arbitrarily selecting one or more of these values. Also, a change in any one of the four parameters of the function will affect the remaining three parameters. This will affect the curve shape and therefore, a life prediction.

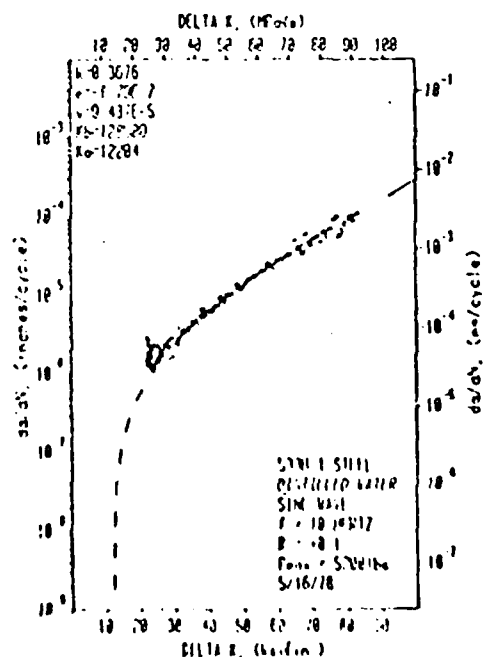
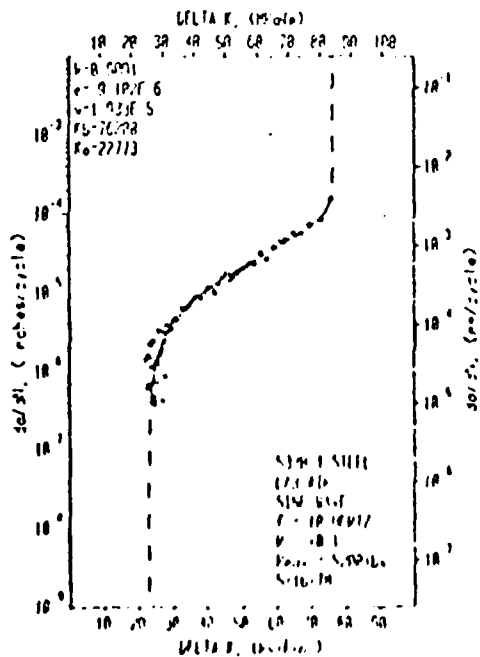
RESULTS AND DISCUSSION

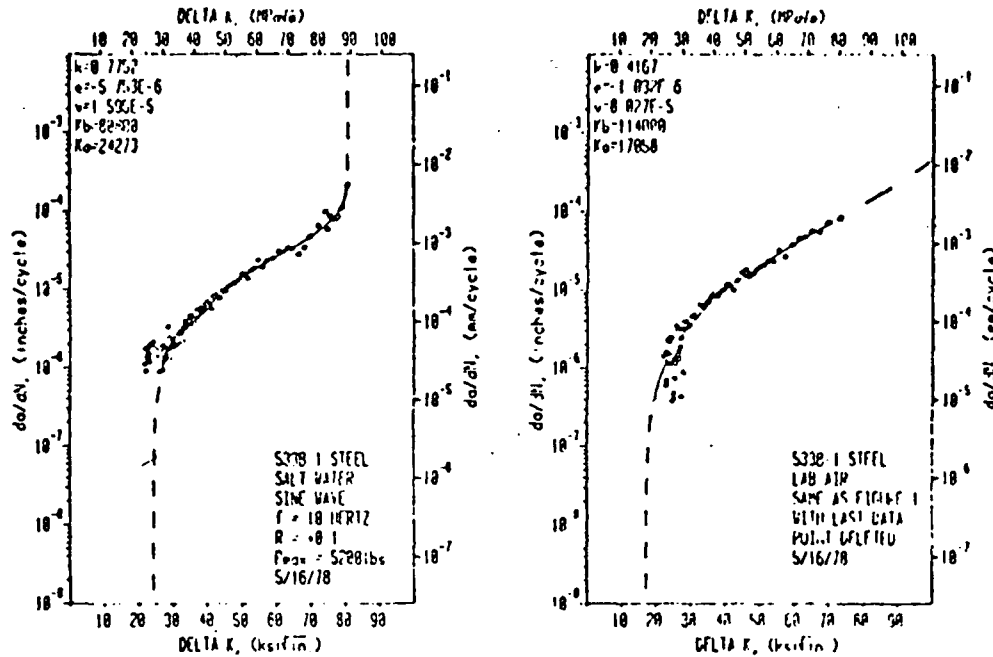
The data obtained from the three tests are plotted in Figs. 1-3 along with the appropriate Weibull curve. Figure 4 is a plot utilizing the data in Fig. 1 with a slight modification. The values of the Weibull parameters for each set of data in the figures are given in Table 1.

The values of the four Weibull parameters for the lab air and the salt water environments are relatively close while the values for the distilled water environment vary significantly (Table 1). The crack propagation in this specimen (distilled water) became unstable shortly after the

Table 1. Values of the Weibull parameters

Environment	$K_b$	$k$	$e$	$v$
Lab air	76,200	0.9091	9.1021 6	1.9331 5
Distilled water	128,500	0.3676	1.791 7	9.4371 5
Salt water	80,800	0.7752	5.7531 6	1.5951 5
Lab air (modified)	114,000	0.4167	1.0321 6	8.0271 5





last data point, however, this is not reflected in the curve in Fig. 2. The curve indicates that the crack propagation continues in a stable manner until a much higher value of  $K_k$  is reached. This higher  $K_k$  value is due to the lack of high crack propagation rate data obtained from the distilled water specimen. The effect of this higher  $K_k$  value will be to change the remaining three parameters and result in a curve that does not fit the physical characteristics of the crack propagation in the specimen.

The threshold of the curve in Fig. 2 is shown as being lower than the thresholds in Figs. 1 and 3. This is partly due to the effect of the higher  $K_k$  value, and also to the lack of near threshold crack propagation data. Some data were obtained in the near threshold region for the lab air specimen (Fig. 1), but little was obtained for the distilled water and salt water specimens (Figs. 2 and 3). The "physical" fit to the data in Fig. 3 results from the last high crack propagation rate data point and its influence on the curve. In Fig. 1 where some near threshold and high crack propagation rate data were obtained, the curve fits the physical characteristics of the data. The curve for the distilled water environment would be similar to the curves for the lab air and the salt water environments, had more data been obtained in both the near threshold and the high crack propagation rate regions.

Evidence of this fact is provided in Fig. 4 where the last data point from the lab air data set (Fig. 1) has been deleted. The resulting curve is similar to Fig. 2 with the  $K_k$  value increasing to 114 ksi√in. The threshold in Fig. 4 is also lower than the threshold in Fig. 1 because of the higher  $K_k$  value. Although a large amount of data was not obtained in either the near threshold or the high crack propagation rate regions for these three specimens, the importance of these data are emphasized by a comparison of the curve fits. A curve that fits the physical characteristics of the crack propagation in the specimen will result when data in these two regions are obtained.

### CONCLUSIONS

The importance of the near threshold and the high crack propagation rate data to the curve fit, is evidenced by a comparison of the values of the Weibull parameters for the distilled water test to the lab air and the salt water tests. The lack of data in these regions can result in a curve that does not fit the physical characteristics of the fatigue crack propagation in the specimen. Although data in these regions of the  $DADN$  vs  $\Delta K$  curve is costly and difficult to obtain, the primary effort of fatigue crack propagation testing should be concentrated in these two areas if accurate life predictions are to result.

*Acknowledgements*—The authors wish to acknowledge Mr. Larry Mueller for his help with and the use of the plotting programs.

#### REFERENCES

- [1] D. W. Hoepfner and W. E. Krupp, Prediction of component life by application of fatigue crack growth knowledge. *Engng Fracture Mech.* 6 (1974).
- [2] G. E. Bowie and D. W. Hoepfner, Numerical modeling of fatigue and crack propagation results. *Nuclear Metallurgy Proc. 1976 Int. Conf. Computer Simulation for Materials Applications*, Vol. 20, Part 2, pp. 1171-1178 (1976).
- [3] R. K. Reeves and D. W. Hoepfner, A Weibull analysis of center cracked panel crack growth data of a 0.40/0.50 carbon steel. *Engng Fracture Mech.* 10(3), 571 (1978).

(Received 22 May 1978; received for publication 5 September 1978)

MODEL FOR PREDICTION OF FATIGUE LIVES BASED UPON  
A PITTING CORROSION FATIGUE PROCESS.

David W. Hoepfner, Ph.D., P.E.  
Cockburn Professor of Engineering Design  
University of Toronto, Toronto Ontario.

Abstract

An earlier paper on fatigue crack initiation discussed the manner in which fatigue cracks are initiated by slip, twinning, strain incompatibility that produces localized cleavage, grain boundary decohesion, constituent particle fracture, and foreign particle fracture. All of these mechanisms of localized deformation or elastic fracture may ultimately lead to a mode I fatigue crack that can be described using conventional fracture mechanics concepts, as long as linear elastic behavior exists. In addition, these mechanisms of initiation of mode I fatigue cracking result from application of cyclically varying external driving force such as load or temperature. The intrinsic characteristics of the material govern the kinetics of the initiation and propagation processes.

However, there are many situations in the fatigue of materials where initiation of mode I cracking results from the combined action of environment and the alternating strains. Sometimes the environment/deformation synergism results in pitting corrosion fatigue. A physical model of the pitting corrosion fatigue process is presented involving the utilization of pitting kinetics and fatigue crack growth kinetics. It is postulated that pitting theory can be used to predict the rate of growth of pits. Utilizing information on the fatigue-crack growth threshold for the material/environment combination of interest it then is postulated that the number of cycles at a given stress to generate a pit of sufficient size to become a mode I fatigue crack can be estimated. An experimental technique to observe the growth of pits forming under cyclic loading has been developed. Verification of the model is presented and some shortcomings and needs for additional research are discussed.

To be published - ASTM presented @ International Conference  
on Mechanism of Fatigue, May 1978, K.C., Mo., ASTM.

Key words: Fatigue, Corrosion Fatigue, Pitting, Fracture Mechanics, Threshold, Kinetics, Mode I, Initiation, Crack Energy.

## INTRODUCTION

A large number of studies have been conducted and reported in the literature related to mechanism(s) of fatigue "initiation" and/or "propagation". It is now clear that many processes of physical deformation can be involved in the fatigue behavior of materials. This paper deals with one such process, viz., pitting corrosion fatigue. A conceptual physical model to explain the process of this insidious failure mode is presented in terms of physical events that subsequently can be mathematically described in order to calculate the time (cycles) to fatigue failure; or to alternately calculate the time (cycles) to a defined physical event in the development of fatigue failure. The model for the pitting corrosion fatigue model is verified herein for 7075-T6 aluminum.

The utility of the model is its potential usefulness in estimating total fatigue life for including pre-Mode I cracking and Mode I crack growth. The basic features of the model are as follows:

- 1) Use pitting rate theory to predict the number of cycles required to generate a pit that is large enough for a Mode I fatigue crack to develop at the pit.
- 2) The size of pit, at a given stress condition, at which a mode I crack will form is determined from the Mode I fatigue crack growth threshold.
- 3) The Mode I fatigue-crack-growth threshold is determined from numerically fitting fatigue-crack-growth data for specific boundary conditions.
- 4) Determine the number of cycles to propagate from a Mode I crack to fracture using fatigue-crack growth prediction methodology.
- 5) Sum the cycles to failure for the total fatigue life.

Aside from using this model for fatigue life prediction it also allows a means whereby quantitative comparisons of materials operating under corrosion fatigue can be made based upon the quantitative assessment of differences in either pitting behavior or fatigue crack growth behavior or both.

Thus, quantitative studies of pitting corrosion fatigue mechanisms will be possible.

The following sections present the model and an experimental procedure used to verify it. It is also elucidated. Further studies are continuing and

3.  
more results on the quantitative verification of the model will be reported at a later date.

BACKGROUND:

During the past thirty years the development of linear elastic fracture mechanics (LEFM) has been very rapid. The application of LEFM, and other areas of fracture mechanics to fatigue offers the attractive feature of dealing quantitatively with the "cumulative damage" (i.e. crack extension) during the fatigue process. Principal quantities of interest in applying fracture mechanics to fatigue are the initial flaw size, applied load, location of the flaw with respect to the stress field, environment, load spectrum and frequency, and the properties of the material of interest. In this case, the properties of interest are the fatigue crack growth threshold ( $K_{th}$  or  $K_0$ ), the crack instability parameter,  $K_{Ib}$ , and the fatigue crack growth curve for the material(s) of interest for the conditions of interest. The apparent relative simplicity of fracture mechanics as a useful tool for dealing with the physical aspects of fatigue has, however, a concomitant difficulty. This difficulty is associated with the initial flaw.

Many investigators have classified the fatigue process as being comprised of three stages, viz. initiation, propagation, and final fracture. On numerous occasions, an attempt has been made to ascertain the quantitative meaning of researchers when they refer to fatigue crack initiation (1-5)\*. Some papers have been published related to either the concept of fatigue crack initiation or a model for fatigue crack initiation. Very few authors, if any, have attempted to characterize "fatigue crack initiation" in terms of a flaw size for a given physical process. It has frequently been discussed in the literature that subsequent to the attainment of a given flaw size (fatigue crack initiation) one need simply apply fatigue crack growth concepts based on LEFM to "predict life"

It is now generally recognized that fatigue of a member (specimen or structure) occurs as the result of either microplastic flow or constraint to flow or both. The physical flow or fracture processes that may lead to the development of a Mode I (Forsyth-Stage II - see Ref. 6) fatigue crack are slip, twinning, cleavage, grain boundary flow or fracture, phase boundary flow or fracture, and particle boundary flow or fracture (4,6). Aside from time

---

\*Numbers in parentheses refer to the references.

dependent synergisms that occur with cyclic loading, one of which is the subject of this paper, these physical deformation processes occur at either an inherent continuum discontinuity (notch, scratch, blowhole, pore, etc.) to create fatigue crack extension or are the processes that may lead to the development of a Mode I crack to which the principles of LEFM or generalized fracture mechanics may be applied. Thus, it is generally recognized that even though a continuum flaw may not be favourably located and of sufficient size for fatigue crack extension from the flaw, a fatigue crack can initiate at another point from pure deformation or localized fracture from point or line defect motion or interaction (7). Since fatigue cracks may therefore be developed without the presence of a continuum flaw, the many methods of potential nucleation must be dealt with in order to formulate fatigue resistant materials and structural/environmental systems.

Many synergisms for accelerating, or generating, the fatigue process are possible (8,9). In this brief paper only one will be dealt with as it relates to fatigue. Pitting corrosion fatigue is one of the most insidious of the synergisms that can occur (1, 5-7). However, very little is understood related to the kinetics of corrosion fatigue. More understanding is required to develop materials, formulate prospective and retrospective corrosion fatigue resistant design methodology, and understand the mechanisms of fatigue in a universal sense.

There are, of course, many types of corrosion that can interact with cyclic loading to produce the corrosion fatigue synergism. One of the corrosion mechanisms is pitting corrosion (1,10). There is very little information in the literature on pitting corrosion fatigue. In a recent ASTM Symposium on Corrosion Fatigue Technology (ASTM-STP 642) two papers were presented that considered the development of corrosion fatigue from a corrosion/mechanical load synergism. A paper by Van derHorst (11) dealt with corrosion fatigue initiated by stress corrosion cracking and thus is not directly relevant to this work except that conceptually it has similarities. The other paper by Kitagawa, et al., dealt more specifically with the nucleation of fatigue cracks at corrosion fatigue induced pits (12). They showed that probabilistic concepts could be employed to predict the corrosion fatigue process. This later reference is the only one in the literature of corrosion fatigue that relates to formulating a prediction of corrosion fatigue life based upon the observation of physical crack size. As with this paper, Kitagawa, et al., had to employ the rationale of fracture mechanics in formulating the analysis methodology.

This effort was indeed noteworthy, since following the dictates of the physical fatigue process these authors attempted to formulate a method of prediction of corrosion fatigue lives by coupling reliability concepts with fracture mechanics to yield a graphical display. This paper provides a slightly different approach to the problem.

This paper, then will review a conceptual model of corrosion fatigue and apply the knowledge of pitting corrosion to predict when a crack depth,  $a_0$ , will be achieved that will yield a value of stress intensity such that the threshold for fatigue crack growth ( $K_{th}$ ) shall be achieved. Subsequent to the presentation of the model, results of experiments that have been completed will be presented. Concepts similar to these have been developed related to fretting fatigue (12-14) and pure fatigue (4) and this paper is intended to, illustrate the universality of the concept.

#### REVIEW OF MODEL:

In Reference (1) a conceptual model for the corrosion fatigue process was presented and the essential elements of the process are as follows:

1. Corrosive attack under cyclic loading
2. Generation of Mode I fatigue crack of observable size.
3. Environmentally enhanced Mode I fatigue crack growth.  
(The opposite is possible).
4. Stress intensity dominated fatigue crack growth (Mode I,II, or III)
5. Unstable fracture.

Pitting corrosion fatigue was initially selected for verification of the model of corrosion fatigue since it physically has all five components above. Component one can be the initiation of pitting corrosion due to the material/environment/cyclic loading combination. Thus, by applying the knowledge of pitting theory it should be possible to ascertain the amount of time (no. of cycles) to propagate a corrosion fatigue pit to become a Mode I crack for the crack type/loading combination. In order to accomplish this prediction, the fatigue crack growth threshold of a Mode I fatigue crack in the material must be known. Thus, the cycles to propagate a pit to a dimension that is adequate to initiate a Mode I fatigue crack at a pit can be determined. In a practical case the Mode I crack then can grow to become an observable (inspectable) crack. It is a known fact that fatigue cracks usually initiate well before they are "observable". Subsequently, if the load is known it is possible to predict the fatigue-crack growth life if a prediction methodology

exists and the crack growth parameters are known. Fortunately, these methods are well established (2). The exact fitting of the fatigue crack growth data remains a subject of study. However, it appears that utilization of the Weibull Survivorship function (15-18) is an effective way to describe fatigue data since the data appear to be distributed on a Weibull basis (15-19). Point above is attained when the fracture toughness,  $K_{Ic}$ , or other suitable measure of crack instability is attained ( $da/dN$  approaches infinity in the limit). Thus, initiation of final fracture (crack instability) occurs when the crack reaches sufficient size at a given load level.

The fitting power of Weibull's relation lies in part in the fact that it fits the physical processes and relates to the physical boundary conditions. A power of the Weibull function also lies in its discriminating power of an effect of a variable on fatigue life. A brief review of fatigue-crack growth curve fitting is given since it is an essential part of the model.

#### FATIGUE CRACK GROWTH CURVE FITTING RELATIONS:

It is usual to plot fatigue-crack propagation test results in the form

$$Da/DN = f(\Delta K) \quad (1)$$

where  $Da/DN$  = crack propagation rate and  $\Delta K$  = stress intensity range.

A suitable curve fitting relation for this type application is one with a mathematical fit to the total physical behavior of fatigue-crack growth.

This relation must have the following properties (12,15):

- (1) The relation should lend itself to distinction between slow and fast crack growth rate segments.
- (2) As  $K$  approaches an upper limit,  $K_b$ , the crack growth rate should increase indefinitely.

$$\lim_{\frac{\Delta K}{K_b} \rightarrow 1} \left[ \frac{Da}{DN} \right] = \infty \quad (2)$$

- (3) As  $K$  approaches a lower threshold limit,  $K_{th}$ , the crack growth rate should diminish to zero

$$\lim_{\Delta K \rightarrow K_{th}} \left[ \frac{Da}{DN} \right] = 0 \quad (3)$$

A new class of exponential curve fitting relations with mathematical form in the fatigue data reduction Weibull distribution function have been explored recently.

Three members of the class are:

Type

Relations

$$A) \quad 1-F = \text{Exp} \left[ - \left( \frac{H - e}{v - e} \right)^k \right], \quad (4)$$

$$\text{or } H = e + (v - e) [(-\log_e(1 - F))]^{1/k};$$

$$B) \quad 1-F = \text{Exp} \left[ - \left( \frac{\log_e(H + 1) - e}{v - e} \right)^k \right], \quad (5)$$

$$\text{or } H = -1 + \text{Exp} \left( e + (v - e) [(-\log_e(1 - F))]^{1/k} \right)$$

$$C) \quad 1-F = \text{Exp} \left[ - \left( \frac{\log_e \log_e(H + \exp(1)) - e}{v - e} \right)^k \right] \quad (6)$$

$$\text{or } H = -\text{Exp}(1) + \text{Exp} \left( e + (v - e) [(-\log_e(1 - F))]^{1/k} \right)$$

These relations meet the three criteria of acceptability previously stated. The fitting routine contains logic for estimating the curve fitting parameters  $k$ ,  $e$ , and  $v$  by a combination of linear regression and correlation coefficient optimization. In practice,  $Da/DN$  and  $\Delta K$  values of a data set are stored as one dimensional arrays  $DaDN$  and  $dK$ . The regression analysis is performed on variables  $X$  and  $Y$ , in terms of the equation of regression

$$(-\log_e Y)^w = bX + a \quad (7)$$

which has alternative form

$$Y = \text{Exp} \left( - \left( \frac{X - e}{v - e} \right)^k \right) \quad (8)$$

where

$$k = 1/w,$$

$$e = -a/b,$$

and

$$v = (1 + bc)/b$$

The following operations are performed, for example, when applying candidate Type-B curve fitting:

```

DO I = 1 TO N
  X = loge(Da/DN(i) + 1)
  Y = (- loge(1 - dK(i)/Kb))w
  .
  .
  .
Regression and Correlation Coefficient Logic
  .
  .
END

```

In this case, the routine yields the Type-B relation

$$1 - \Delta K/K_b = \text{Exp} \left[ - \left( \frac{\log_e(Da/DN + 1) - e}{v - e} \right)^k \right], \tag{9}$$

where  $\Delta K/K_b = F$ , and  $Da/DN = H$

Parameter  $K_b$  is the stress intensity range where  $Da/DN$  is indefinitely large. Estimation of  $K_b$  requires exercise of judgement in addition to interactive computing effort. At the outset of data set analysis, all three types of exponential curve fitting relations are tested, with  $F = \Delta K/K_b$  and  $H = Da/DN$  for each type. Measures of goodness of fit are used in deciding which, if any, type is suitable. For all three types, the particular stress intensity range where  $Da/DN = 0$  is called the threshold stress intensity,  $K_{th}$ , where

$$K_{th} = K_b \left( 1 - \text{Exp} \left( - \left( \frac{-e}{v - e} \right)^k \right) \right). \tag{10}$$

Physical significance is attached to threshold  $K_{th}$  for cases where threshold parameter  $e \leq 0$ .

- a. For  $e = 0$ ,  $K_{th} = 0$
- b. For  $e < 0$ ,  $K_{th} > 0$
- c. For  $e > 0$ , the suggestion is that crack growth begins at some  $Da/DN > 0$  for arbitrarily small  $\Delta K > 0$ .

Methods of determining goodness of fit are being developed (19) and are discussed to some extent in reference (16-18). In addition, procedures for distinguishing between fast and slow crack growth are available. Neither of these procedures will be discussed here since they are rather lengthy numerical statements.

In noting equation (9) it certainly is somewhat more complex than the typical Paris relation  $da/dN = D(\Delta K)^n$  utilized in a great deal of crack growth correlation. However, since it is desirable to formulate an accurate fatigue life prediction methodology herein, it is worth noting that equation (9) fits the physical data over the entire range of fatigue-crack growth whereas equation (1) does not. Thus, it would be difficult, if not impossible, to apply the Paris relation to pitting corrosion fatigue situations since a change in C or n would not necessarily yield a change in  $K_{th}$  or  $K_b$  ( $K_{IC}$ ). Thus, a life calculation could be in serious error. Thus, if procedures for optimizing the fit of equation (9) were available, and if a generalized integration routine can be established, a physically rational and reliable fatigue life prediction methodology would be available for pitting corrosion fatigue. This is the subject of other efforts but the Weibull technique has been developed adequately to test it on the pitting corrosion fatigue model.

The four Weibull parameters of interest here are;

- $K_b$  - the crack instability parameter,
- $e$  - threshold parameter,
- $v$  - characteristic value,
- $K$  - shape parameter.

Equation 10 gives the threshold value of stress intensity required to establish when a pit becomes of sufficient physical size to become a Mode I crack, for a defined load/environment/frequency to propagate in the regime where equation (9) can be applied.

In order to apply the model an analytical and experimental method must be available to establish the size of pit and time (or cycles) to develop a pit of given size. This is available from pitting theory as it now stands (15,20). However, it is noted after a review of pitting literature that it has not been established if dynamic loading accelerates pitting or not. This was not a subject of this study but needs to be established in order to fully understand the mechanisms of corrosion pitting fatigue. Current research is being directed at this crucial question. In addition, the specific mechanism(s) of corrosion pitting

are not dealt with herein. This is not to say they are not important but the postulated model does not require knowledge of the mechanism, only knowledge of the pitting rate and pitting geometry.

PITTING:

Corrosion pitting has been found to be related to area of exposure, time of exposure and the material/environment under consideration. At this time the equations that are used to determine pit depth are those due to Scott (21), et al., and Godard (22). They are, respectively,

$$d = bA^2 \quad (11)$$

and

$$d = C(t)^{1/3} \quad (12)$$

where

d = maximum pit depth

A = area of exposure

t = time

C = a parameter related to the material/environment combination

Although extreme value statistics also can be used to represent pitting data (16) it will not be used in this paper. Conceptually, it is now clear that to determine the pit depth as a function of time it is necessary to conduct experiments to get the value of C in equation (12) above. This procedure was employed to obtain the pit depth at which, for a defined load/environment combination, the fatigue-crack growth threshold will be attained.

It must be emphasized that very limited information on pitting rates is available. The author has numerous studies of this nature underway at present and this will allow confirmation of equation (12) or further development of the model.

Summary of Model  
for the Prediction of Fatigue Life Based  
Upon Pitting Corrosion  
Fatigue Mechanism  
-----

The model can now be summarized as follows:

1. Calculate the time (cycles) for a pit to develop to sufficient depth,  $a_{th}$ , to attain the fatigue-crack growth threshold at the stress level of interest. The environment and alloy must be known. Pitting data must be available. A flaw geometry must be assumed. If a surface flaw\* is assumed, an  $a/2c$  ratio must be assumed for the pit growth.

$$1a) K_{sf} = 1.1 S \sqrt{\pi(a/Q)}$$

$$Q = f \left[ (a/2c), S_{ty} \right]$$

- 1b)  $\Delta K_{th}$  (fatigue crack growth threshold for Mode I crack) must be known from experiments for the environment/material/frequency/spectrum/wave form combination.

2. Calculate the cycles (time) required to grow the Mode I crack that initiated from the pit to final fracture. Fatigue crack-growth data must be available for the alloy and environment determined at the proper test condition. Fracture toughness data should be available if applicable.

It should be noted that for those conditions where LEFM does not apply, plane stress or "large" strain, some modification of the model will be necessary, this effort also is currently underway.

Thus, this model must be verified and tested. In order to test the model based upon the pitting/corrosion fatigue mechanism experiments on pitting corrosion fatigue and fatigue-crack growth must be conducted. The verification experiments are reported in the remainder of the paper.

\* A surface flaw is assumed as an idealization of the pitting process. It is recognized that other pit geometries can occur.

It is worth noting that several initiation and propagation events are involved in this mechanism of fatigue failure. They are:

- 1) Initiation of corrosion pits,
  - 1p) Propagation of pits
- 2) Initiation of a Mode I crack at a corrosion pit site,
  - 2p) Propagation of the Mode I crack
- 3) Initiation of fracture instability,
  - 3p) Unstable crack propagation

Thus, to attempt to simply characterize the corrosion fatigue mechanism by terms such as initiation and propagation is a conceptual misunderstanding of the physical process. With this mechanism of fatigue it is possible to mathematically determine, for a given material in a given loading condition, the point at which processes 2 and 3 occur. However, in a relativistic sense, it does not today appear possible to be able to mathematically determine the precise nucleus size which leads to the initiation of corrosion pits. However, we can determine, on a statistical basis, the factors that control the growth of pits.

#### EXPERIMENTAL VERIFICATION OF THE MODEL:

In order to verify the proposed model it was decided to use 7075-T6 aluminum alloy tested in air and salt water. This material was selected since LEFM can be used to describe its behavior and also because it is known to undergo pitting in salt water. Although some steels yield greater pitting rates in some environments, aluminum was selected for the initial verification studies in order to avoid oxidation contamination which would make production of the movies difficult. The unnotched specimen used for the studies is shown in Figure 1.

The experimental apparatus used for the observation of crack development is shown in Figure 2 with the specimen position indicated

In the upper left hand portion of the figure. A viewing eyepiece was positioned to allow the observer to view the specimen and select the for detailed studies with recording on the film as shown. The movie system was quite elaborate and my colleague Vance Danford and I named the overall observation scheme A Sync-Strobe System for In-Situ Study of Fatigue some years ago. The system was designed to allow synchronization of the movies with the fatigue cycle or to allow the synchronization to be slipped over numerous cycles if desired. In this manner the motion can be stopped for easier viewing.

The unnotched fatigue tests were conducted under constant deflection axial loading with a sine wave at a frequency of 30 Hz. An R ratio ( $R = S_{min}/S_{max}$ ) of +0.1 was utilized for the initial verification studies. A small transparent container was constructed to contain the environment around the central section of the unnotched specimen. The environment always was introduced within minutes of starting the test. Tests were conducted on a continuous basis from start to fracture. Fatigue-crack growth data for these verification studies were taken from a previous effort (23) and other unpublished work of the author.

#### RESULTS:

The results on the unnotched specimens tested in laboratory air, distilled water, and 3.5% NaCl are shown in Figure 3. As expected, the salt water reduces the fatigue life a considerable amount. The initiation points indicated on Figure 3 are for development of a 0.127mm crack. The lines drawn through the data are in no way numerical fits of the data and should not be construed as such. Figures 4 and 5 present the fatigue-crack growth curves utilized for the model verification for the air and salt water fatigue crack growth tests. Tests were conducted on 15.24cm wide center cracked panels tested in closed loop load control with a sine wave at 10 Hz. It was determined from previous work (23) that no effect of frequency would occur between 10 Hz and 30 Hz. The Weibull parameters are shown in the upper left portion of the figures.

Figures 6 and 7 present several photographs that were selected for reproduction from the movies that were made during the tests. The specimen that was tested at 103.4 MPa ( $N_f = 357,810$  cycles) yielded most of the photographs shown. Figure 6a is a typical pit from the specimen tested at 275.8 MPa ( $N_f = 21,822$  cycles). From pitting data on 7075 In salt water a prediction of time to develop a Mode I crack will be made for the specimen tested at 103.4 MPa. Figures 6b through 7d will be used in conjunction

with the prediction. From Figure 4 the Weibull parameters are used to calculate the threshold from equation 10.\* Using the values indicated in the figure, a threshold value of 57.74 MPa√cm results. For an edge crack, through the edge in this case, a pit depth of

$$a_{th} = \frac{1}{\pi} \left( \frac{57.74}{1.15} \right)^2 = \frac{1}{\pi} \left( \frac{57.74}{1.1 \times 103.4} \right)^2 = 0.08 \text{ cm results.}$$

The actual pit (through edge crack) that resulted in size sufficient to generate a Mode I crack is .00635 cm. This is reasonable agreement. Further refinement can occur dependent on the number of specimens used to obtain the Weibull parameters and care with which the pit depth is determined.

Use of equation 12 in conjunction with the C value and time yield a number of cycles to a crack depth of:

$$d = C(t)^{1/3}$$
$$t = \left( \frac{d}{C} \right)^3$$

substitute the actual  $a_{th}$  for d

$$t = \left( \frac{a_{th}}{C} \right)^3 = \left[ \frac{0.00635 \text{ cm}}{0.000305 \text{ cm/sec}^{1/3}} \right]^3$$

= 9050 seconds.

in 9050 sec at 30 Hz approximately 300,000 cycles was required to initiate the Mode I crack. It is noted from Figure 6d and 7a that the Mode I crack developed somewhere between 204,000 cycles. Figure 6d and 324,412 cycles. A value of 300,000 cycles appears reasonable when an extrapolation on the one-third power of time is taken. Unfortunately, the exact t(N) at initiation of the Mode I crack was not obtained. Nonetheless, very good agreement is obtained and the conceptual model has been verified for this material and environment.

SUMMARY AND CONCLUSIONS:

It is clear from the photos shown in Figures 6 and 7 that corrosion pits produce a local discontinuity that acts as the site of initiation of a Mode I fatigue crack. The fatigue process, represented as the total number of cycles, is comprised of the cycles needed to produce the pit and the cycles needed to propagate the Mode I crack that initiates at the pit to failure. This is depicted in the simple a-N plot shown in Figure 8 below and in Figure 9, a representation of the Stress-Cycles to failure curve.

\* The computer programs currently are written for dealing with data acquired in English units; thus, the parameters listed in fig. 4 and 5 are for English units except for  $K_0$  and  $K_1$ .

The four parameter Weibull fits to the fatigue crack growth data that resulted for the 7075-T6 tested in salt water yield the fatigue-crack growth threshold,  $K_0$ . This value is then used to determine the size pit that will produce a stress intensity of sufficient magnitude to initiate a Mode I fatigue crack. The verification of the model worked well for the tests that were conducted. Further refinements appear probable as discussed in the recommendations section.

Figure 10 shows transmission electron fractographs taken from the vicinity of the origin for the air tests (Figure 10A and 10B) and the salt water tests (Figure 10C and 10D). A pronounced difference in the fracture appearance is noted in the origin areas. The air results show well defined fatigue striations whereas the salt water results show the more typical "brittle striations" (6). Additional effort will be needed to clarify the detailed deformation mechanisms that produce the difference in fracture surface detail.

It is concluded that:

- 1) Corrosion pits act as initiation sites for Mode I fatigue cracks in 7075-T6 cyclically loaded in salt water.
- 2) Pitting theory can be used to predict the rate of growth of pits and their size at various times.
- 3) The four-parameter Weibull fit to fatigue crack growth data can be used to obtain the fatigue-crack growth threshold.
- 4) Using the combined knowledge on pitting rates and the fatigue-crack growth threshold it is possible to predict either the size pit that will produce a Mode I fatigue crack or the cycles to do so or both.
- 5) The total number of cycles to failure can be predicted from a combined knowledge of the kinetics of pitting corrosion and fatigue-crack growth.
- 6) Continued emphasis must be placed on the kinetics of all potential fatigue mechanisms in order to formulate fatigue resistant materials and fatigue design concepts.
- 7) The concepts elucidated herein can be applied in failure analysis as well as to understand the mechanism of the fatigue process.

RECOMMENDATIONS:

From the success of this model and the experimental techniques developed to verify it is believed that other forms of the corrosion fatigue process could be modelled and studied in the same manner. Particular success should be attained with stress corrosion induced cracks, erosion, cavitation, crevice corrosion. As indicated in the text, very good success has already been attained in modelling fretting initiated fatigue. Much more data is needed however.

Several areas of corrosion pitting fatigue need increased attention to improve our understanding of this mechanism. First, we need to ascertain whether dynamic loading changes the kinetics of pitting. I have several students working on this now but this is a critical question. A great deal of additional statistically based pitting data also are needed. A great deal of attention must be dedicated to determining statistical distributions of fatigue-crack growth data in order to improve the predictions made with the model.

Finally, very little is known about the fundamental mechanism of pitting corrosion (under either static or dynamic loading) and some effort should be devoted to understanding this mechanism as it relates to the fatigue mechanism in general.

ACKNOWLEDGMENT AND DEDICATION:

The research reported herein was initiated as part of the Lockheed California Company Independent Research Program in 1969 and was continued during the author's tenure with Lockheed. In 1974, when the author joined the University of Missouri, Lockheed and the Alcoa Foundation continued support of this work through a research grant and gift, respectively, to the University of Missouri with Mr. William Krupp as the Lockheed technical monitor and Mr. D. Mauney as the Alcoa liaison. The author is grateful to his many colleagues at Lockheed for their many stimulating discussions over the past years. I want to express particular appreciation to Mr. William Krupp, Mr. Don Pettit, Mr. E.K. Walker, Mr. J.C. Ekvall, Mr. Gary Goss (now with Lockheed Missiles and Space Company), Dr. J.C. Ryder, Dr. G. Bowie, Mr. J. Fritzen, Mr. Vance Danford, Mr. Paul Sandifer, Mr. J. Van Orden, Mr. S. Bocarsly, and Dr. K.E. Weber. I am indebted to Mr. David Mauney of Alcoa and Mr. R. Jeal, Rolly Royce-Derby, for many discussions of these areas of endeavor. Mrs. Geraldine Hoch provided many stimulating thoughts on the corrosion aspects of this effort and her death during its progress was, in a sense, a serious loss. I have tried to continue this effort based upon many of the ideas shared with Geraldine and John Fritzen and I dedicate this paper to the living memory of Mrs. Geraldine Hoch.

In recent years the Office of Naval Research, and Air Force Office of Scientific Research also have provided support to my researchers on Corrosion Fatigue under contracts N 00014-75-C-0670 and AFOSR 77 3178, respectively, with Dr. Phillip Clarkin and Dr. William Walker, the respective technical monitors.

I am extremely grateful to all of the persons for their support, stimulation and encouragement in the pursuit of this subject.

REFERENCES

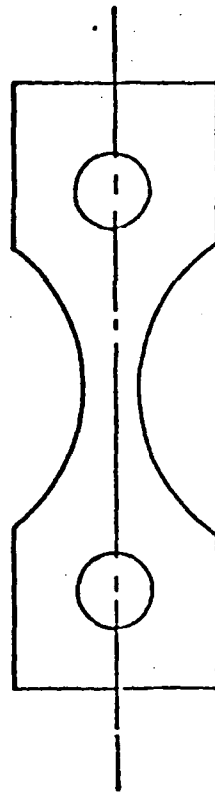
1. D.W. Hoepfner, "Corrosion Fatigue Considerations in Materials Selection and Design", Corrosion Fatigue: Chemistry, Mechanics, and Microstructure, NACE-2, National Association of Corrosion Engineers, 1972, pp. 3-11.
2. D.W. Hoepfner, W.E. Krupp, "Prediction of Component Life by Application of Fatigue Crack Growth Knowledge", Engineering Fracture Mechanics, 1974, Vol. 6, pp. 47-70.
3. A.H. Freudenthal, "Fatigue and Fracture Mechanics", Engineering Fracture Mechanics, 1973, Vol. 5, pp. 403-414.
4. D.W. Hoepfner, "Fatigue Crack Initiation Concepts in Solids", Submitted to Journal of Mechanics and Physics of Solids for publication, 1978.
5. L.F. Coffin, Jr., "The Multi-Stage Nature of Fatigue", Metal Science, February 1977, pp. 68-71.
6. P.J.E. Forsyth, "Fatigue Damage and Crack Growth in Aluminum Alloys", Acta Metallurgica, Vol. 11, No. 7, July 1963, pp. 703-717.
7. J.C. Grosskreutz, "The Mechanisms of Metal Fatigue (II)"; Phys. Stat. Sol. (b), Vol. 47, (1971), pp. 359-396.
8. C. Laird, D.J. Duquette, "Mechanisms of Fatigue Crack Nucleation", Corrosion Fatigue: Chemistry, Mechanics and Microstructure, NACE-2, National Association of Corrosion Engineers, 1972, pp. 68-117.
9. "Fatigue-1977", Metal Science, The Metals Society, August/September 1977, Entire proceedings.
10. Galvanic and Pitting Corrosion-Field and Laboratory Studies, ASTM STP 576, American Society for Testing and Materials, Philadelphia, Pa., 1976, pp. 117-295.
11. J.H.A. Van der Horst, "Corrosion Fatigue Initiated by Stress Corrosion Cracking", personal communication.
12. H. Kitagawa, T. Fugita, K. Miyazawa, "Small Randomly Distributed Cracks in Corrosion Fatigue", ASTM-STP 642, pp. 98-117.
13. D.W. Hoepfner, G.L. Goss, "A Fretting-Fatigue Damage Threshold Concept", Wear, Vol. 27, 1974, pp. 61-70.
14. P.R. Edwards, R.J. Ryman, R. Cook, "Fracture Mechanics Prediction of Fretting Fatigue", Royal Aircraft Establishment Publication presented at the International Conference on Aeronautical Fatigue--1977, to be published.

15. K. Endo, H. Goto, "Initiation and Propagation of Fretting Fatigue Cracks", Wear, Vol. 38 (1976), pp. 311-324.
16. G. Bowie, D. Hoepfner, "Numerical Modeling of Fatigue and Crack Propagation Test Results", Proceedings of the International Conference on Computer Simulation for Material Applications, Nuclear Metallurgy, Vol. 20, part 2, 1976.
17. K. R. Kondas, "Influence of Microstructural and Load Wave Form Control on Fatigue Crack Growth Behavior of Precipitation Hardening Stainless Steels", UM-C, Ph.D. dissertation, July 1976.
18. R. K. Reeves, "Microstructural and Environmental Effects on Fretting Fatigue", UM-C, Ph.D. dissertation, May 1977.
19. R. K. Reeves, D. W. Hoepfner, "A Weibull Analysis of Center Cracked Panel Crack Growth Data of a .40/.50 Carbon Steel", Accepted for publication in Engineering Fracture Mechanics.
20. L. Mueller, "The Optimization of the Weibull Survivorship Function in Fitting Fatigue Crack Growth Data", M.S. thesis, University of Missouri-Columbia, May 1978.
21. L. C. Rowe, "Measurement and Evaluation of Pitting Corrosion-Field and Laboratory Studies", ASTM-STP 576, American Society for Testing and Materials, 1976, pp. 203-216.
22. H. P. Godard, Canadian Journal of Chemical Engineering, Vol. 38, October 1960, p. 1671.
23. W. E. Krupp, D. W. Hoepfner, E. K. Walker, "Crack Propagation of Aluminum Alloys in Corrosive Environments", Corrosion Fatigue: Chemistry, Mechanics and Microstructure, NACE-2, National Association of Corrosion Engineers, 1972, pp. 468-483.

FIGURE CAPTIONS:

Figure No.

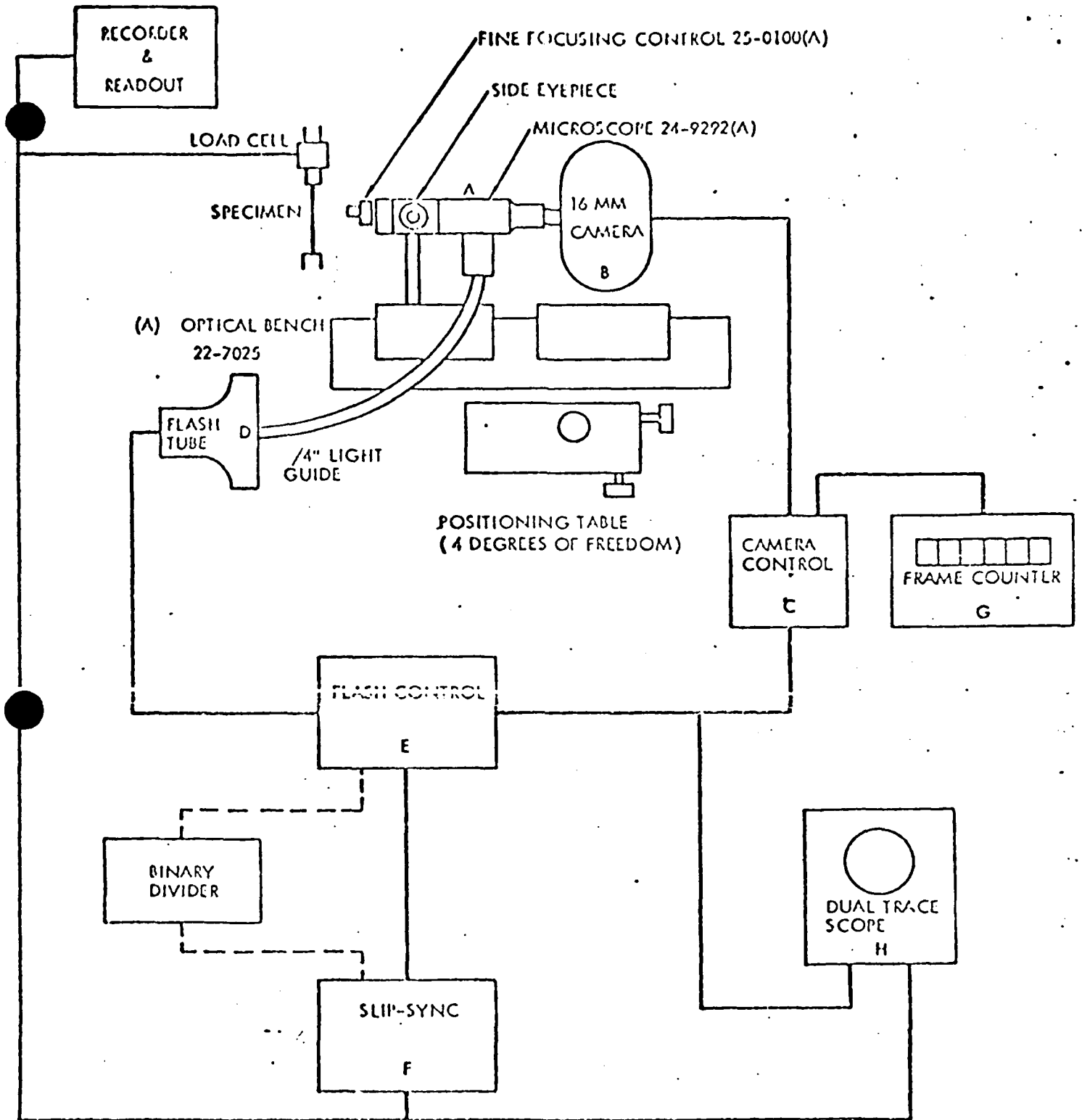
1. Fatigue Specimen Used for Pitting Studies.
2. Instrumentation for Observation of Fatigue Specimens During Cyclic Loading. Specimen is located at upper left.
3. Fatigue Results for Unnotched Fatigue Specimens Tested in Air, Distilled Water, and Salt Water. "Initiation" is to a crack 0.127mm long.
4. Typical Fit to Fatigue Crack Growth Data for 7075-T6 15.24cm wide Panel Fatigue Tested in Air.
5. Typical Fit to Fatigue Crack Growth Data for 7075-T6 15.24cm wide Panel Fatigue Tested in 3.5% NaCl Solution.
6. Photomicrographs Taken from Movies for Specimens Tested at (A) - 275.8MPa and (B), (C), (D) - 103.4MPa
  - A. Typical pit with Mode I fatigue crack.
  - B. Edge of specimen showing area where corrosion pit initiated that developed a Mode I crack.
  - C. Pit area after 146,000 cycles.
  - D. Pit area after 204,000 cycles.
7. Photomicrograph taken from Movie for Specimen Tested at 103.4 MPa
  - A. Pit area after 321,292 cycles.
  - B. Pit area after 330,592 cycles.
  - C. Pit area after 346,700 cycles.
  - D. Final fracture 354,700 cycles.
8. A Conceptual Crack Length (a) versus Cycles (N) Plot for the Corrosion Pitting Fatigue Model.
9. Various Critical Event Curves on the Stress-Cycles to Event Plot.
10. Electron Fractographs in Origin Areas for Fatigue Test In Air (A), (B), Fatigue Test in Salt Water (C), (D).



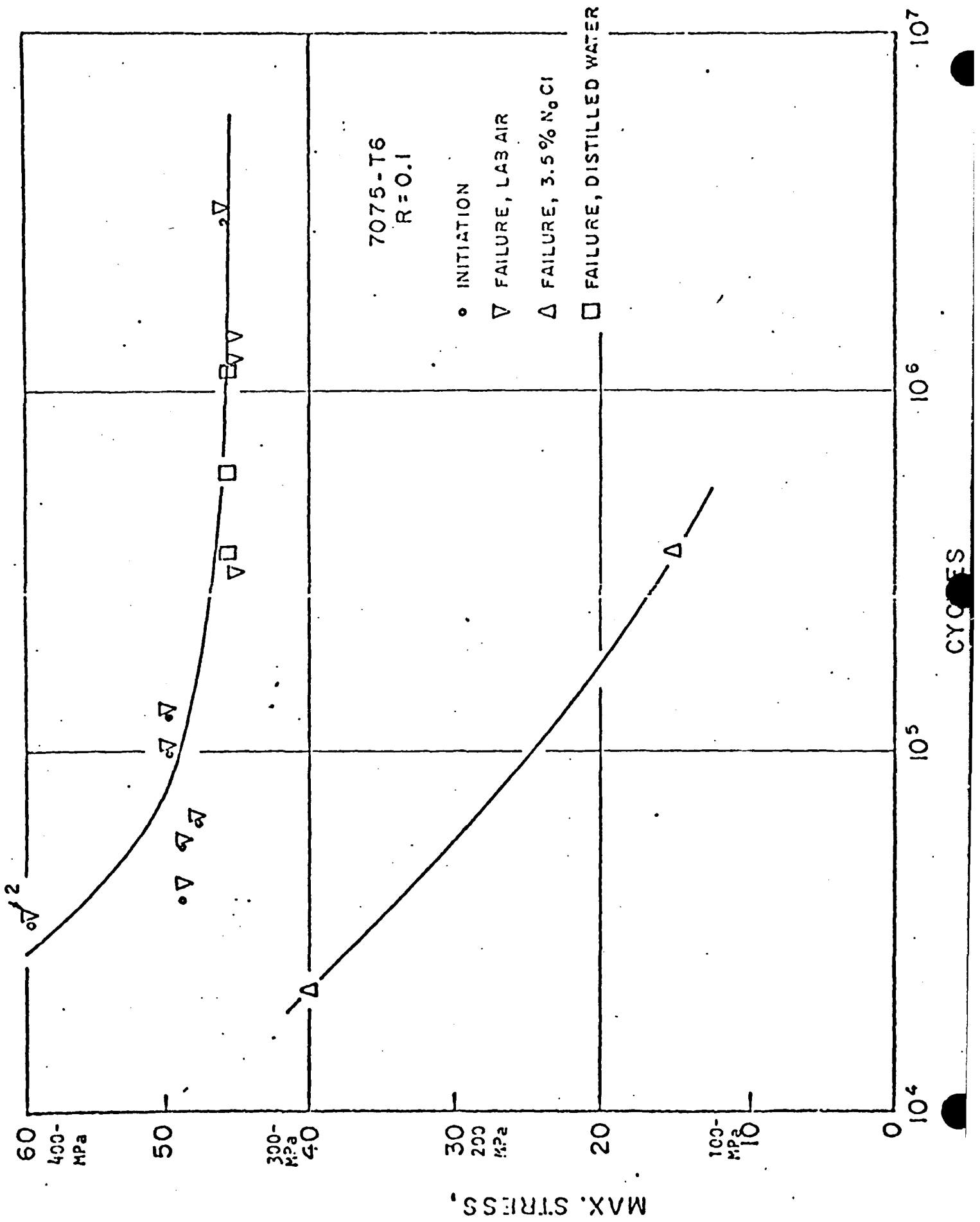
FULL SCALE

┌───┐  
10 m m

FIGURE 1 FATIGUE SPECIMEN USED  
FOR PITTING STUDIES



UNIT	MODEL	MANUFACTURER
A MICROSCOPE & BENCH	SEE ABOVE	EALING
B CAMERA	370	CHADWICK-HELMUTH
C CAMERA CONTROL	352A	CHADWICK-HELMUTH
D FLASH TUBE	71	CHADWICK-HELMUTH
E FLASH CONTROL	136	CHADWICK-HELMUTH
F SLIP-SYNC	107	CHADWICK-HELMUTH
G COUNTER	5221B	HEWLETT-PACKARD
H SCOPE	561A	TECFONIX



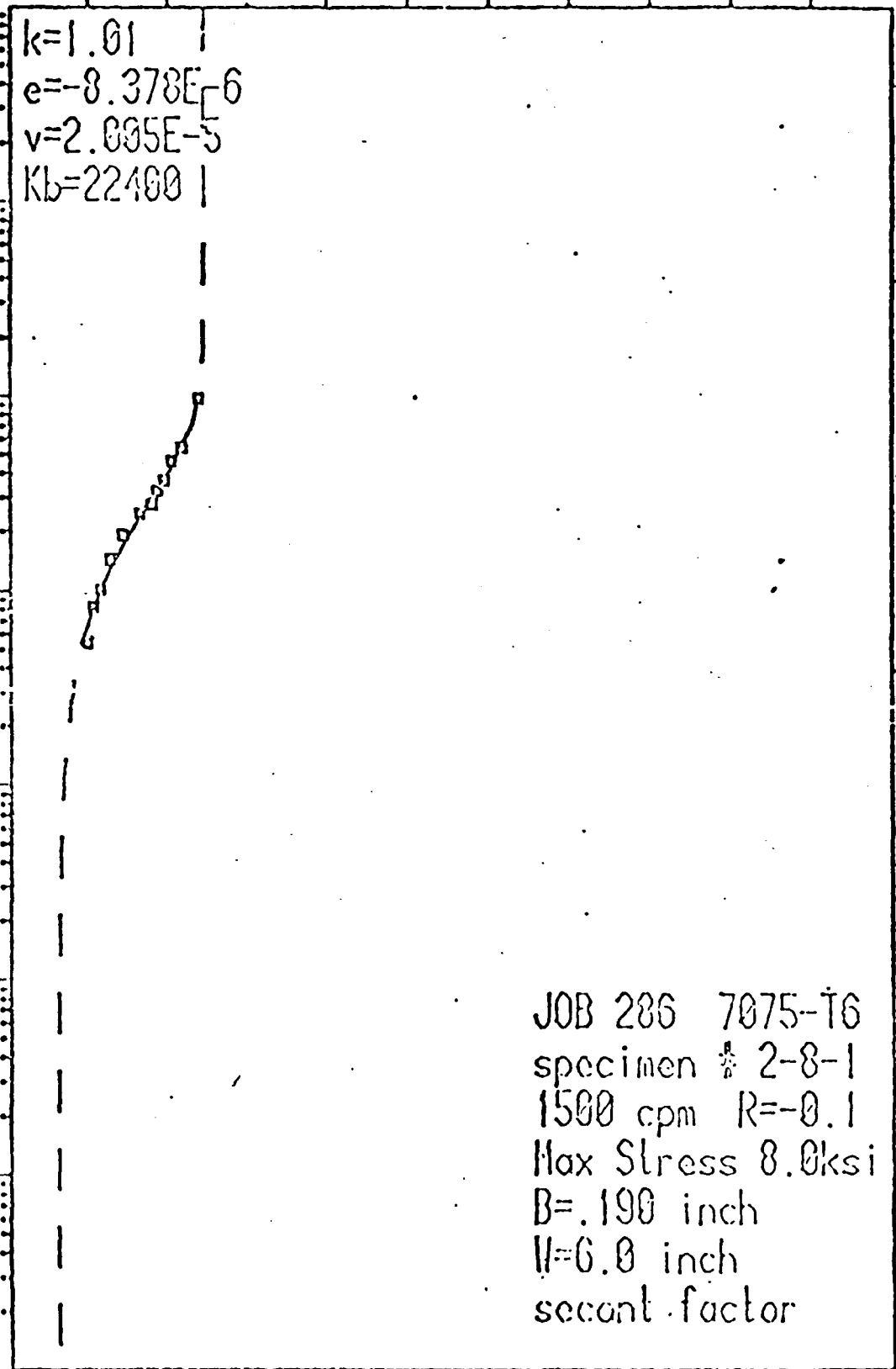
DELTA K, (MPa√in)

10 20 30 40 50 60 70 80 90 100

k=1.01  
e=-8.378E-6  
v=2.095E-5  
Kb=22400

da/dN, (inches/cycle)

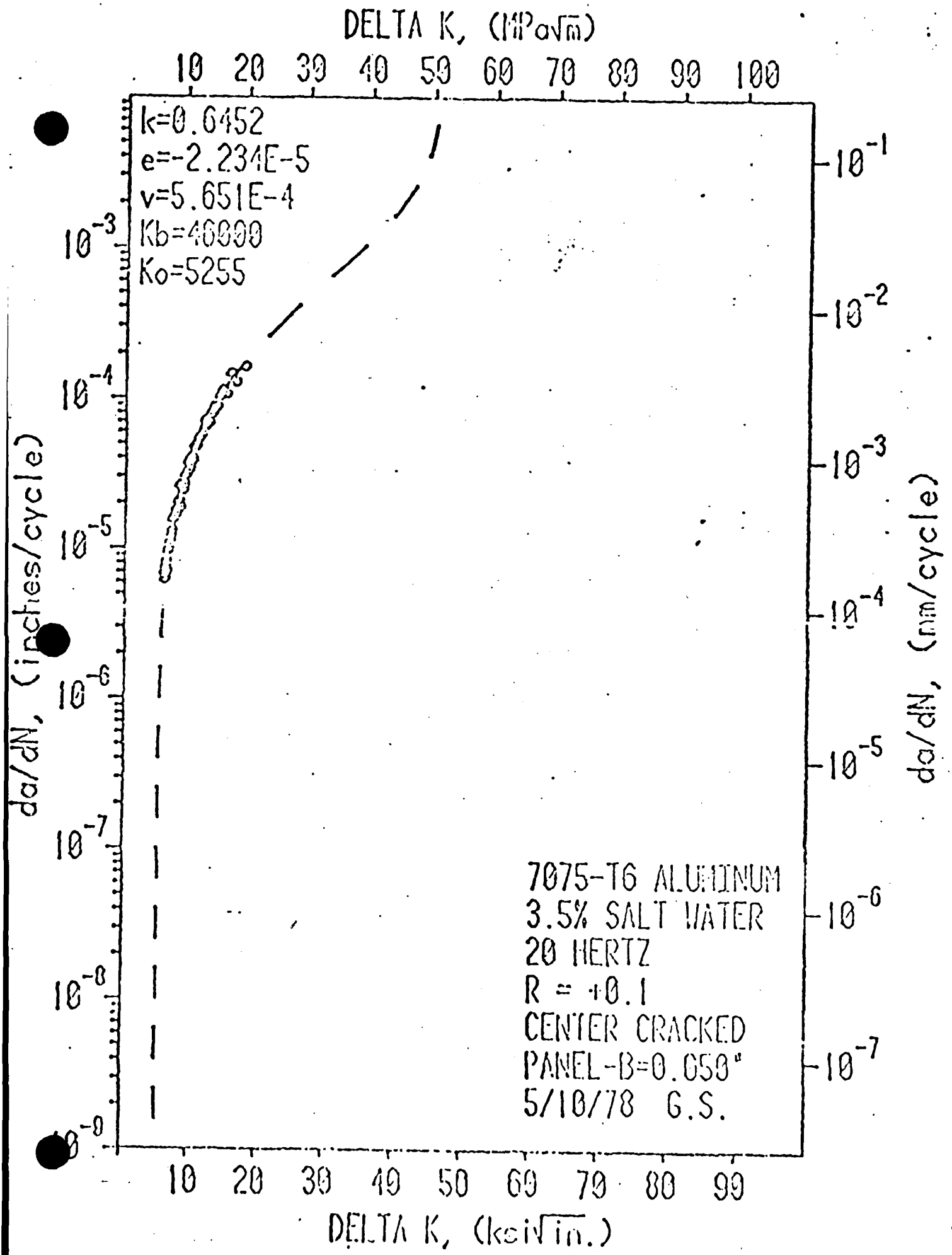
da/dN, (mm/cycle)

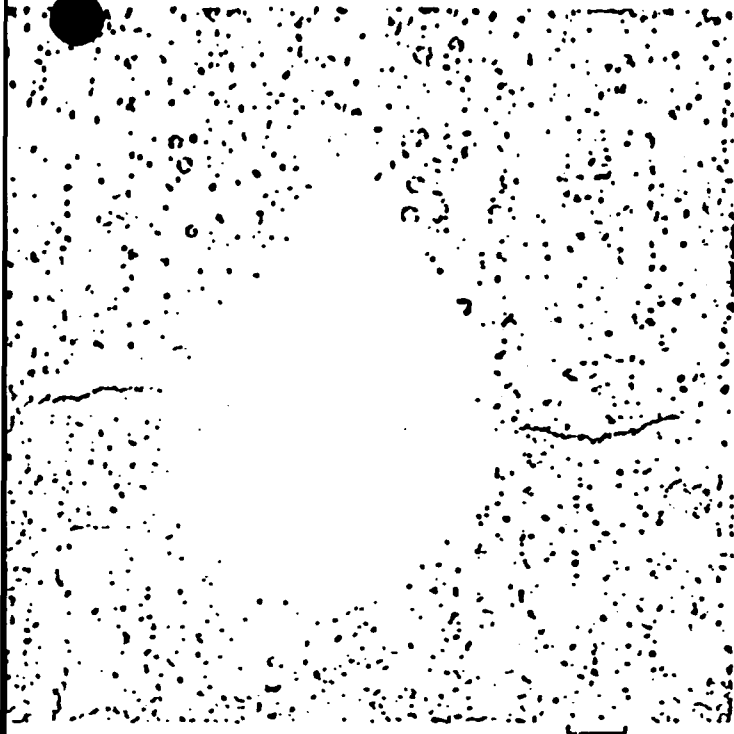


JOB 286 7075-T6  
specimen # 2-8-1  
1500 cpm R=-0.1  
Max Stress 8.0ksi  
B=.190 inch  
W=6.0 inch  
second factor

10 20 30 40 50 60 70 80 90

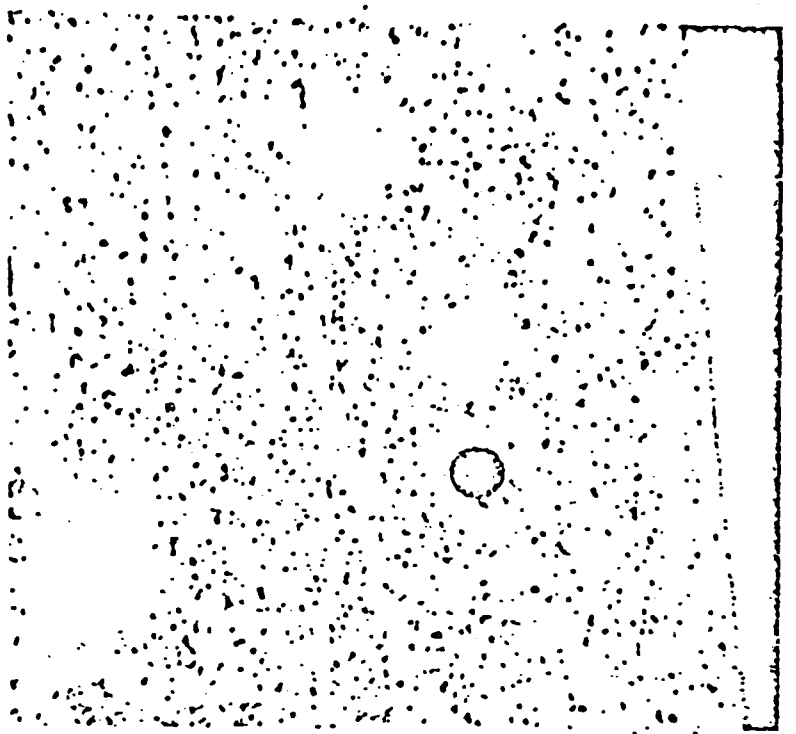
DELTA K, (ksi√in.)





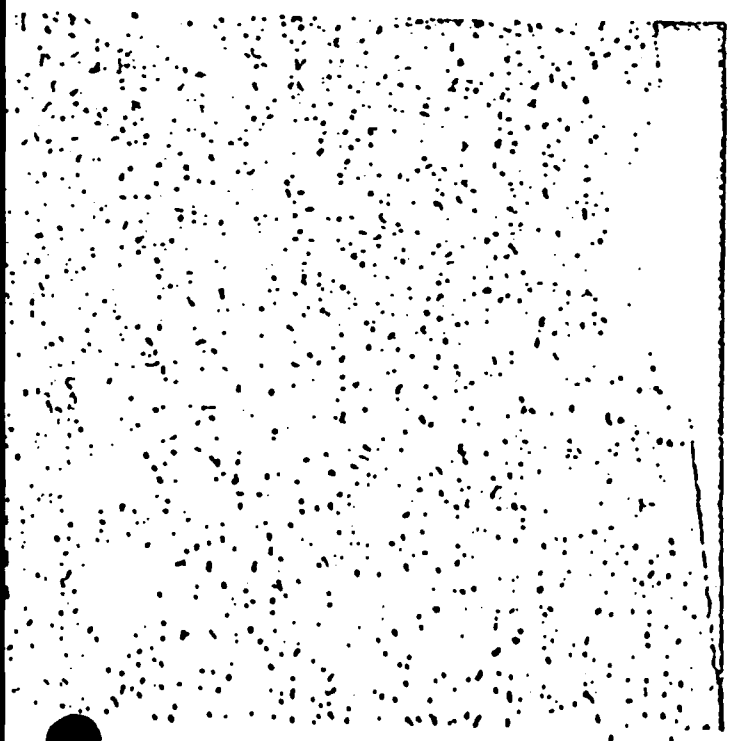
A

0.1 mm



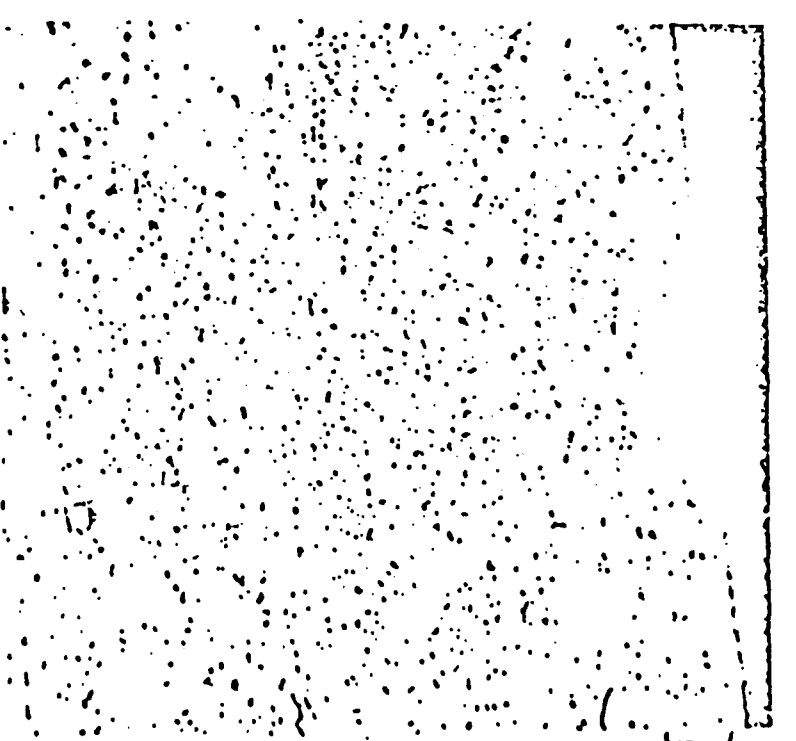
B

0.1 mm



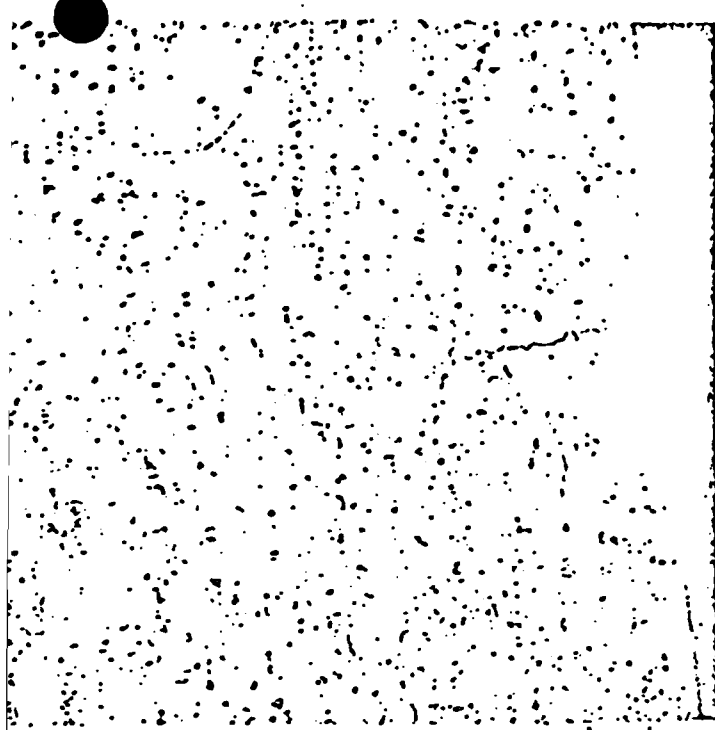
C

0.1 mm



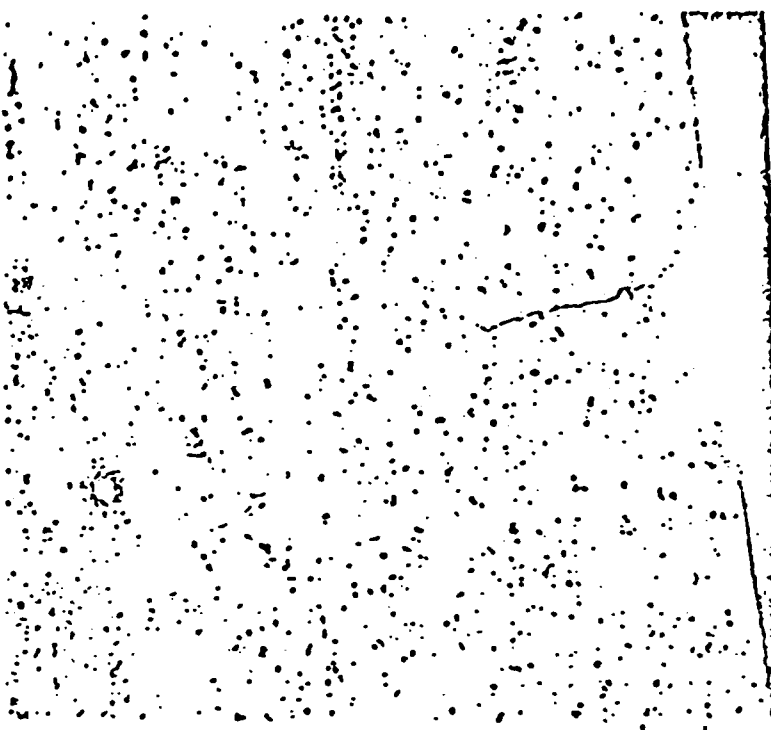
D

0.1 mm



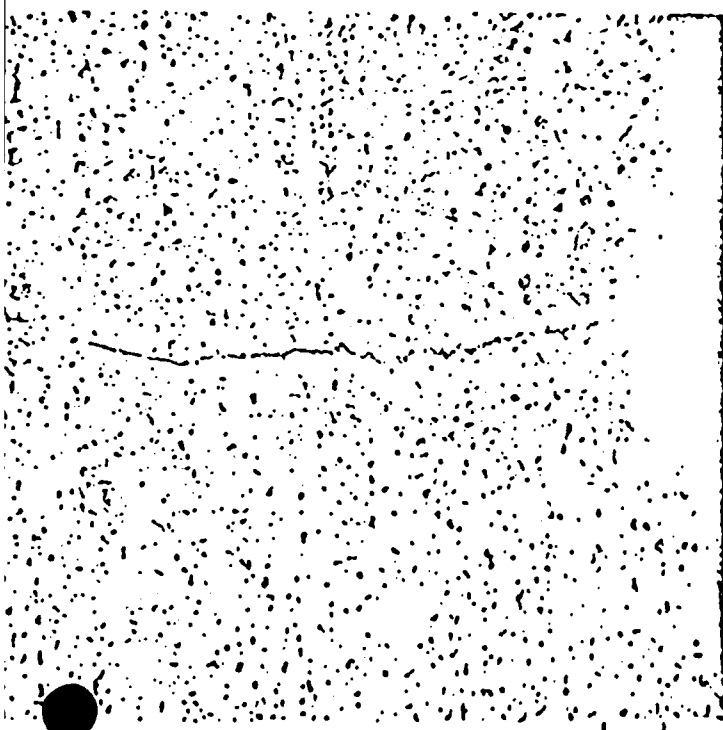
A

0.1mm



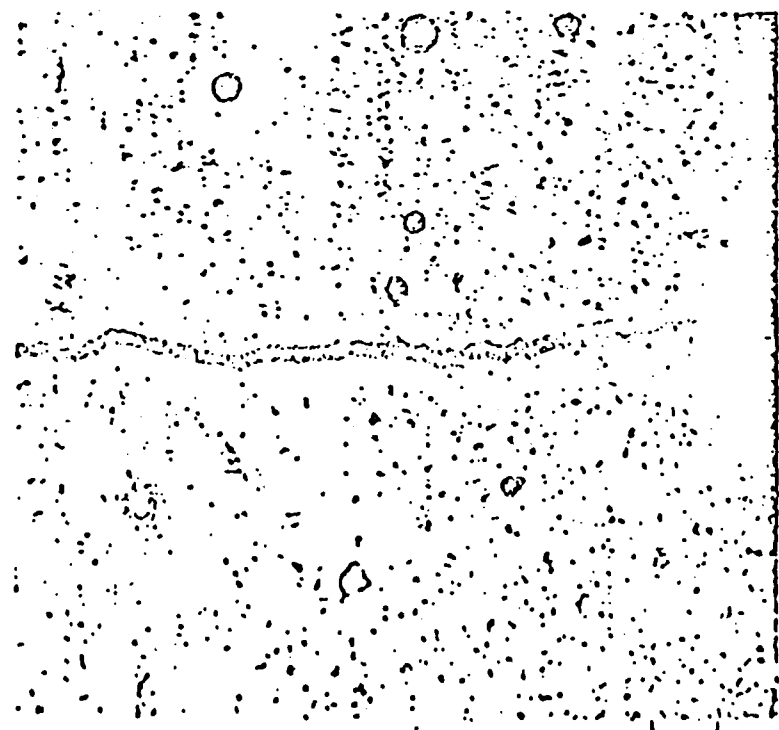
B

0.1mm



C

0.1mm



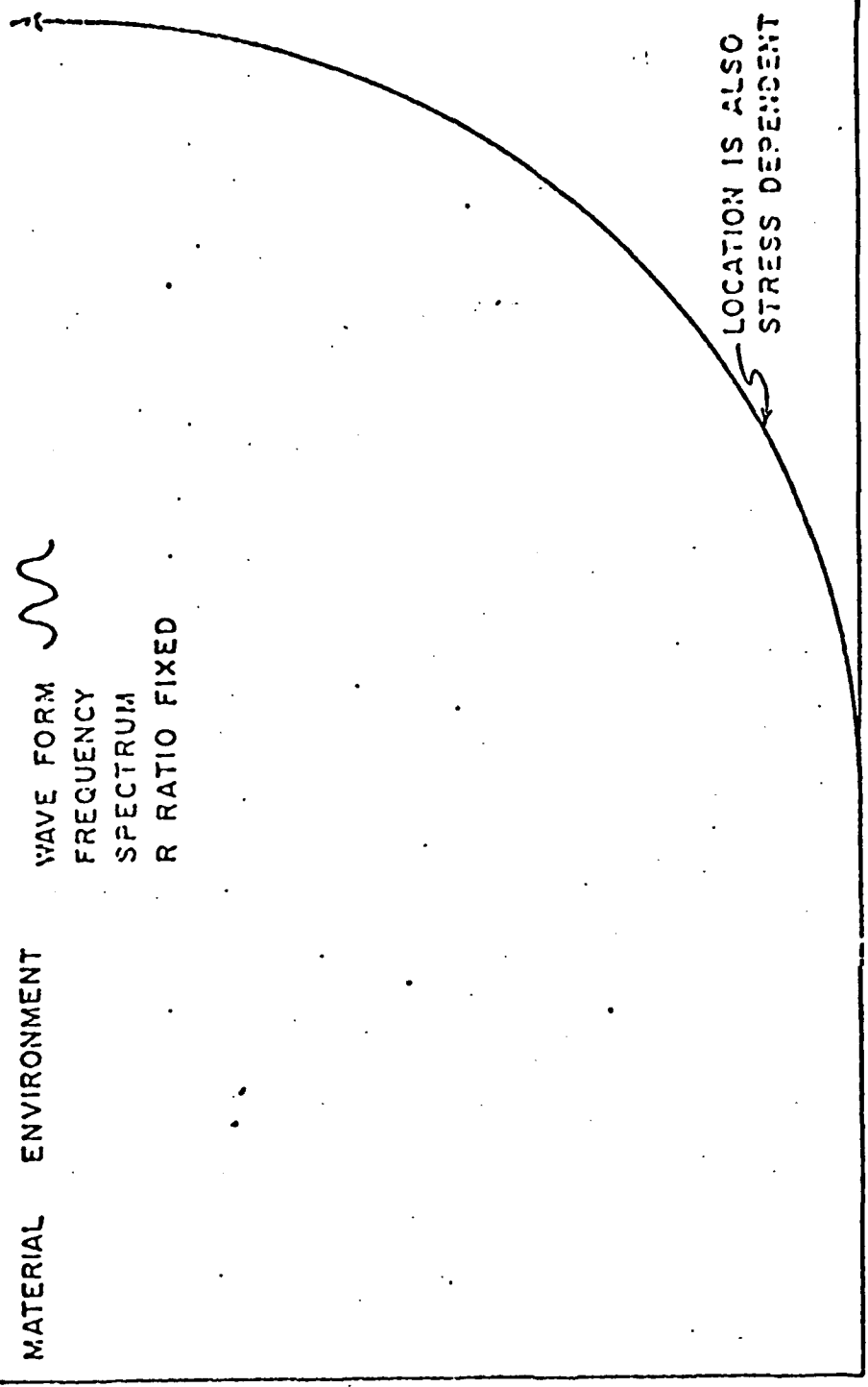
D

0.1mm

WAVE FORM   
 FREQUENCY  
 SPECTRUM  
 R RATIO FIXED

MATERIAL ENVIRONMENT

CRACK SIZE,

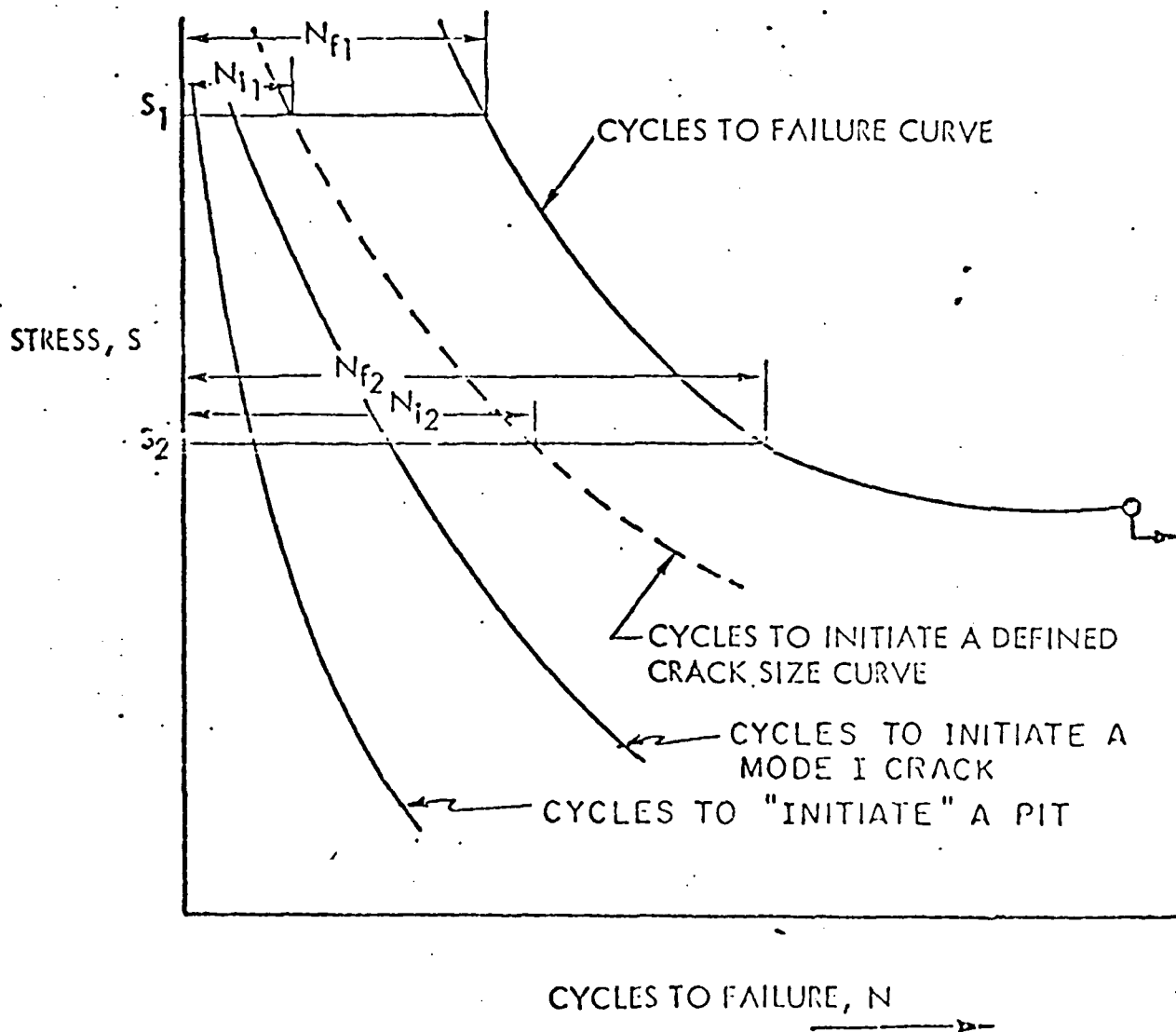


CYCLES, N  
(TIME)

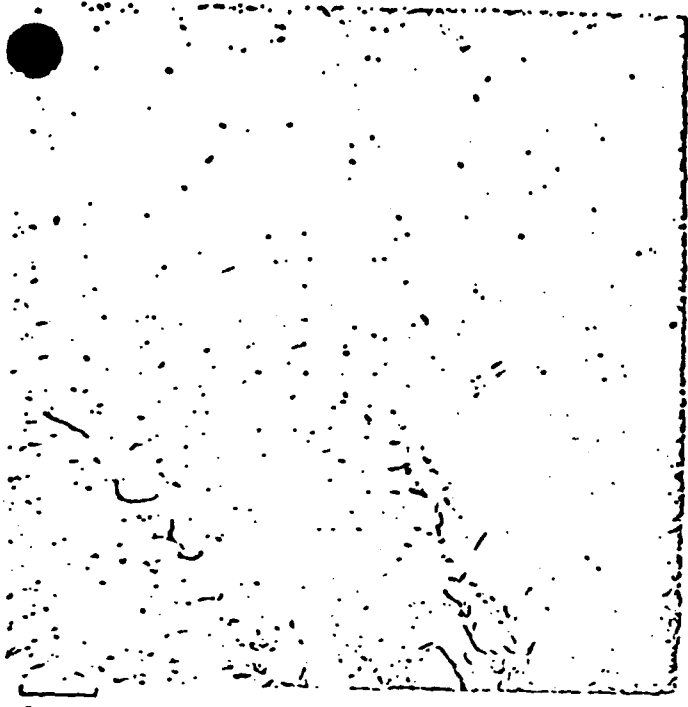
LOCATION IS ALSO  
STRESS DEPENDENT

① DEVELOPMENT OF PIT LARGE ENOUGH TO INITIATE A MODE I CRACK

GIVEN MATERIAL  
ENVIRONMENT FIXED  
FREQUENCY FIXED

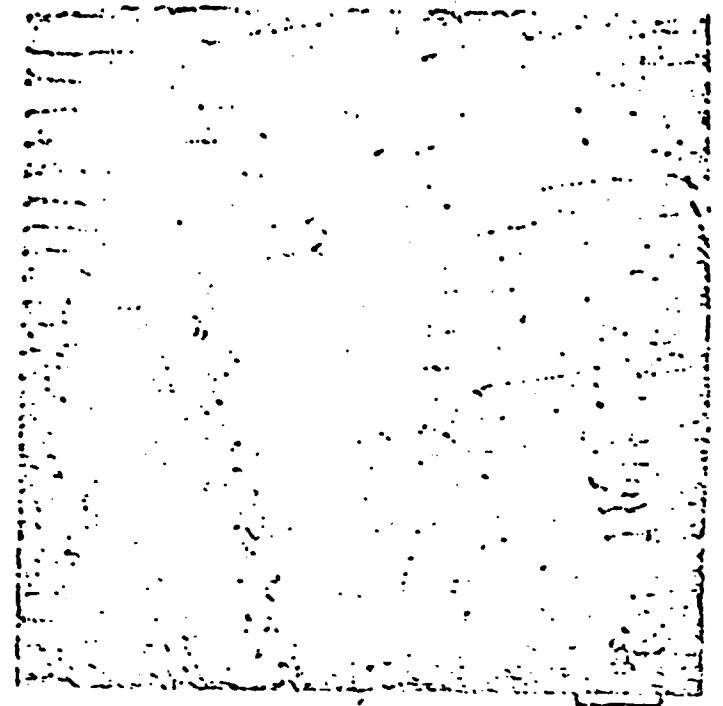


$$C_R = \frac{N_i}{N_f} = \text{CYCLE RATIO, THE RATIO OF THE NUMBER OF CYCLES TO INITIATE A CRACK AT A GIVEN STRESS TO THE NUMBER OF CYCLES TO FAILURE AT THE AT THE SAME STRESS}$$



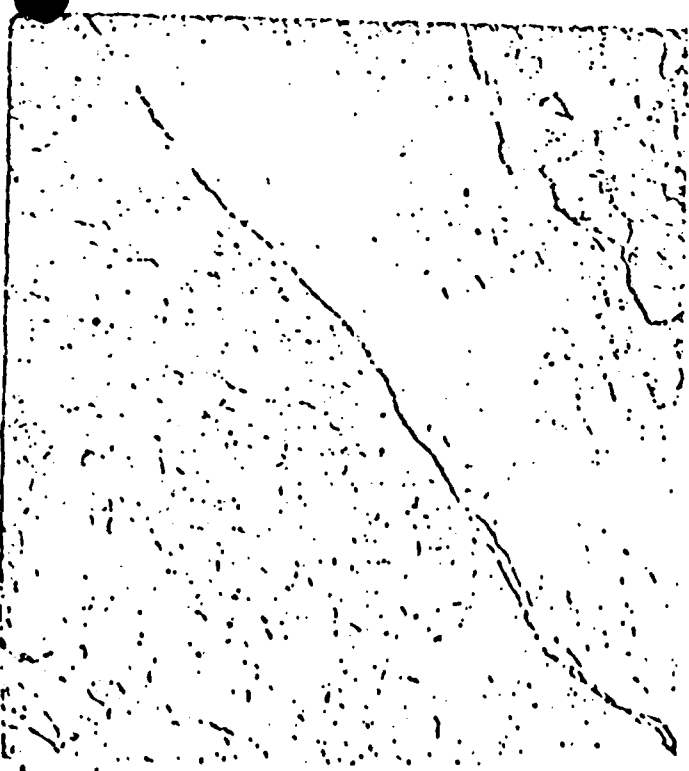
0.15 μm

A



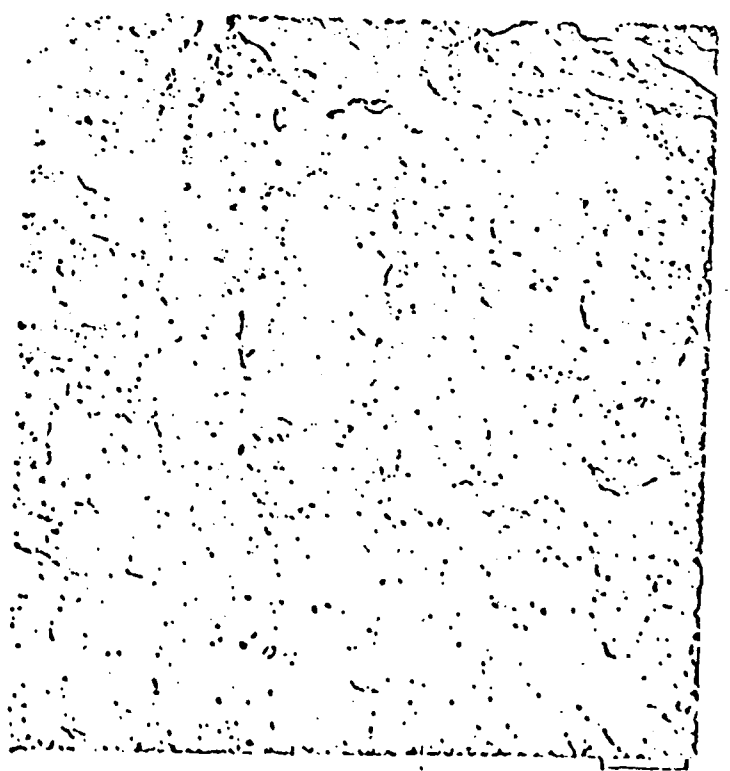
0.15 μm

B



0.15 μm

C



0.15 μm

D

PITTING AND FATIGUE CRACK  
INITIATION OF 2124-T851 ALUMINUM  
IN 3.5% NaCl SOLUTION

---

A Thesis  
Presented to  
The Faculty of the Graduate School  
University of Missouri-Columbia

---

In Partial Fulfillment  
of the Requirements for the Degree  
Master of Science

---

by  
James Michael Cox  
May, 1979

Dr. David W. Hoepfner

Thesis Supervisor

PITTING AND FATIGUE CRACK  
INITIATION OF 2124-T851 ALUMINUM  
IN 3.5% NaCl SOLUTION

James Michael Cox

Dr. David W. Hoepfner

Thesis Supervisor

ABSTRACT

The presence of a corrosive environment may have an effect upon the mechanical properties of a material. In addition, the corrosive properties of a material may be affected by mechanical loads. The following effort deals with several aspects of corrosion pit growth and fatigue-crack initiation in 2124-T851 Aluminum. Pitting rates under cyclic loading were to be determined and the pit dimensions at initiation were to be evaluated.

The results of this investigation indicates: 1) that under the given test conditions fatigue-crack growth rates are not altered by environment, 2) that a pitting environment significantly reduces the fatigue life of an unflawed specimen, 3) that there appears to be an endurance limit regardless of environment and 4) that fatigue-crack initiation from corrosion pits is poorly predicted by the method employed. Empirical pitting rate constants under cyclic loading could not be evaluated.

## ACKNOWLEDGMENTS

The author would like to thank Dr. David Hoeppe for his guidance and support throughout this study.

The author also wishes to acknowledge the support of this study by the Air Force Office of Scientific Research, contract number AFOSR 773178. The donation of the optical components and permission to carry forward the development of in situ observational techniques, initially developed at Lockheed California Company under the direction of Hoeppe and Danford, is greatly appreciated. Also the donation of the material used in this investigation by the Alcoa Company is appreciated.

A special thanks to Dr. Sharon Langenbeck and Mike Mayfield is due for their assistance in the compiling of this document and the preparation of the test system. The advice and technical assistance given by fellow graduate students is also greatly appreciated.

Finally, a very special thank you to Francis Hilliard to whom the author owes all.

## NOMENCLATURE

a	Crack length or Pit depth (in or mm)
$a_0$	Crack length of minimum detectible crack (in or mm)
$a/W$	Crack aspect ratio, or dimensionless crack length (in/in or mm/mm)
B	Thickness of specimen (in or cm)
C	Constant in Paris type equation
$C_s$	Cycle ratio ( $N_i/N_f$ )
d	Pit depth (in or mm)
$da/dN$	Crack growth rate (in/cycle or mm/cycle)
$d\sigma/dt$	Stress transient
e	Symbol for a single electron <u>or</u> Empirical Constant In Weibull Curve Fit Equation
$H^\circ$	Symbol for atomic hydrogen
$H^+$	Symbol for ionic hydrogen
k	Empirical constant
K	Stress intensity ( $ksi\sqrt{in}$ or $MPa\sqrt{m}$ ) <u>or</u> Empirical constant for pitting rate equation
$K_b$	Stress intensity at instability ( $ksi\sqrt{in}$ or $MPa\sqrt{m}$ )
$K_{Ic}$	Critical intensity at instability ( $ksi\sqrt{in}$ or $MPa\sqrt{m}$ )
$K_{max}$	Maximum stress intensity ( $ksi\sqrt{in}$ or $MPa\sqrt{m}$ )
$K_{min}$	Minimum stress intensity ( $ksi\sqrt{in}$ or $MPa\sqrt{m}$ )
$K_0$	Fatigue crack threshold stress intensity ( $ksi\sqrt{in}$ or $MPa\sqrt{m}$ )
ksi	Kilo-pounds per square inch (1 ksi = 6.895 MPa)

MPa	Mega Pascal or $10^6$ Pascal (unit of pressure or stress)
$m, n$	Empirical rate exponents
$N$	Number of cycles
$N_i$	Number of cycles to fatigue crack initiation
$N_f$	Number of cycles to failure
$P$	Load (lb or nt)
$P_f$	Fatigue loading
$P$	Stress ratio ( $S_{min}/S_{max}$ )
$S$	Stress (lb/in <sup>2</sup> or nt/cm <sup>2</sup> )
$S_A$	Alternating stress (kip or nt)
$S_{max}$	Maximum stress (kip or nt)
$S_{min}$	Minimum stress (kip or nt)
$t$	Time
$v$	Empirical constant
$W$	Specimen width (in or cm)
$\Delta K$	Stress intensity range ( $K_{max} - K_{min}$ ) (ksi $\sqrt{in}$ or MPa $\sqrt{m}$ )
$\sigma$	Stress (ksi or MPa)
$\sigma_{ys}$	Yield stress (ksi or MPa)
$\epsilon$	Strain (in/in or m/m)
$\phi$	Elliptical integral

## TABLE OF CONTENTS

	<u>Page</u>
Acknowledgements . . . . .	i
Nomenclature . . . . .	ii
Table of Contents . . . . .	iv
List of Figures . . . . .	vi
List of Tables . . . . .	x
 <b>Chapter</b>	
1.0 Introduction . . . . .	1
2.0 Objectives . . . . .	3
3.0 Technical Discussion . . . . .	4
3.1 Fatigue . . . . .	4
3.1.1 Fatigue Crack Propagation (FCP) . . . . .	9
3.1.2 Fatigue Crack Initiation . . . . .	12
3.1.3 Corrosion Fatigue . . . . .	14
3.2 Localized Corrosion-Pitting . . . . .	21
3.2.1 Pit Initiation . . . . .	22
3.2.2 Pit Growth . . . . .	30
3.2.3 Pit Growth Rates . . . . .	31
3.3 Stress In A Pit . . . . .	33
4.0 Material Characterization . . . . .	41
4.1 Chemical Analysis . . . . .	42
4.2 Orientation Terminology . . . . .	42
4.3 Hardness and Tensile Tests . . . . .	44
4.4 Fracture Toughness . . . . .	48
4.5 Microstructure . . . . .	48
4.6 Summary of Material Characteristics . . . . .	51
5.0 Experimental Program and Procedure . . . . .	59
5.1 Experimental Hypothesis . . . . .	59
5.2 Test Matrix . . . . .	60
5.3 Test Equipment . . . . .	60

	<u>Page</u>
5.4 Testing Procedure and Data Acquisition . . . . .	75
5.4.1 Testing Procedure and Data Acquisition For FCG Tests . . . . .	75
5.4.2 Testing Procedure and Data Acquisition For S-N Tests . . . . .	79
5.5 Data Reduction . . . . .	81
5.5.1 Data Reduction For FCG Tests . . . . .	81
5.5.2 Data Reduction For S-N Tests . . . . .	82
5.6 Fractography Procedure . . . . .	85
6.0 Results and Discussion . . . . .	86
6.1 Results and Discussion of FCG Tests . . . . .	86
6.2 Results and Discussion of S-N Tests . . . . .	98
6.2.1 Results and Discussion of S-N Data . . . . .	98
6.2.2 Results and Discussion of Pit Growth Analysis (Photographic Technique) . . . . .	102
6.2.3 Results and Discussion of Fatigue Loaded Pit Geometry . . . . .	102
6.2.4 Results and Discussion of the Semielliptical Surface Flaw Model of a Pit . . . . .	113
6.3 Results and Discussion of Fractographic Examination . . . . .	118
7.0 Conclusions . . . . .	137
8.0 Recommendations . . . . .	139
9.0 References . . . . .	140
Appendix . . . . .	145

## LIST OF FIGURES

	<u>Page</u>
1. Factors Affecting Response To Fatigue Loading . . . . .	2
2. Typical Loading Cycle and Terminology . . . . .	5
3. Typical S-N Curve . . . . .	7
4. Fatigue Process - Cycles To Initiation, Cycles To Failure . . . . .	8
5. Fatigue Design Problem . . . . .	10
6. The Three Regions of FCG . . . . .	11
7. Schematic of Intrusions and Extrusions Due To Slip . . .	15
8. Schematic Representation of Crack Tip Dissolution . . .	18
9. Schematic Representation of Crack Tip Dissolution and Hydrogen Embrittlement . . . . .	20
10. Pit Initiation Sequence . . . . .	24
11. Passive Material Subject to a Stress Transient . . . . .	27
12. Fracture of Oxide Layer Perpendicular to Stress Transient . . . . .	28
13. Fracture of Base-Oxide Interface . . . . .	29
14. Pit Growth Process . . . . .	32
15. Fatigue Process Resulting From Pitting Corrosion . . . . .	34
16. Pit Shape and Dimensioning . . . . .	36
17. Three Dimensional Idealization of Flaw (Pit) . . . . .	37
18. Semielliptical Surface Flaw . . . . .	39
19. Elliptical Integral Curve for Elliptical Flaws as a Function of Flaw Configuration . . . . .	40
20. Orientation Terminology . . . . .	45
21. Tensile Specimen . . . . .	47

	<u>Page</u>
22. Microstructural Specimens' Locations . . . . .	50
23. Microstructure of 2124-T851 Aluminum - Near Surface . . .	53
24. Microstructure of 2124-T851 Aluminum - 1/4 Deep . . . . .	55
25. Microstructure of 2124-T851 Aluminum - 1/2 Deep . . . . .	57
26. Test System Block Diagram . . . . .	62
27. Block Diagram of Camera System . . . . .	64
28. Optical Train Schematic Diagram . . . . .	66
29. Camera System Component Arrangement . . . . .	68
30. Optical Train and Camera . . . . .	68
31. Camera System and Hydraulic Lift Table . . . . .	70
32. Load Frame and Control Electronics . . . . .	70
33. Load Frame and Environment System . . . . .	72
34. S-N Specimen Chamber (Front) . . . . .	73
35. S-N Specimen Chamber (Back) . . . . .	74
36. Specimen, Chamber and Grip Arrangement . . . . .	77
37. WOL Specimen . . . . .	78
38. S-N Specimen . . . . .	80
39. a-N Data, Lab Air - Test 1 . . . . .	87
40. a-N Data, Lab Air - Test 2 . . . . .	88
41. a-N Data, Salt Water - Test 3 . . . . .	89
42. a-N Data, Salt Water - Test 4 . . . . .	90
43. FCP Data, Lab Air - Test 1 . . . . .	91
44. FCP Data, Lab Air - Test 2 . . . . .	92
45. FCP Data, Salt Water - Test 3 . . . . .	93

	<u>Page</u>
46. FCP Data, Salt Water - Test 4 . . . . .	94
47. FCP Curve Fit - Lab Air . . . . .	95
48. FCP Curve Fit - Salt Water . . . . .	96
49. FCP Curve Comparison; Lab Air - Salt Water . . . . .	97
50. S-N Data . . . . .	101
51. Bubbles Obscuring Pits During Testing . . . . .	104
52. Specimen With Corrosion Debris and Bubbles Near End of Test . . . . .	104
53. Pit Size Obscured by Corrosion Debris . . . . .	106
54. Example of Pit Dimension Measurements . . . . .	108
55. Example of Pit Dimension Measurements . . . . .	110
56. Example of Pit Dimension Measurements . . . . .	112
57. Pit Depth - Maximum Stress Correlation . . . . .	115
58. Pit Geometry - Maximum Stress Correlation . . . . .	116
59. Stress Intensity - Maximum Stress Correlation . . . . .	117
60. Actual - Calculated Pit Depth Comparison . . . . .	119
61. Pit Depth Ratio - Maximum Stress Correlation . . . . .	120
62. Typical Fracture Surface In Low $\Delta K$ Region - Lab Air - WOL . . . . .	122
63. Typical Fracture Surface In Lower Intermediate $\Delta K$ Region - Lab Air - WOL . . . . .	122
64. Typical Fracture Surface In Intermediate $\Delta K$ Region - Lab Air - WOL . . . . .	124
65. Typical Fracture Surface In High $\Delta K$ Region - Lab Air - WOL . . . . .	124
66. Typical Fracture Surface in Lower Intermediate $\Delta K$ Region - Salt Water - WOL . . . . .	126

	<u>Page</u>
67. Typical Fracture Surface In Intermediate $\Delta K$ Region - Salt Water - WOL . . . . .	126
68. Typical Fracture Surface In High $\Delta K$ Region - Salt Water - WOL . . . . .	128
69. Fracture Surface Near the Initiation Point - Lab Air - S-N . . . . .	130
70. Fracture Surface Away From the Initiation Point - Lab Air - S-N . . . . .	130
71. Fracture Surface Near the Initiation Point - Salt Water - S-N . . . . .	132
72. Fracture Surface Away From the Initiation Point - Salt Water - S-N . . . . .	132
73. Striations On Air Specimen At Cleavage - Ductile Tearing Transition - S-N . . . . .	134
74. Striations On Salt Water Specimen At Cleavage - Ductile Tearing Transition - S-N . . . . .	134

## LIST OF TABLES

	<u>Page</u>
1. Comparison Of Chemical Compositions . . . . .	43
2. Mechanical Properties Of 2124-T851 And 2024-T851 . . . . .	46
3. Fracture Toughness Values For 2124-T851 And 2024-T851 . . . . .	49
4. Test System Component List . . . . .	63
5. S-N Data And Reduction . . . . .	99
6. Pit Dimensions And Calculations For Fatigue Crack Initiation . . . . .	114

## 1.0 INTRODUCTION

As progress has been made in fatigue life analysis, the material structure, R-ratio, frequency, waveform, load spectra, stress state and flaw type have emerged as important factors. Recently it has become more and more apparent that environment also plays a major role and that synergistic effects between all of the above factors are more severe than previously anticipated. These factors and their interactions are shown in Figure 1 (1)\*.

This relatively new knowledge is quite disturbing in that it seems to necessitate fatigue tests for each particular combination of material structure, R-ratio, frequency ... and environment encountered in order that we might design reliable structures. However, if the mechanisms by which the above phenomena occur can be understood, then it will be possible to circumvent at least part of that testing. This work considers one such mechanism, what might be termed the mechanism of mode I fatigue crack initiation by pitting corrosion, and provides a preliminary attempt at quantifying its effects.

---

\*Numbers in parentheses ( ) refer to References, page 140.



## 2.0 OBJECTIVES

The general objective of this investigation was to advance the development of a method of determining the fatigue life of a structure subjected to a pitting attack. The specific objectives were:

- a) To determine the feasibility of surface photography in establishing pit growth rates in 2124-T851 aluminum.
- b) To illustrate environmental effects on both initiation and propagation of fatigue cracks.
- c) To apply an empirical pitting rate method to actual fatigue pitting.
- d) To determine if crack initiation values ( $K_{oc}$ ) derived from pit dimensions and a semielliptical surface flow model correlate with crack initiation values ( $K_{ocp}$ ) derived from a linear regression Weibull curve fit of crack propagation data ( $da/dN$  vs  $\Delta K$ ).
- e) To correlate fracture modes found on pitting initiated fracture surfaces with those found on the more common crack propagation type specimen.

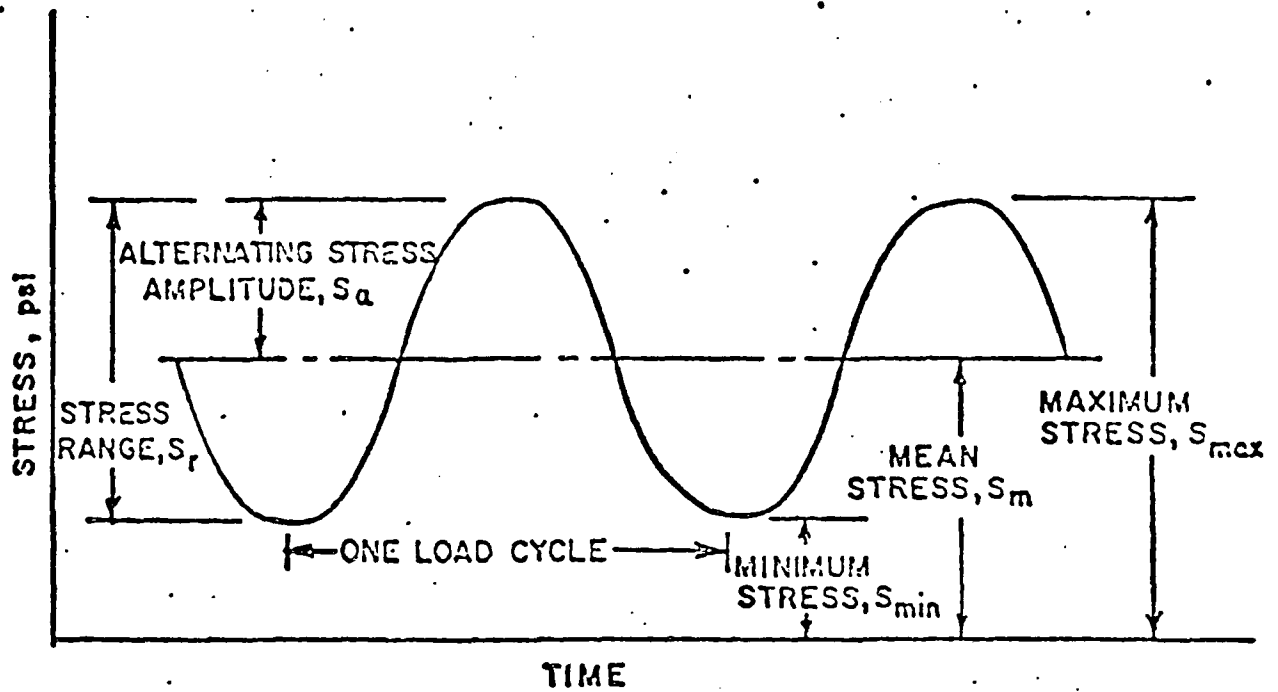
### 3.0 TECHNICAL DISCUSSION

To understand the phenomenon of a fatigue crack initiating at a corrosion pit and to meet the objectives of this investigation, knowledge must be acquired from a variety of fields. These fields have been loosely arranged into three areas and are reported upon in the following sections.

#### 3.1 Fatigue

Fatigue might be generally described as the degradation of structural reliability due to an alternating stress field. More precisely it might be termed as subcritical flaw extension due to an alternating stress field. (A representation of an alternating stress field along with other terms typically associated with fatigue is illustrated in Figure 2.) Since nearly all structures are subjected to alternating stress fields, the potential for fatigue to occur is enormous. This is borne out by the numerous failures which are attributed to fatigue every year.

The fatigue phenomenon has been recognized for centuries but the first significant analysis did not occur until slightly over one-hundred years ago (2). From that time until the middle of this century, fatigue was treated by what may be termed as "the classical treatment of fatigue" (3). This treatment involved the testing of what were thought to be unflawed specimens at constant amplitude alternating stress levels. The data generated from such tests were plotted as a stress (S) vs number of cycles (N) to failure curve.



NOTE THAT:  $S_m = \frac{S_{max} + S_{min}}{2}$ ,  $S_r = S_{max} - S_{min}$ ,

$$S_a = \frac{S_r}{2} = \frac{S_{max} - S_{min}}{2}$$

R or A = STRESS RATIO

$$R = \frac{S_{min}}{S_{max}}, \quad A = \frac{S_a}{S_m}$$

$$\text{and } R = \frac{1-A}{1+A}, \quad A = \frac{1-R}{1+R}$$

Figure 2: Typical Loading Cycle and Terminology

This curve, Figure 3, has become commonly known as an S-N diagram. Fatigue design during this period was relatively simple and consisted of keeping the nominal stresses in a component at levels below the endurance limit (the endurance limit being the maximum stress level at which failure due to cyclic loading does not occur).

The next major innovation in fatigue technology, which did not occur until the 1940's, was conceptually based upon the work of C.E. Inglis in 1913 (4). Inglis was the first to acknowledge the presence of flaws in a material and their role as stress raisers. Shortly after the work by Inglis, Alan A. Griffith proposed the first viable interpretation of flaw extension and developed a mathematical expression relating the extension of a crack to elastic strain energy at the crack tip (5).

Based upon Griffith's model and the observation of subcritical fatigue crack growth, researchers in the forties and fifties proposed that the fatigue phenomenon occurred in three separate stages, namely initiation, propagation, and unstable fracture. For a period, fatigue analysis was concentrated almost exclusively upon the propagation phase and it was not until recently that attention has been directed toward that portion of the fatigue life devoted to initiation (6,7). The importance of initiation studies is revealed when one considers that, dependent upon several factors, initiation can account for a major portion of fatigue life (Figure 4).

A proper fatigue analysis must account for all three regimes of crack growth (the third regime, unstable fracture, must be taken into

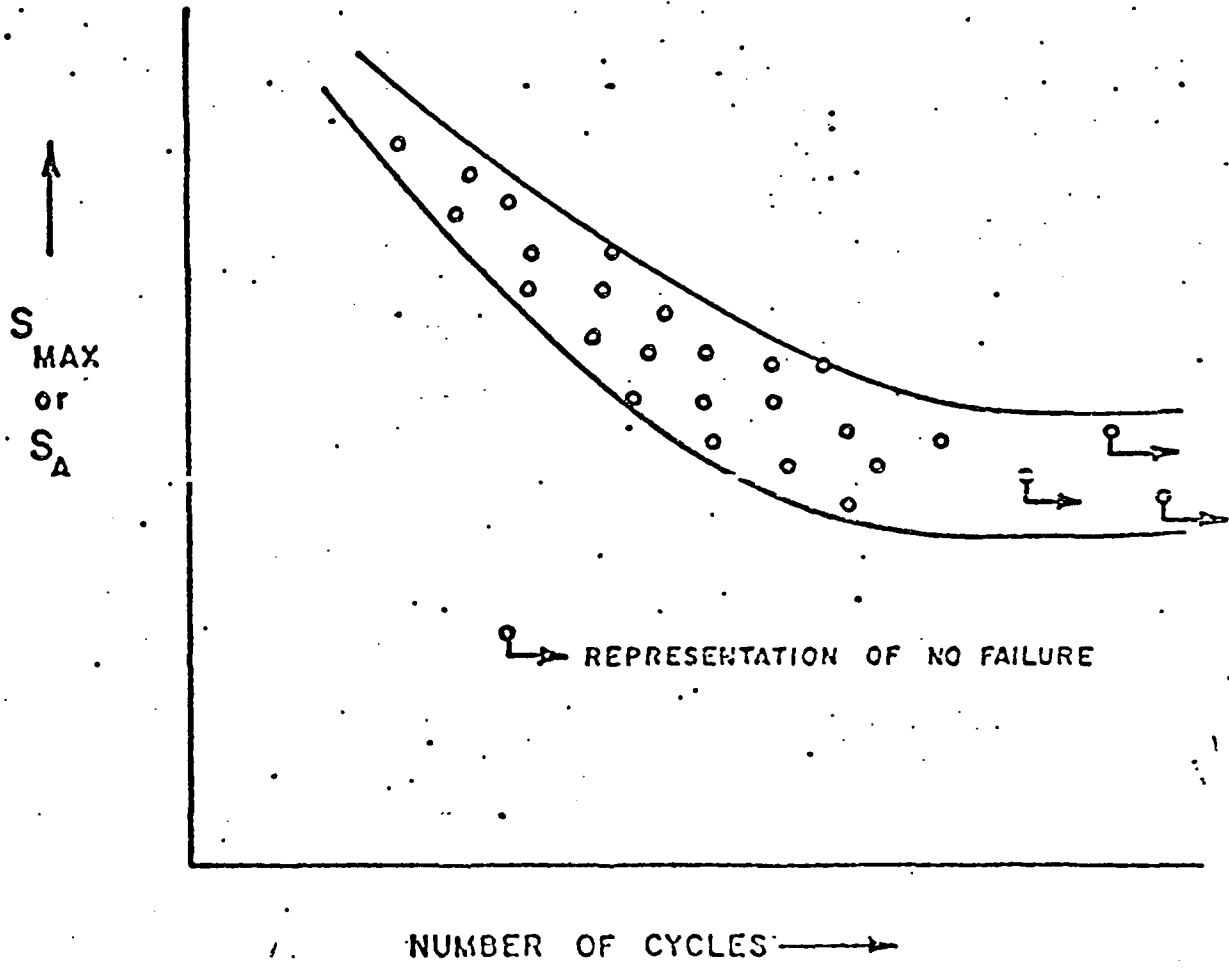


Figure 3: Typical S-N Curve

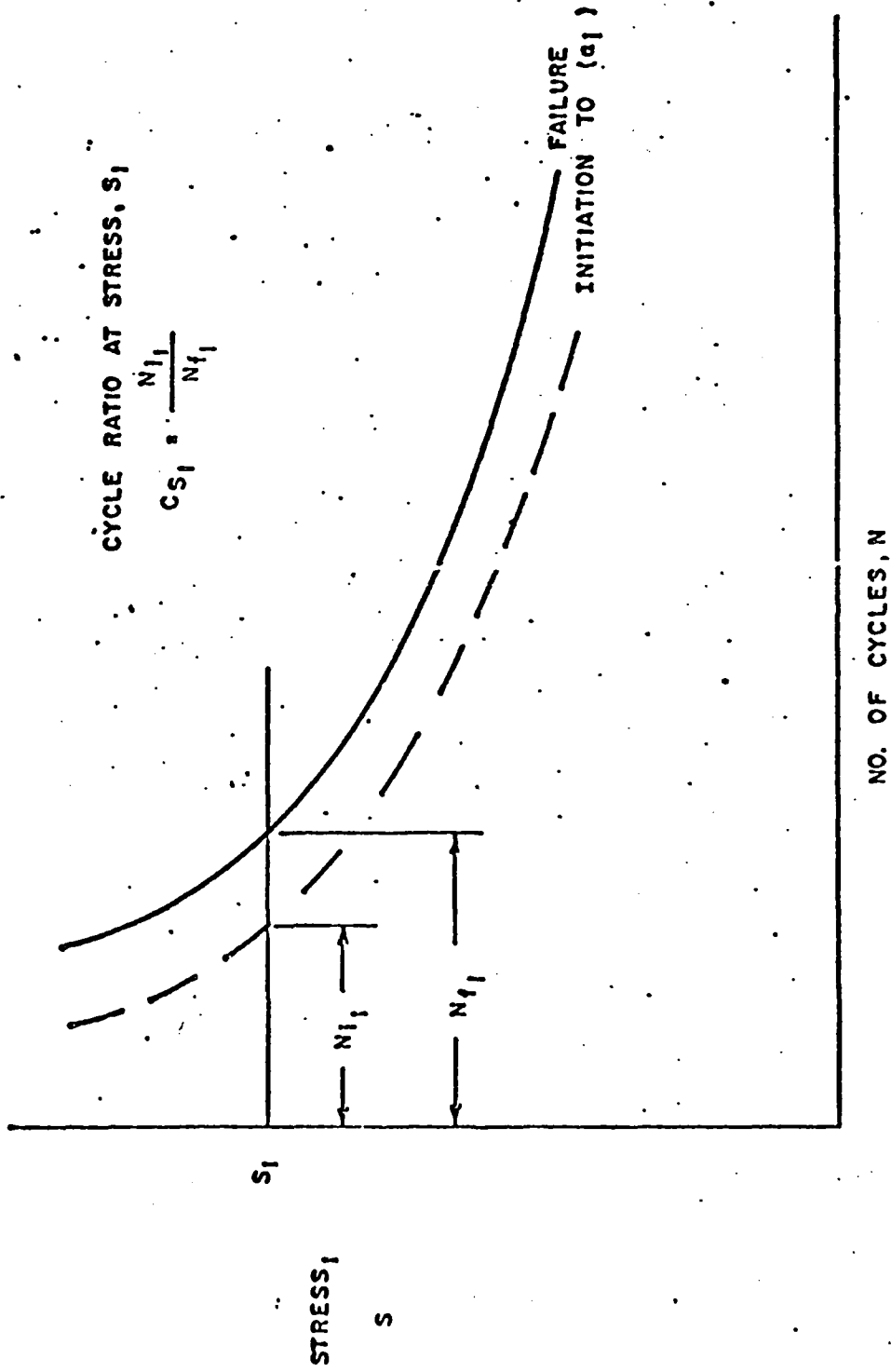


Figure 4: Fatigue Process - Cycles To Initiation, Cycles to Failure

account for the obvious reason that it terminates the process). Figure 5 identifies the fatigue designer's problem and suggests some of the variables which might tend to emphasize one regime or another.

### 3.1.1 Fatigue Crack Propagation (FCP)

Over the past thirty years fatigue crack growth (FCG) design technology has rapidly evolved (8, 9 and 3). The general procedure is to determine crack growth rates for given conditions and then to somehow integrate an equation which describes the growth rate thereby establishing a 'safe life'. The rate equation is typically of the form:

$$\frac{da}{dN} = f(S, a, \phi) \quad (1)$$

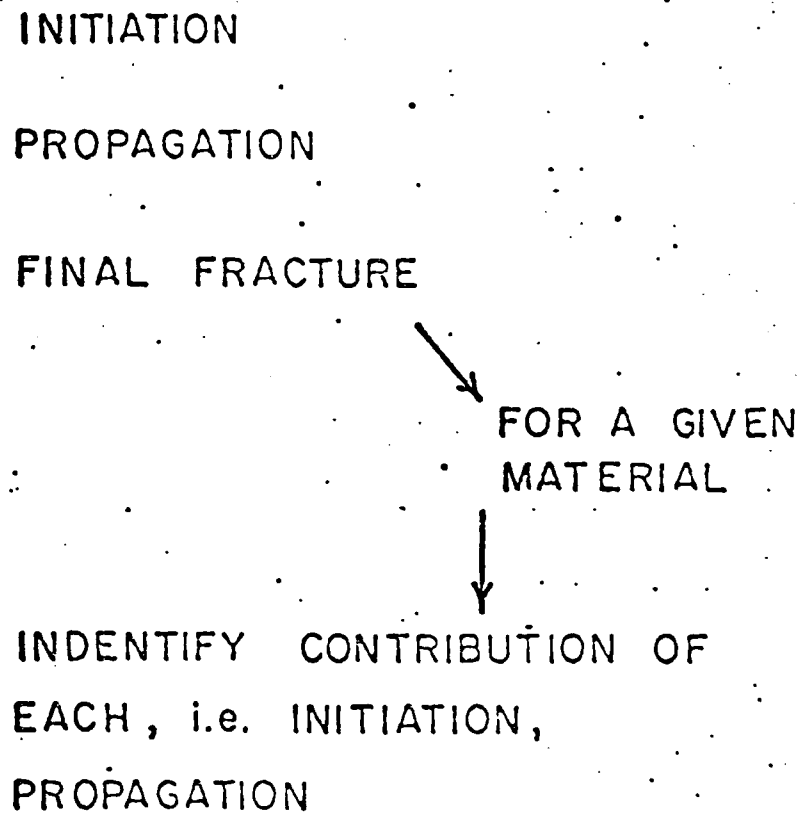
where  $da/dN$  is the FCG rate (in/cycles), and  $f(S, a, \phi)$  is a function of the gross stress ( $S$ ), the crack length ( $a$ ), and the geometrical or shape conditions ( $\phi$ ).

Numerous proposals for fatigue crack propagation 'laws' in the form of Equation (1) have been developed recently. Several of these may be found in a paper by Hoepfner and Krupp (3). Almost all of these proposed FCG 'laws' suffer from the same inadequacy. Briefly stated, most of these FCG 'laws' are inadequate either because they fail to describe all three regions of crack growth (Figure 6) or because they require one to assume the FCG threshold ( $K_0$ ) and/or the FCG instability stress intensity ( $K_b$ ).

INITIATION

PROPAGATION

FINAL FRACTURE



FOR A GIVEN  
MATERIAL

IDENTIFY CONTRIBUTION OF  
EACH, i.e. INITIATION,  
PROPAGATION

THE CONTRIBUTION OF EACH WILL VARY WITH MATERIAL,  
PROCESSING, APPLIED LOAD LEVELS, GEOMETRY, ENVIRONMENT  
CONTAMINANT, FREQUENCY, CONTAMINANT CONCENTRATION

Figure 5: Fatigue Design Problem

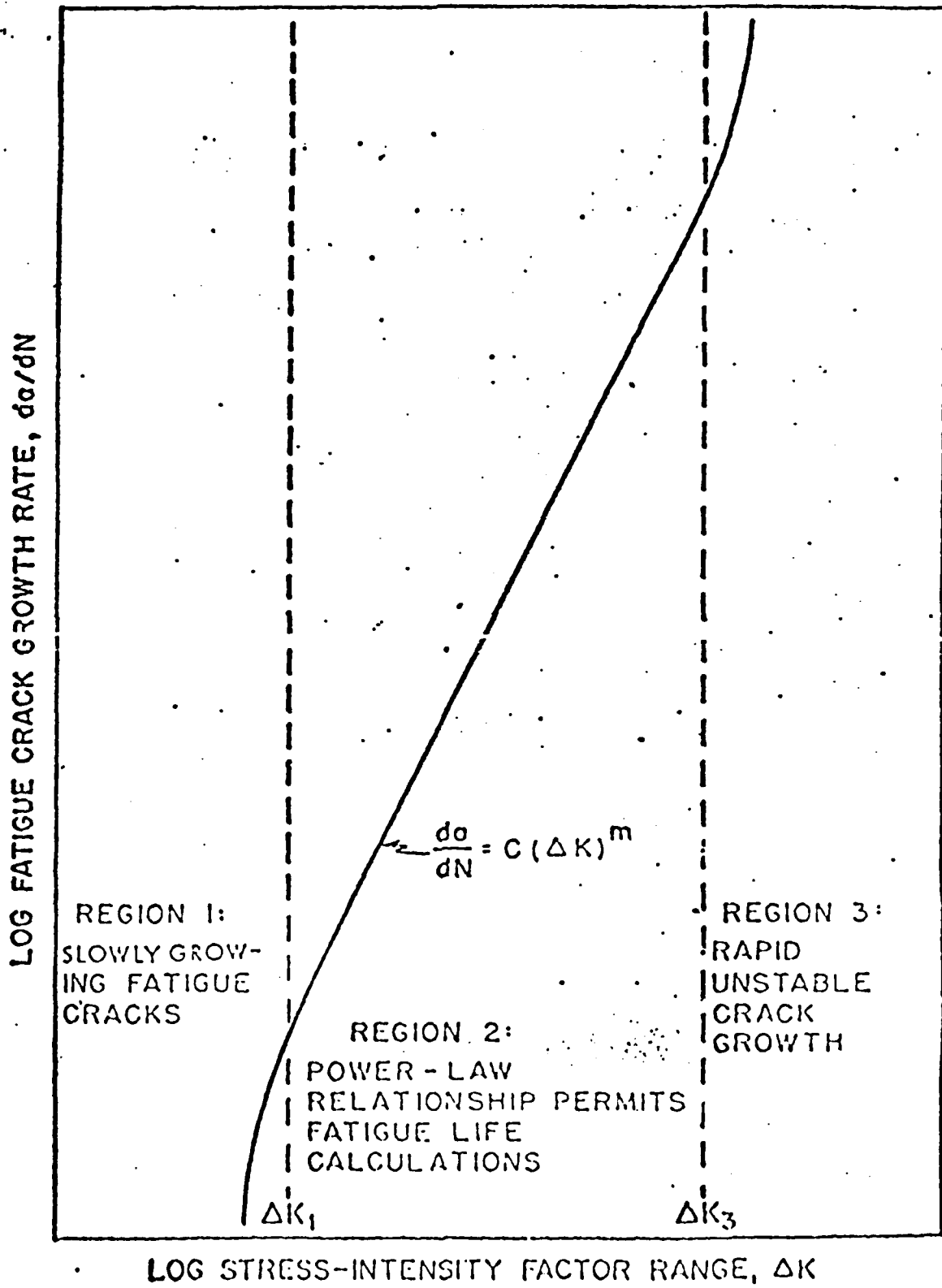


Figure 6: The Three Regions of FCG

A relationship which does not suffer from either of the above mentioned inadequacies was developed by Bowie and Hoepfner (10). The relationship, known as "the four parameter Weibul survivorship function", is given as:

$$\frac{da}{dN} = e + (v-e) \left( -\ln \left( 1 - \frac{K}{K_b} \right) \right)^{1/k} \quad (2)$$

where  $k$ ,  $e$ , and  $v$  are empirical constants and  $K_b$  is the stress intensity range where  $da/dN$  is infinitely large. All four of these parameters may be analytically determined through a regression analysis. The details of this analysis (which was further developed at the University of Missouri - Columbia (11, 12)) will not be discussed here. The reader is referred to the work of Mueller (13) for an in depth discussion.

A unique feature of this relationship is realized by extrapolating to the lower asymptotic, condition,  $da/dN = 0$ . When this is done the threshold stress intensity,  $K_0$  can be solved for, as done in Equation 3:

$$K_0 = K_b \left\{ 1 - \exp \left[ -\left( \frac{v-e}{v} \right)^k \right] \right\}^{1/k} \quad (3)$$

### 3.1.2 Fatigue Crack Initiation

Whenever fatigue crack initiation is discussed a basic difficulty is always encountered. That difficulty being the definition of initiation itself. In the field, initiation is most often defined as a fatigue crack of size  $a_0$  which is the smallest size the nondestructive

testing (NDT) equipment employed can detect. Initiation, defined in this manner, then becomes a function of the NDT technique involved, the NDT properties of the material tested, and the location and orientation of any particular flaw sought. While this particular definition is adequate and applicable to many situations, it is not related in any way to fatigue crack initiation. Since the mechanistic theory of initiation is just beginning to emerge it would be presumptuous for this author to define what constitutes true initiation at this time. Instead, some proposed fatigue crack initiation mechanisms will be discussed. From this discussion it is hoped that at least a basis for the definition of initiation can be found for the case at hand.

It is becoming generally recognized that both fatigue crack initiation and propagation are a result of microplastic flow and constraint to deformation. The known processes that may lead to fatigue crack initiation are slip, twinning, cleavage, grain boundary flow or fracture, phase boundary flow or fracture, and particle boundary flow or fracture (14, 15). These processes are generally thought to occur at continuum discontinuities, however under specific conditions they may develop from pure deformation and the subsequent interaction of point or line defects. It is interesting to note that all processes mentioned are internal phenomena rather than surface phenomena.

As a result of this plastic flow theory some researchers (16) have attempted to determine  $K_0$  values from plastic parameters such as the shear modulus. Attempts of this sort, while claiming success, seem to neglect the fact that macroscopically determined parameters, such

as the shear modulus, are gross generalizations when they are applied to the microscopic level (17).

It now appears that the dislocation structures generated near a fatigue crack are different from those found in the general bulk (18, 19). In the bulk, the dislocations are arranged in veins or cell walls in what might be termed an open weave density. Near the crack tip, dislocations are found to arrange themselves in well defined ladder or cell structures (18, 19). These dislocation structures near the crack tip are the result of both generation and transfer of dislocations from the surrounding matrix. The highly defined ladder or cell structure approximately corresponds to the plastic zone size calculated by fracture mechanics (18).

While the above discussion pertains to a preexistent crack it is found that the same type of structure develops at initiation sites. When these structures are found at initiation points they have been termed persistent slip bands (PSB). Some researchers have theorized that the PSB result in intrusions and extrusions (Figure 7) which develop into fatigue cracks (19, 20). While this particular theory is far from proven it does appear that the development of bands of high dislocation density surrounding a matrix of relatively low dislocation density is a prerequisite for both initiation and propagation of fatigue cracks.

### 3.1.3 Corrosion Fatigue

As fatigue research has progressed, it has become more apparent

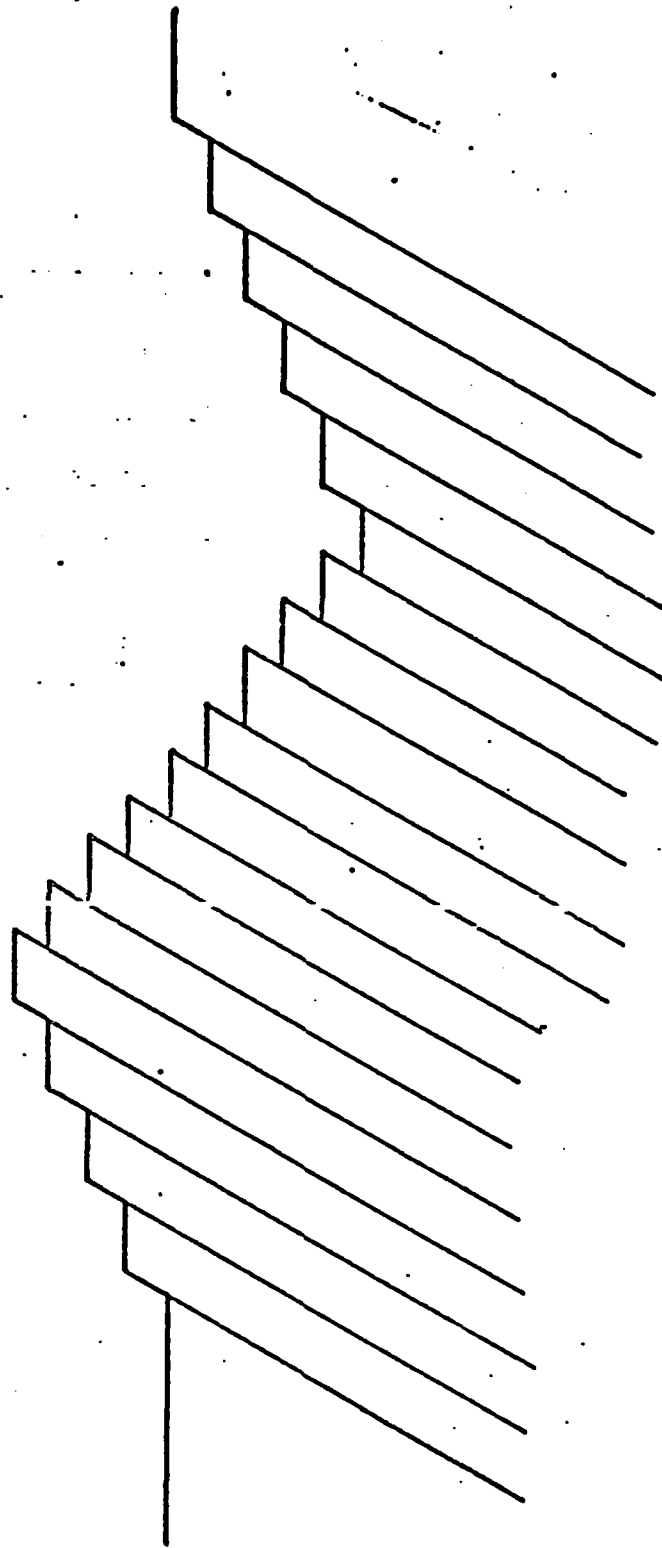


Figure 7: Schematic of Intrusions and Extrusions Due to Slip

that environment is an important factor. Laboratory air tests which were once thought to represent pure fatigue have since been shown to be sensitive to the testing humidity among other environmental parameters. As a result, extensive research on corrosion fatigue has led to the traditional model which superimposes the stress corrosion cracking phenomenon upon the fatigue phenomenon. As a result the phrase, 'the synergistic effects between corrosion and fatigue', has become popular in recent years. This synergistic interaction is known to affect both the initiation and propagation stages of corrosion fatigue in several ways (21). In general, the more severe the environment the less time is required to initiate a fatigue crack and the higher the fatigue crack growth rate.

Since fatigue crack initiation is poorly understood it is no wonder corrosion aided fatigue crack initiation is even less well understood. It has been reported that there is a relationship between the previously mentioned persistent slip bands and the electrochemical dissolution rate (22). It is theorized that more severe environments accelerate the process by which PSB lead to initiation (19). It is not clear at this time whether this acceleration is due to the dissolution of certain structures within the PSB or some other mechanical-chemical process. However, it does seem evident that any comprehensive theory on corrosion fatigue crack initiation must take into consideration the process of oxide or film growth, passivation, and diffusion, and their effects upon the near-surface dislocation structures and local mechanical properties.

When fatigue crack growth occurs in an active environment, interactions occur at the crack tip which generally decreases the fatigue life. Several different theories have been developed which attempt to explain these interactions, however most of them are based upon the same theoretical driving force. That driving force might be explained in the following way. As the local stress is increased and the crack begins to propagate, resulting in the formation of two new surfaces, the freshly exposed surfaces are anodic to the rest of the structure. Under normal circumstances the anodic crack tip area is much, much smaller than the area of the rest of the structure and thus extremely high dissolution rates should occur there, Figure 8 (23). As a result, transient oxidation or passivation effects on the order of milliseconds become very important (19). This explains the often observed frequency effects in corrosion fatigue growth rates (24, 25). Another parameter which is often seen to have an effect on the growth rate is the R-ratio (26, 27). This effect may be explained on the basis of the crack tip opening displacement which limits the access of the corrosive environment to the freshly exposed surfaces. It should be noted that the local chemistry near the crack tip is quite different from that of the bulk solution (19).

As mentioned previously, several theories, all based on the same theoretical driving mechanism, have been developed which attempt to explain corrosion fatigue. These theories might be divided into three separate categories (19):

- 1) theories involving dissolution of metal at the tip,

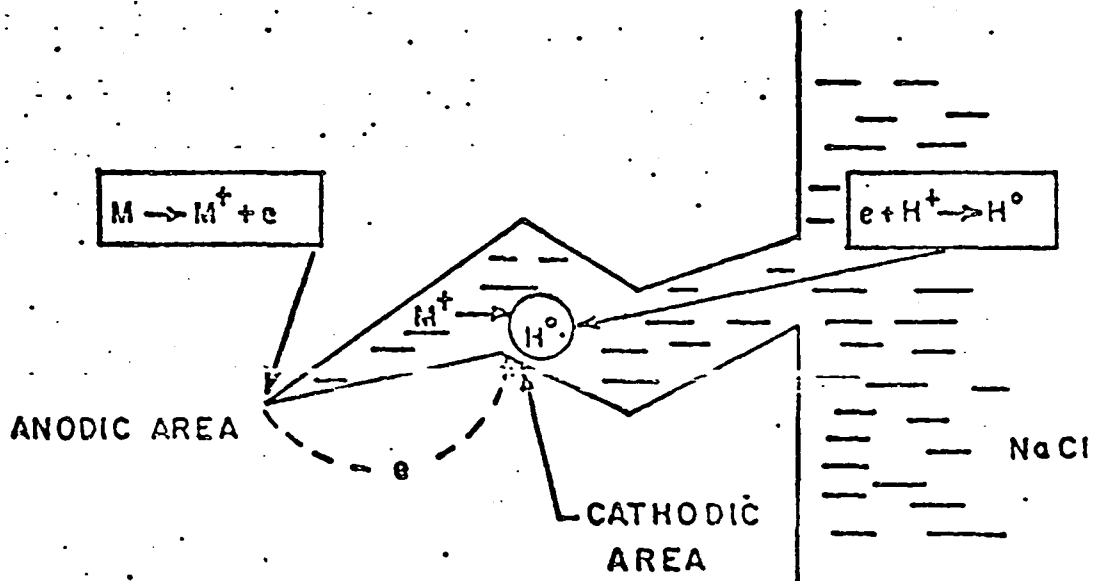


Figure 8: Schematic Representation of Crack Tip Dissolution

- 2) theories involving essentially mechanical crack tip effects,
- 3) theories involving changes in the local deformation character of the material at the crack tip.

Theories of the first type (28) simply attribute the increased crack growth rates to the anodic dissolution at the crack tip. From this type of theory it follows that increased anodic reactions result in increased growth rates. However this is not always the case (29).

The second group of theories suggests that the mechanical properties at the crack tip are altered or that the crack tip geometry itself is altered. This alteration results from the environmentally controlled change in the crack tip oxide film and film growth. As an example, a ductile to brittle transition of the oxide film might increase the growth rate by effectively sharpening the crack tip (30).

The third group of theories relates the changes in crack growth rate to changes in the mechanical properties in the plastic zone. These theories depend upon the diffusion of elemental species into the metallic lattice. It is proposed that the diffused specie either reduces the cohesive strength of the material sufficiently to promote a cleavage mode of fracture (31) or, dependent upon the conditions, has a hydrogen embrittlement type effect (32). Interestingly, hydrogen would be expected to be generated near a propagating crack tip in an aqueous environment (23). Figure 9 (23) conjecturally illustrates how crack tip dissolution could result in atomic hydrogen entering the metallic lattice. For an in-depth review of hydrogen embrittlement

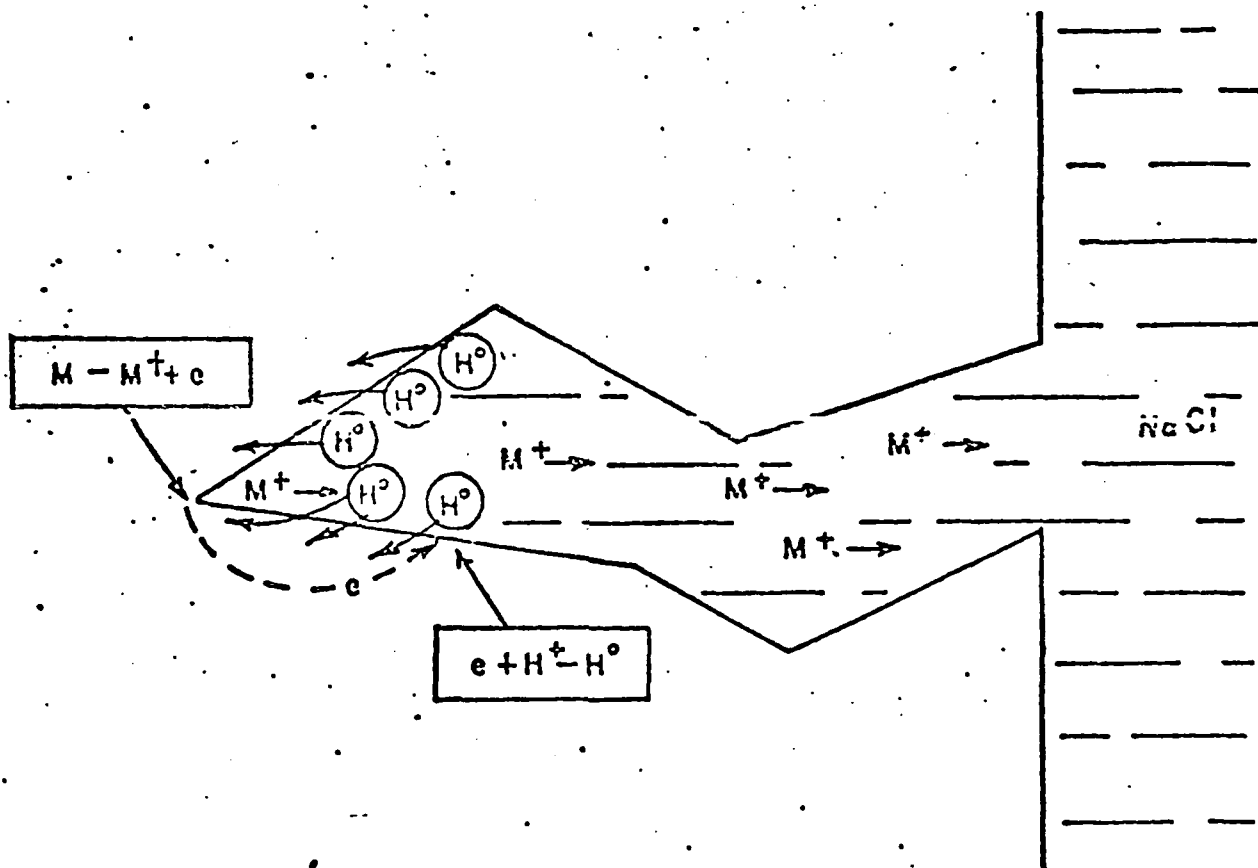


Figure 9: Schematic Representation of Crack Tip Dissolution and Hydrogen Embrittlement

the reader is referred to references 33, 34, 35 and 36.

Since none of the above mentioned theories can completely account for all cases of environmentally accelerated fatigue crack growth, it is suggested that all of them may play a role with particular environments in combination with specific materials determining which mechanism(s) is (are) dominant. If this is indeed true, corrosion fatigue effects will not be analytically predicted for some time to come.

### 3.2 Localized Corrosion - Pitting

Corrosion has been described as the destructive attack of a metal by chemical or electrochemical reaction with its environment (37). The monetary cost of corrosion to the civilized world each year is staggering. Much of this monetary loss is accounted for by forms of corrosion which lead to an obvious degradation and eventual replacement of a part. But perhaps ethically more important are those types of corrosion which are difficult to detect, since they could often lead to the leakage of hazardous materials or to sudden fracture, either of which could endanger human lives. A prime example of this type of corrosion is known as pitting. While pitting occurs in many materials, attention here will be directed specifically to the pitting of aluminum alloys in a sodium chloride solution.

Metals which owe their corrosion resistance to passivation (passivation is a result of an oxide barrier film between the base metal and the environment) may be susceptible to pitting when certain environments are encountered (38). Aluminum is generally resistant to corrosion due to its passive film and therefore is potentially susceptible

to pitting. For pitting to occur the environmental presence of certain anions is required. The most prevalent pitting anion is  $\text{Cl}^-$ , however  $\text{Br}^-$ ,  $\text{I}^-$ , and  $\text{F}^-$  are also encountered (39). Pitting is an extremely localized attack of a metal. Corrosion pits may generally be described as semielliptical cavities in a material and are caused by chemical or electrochemical reactions. Pits may be found singly, or more often, distributed in an apparently random fashion across the metal's surface (38). The pits' small size plus the fact that they are often filled and obscured by corrosion products and other debris, makes them difficult to detect (38).

Any evaluation of pitting must address two distinct and sequential subjects: 1) pit initiation and 2) pit growth. Pit initiation involves the understanding of the mechanism and the possible retardation of that mechanism. Pit growth involves the chemical kinetics of a pit once it has been initiated.

### 3.2.1 Pit Initiation

When approaching the subject of pit initiation on an unstressed aluminum surface exposed to a brine solution, two major questions present themselves:

- a) By what mechanism does pit initiation occur?
- b) Why do certain areas on the aluminum surface induce a pit to initiate? In other words, what kind of physical discontinuities, in either the metal or the solution, establish the chemical or electrochemical forces necessary to initiate a pit?

The first question might be answered in the following way. Aluminum immersed in a sodium chloride solution forms a protective surface film (i.e. it becomes passive) which slows the corrosive process to a minimum. It is hypothesized that chloride ions ( $\text{Cl}^-$ ) locally breakdown this passivity and initiate pits. The process by which this breakdown occurs is not definitely known but is thought to involve two steps: 1) adsorption of  $\text{Cl}^-$  on the oxide-solution interface under the influence of an electric field and 2) the formation of a basic hydroxy chloride aluminum salt which is readily soluble (Figure 10). As the passive layer is locally dissolved, chloride ions are drawn to that area due to the increased local corrosion rate. This increase in  $\text{Cl}^-$  concentration causes an increased dissolution of the oxide layer, which causes more  $\text{Cl}^-$  to be drawn to the site and on and on until the oxide layer no longer forms because its constituents immediately go into solution (37). At that point, the pit can be said to have completed initiation and be in the pit growth phase.

The answer to the second question has not yet been formalized into a precise theory, but general observations may be made. First it seems obvious that the initiation site is determined by some sort of local discontinuity since a localized attack occurs. The cause of the initial imbalance in corrosion rates (and therefore the initial imbalance in  $\text{Cl}^-$  concentration) could be due to any number of things such as a small surface scratch, a discontinuity in the protective oxide film, a dislocation which intersects the surface of the metal, certain grain orientations, grain boundaries, or perhaps just the random variations in

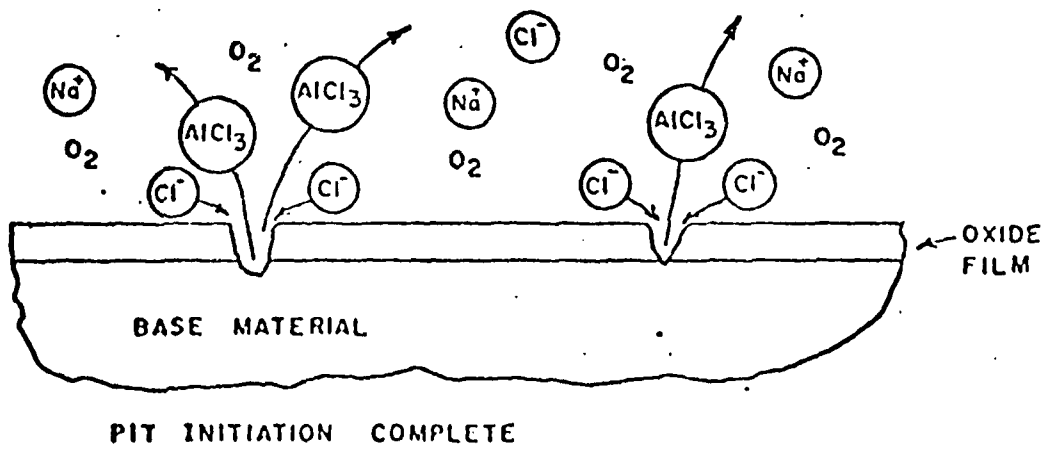
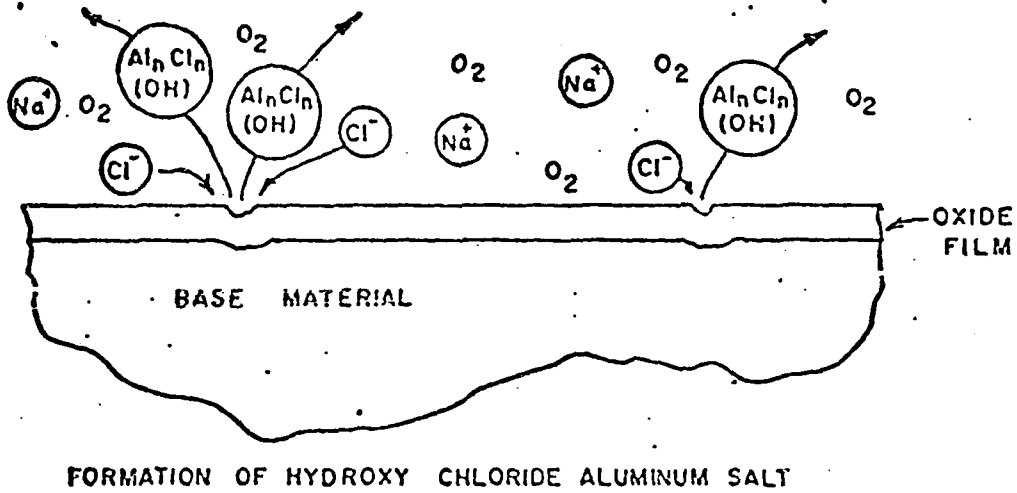
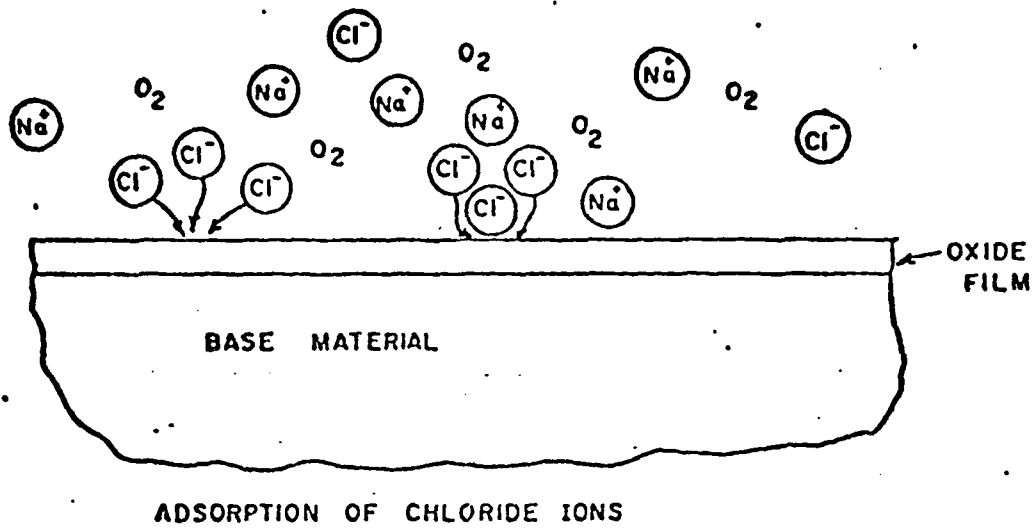


Figure 10: Pit Initiation Sequence

solution composition (37, 38). It is apparent that during the initiation and early growth stages of a pit, conditions are especially unstable in that any stray convection current can easily sweep away the localized chloride ions responsible and thus allow the relatively stable surface film to return. This instability has been experimentally observed (38).

Pit initiation up to this point has only been discussed for the situation where the material is statically stressed. Literature concerning how the mechanism is altered when the base material is experiencing a stress (and necessarily a strain) transient is sparse. This is surprising since most materials experience stress transients of one type or another. Since little has been published on this subject the author will propose a theory based upon a projection of what has been published and upon the author's basic mechanical knowledge. It should be remembered that this theory has not, to the author's knowledge, been experimentally proven.

Since the oxide film is both chemically and structurally different from the base material we must consider the mechanical system to consist of two separate materials with different physical properties. A truly effective passive film (such as the type typically associated with aluminum) is continuous and coherent. It also has a strong affinity for the base metal and is normally very thin relative to the base material (38). Also oxide films tend to be much more brittle than their base materials.

When a structure which is immersed in a pitting environment is

subjected to a stress transient (in this case simple tension (Figure 11)) the base material may be under either stress controlled or strain controlled conditions. It seems reasonable to assume that the oxide film's addition to the load carrying capacity is negligible. Therefore the oxide film is always subjected to strain controlled conditions since it adheres to the base material. When certain strain levels are attained the brittle oxide layer should fracture exposing base material and thus accelerating initiation.

The fracture of the oxide layer might occur in either of two ways. The first way would involve fracture through the oxide layer in a direction normal to the tensile strains. Since the strain is primarily transferred from the base material to the film through shear loading along the interface rather than through the oxide layer itself, fracture should occur in numerous places causing a ladder type appearance (Figure 12). As a result we would expect numerous initiation sites. The second type of fracture which might occur would begin along the oxide-base interface effectively separating the oxide layer from the base on a local level. As these local separations become larger, fracture would eventually occur in a direction normal to the surface causing the oxide layer to flake off. This type of process would expose relatively large areas of base metal to the environment thus significantly accelerating pit initiation (Figure 13).

When strains in the oxide layer are insufficient to cause fracture, pit initiation should still be accelerated. The acceleration would be due to higher diffusion rates in a strained structure. This

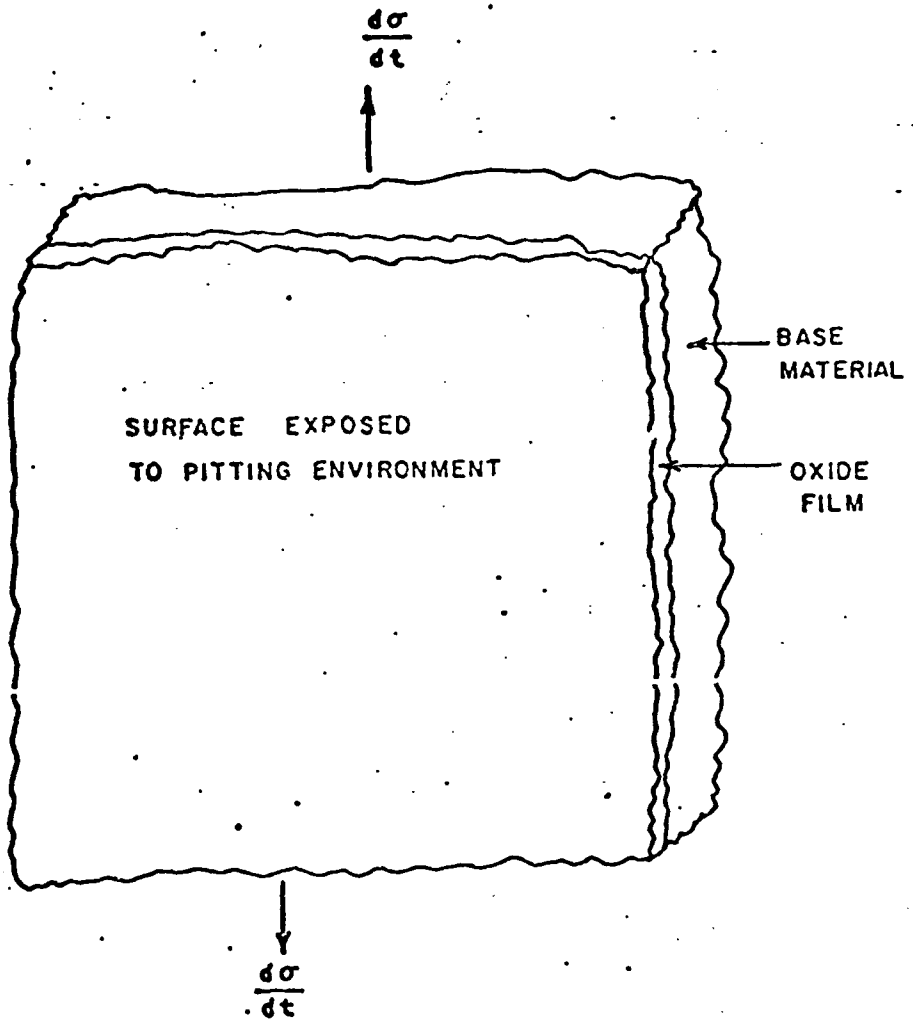


Figure 11: Passive Material Subject to a Stress Transient

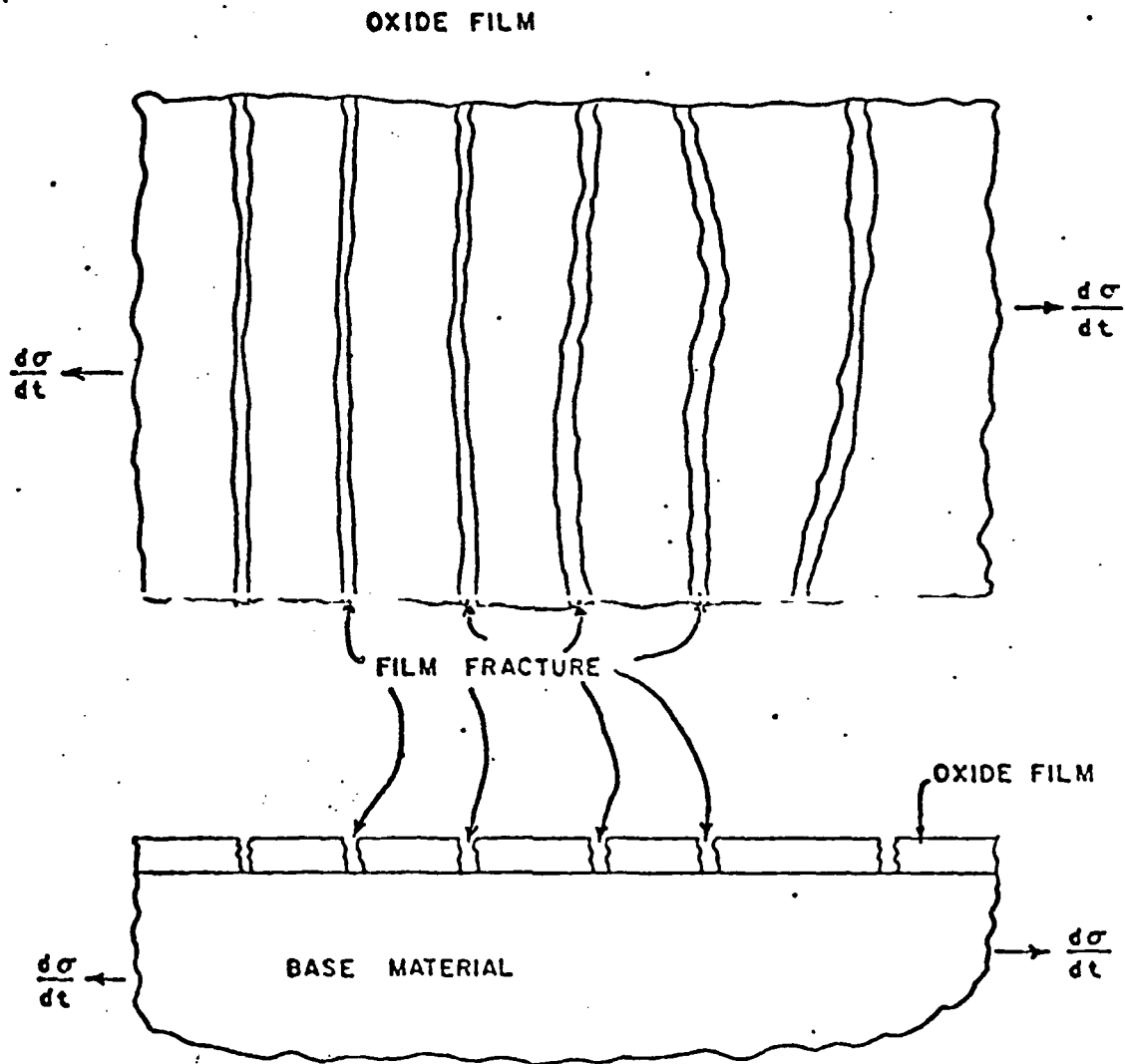


Figure 12: Fracture of Oxide Layer Perpendicular to Stress Transient

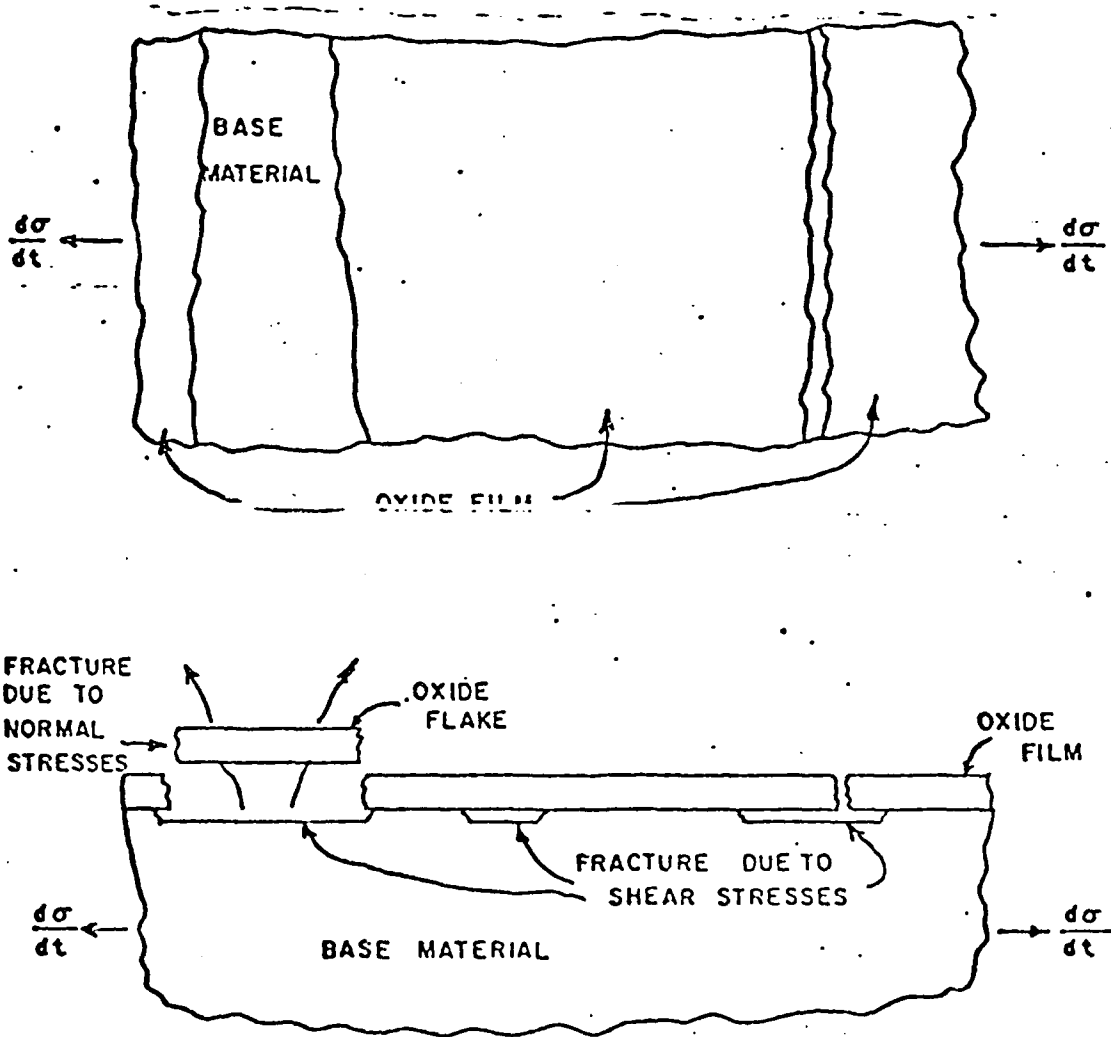


Figure 13: Fracture of Base-Oxide Interface

is assuming that pit initiation is in fact at least partially controlled by a diffusion process.

When a structure is subjected to a fatigue type loading rather than a single transient, one would expect the minimum strain at which oxide fracture occurs to be lowered. In addition, if the mechanically induced, newly exposed surfaces repassivate the process would start again. This suggests that under certain conditions, fatigue crack initiation might occur as a result of successive cracking and subsequent passivation.

### 3.2.2 Pit Growth

Once a pit has been initiated the question arises as to what mechanism continues its growth. A corrosion pit is a unique type of anodic reaction. It is an autocatalytic process (37). That is, the corrosion process within a pit produces conditions which are both stimulating and necessary for the continued growth of the pit. The mechanism in effect involves the rapid dissolution of aluminum ions within the pit, while oxygen reduction takes place on adjacent surfaces (37). (The presence of copper containing phases accelerates the reduction of oxygen and thus the pitting process (38)). The rapid dissolution of metal within the pit tends to produce an excess of positive charge in this area resulting in the migration of chloride ions so as to maintain electroneutrality (38). These chloride ions combine with the aluminum ions, usually in the form of  $AlCl_3$  (40), and disperse into the solution due to that compound's high solubility. This then adds to the force driving the pit's growth at an ever-

accelerating pace which is limited only by the diffusion rates. In a sense, pits cathodically protect the rest of the metal's surface (37). Figure 14 illustrates the pit growth mechanism.

The effect of stress, and in particular fatigue stresses, upon pit growth is about as poorly understood as it is for pit initiation. However, in the author's opinion, at least two opposing effects are involved. The first effect would be that the dissolution of aluminum would be aided by the potential energy increase due to the material straining. The second effect is a result of the volume change within the pit as the structure is cycled. As the volume is expanded and then contracted a pumping action would occur which would tend to aid in the dispersion of the localized chloride concentration and thus add to pit growth instability.

### 3.2.3 Pit Growth Rates

Corrosion pitting has been found to be related to area of exposure, time of exposure and the material/environment under consideration. At this time the two equations used to determine pit depth are due to Scott (41) et al., and Godard (42). They are, respectively,

$$a = bA^2 \quad (4)$$

and

$$a = C_1 (t)^{1/3} \quad (5)$$

where

a = maximum pit depth

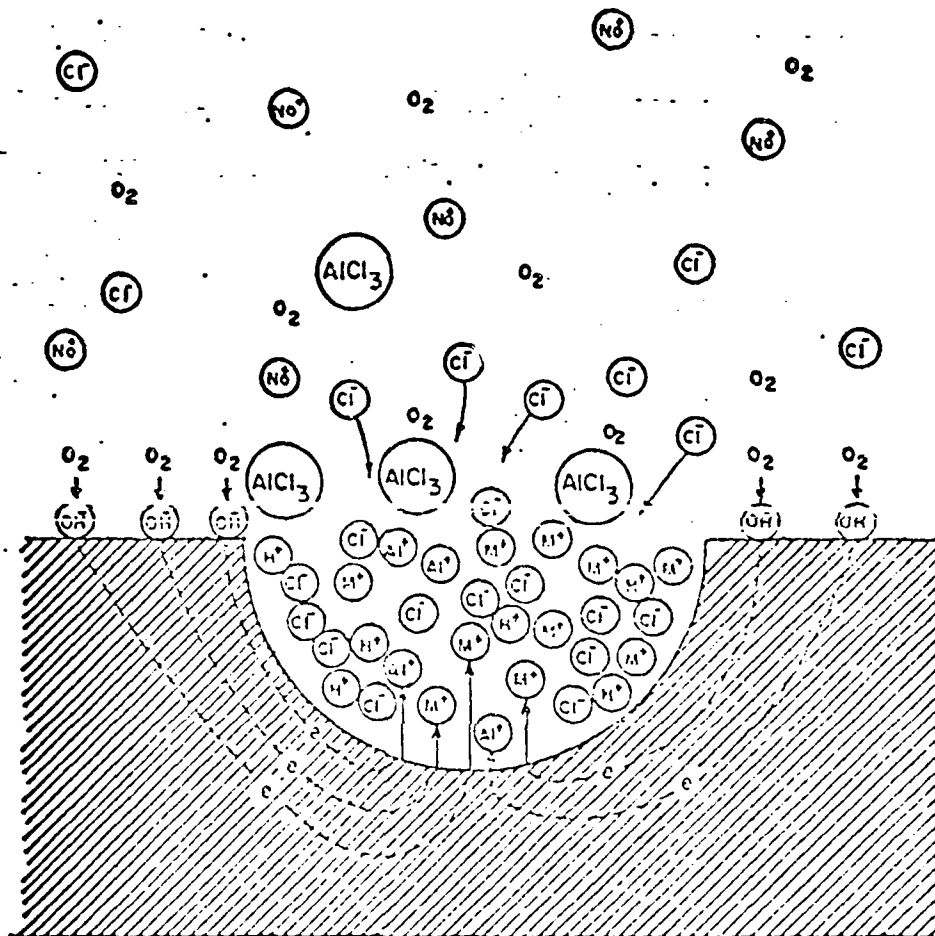


Figure 14: Pit Growth Process

$A$  = area of exposure

$t$  = time

$b, C_1$  = are parameters related to the material/environment combination

The first equation above is based upon allowing exposure time to be constant while the second is based upon allowing exposure area to be constant. Since  $C_1$  and  $b$  are material/environment parameters they must be determined experimentally.

Another applicable method of determining pitting rates under specific conditions is the use of extreme value statistics. An excellent analysis on this subject is presented by Aziz (43).

### 3.3 Stress In A Pit

The importance of pitting to the present work is that pits are natural stress raisers and therefore potential sites for fatigue crack initiation (Figure 15). As such it is important to establish an analytical method for determining the stress at the pit. The first step in determining any analytical method is to geometrically describe the flaw (pit). As is generally the case, this step is a major barrier which can only be overcome by idealization of the true geometrical shape (most often extremely complex) into a manageable shape. Manageable shape in this case being a shape which is easily defined mathematically. The validity of any evaluation will be dependent upon the degree of idealization. Therefore it seems necessary to determine the true geometrical shape of the flaw before the validity

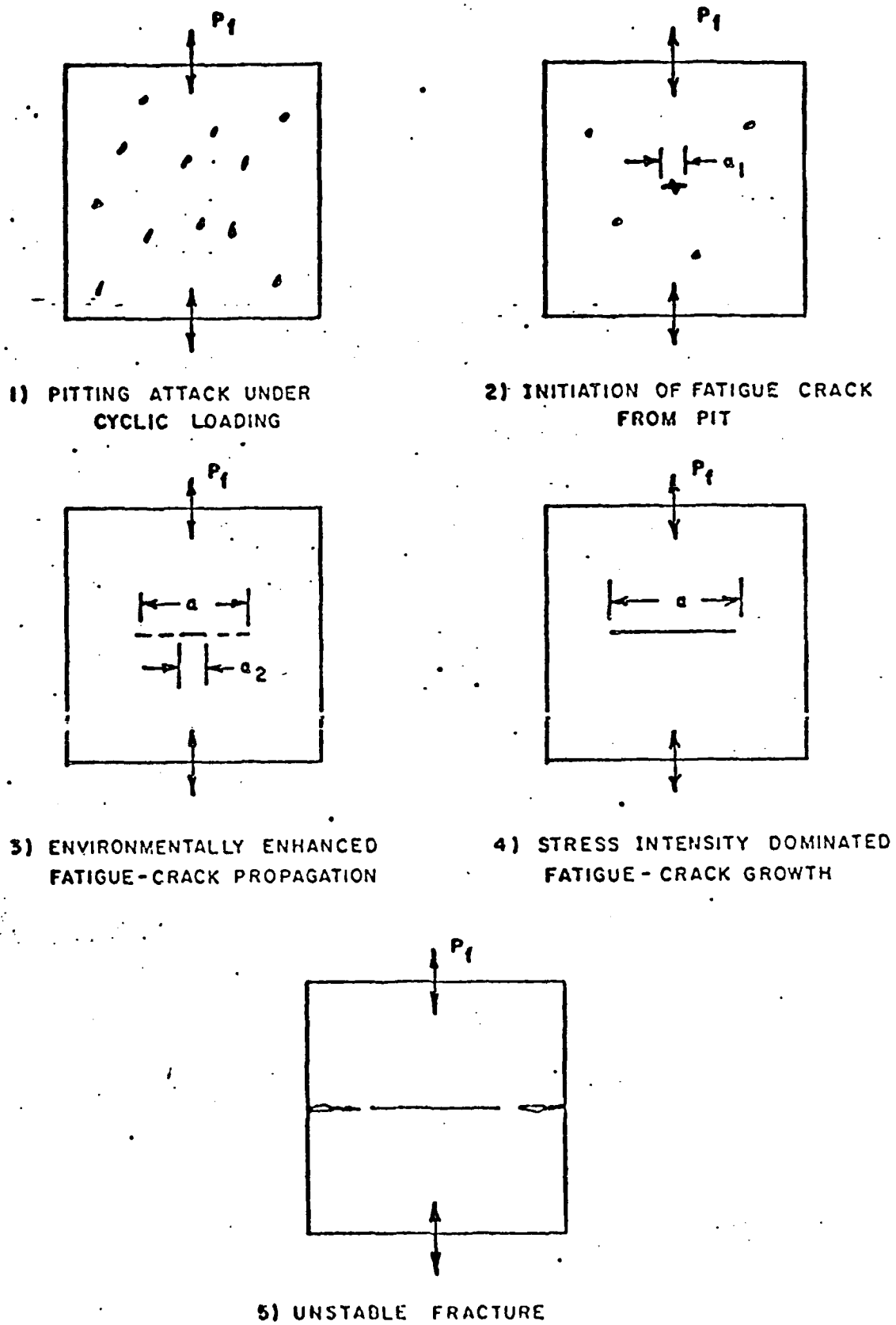


Figure 15: Fatigue Process Resulting From Pitting Corrosion

of any analytical method can be evaluated.

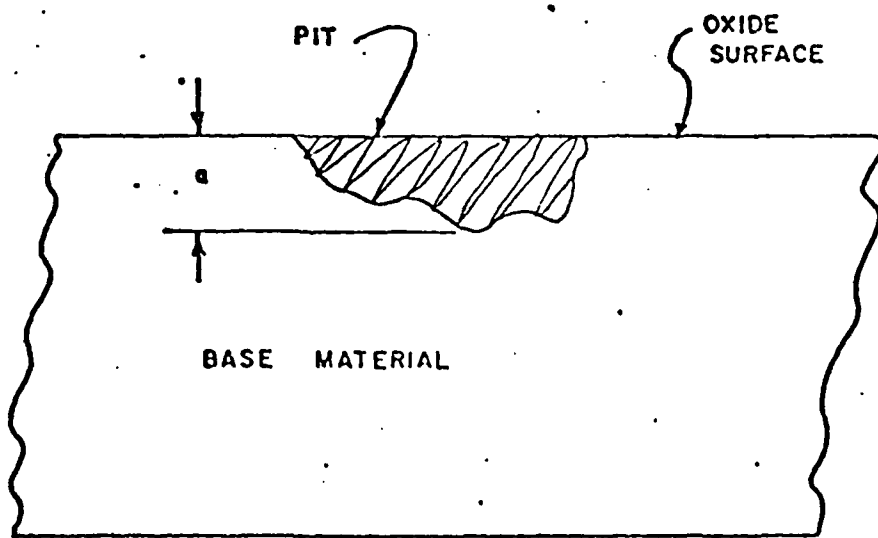
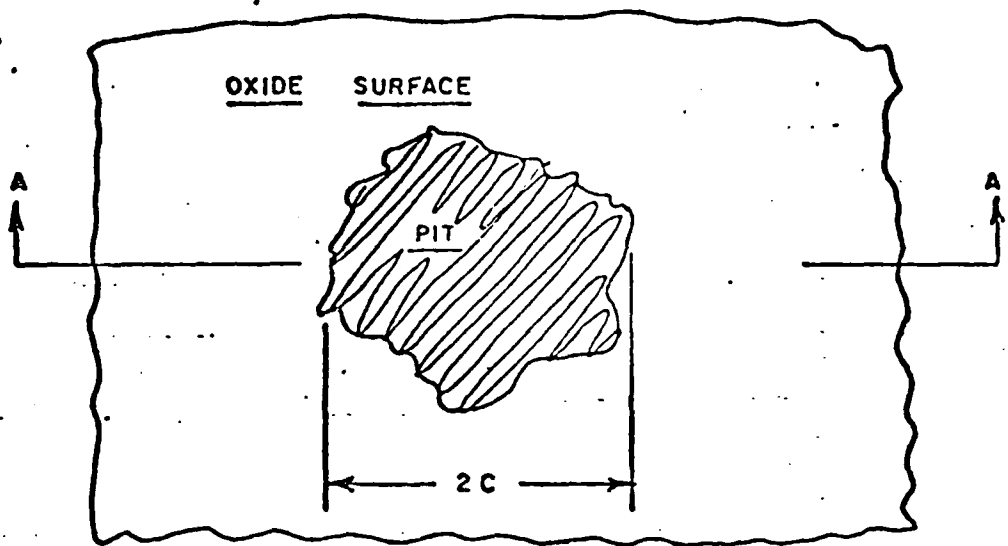
Pits come in a wide range of shapes and sizes however most of them which are encountered may be generally described as semielliptical surface cavities (38). As such they are typically described by two parameters, the pit depth ( $a$ ) and the pit diameter at the surface ( $2c$ ) (Figure 16). Being cavities they are three dimensional in nature. These cavities are rarely smooth surfaced and in fact can often be extremely irregular. From the above it can be concluded that the optimum mathematical shape would account for:

- 1) the three dimensional nature of the flaw,
- 2) the irregularities along the cavity walls,
- 3) the statistical variations of both one and two above.

The first requirement could easily be satisfied either analytically or more probably numerically. The second requirement is more difficult to satisfy but might be handled by modeling of the 'largest' surface irregularity at the point of maximum stress and then idealizing the remainder of the cavity as being smooth (Figure 17). The third requirement is without doubt beyond the capability of present day technology and is therefore impossible to analytically treat at this time.

One analytical method would be to devise a three dimensional finite element analysis around the geometrical shape shown in Figure 17. This method seems to approach the problem with the least distortion of the actual shape.

An alternative approach would be to idealize the three-dimensional



SECTION A-A

Figure 16: Pit Shape and Dimensioning

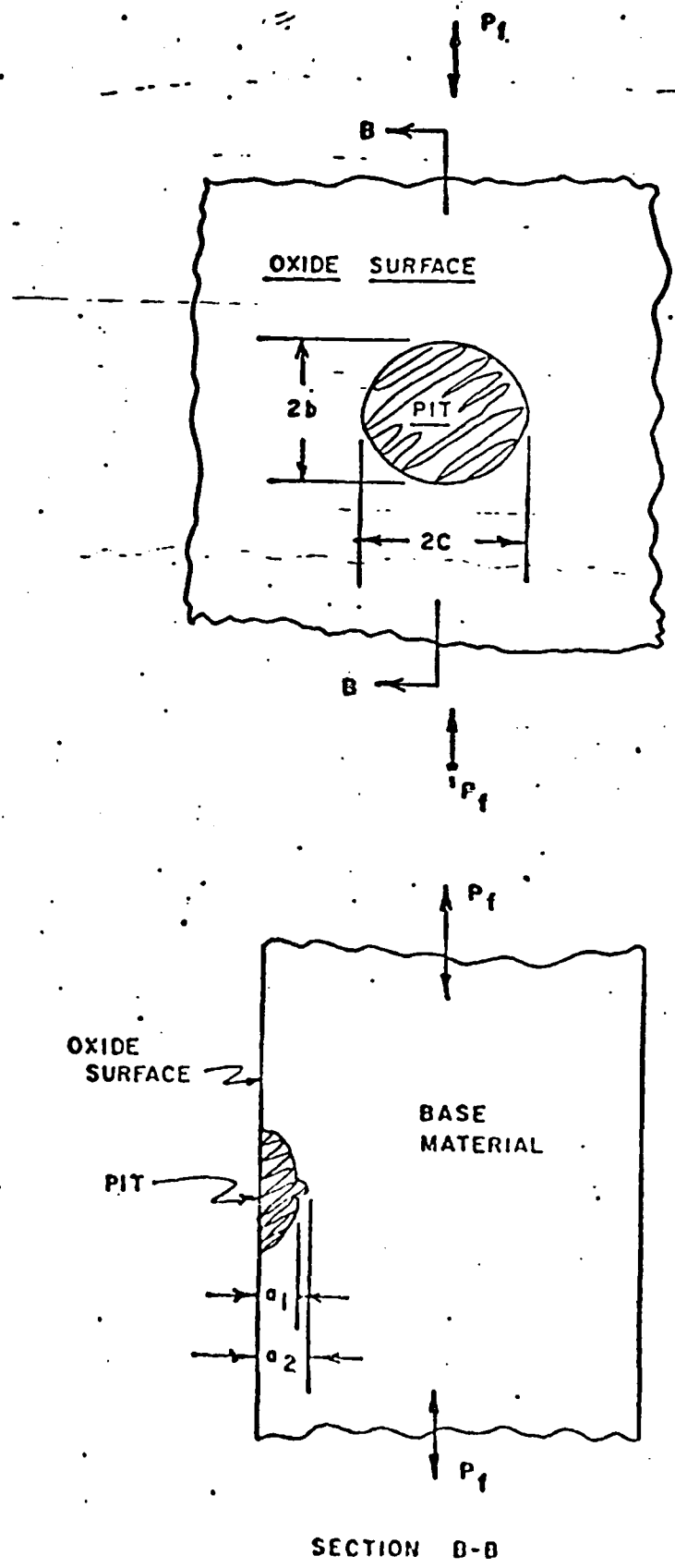


Figure 17: Three Dimensional Idealization of Flaw (Pit)

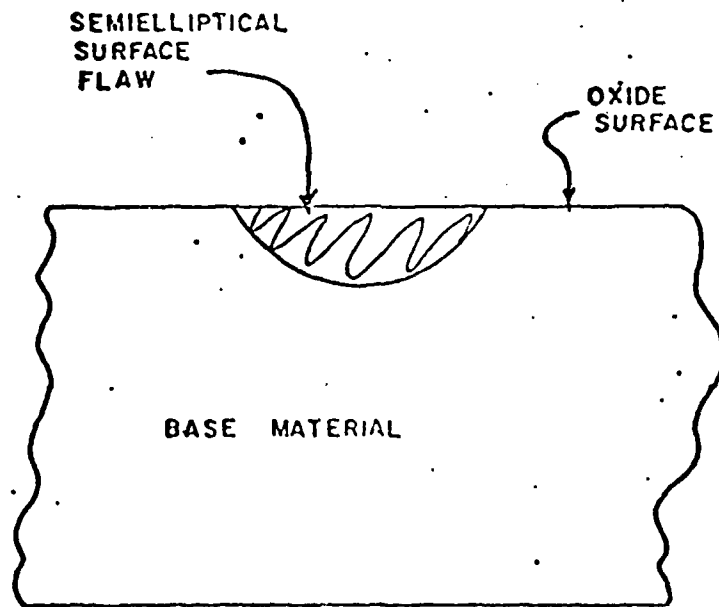
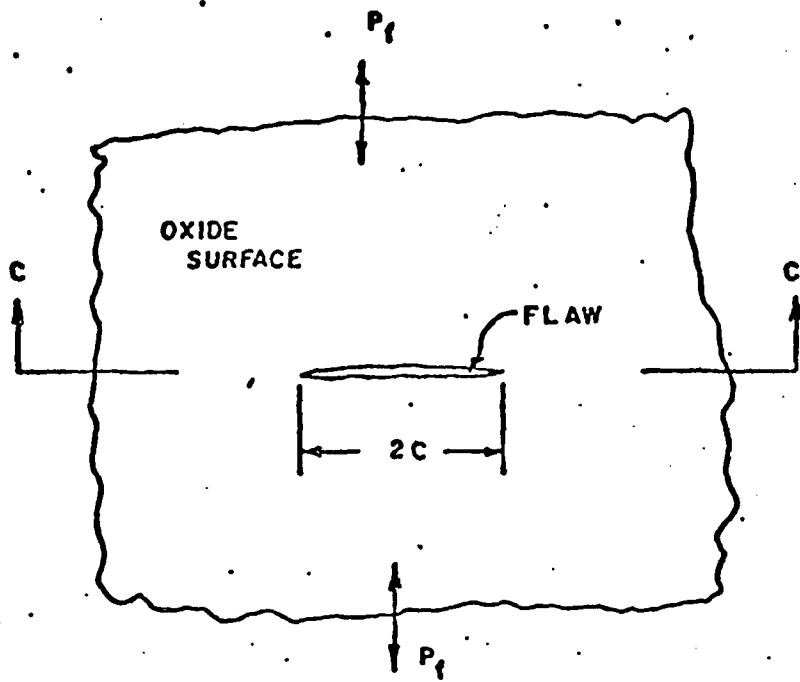
shape of the pit as a two dimensional semielliptical surface flaw (Figure 18). While this at first appears to be a gross idealization it does provide a simplified nonnumerical method for evaluating the stresses surrounding the flaw. In addition, if pit initiation occurs by means of oxide fracture as mentioned in the previous section, the semielliptical surface flaw idealization error would tend to greatly diminish. It should be noted that this type of idealization would result in the prediction of higher stresses than actually would occur (44).

The initial analysis of a semielliptical surface flaw is credited to Irwin (45) and was later refined by Paris (46). The form of the equation for the stress intensity (K) at the bottom of a semielliptical crack is of the form:

$$K = \left( \frac{\sigma^2 \pi a M}{\phi^2 - 0.177 M \left( \frac{\sigma}{\sigma_{ys}} \right)^2} \right)^{1/2} \quad (6)$$

where  $M = 1 + 0.12 (1 - a/c)$  and is the front-face free surface correction factor,  $\phi$  is the elliptical integral as is described in Figure 19,  $\sigma$  is the gross stress,  $\sigma_{ys}$  is the yield stress of the material, and  $a$  and  $c$  are as defined before. The above equation assumes that there are no back surface or net section effects (i.e. the crack dimensions are much, much smaller than the part dimensions).

Having developed the technical background to support the objectives, the theory was investigated experimentally using 2124-T851 aluminum.



SECTION C-C

Figure 18: Semielliptical Surface Flaw

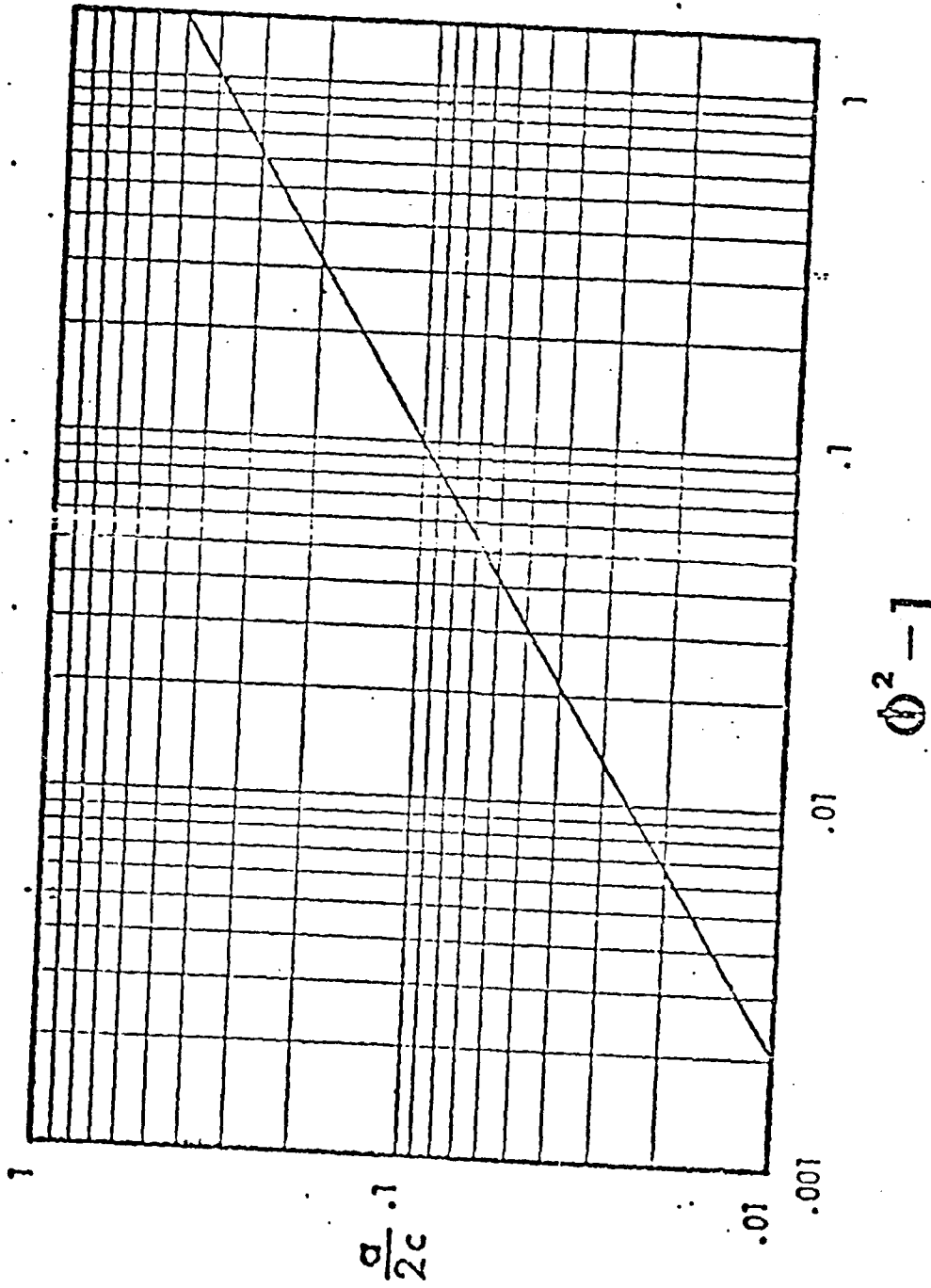


Figure 19: Elliptical Integral Curve for Elliptical Flaws as a Function of Flaw Configuration

#### 4.0 MATERIAL CHARACTERIZATION

For this investigation the aluminum alloy 2124-T851, in the form of a 3"-thick plate, was chosen, (formerly designated, "Alcoa 417 Process 2024") (47). (Note: since 2124 and 2024 are so similar they will be compared throughout this material characterization.) The alloy itself is 2124 while T851 indicates the heat treatment. In this case, a solution heat treatment followed by cold working, artificial aging, and stress relief provided by stretching to a 0.5 to 3% permanent set (48). Alloy 2124 is a high purity derivative of 2024 in which iron and silicon concentrations are more closely controlled (47). The 2000 series, of which 2024 and 2124 are both a part of, can normally be identified by their high copper content (5.5 - 2.3%) (49).

Copper is one of the most important alloying elements in aluminum systems because of its high solubility and strengthening effects (48). Copper can contribute to the strengthening of aluminum alloys in two ways, 1) as a solid solution inhibiting dislocation movement and, 2) as part of a precipitate which also inhibits dislocation movement but to a much greater degree (48). It is this second feature, precipitation hardening, which is by far the most important. By using various heat treatments a wide range of properties may be obtained (48).

The precipitates normally encountered are either  $\text{CuAl}_2$  or, if enough magnesium is present,  $\text{CuMgAl}_2$  (48). The magnesium is normally added to increase and accelerate age hardening at room temperature (48). Other phases one might possibly encounter are  $\text{Mg}_2\text{Al}_3$ ,  $\text{Mg}_2\text{Si}$ , and  $\text{MgZn}$ ,

provided adequate concentrations of these elements are available (48).

Other general properties of the 2000 series alloys are that they do not have a corrosion resistance as good as that of most other aluminum alloys and under given conditions are sometimes subject to intergranular corrosion (50). However the alloys in this series are generally thought to be highly resistant to stress corrosion cracking (51). When these alloys are in the heat-treated condition they have mechanical properties approximately equivalent to those of mild steel (50).

#### 4.1 Chemical Analysis

In Table 1 the chemical compositions of 2124 and 2024 aluminum systems are given. The constituent limits are listed along with the composition experimentally determined for the 2124 plate used in this investigation (52). The experimentally determined composition falls within all given limits set for this alloy.

When comparing 2124 composition limits to 2024 composition limits the only differences are for the elements iron, 0.30 max to 0.50 max; silicon, 0.20 max to 0.50 max; and titanium 0.05 max to 0.20 max, respectively. In other words, assuming that these are tramp elements, 2124 is a slightly cleaner alloy. The reduction of iron and silicon concentrations would be expected to improve the fracture toughness of this alloy (20).

#### 4.2 Orientation Terminology

In order to describe the anisotropic properties in the following sections it seems best to introduce a reference system at this time

**TABLE 1**  
**COMPARISON OF CHEMICAL COMPOSITIONS**

<u>Element</u>	<u>2124 Actual, %</u>	<u>2124 Green Letter Limits, % (47)</u>	<u>2024 ASTM Limits, % (53)</u>
Copper	3.88	3.8 - 4.9	3.8 - 4.9
Magnesium	1.34	1.2 - 1.8	1.2 - 1.8
Manganese	0.52	0.30 - 0.9	0.30 - 0.90
Zinc	0.08	0.25 max	0.25 max
Iron	0.06	0.30 max	0.50 max
Silicon	0.06	0.20 max	0.50 max
Titanium	0.02	---	0.10 max
Chromium	0.01	0.10 max	---
Nickel	0.01	---	---
Lead	0.01	---	---
Tin	0.01	---	---
Others			
Each	---	0.05 max	0.05 max
Total	---	0.15 max	0.15 max

which will be adhered to throughout the remainder of this work. Referring to Figure 20, three directions are required, rolling (R), thickness (T), and width (W).

With these directions as a reference, a plane is specified by the direction normal to it. For example, a T-plane is any plane which is parallel to the rolled surface. Whenever a specimen is under consideration, two letters shall be used, the first letter specifies the loading direction while the second letter specifies the direction in which the crack will propagate. For example, a specimen in the RW orientation is loaded in the R-direction and fractures in the W-direction. When a specimen is to fracture in more than one direction (i.e. radially on a plane) it shall be described by two letters. The first letter specifies the loading direction as before but the second specifies the normal to the fracture plane. For example, a specimen in the RR orientation is loaded in the R-direction while the fracture occurs in both the W and the T directions.

#### 4.3 Hardness and Tensile Tests

Hardness and tensile tests were conducted at midthickness of the three inch plate. The averaged values for those tests are found in Table 2 along with the tensile properties for 2124-T851 as specified in Alcoa's Green Letter (47) and those for 2024-T851 as specified by ASTM (53). The tensile specimens, (three separate specimens were tested and the results averaged), were machined from the midplane of the plate according to Figure 21 and were in the RR orientation.

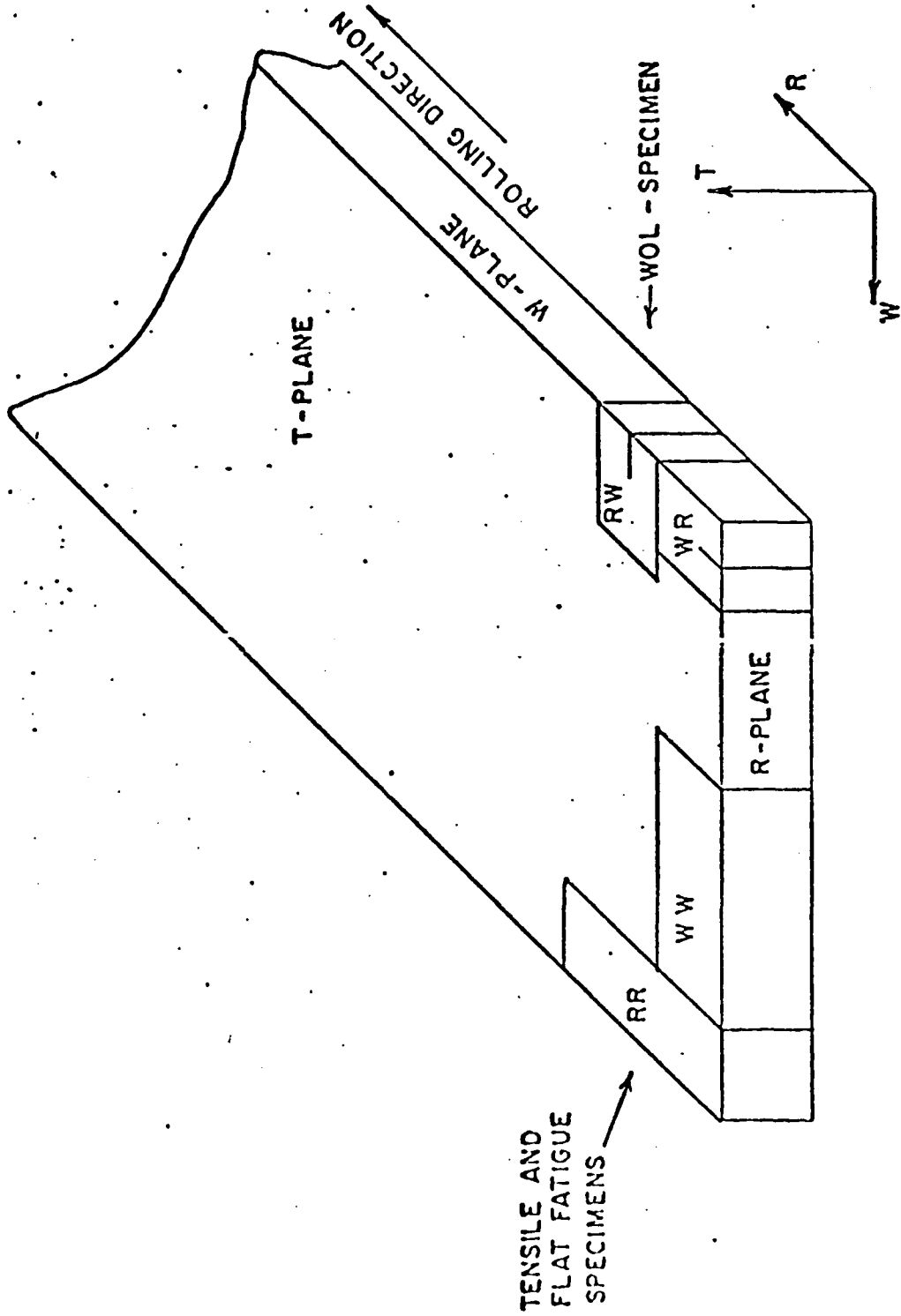


Figure 20: Orientation Terminology

TABLE 2

MECHANICAL PROPERTIES OF 2124-T851 AND 2024-T851

<u>Property</u>	<u>RR - Orientation</u>		
	<u>2124-T851</u>		<u>2024-T851</u>
	<u>Actual</u>	<u>Specified, (47)</u>	<u>Specified, (53)</u>
Tensile Strength Ksi (MPa)	72.5(500)	65.0(448) min 69.8(481) avg	66.0(455) min 70.0(483) avg
Yield Strength Ksi (MPa)	63.0(434)	57.0(393) min 63.5(438) avg	58.0(400) min 65.0(448) avg
Elongation, %		6 min 9.0 avg	5 min 8.0 avg

Hardness (2124-T851)

<u>Plane</u>	<u>Hardness, (Rockwell - B)</u>			
	<u>1</u>	<u>2</u>	<u>3</u>	<u>Avg.</u>
R	79.9	79.0	80.0	79.6
W	74.9	76.8	74.0	75.2
T	77.5	78.5	79.5	78.5

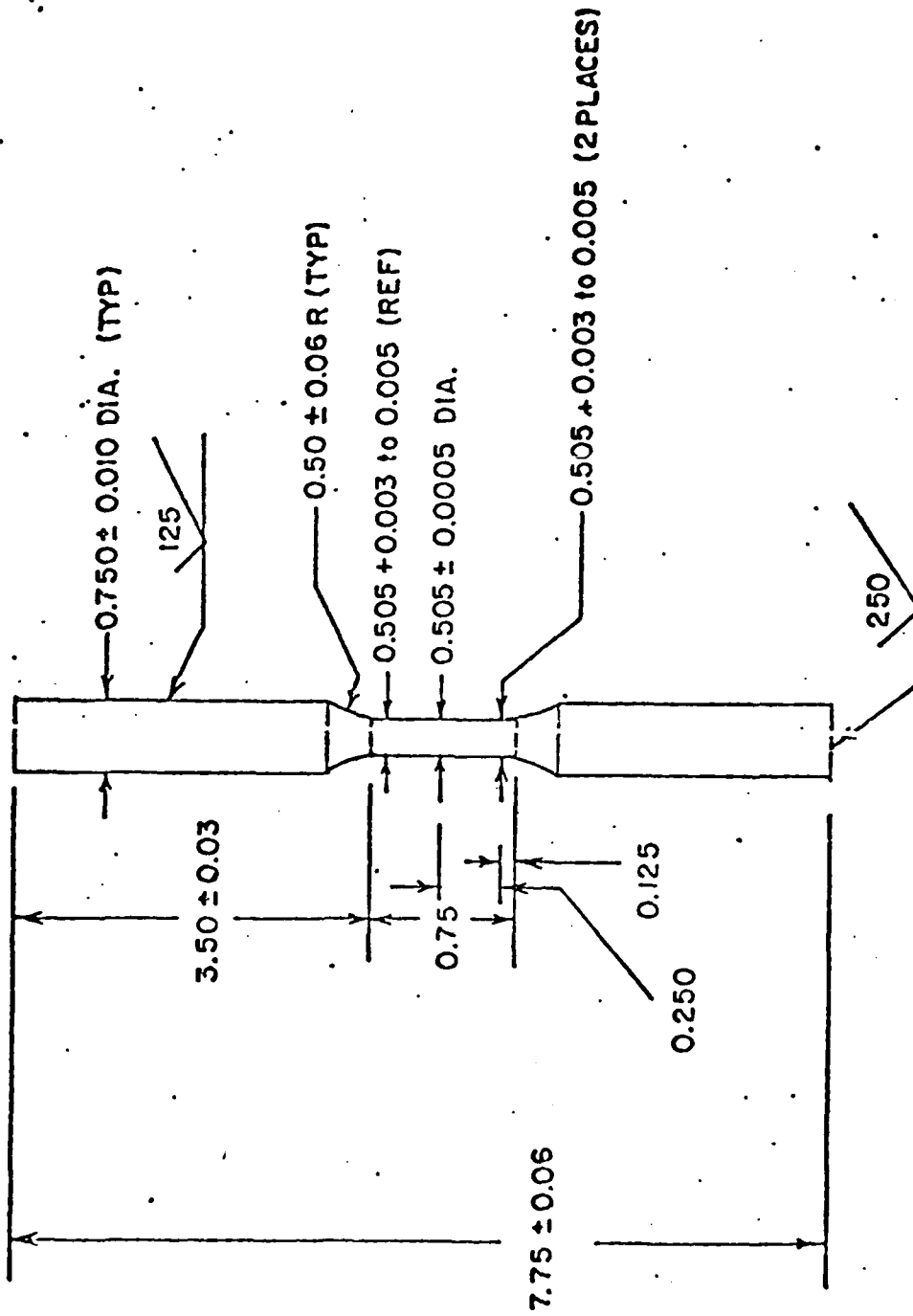


Figure 21: Tensile Specimen

From the mechanical properties table we see that the actual tensile and yield strengths for the 2124-T851 3-inch plate compare favorably with those specified. Also the specified 2124-T851 tensile and yield strengths are slightly less than those specified for 2024-T851 while the 2124-T851 is slightly more ductile.

#### 4.4 Fracture Toughness

Fracture toughness tests were not performed on the test material, however  $K_{IC}$  values from the literature (54) have been included in Table 3 for both 2124-T851 and 2024-T851. While these values must be viewed cautiously in reference to the particular material used in this investigation they give a general idea as to the probable ranges and indicate the fracture toughness superiority of 2124-T851 over 2024-T851.

#### 4.5 Microstructure

The microstructure was examined at three different levels through the plate thickness: a) near the surface, b) at the quarter plane (1/4-deep) 0.75 inches below the surface, and c) at the mid plane (1/2-deep) 1.5 inches below the surface, (Figure 22). The three principal orthogonal planes, (R, W. and T), were prepared for each level. Each specimen was metallographically prepared and then etched with Keller's etching reagent (55). The three levels were chosen with the intent of showing microstructural variation through the thickness of the three inch plate.

The resulting photomicrographs are shown in Figures 23, 24, and

TABLE 3

FRACTURE TOUGHNESS VALUES FOR 2124-T851 AND 2024-T851

ENVIRONMENT - LAB AIR

<u>Orientation</u>	<u>Published <math>K_{IC}</math> (Ksi <math>\sqrt{in}</math>) 2124-T851, (54)</u>	<u>Published <math>K_{IC}</math> (Ksi <math>\sqrt{in}</math>) 2024-T851, (54)</u>
RW	23.6*	21.6**
WR	22.8*	18.4**

\*Thickness = 0.75 inches

\*\*Thickness = 0.625 inches

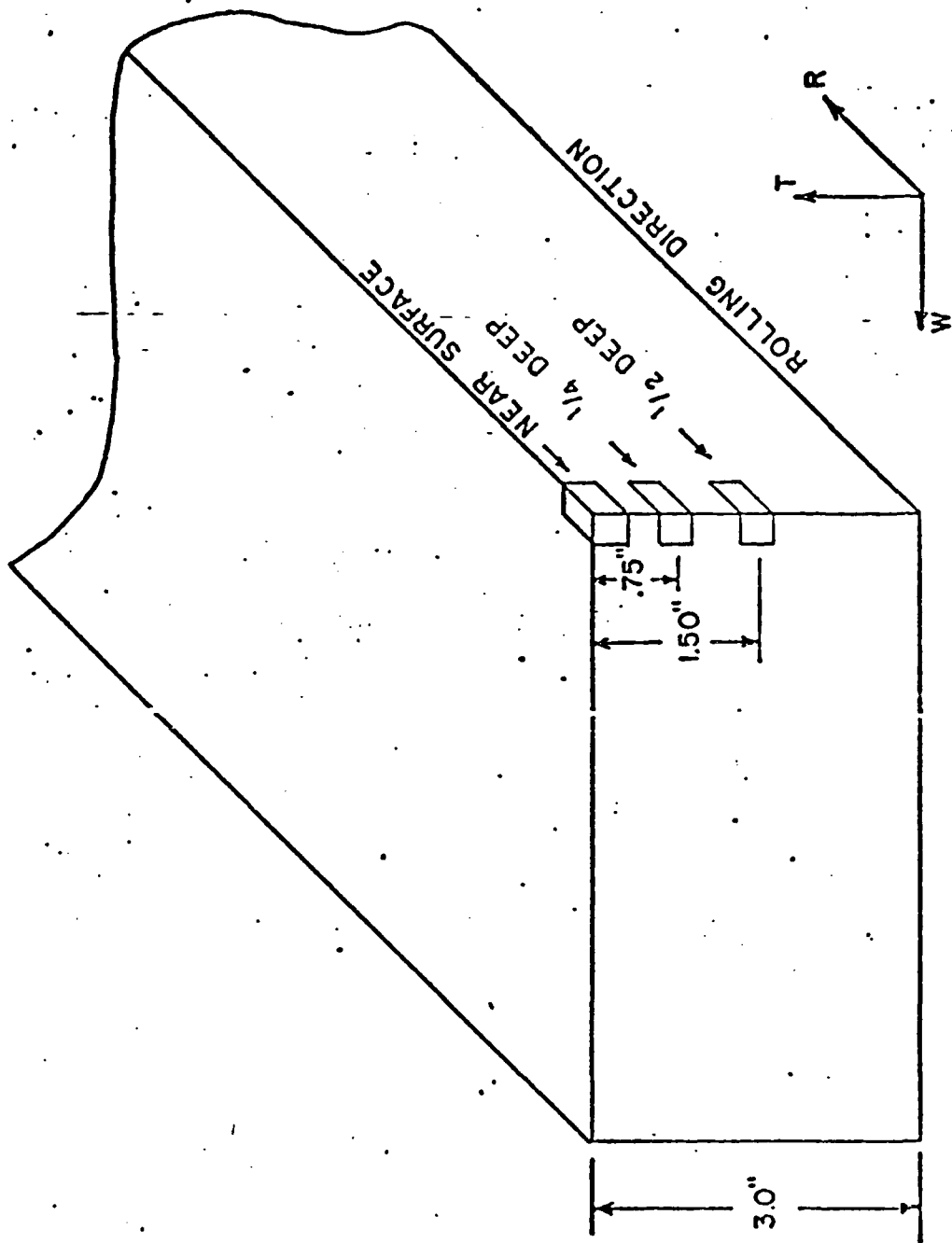


Figure 22: Microstructural Specimen's Locations

25. From these photomicrographs it was noted that:

- 1) The concentration of dark spherical particles, ( $\text{CuMgAl}_2$  or  $\text{Cu}_2\text{Mn Al}_{20}$  precipitates), decreases as the center of the plate is approached.
- 2) The degree of deformation of the grains decreases as the center of the plate is approached.
- 3) Strain lines appear at all levels and in all orientations.
- 4) There is a high contrast between grains which is normally associated with the precipitation of the hardening phase,  $\text{CuMgAl}_2$ , on the matrix slip planes (1).
- 5) In comparing these micrographs with those in literature, (26,56), for 2024, one may observe that the precipitates are much smaller and more dispersed in the 2124 alloy.

From the above observations, it was concluded that:

- 1) The test material is typical of cold rolled, artificially aged aluminum, with grains flattened in the thickness direction and elongated in the rolling direction.
- 2) The reduction in size and density of distribution of the large precipitate particles correlates with the increased fracture toughness properties found for the 2124 alloy.
- 3) Specimens should be machined from the midplane so as to provide the most uniform microstructure and properties.

#### 4.6 Summary of Material Characteristics

In summary, the material used in this investigation, (2124-T851

**Figure 23**  
**Microstructure of 2124-T851 Aluminum**  
**Near Surface**

**(Keller's Etching Reagent)**

**(a) R-orientation      50x**

**(b) W-orientation      50x**

**(c) T-orientation      50x**

**Figure 24**  
**Microstructure of 2124-T851 Aluminum**  
**1/4-Deep**

**(Keller's Etching Reagent)**

**(a) R-orientation      50x**

**(b) W-orientation      50x**

**(c) T-orientation      50x**

Figure 25

Microstructure of 2124-T851 Aluminum

1/2-Deep

(Keller's Etching Reagent)

(a) R-orientation 50x

(b) W-orientation 50x

(c) T-orientation 50x

in the form of a three inch thick plate), meets or exceeds all property specifications which were evaluated and is typical of heavily cold worked, solution heat treated aluminum alloys. Furthermore, this material is very similar to the more widely known 2024-T851 and has similar mechanical properties with the exception of fracture toughness values which range somewhat higher for the 2124-T851. Finally, the material may be susceptible to intergranular corrosion but should show a high resistance to stress corrosion cracking.

## 5.0 EXPERIMENTAL PROGRAM AND PROCEDURE

Up to this point the objectives have been stated, the technical background presented, and the material characterized. This chapter will present the actual research conducted in order that the initial objectives might be met. In so doing, this chapter covers all aspects of the research project, from the planning and actual testing stages through to the reduction of the data acquired.

### 5.1 Experimental Hypothesis

The hypothesis suggested for this investigation consists of six parts;

- 1) Test environment will alter fatigue crack growth rate with the brine solution resulting in higher growth rates.
- 2) A brine environment will accelerate initiation of fatigue cracks on polished 2124-T851 aluminum surfaces and thus lower the S-N curve.
- 3) S-N tests of 2124-T851 aluminum in a brine solution will not show a fatigue limit.
- 4) Pit growth can effectively be monitored using a photographic system which is described later.
- 5) The empirical pitting rate equation
$$a = C_1 t^{1/3} \quad (5)$$
can be applied to pitting under fatigue conditions.
- 6) Fatigue crack initiation from corrosion pits can accurately be predicted by modeling the pit as a semielliptical surface

flaw and the use of a threshold stress intensity determined from propagation data.

## 5.2 Test Matrix

The test matrix followed in this investigation consisted of two parts. The first part consisted of crack propagation tests, two tested in lab air and two tested in a 3.5% sodium chloride solution. The second part consisted of S-N tests, some to be tested in lab air, with the majority to be tested in a 3.5% sodium chloride solution.

Since S-N data for this material was not available the exact number of tests of this type, in any particular environment could not be established before actual testing began. Eighteen specimens were available for testing. It was expected that three to four tests would be required to establish the lab air baseline with the remainder of the specimens available for salt water pitting tests. The objective was to establish a cycles-to-failure range extending from around twenty thousand cycles to runout (four million cycles, plus). In addition, a minimum of five salt water tests were to be tested at the same stress level (that level corresponding to the S-N midrange). Both propagation and S-N tests were to be conducted under sinusoidal loading (load control) at a frequency of 10 Hz and an R-ratio of +0.1.

## 5.3 Test Equipment

The test system employed for the fatigue crack growth and S-N experiments used MTS Systems Corporation control electronics and a load frame designed and constructed at the University of Missouri-

Columbia (26). A schematic representation of the system is shown in Figure 26. Table 4 lists the components of the system.

The operation of the test system may be summarized as follows:

- 1) A program signal is produced by the function generator and routed to the 406 controller.
- 2) The program signal is used to provide a drive current to the servo valve on the actuator. The actuator is 'slaved' to the servo-valve and thus responds to movement of this valve.
- 3) A signal is produced by the load cell (for load control operation) or the LVDT (for stroke or displacement control operation). This so-called feedback signal is routed to the 406 controller.
- 4) The feedback signal is compared to the program signal and any deviation results in the addition of an 'error' current to the program current. This alters the servo-valve drive current, thus completing the 'loop'.
- 5) The purpose of the 436 control unit is simply to allow remote control of the hydraulic power supply and the function generator.
- 6) The relative magnitudes of the load and stroke signals are displayed on the digital voltmeter.

The photographic system used in this investigation (used for S-N tests only) is shown schematically in Figure 27. Essentially, the system amounts to a pulsed illumination source and a camera, with

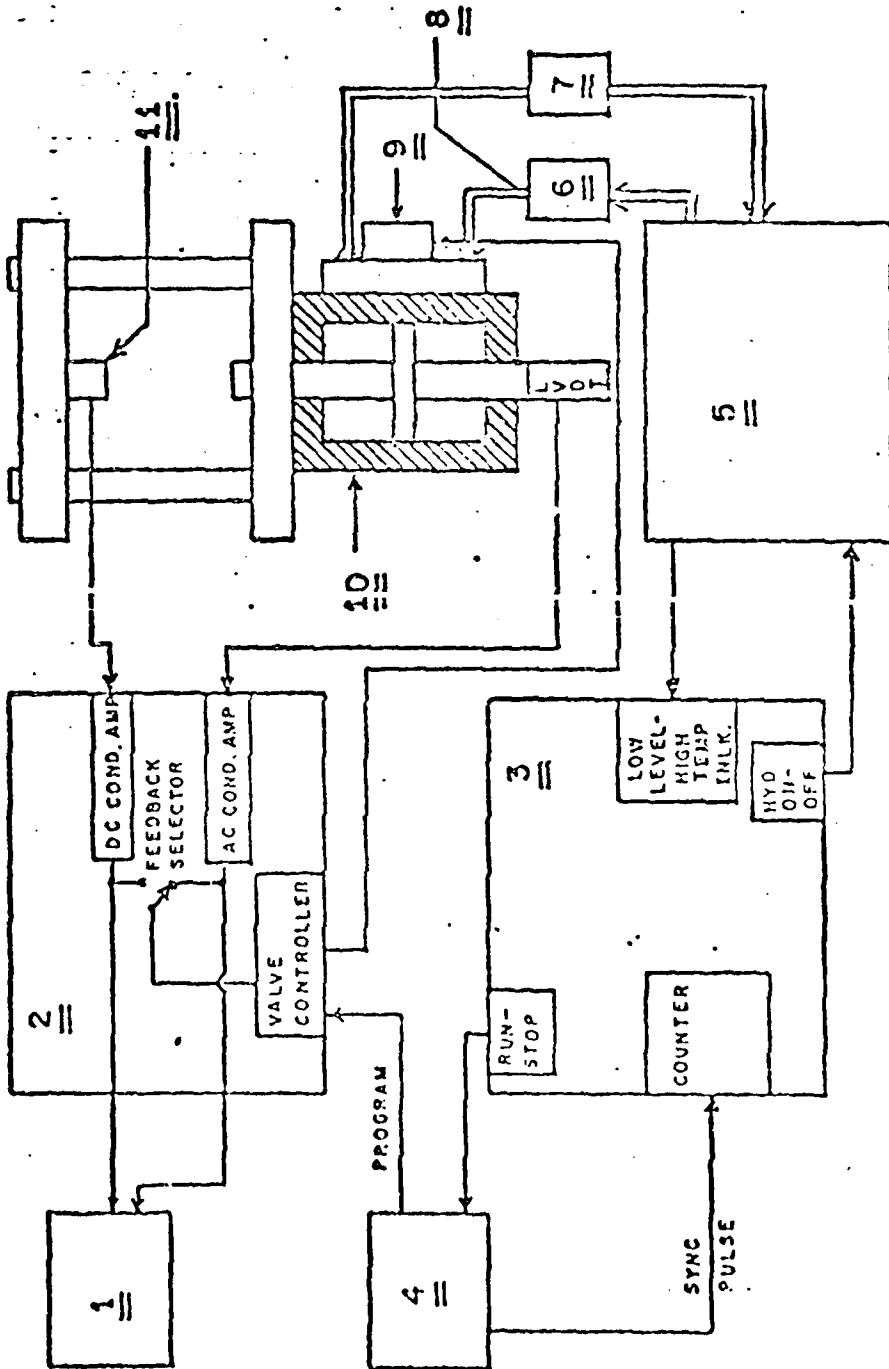


Figure 26: Test System D'ock Diagram

TABLE 4

Test System Component List

<u>Number</u>	<u>Component Description</u>	<u>Model or Part Number</u>
1	Digital Indicator	MTS Model 430
2	Controller	MTS Model 406
3	Control Unit	MTS Model 436
4	Function Generator	MTS Model 410
5	Hydraulic Power Supply	See Reference (26)
6	Accumulator	Greer Model A107-200
7	Accumulator	Greer Model A108-200
8	Hand Valve	----
9	Servo-Valve	Moog 5 gpm Valve
10	Hydraulic Actuator	MTS Model 204.62
11	Load Cell	

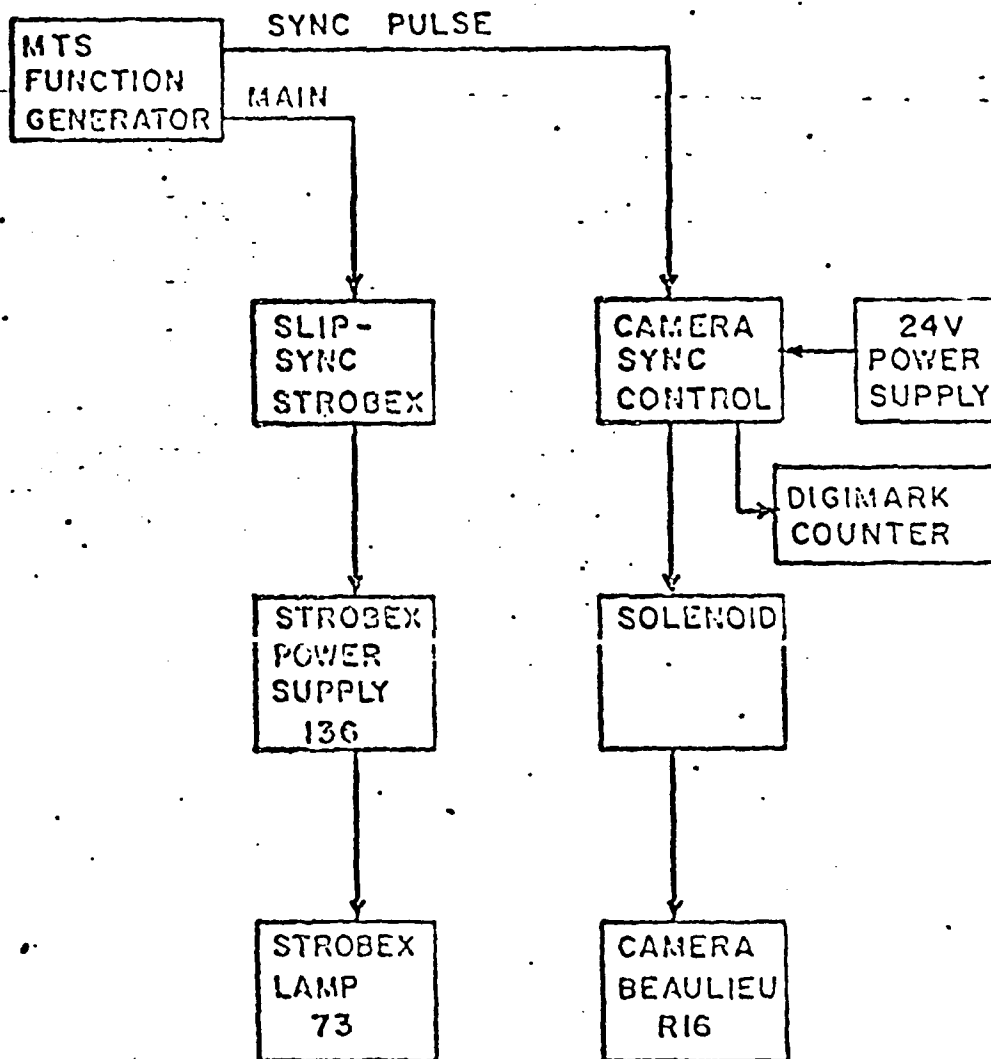


Figure 27: Block Diagram of Camera System

both synchronized to the function generator program signal. A detailed explanation of the camera system may be found in Reference (26). The only major modification to the system was that a 35 mm SLR camera was attached to the eyepiece. This allowed for single 35 mm photographs to be taken as well as 16 mm movies proving the diversity of this basic test system.

Figure 28 is a schematic of the optical train, while Figures 29, 30 and 31 show different views of the camera system. Figure 32 shows the complete test system as used in the lab air tests. Some changes were made for the salt water tests and will be discussed below.

The environment system for the S-N tests was designed to provide a continuously flowing corrosive environment while effectively isolating the specimen from possible galvanic corrosion with the grips or other parts of the test system. The system, shown in Figure 33, consists of a sump (1500 ml beaker), a chamber that fits around the specimen, and a pump to provide the constant flow of corrosive fluid.

The environment chambers were designed to fit around the specimen. This arrangement effectively contains the fluid, eliminating the problems of galvanic corrosion between the specimen and grips. Small slots were cut in the container and glass plates epoxyed in these slots. These 'windows' allowed a clear view of the specimen surface, essential to this photographic technique. Inlet and outlet ports were provided on each side of the chamber (Figures 34 and 35).

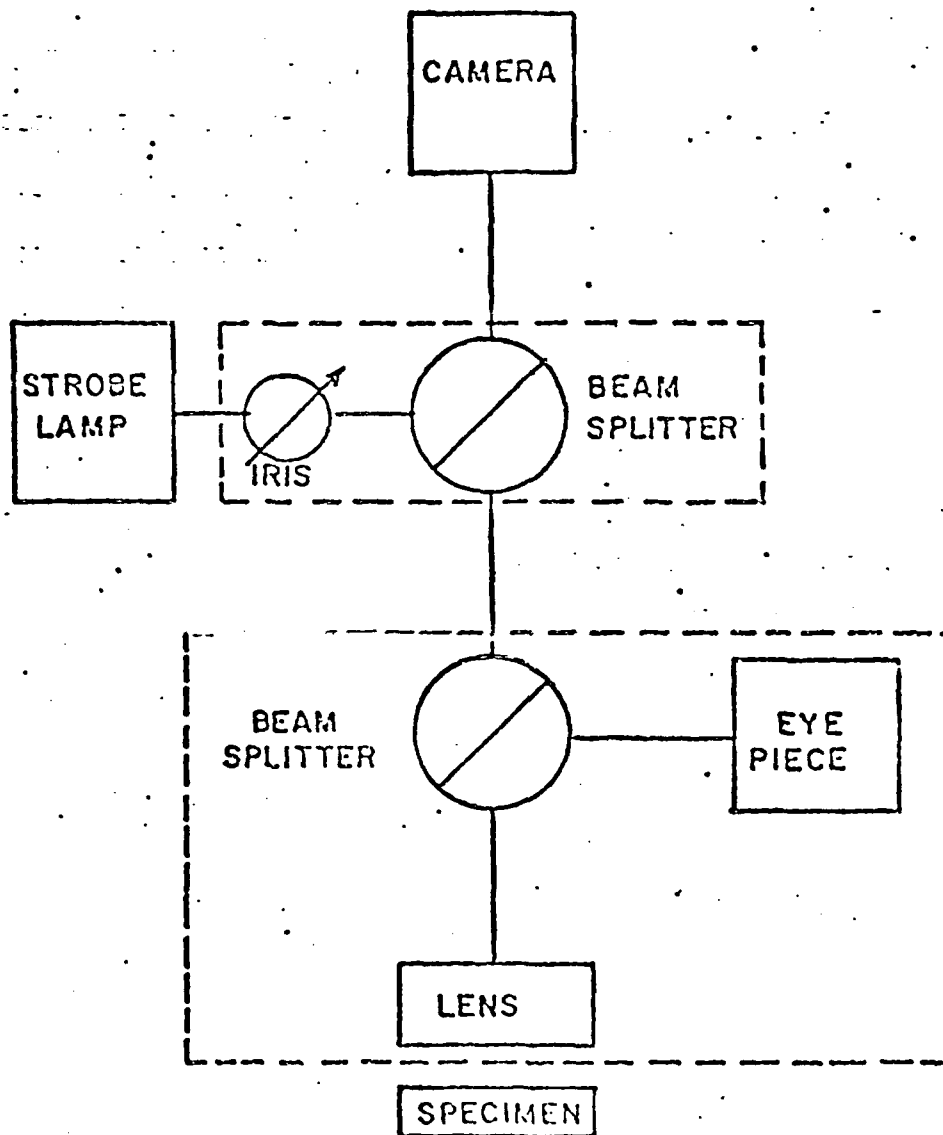


Figure 28: Optical Train Schematic Diagram

Figure 29: Camera System Component Arrangement



Figure 30: Optical Train and Camera

Figure 31: Camera System and Hydraulic Lift Table

Figure 32: Load Frame and Control Electronics

Figure 33: Load Frame and Environmental System

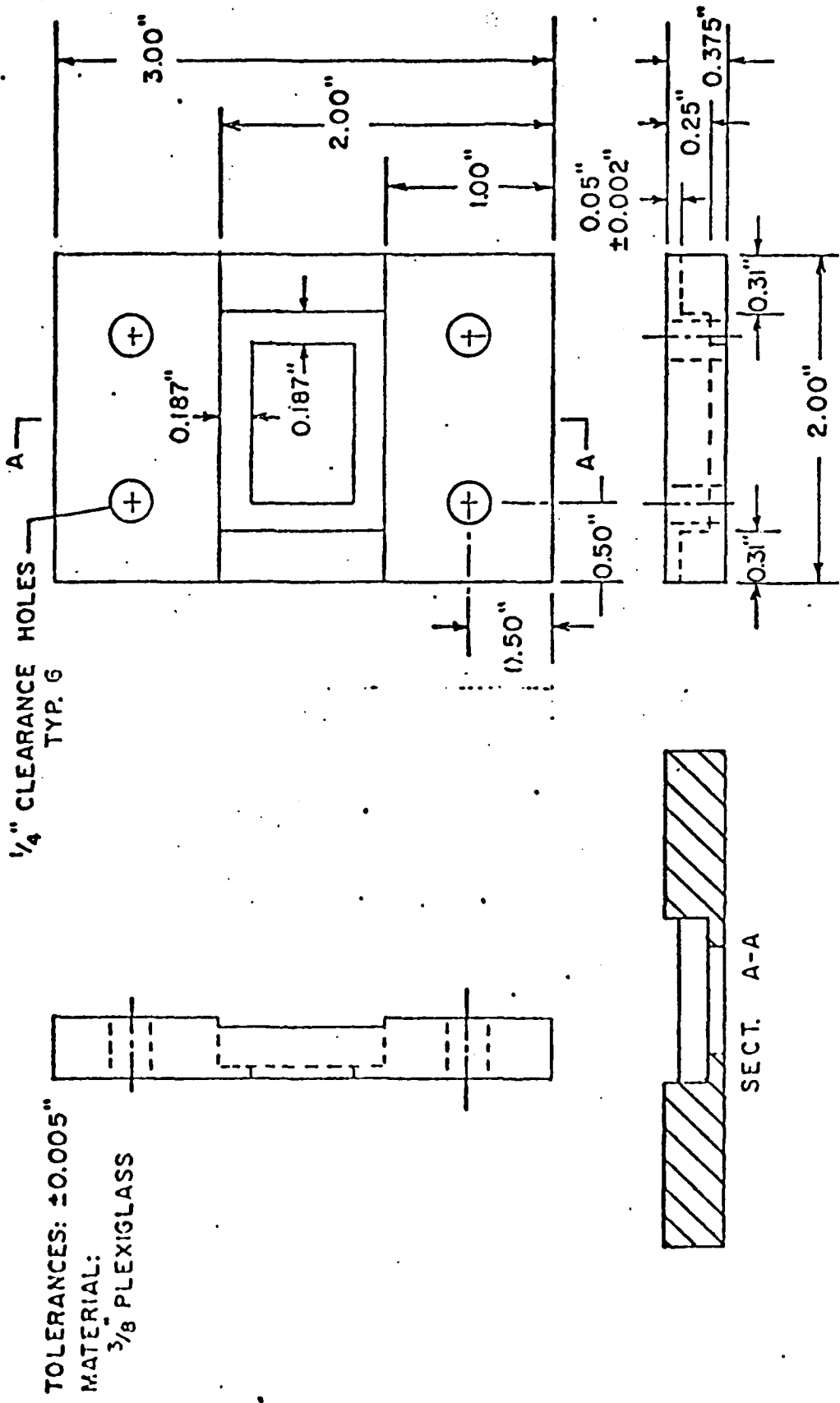


Figure 34: S-N Specimen Chamber (Front)

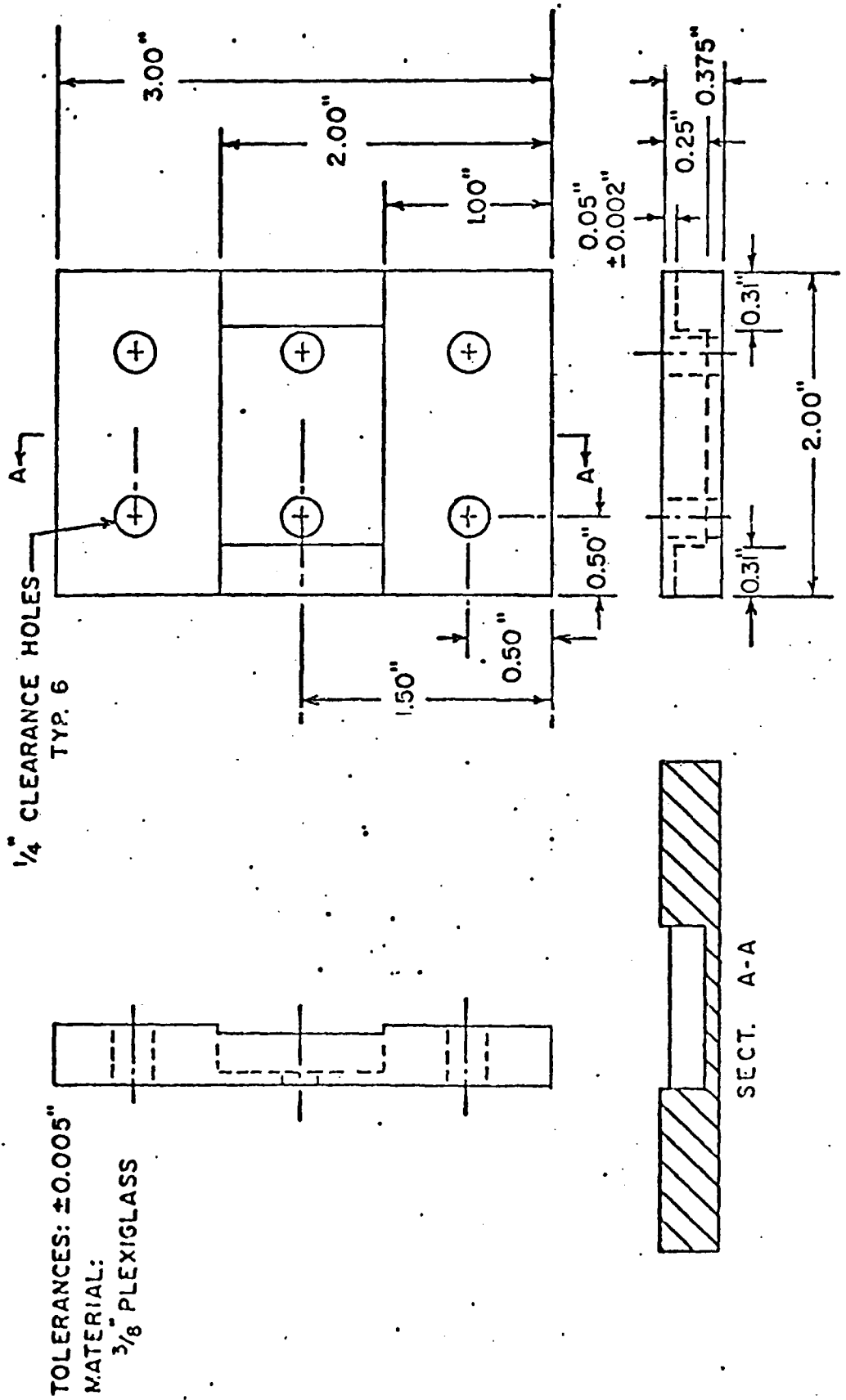


Figure 35: S-N Specimen Chamber (Back)

Figure 36 shows the arrangement of specimen, chamber, and grips. Only those tests conducted in salt water had the environment chamber attached. However, tests on the chambers effects on the loading of the specimen showed it to have negligible effects.

Crack propagation tests did not include the photographic system. The air tests were conducted according to ASTM Standard E399-74 (57) with the crack lengths being monitored using a Gaertner 40X traveling optical micrometer. The crack propagation environmental tank was constructed by Poon (25) and Panhise (24). This tank was constructed of plexiglass allowing for the same type of crack growth monitoring as mentioned for the air tests.

#### 5.4 Testing Procedure and Data Acquisition

Since two entirely different types of tests were conducted, this section will be divided into two subsections. The first subsection will describe the testing procedure and data acquisition for the propagation tests while the second will describe that for the S-N tests.

##### 5.4.1 Testing Procedure and Data Acquisition For FCG Tests

The specimen type used in the FCG portion of this investigation was a modified WOL specimen (wedge opening loading) of the Mode I design (crack propagation orthogonal to loading direction) with a height-to-width ration,  $h/W$ , of 0.486, where  $h$  is the half height of the specimen and  $W$  is the distance from the centerline of the pin holes to the edge of the specimen (Figure 37). The specimens were machined from the midplane of the three-inch-thick plate and were in

Figure 36: Specimen, Chamber and Grip Arrangement



the RW orientation.

Each specimen was precracked one tenth of an inch or more. Both the air tests and the salt water tests were then tested under sine wave loading at a frequency of 10 Hz and an R-ratio of +0.1. Data was acquired in the form of crack length and number of loading cycles.

#### 5.4.2 Testing Procedure and Data Acquisition For S-N Tests

Unnotched axial fatigue specimens were used for the S-N tests. Figure 38 shows the specimen geometry. The specimens were machined from the midplane of the three inch plate in the RR orientation, with the specimen thickness in the same direction as the plate thickness. The stress concentration for this type of specimen is approximately 1.0 (Neuber theory gives the stress concentration,  $K_t$ , as between 1.0 and 1.1 (54)). Axial tensile, sine wave loading was applied to the specimens at a frequency of 10 Hz and an R-ratio of +0.1.

Prior to testing, all of the specimens were sanded to a 600 carbide grit quality on all surfaces (front face, back face, and radii). Subsequent to the sanding, the 'front' surface was polished to the nine micron aluminum oxide level and then cleaned with ethyl alcohol. Next, the back surfaces and radii were completely covered with epoxy. The front surfaces except for an area approximately .25 by .25 in. centered at the point of maximum stress were also covered with epoxy. (This was done to isolate the area of pitting attack thus aiding the photographic technique.)

Two types of data were acquired during the actual testing

- 1) photographic scans of the pitted surface at times  $t_1, t_2, t_3, \dots$

TOLERANCES:  $\pm 0.005$ "  
MATERIAL: 2124-T 851 ALUMINUM  
FROM CENTER 3" PLATE

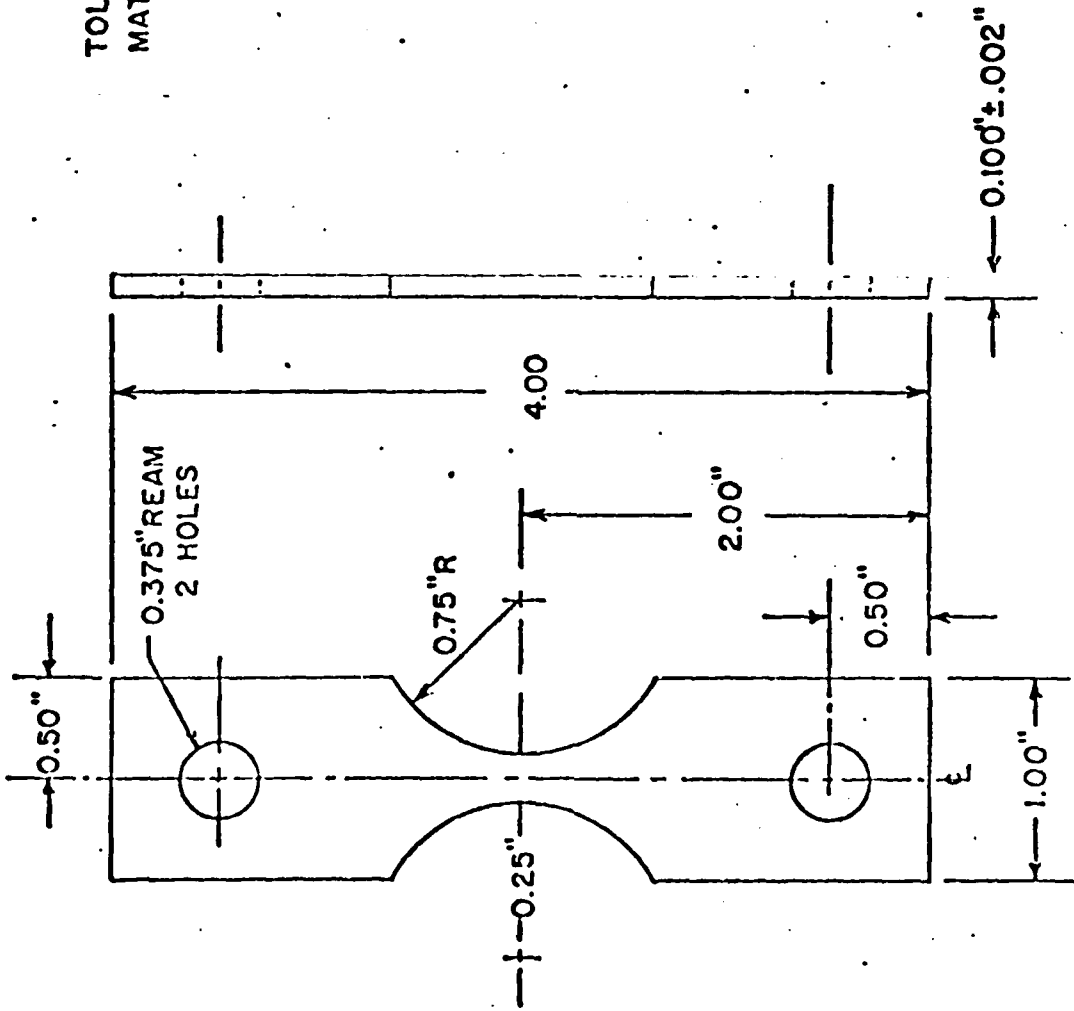


Figure 38: S-N Specimen

$t_f$  (for those specimens subjected to pitting environment only) and 2) number of cycles to failure at a given load. Subsequent to the actual tests the photographic scans were to be examined to determine 1) the diameters of all observable pits at different times and 2) pit diameter at first observable crack. Also fractographic examination was to yield the (a) and (2c) of the 'fracture' pit providing a 'characteristic' geometry.

## 5.5 Data Reduction

This section will also be divided into two subsections for the same reason as before.

### 5.5.1 Data Reduction For FCG Tests

The raw a-N data are used to calculate values for  $da/dN$  and  $\Delta K$ . These values are obtained from the following equations:

$$\frac{da}{dN} = \frac{a_{i+1} - a_i}{N_{i+1} - N_i} ; \text{ where } i = 0, 1, \dots, n \quad (7)$$

$$K_{\max} = \frac{P_{\max}}{BW} (a)^{1/2} (Y_a)$$

for  $L/W = 0.486$

$$Y_a = 30.96 - 195.8 (a/W) + 730.6 (a/W)^2 - 1186.3 (a/W)^3 + 754.6 (a/W)^4 \quad (8)$$

and

$$\Delta K = K_{\max} (1-R) \quad (9)$$

where

$P_{\max}$  = the maximum load applied

$B$  = specimen thickness

$W$  = specimen width

$a$  = crack length

$R$  = stress ratio ( $\sigma_{\min}/\sigma_{\max}$ )

$K$  has units of  $\text{ksi}\sqrt{\text{in}}$  and may be converted to  $\text{MPa}\sqrt{\text{m}}$  by multiplying  $K$  by 1.098855.

Weibull curve fits (of the form given in Equation 2) to the combined air and the combined salt water  $da/dN - \Delta K$  data are determined numerically on a computer. With the  $k$ ,  $e$ ,  $v$ , and  $K_b$  constants evaluated, the threshold stress intensity  $K_{o_{cg}}$ , determined by crack growth tests can be evaluated from Equation 3 which is reprinted here:

$$K_{o_{cg}} = K_b \left\{ 1 - \exp \left[ - \left( \frac{-e}{v-e} \right)^k \right] \right\} (1-R) \quad (3)$$

### 5.5.2 Data Reduction For S-N Tests

For the S-N fatigue tests the stress is determined as the maximum gross cross-sectional stress without stress concentration correction. This is done by dividing the maximum load ( $P_{\max}$ ) by the minimum cross-sectional area ( $A'$ ) as given by:

$$S = \frac{P_{\max}}{A'} \quad (10)$$

where  $A'$  = minimum width times thickness.

From an SEM examination of the fracture surface, the (a) and (2c) measurements of all pits which initiate cracks and are in the fracture plane are made. From these measurements, a/2c ratios are calculated for each pit. This provides an estimate of the a/2c ratio for the remainder of the pits on that specimen (when there are more than one pit on the fracture plane the a/2c ratios are averaged).

Pit diameters (2c), at times  $t_1, t_2, \dots, t_n$ , for all observable pits (which are measured from the photographic scans at times  $t_1, t_2, \dots, t_n$ ) are then multiplied by that particular specimen's 'characteristic' a/2c ratio. This results in an estimated pit depth (a) at time t for each pit on the surface of each specimen.

From this data the pitting rate constant ( $C_1$ ) for each specimen can be calculated from the following equations:

$$C_{1ij} = \frac{a_{ij}}{t_j^{1/3}} \quad (11)$$

$$C_1 = \frac{\sum_{j=1}^m \sum_{i=1}^n C_{ij}}{mn} \quad (12)$$

where

$a_{ij}$  = estimated pit depth for pit i at time  $t_j$

$t_j$  = time to photographic scan

n = number of pits on the particular specimen's surface

m = number of photographic scans

This results in pitting rate constants ( $C_i$ ) for various alternating stress levels. Also for the specimens tested at the same load, variance in  $C_i$  can be determined (for that alternating stress level only) from the standard statistical equation for variance.

Finally, the validity of the model for the stress in a pit (semi-elliptical surface flaw) is evaluated from the (a) and (2c) measurements made by examination of the fracture surfaces in the SEM. This is done for each pit observed to initiate a crack in two ways. First the actual pit depth ( $a_a$ ), the actual pit diameter ( $2C_a$ ), and the maximum cross-section gross stress ( $\sigma_{max}$ ) are used in Equation 6, which is reprinted below:

$$K_{oc} = \frac{\sigma_{max}^2 \pi a M^{1/2}}{\phi^2 - 0.177 M \left(\frac{\sigma}{\sigma_{ys}}\right)^2} \quad (6)$$

where  $M$ ,  $\phi^2$ , and  $\sigma_{ys}$  are as described before, to determine a calculated threshold stress intensity,  $K_{oc}$ . The calculated threshold stress intensity for each pit is then compared to the threshold stress intensity determined from the propagation tests. The second way in which the validity of the model for the stress in a pit is evaluated begins by determining the actual  $a/2c$  ratios. Next pit depth values are calculated from Equation 13 (which is Equation 6 rearranged);

$$a_c = \frac{K_{oc}^2 \phi^2 - 0.177 M \left(\frac{\sigma}{\sigma_{ys}}\right)^2}{\sigma_{max}^2 \pi M} \quad (13)$$

where  $a_c$  is the pit depth calculated using actual  $a/2c$  ratios and  $K_{o_{cp}}$ ,  $M$  is determined from actual  $a/2c$  ratios, and the remainder of the terms are as described before.

The calculated pit diameter values ( $2c_c$ ) result from dividing  $a_c$  by the  $a/2c$  ratio.

### 5.6 Fractography Procedure

The fracture surfaces from both the propagation and S-N tests were removed from each test specimen. These surfaces were prepared for examination in a scanning electron microscope (SEM). A Bausch and Lomb SEM-II was utilized in examining these fracture surfaces.

The primary effort of this examination was to correlate fracture modes in the S-N specimen with those in the propagation specimen.

## 6.0 RESULTS AND DISCUSSION

### 6.1 Results and Discussion of FGG Tests

A total of four fatigue-crack growth tests were conducted, two in lab air and two in salt water. The raw data was obtained and processed as described in Chapter 5. The raw data along with the processed data may be found in the Appendix. The a-N data and the reduced  $da/dN - \Delta K$  data for each test are plotted in Figures 39 through 46. Weibull curve fits for the combined tests are plotted in Figures 47 and 48 along with their respective threshold change in stress intensity values  $\Delta K_{o_{cp}}$  calculated from Equation 3. Figure 49 compares the curve fit of the air tests to that of the salt water tests.

In comparing the curves several things may be observed. These observations are listed below.

- 1) Both curves are fitted to data which is 'heavy' in the low  $da/dN$  range.
- 2) The low end of the lab air curve fit appears to be shifted to the right of the actual data.
- 3) The instability stress intensities ( $K_b$ ) for lab air and salt water are separated by a large range of stress intensity.
- 4) For intermediate values of  $da/dN$  the two curves are approximately equivalent and actually cross each other.

These observations are interpreted as follows:

- 1) The  $K_b$  difference is most likely a result of the lack of high end data rather than any actual difference in  $K_b$ .

A-N DATA FOR SPECIMEN AF1

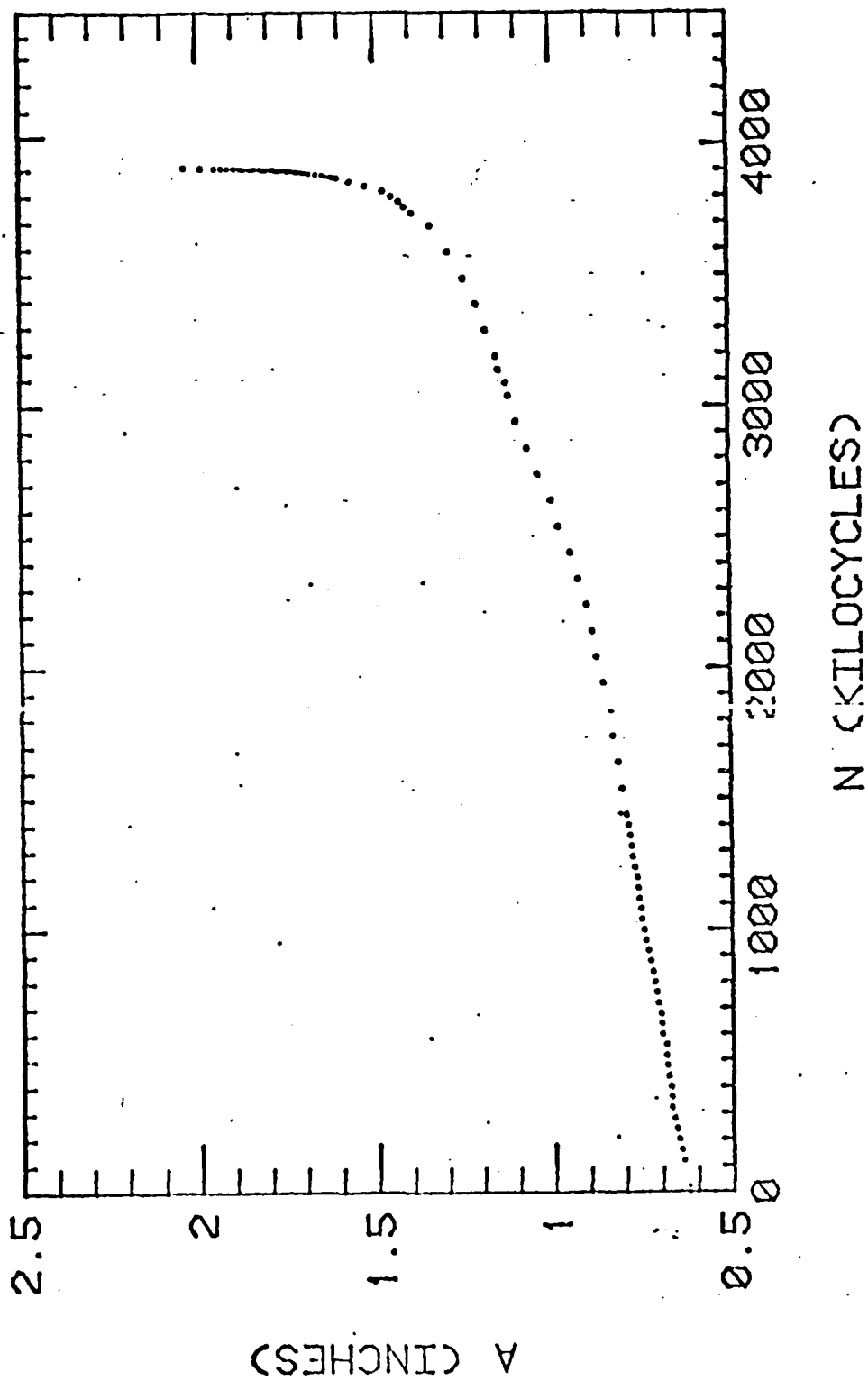


Figure 39: a-N Data, Lab Afr - Test 1

A-N DATA FOR SPECIMEN AF2

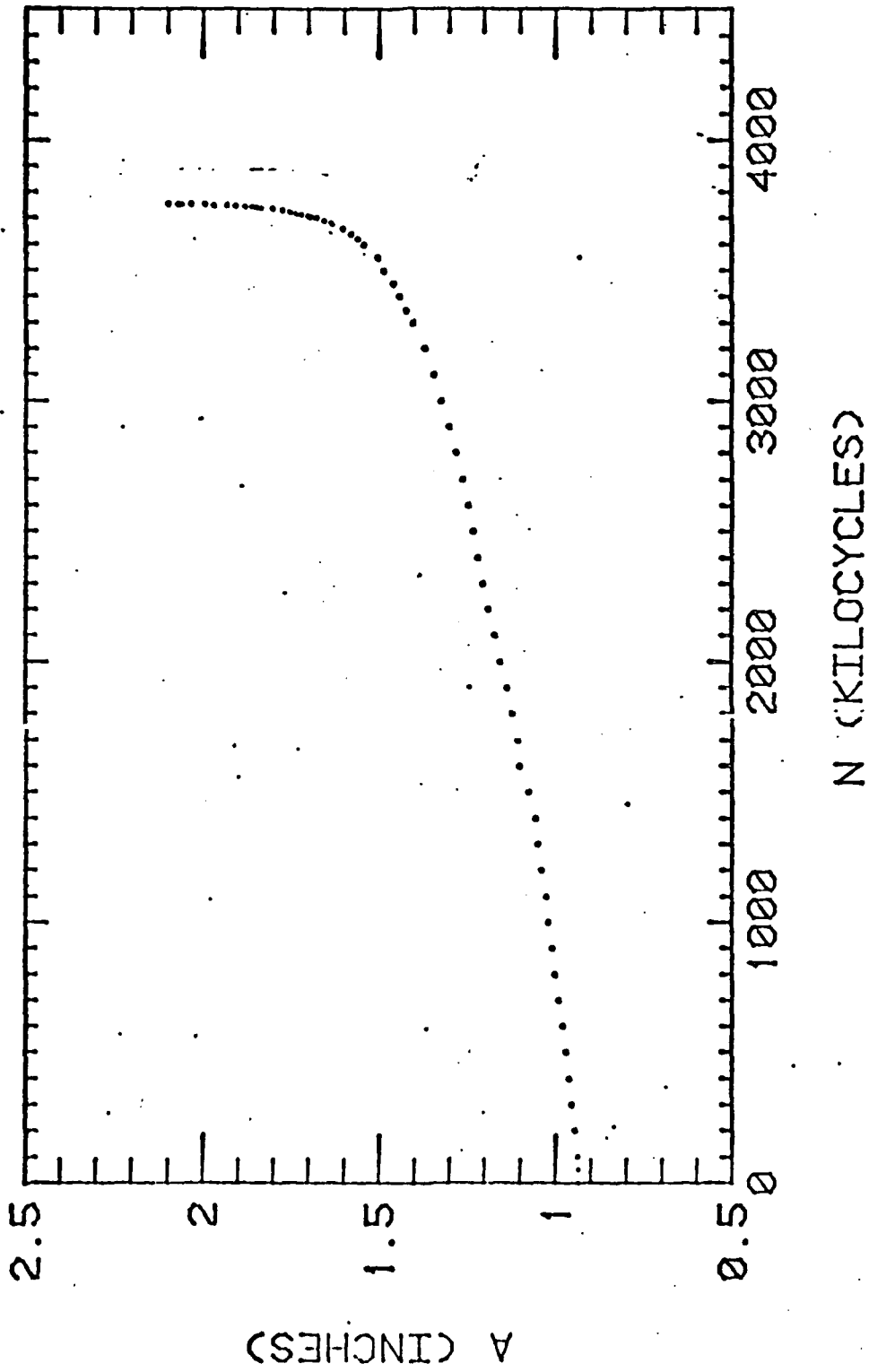


Figure 40: a-N Data, Lab Air - Test 2

A-N DATA FOR SPECIMEN AF3

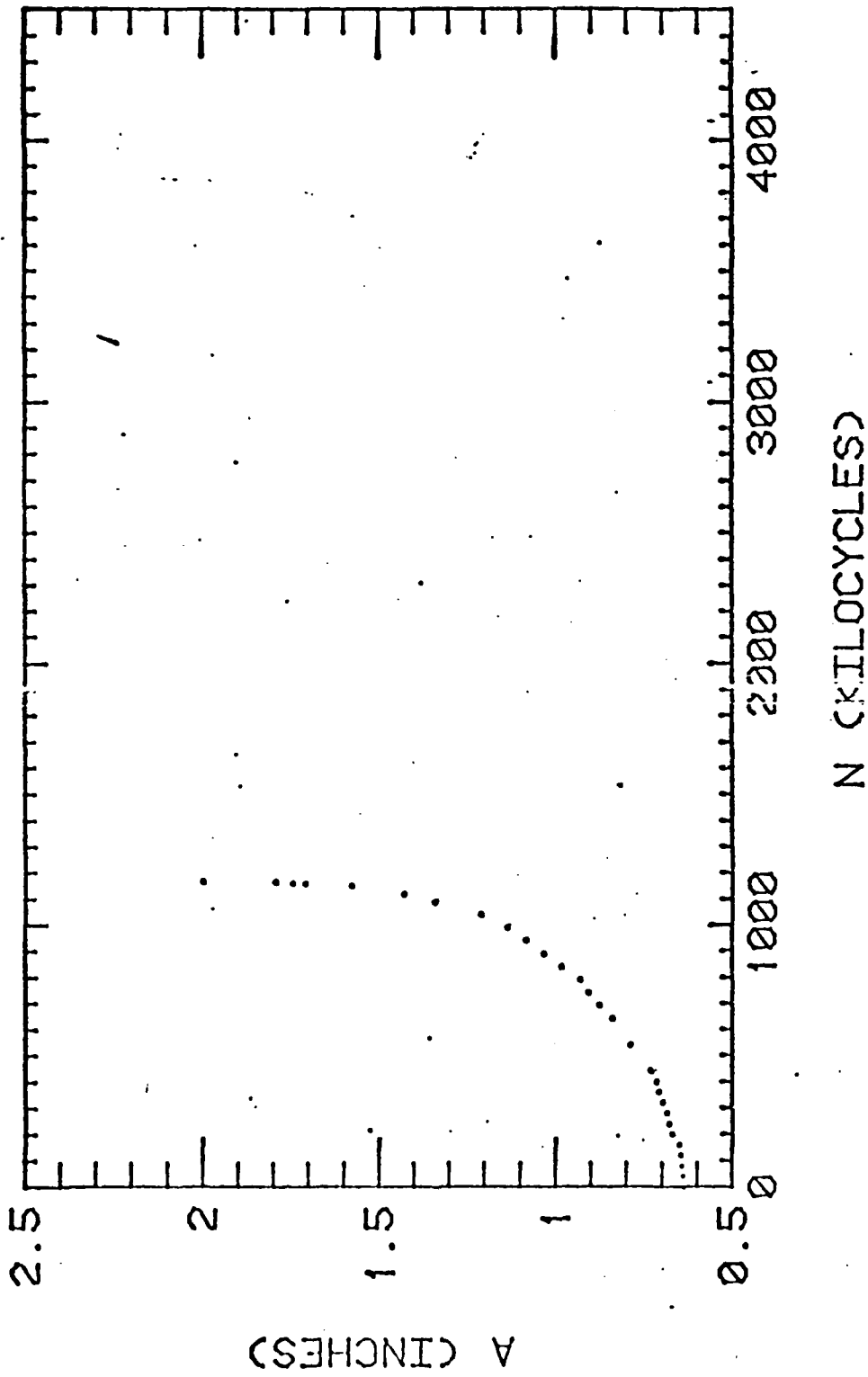


Figure 41: a-N Data, Salt Water - Test 3

A-N DATA FOR SPECIMEN AF4

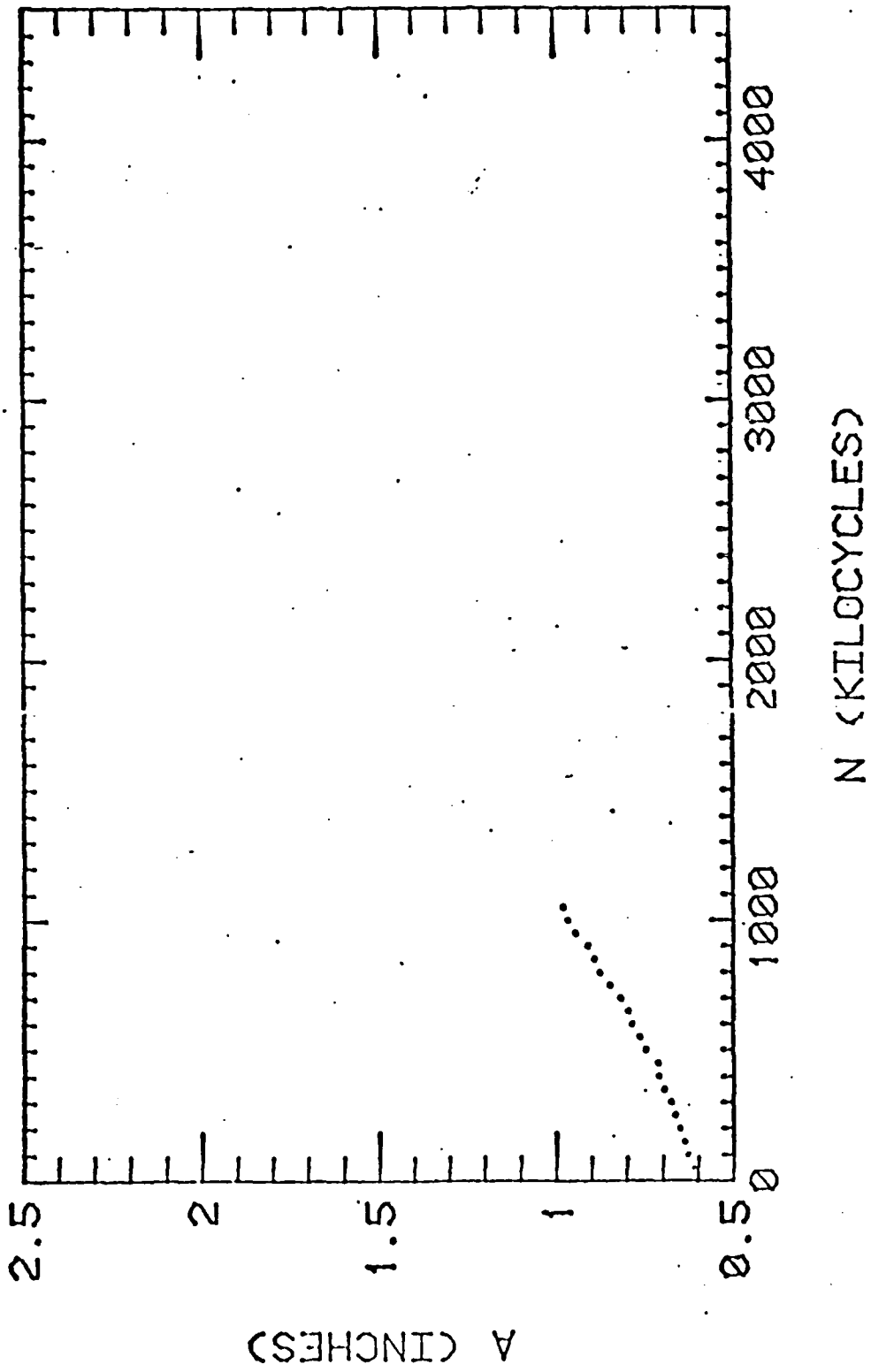


Figure 42: a-N Data, Silt Water - Test 4

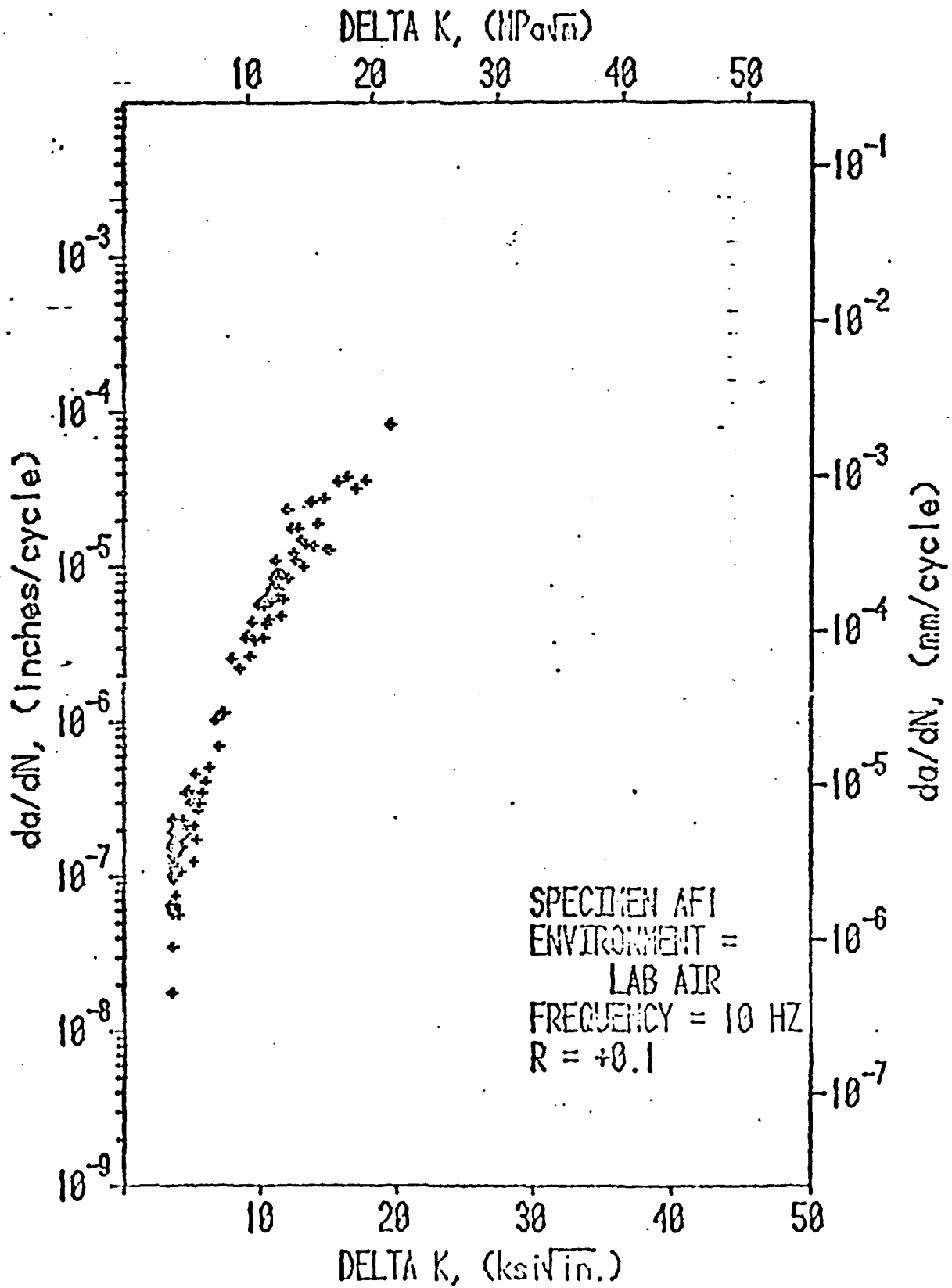


Figure 43: FCP Data Lab Air - Test 1

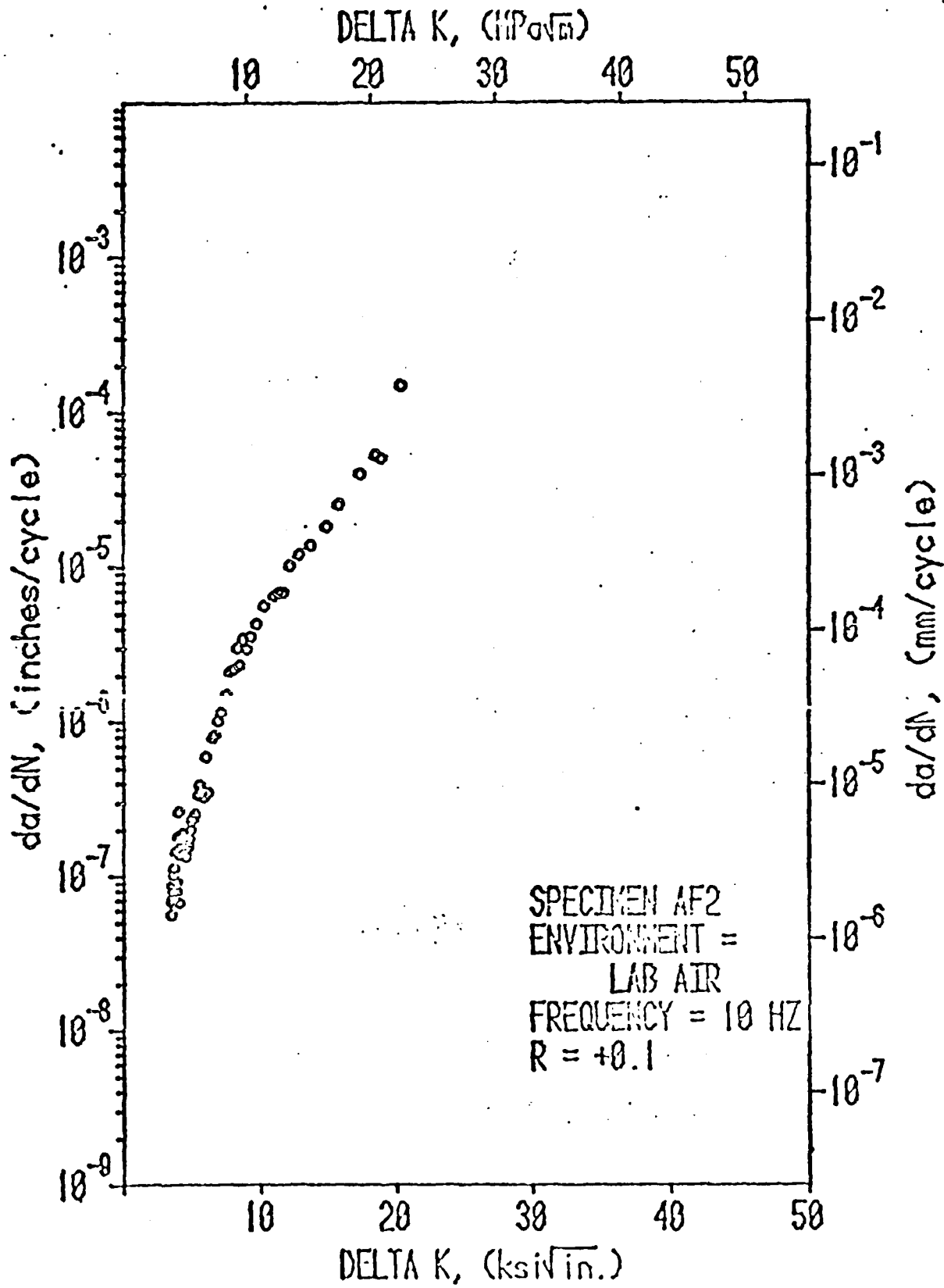


Figure 44: FCP Data Lab Air - Test 2

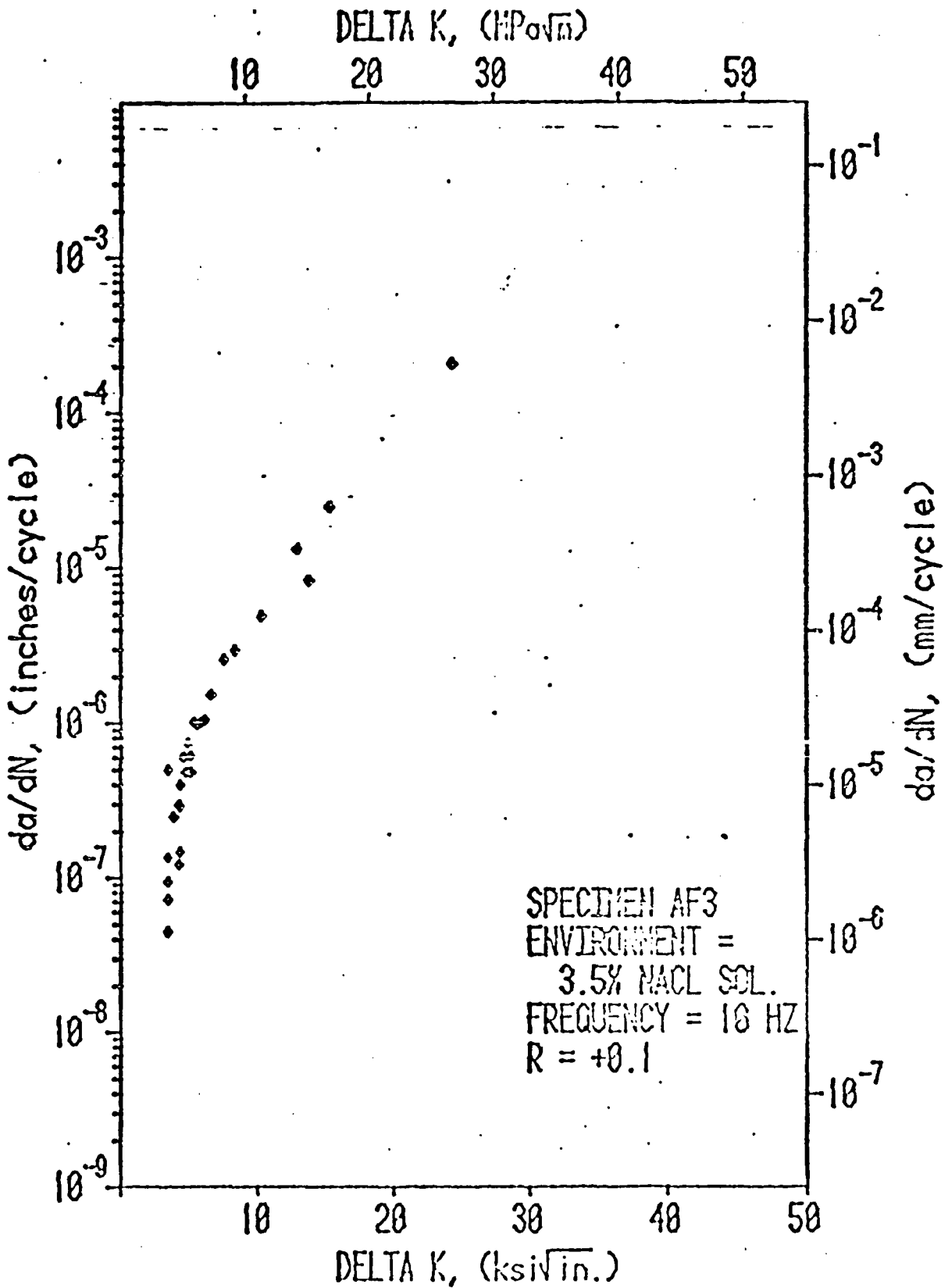


Figure 45: FCP Data Salt Water - Test 3

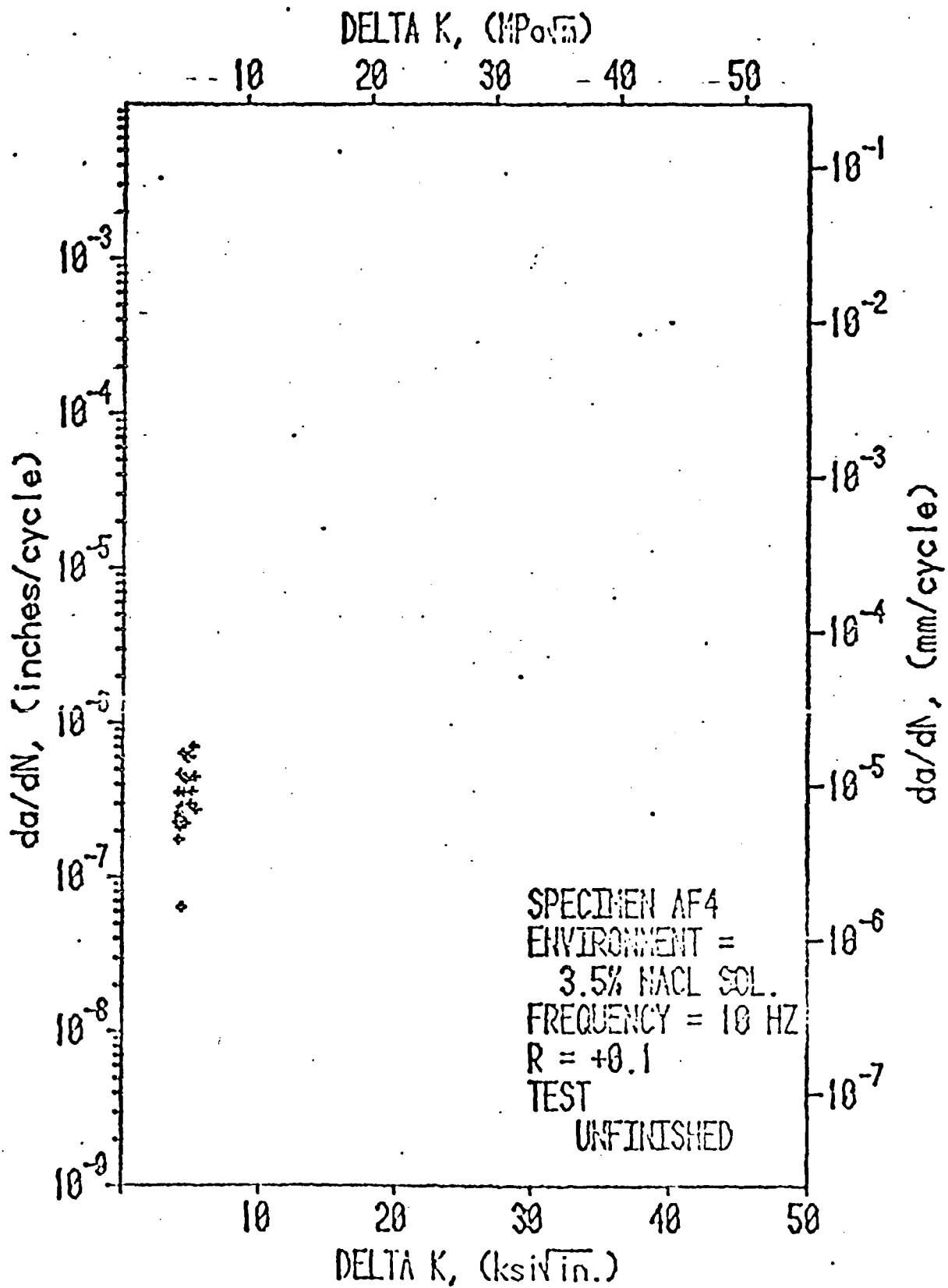


Figure 46: FCP Data Salt Water - Test 4

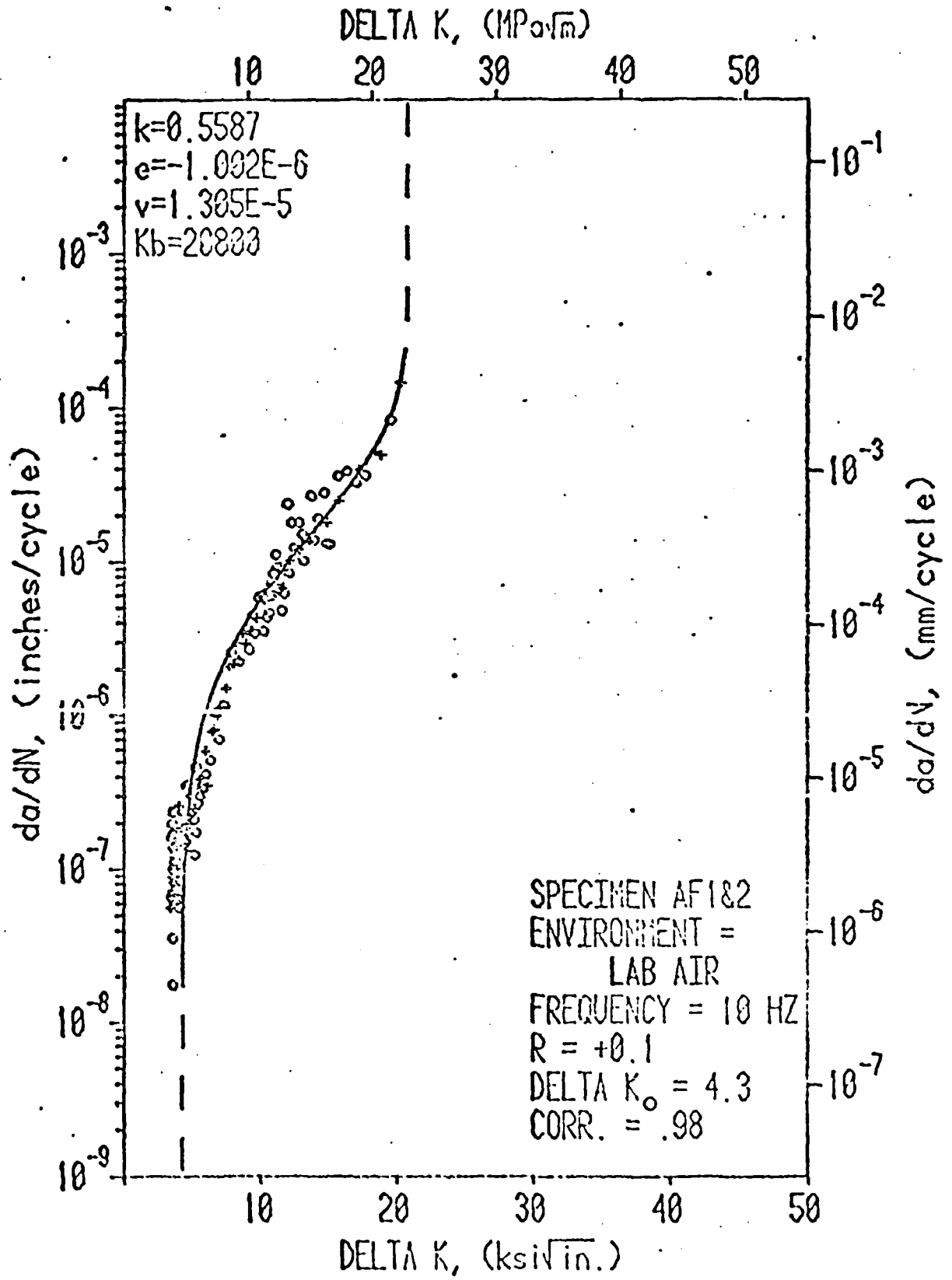


Figure 47: FCP Curve Fit - Lab Air

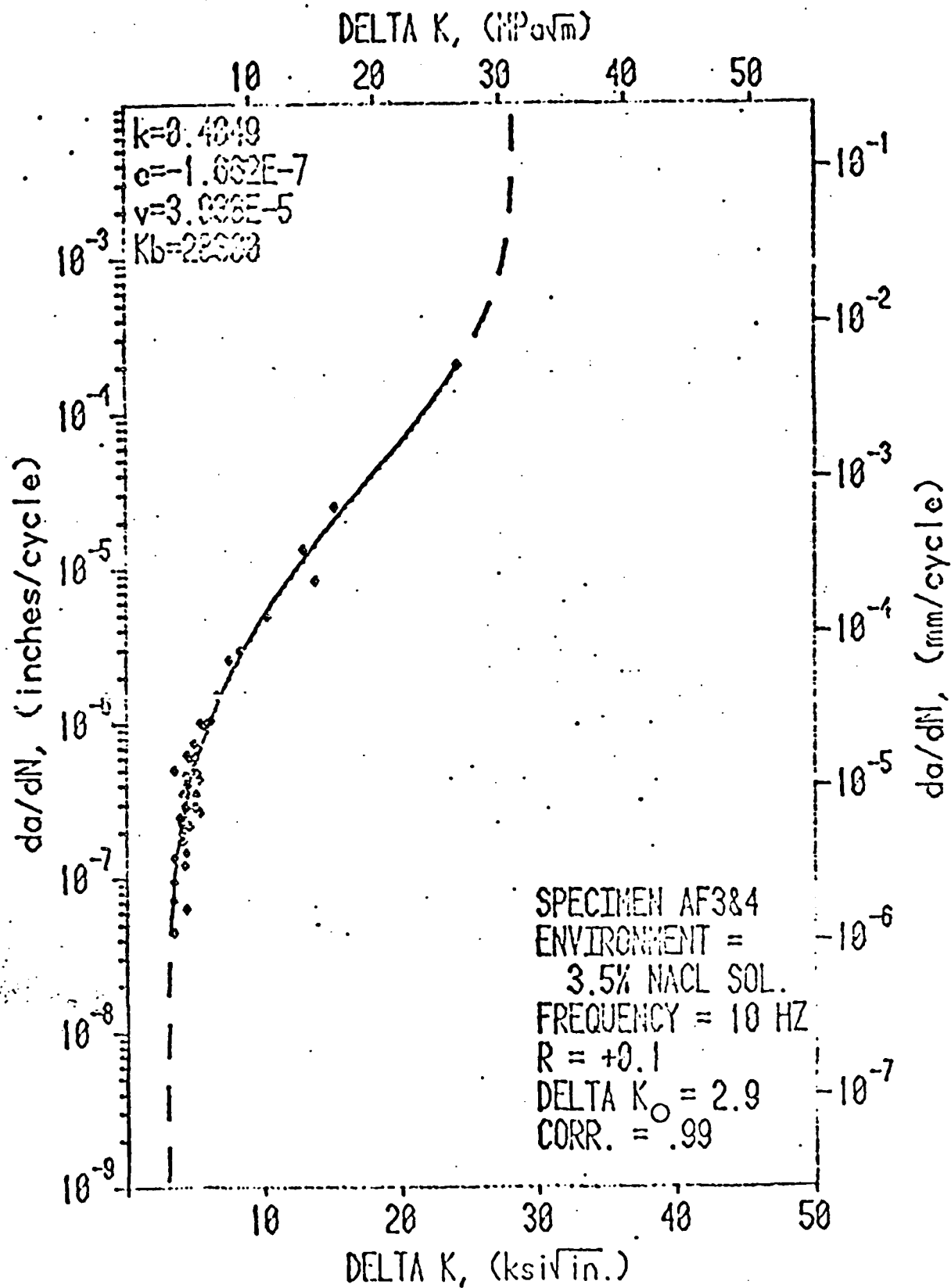


Figure 48: FCP Curve Fit - Salt Water

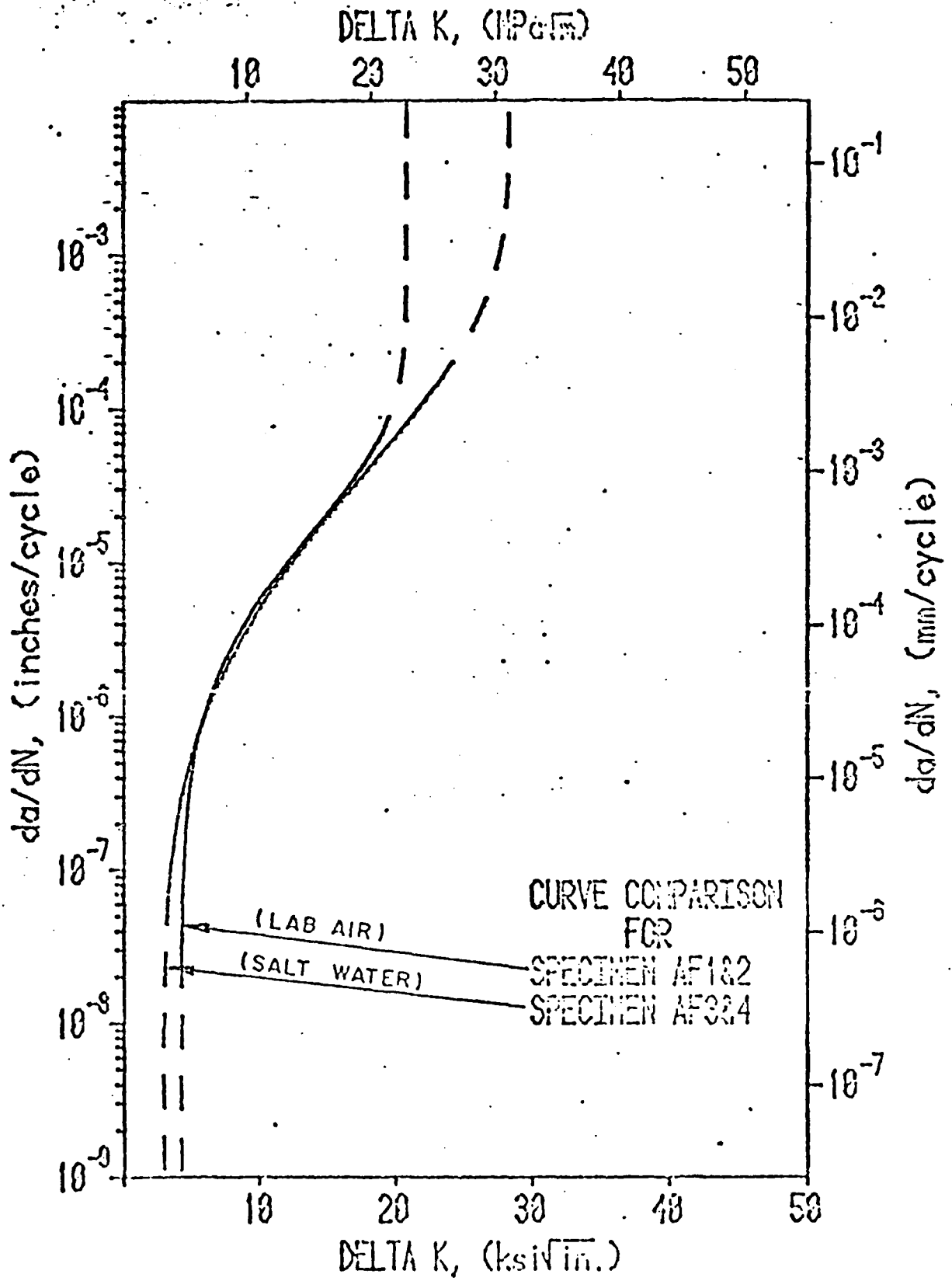


Figure 49: FCP Curve Comparison  
Lab Air - Salt Water

- 2) The  $K_{o_{cp}}$  difference between the two environments is suspect because of the seemingly poor curve fit for the lab air low end data.
- 3) The above two interpretations (along with the fact that the intermediate portion of the  $da/dN$  curves are approximately equivalent) indicate that the crack growth curves for the four tests are not detectably different from one environment to another.

This at first seems inconsistent with reported results (Chapter 3) indicating that salt water environments increase crack propagation rates over lab air base line crack propagation rates. However, if one considers the frequency effects on corrosion fatigue, the above similarity in  $da/dN$  curves could be explained by assuming that the 10 Hz test frequency did not allow time for the corrosion effects to occur. Another possible reason for this apparent inconsistency would be that the test procedure biased the data somehow. The author has no reason to suspect this.

## 6.2 Results and Discussion of S-N Tests

This section is divided into four separate parts each of which center upon one particular aspect of the data generated from the S-N tests.

### 6.2.1 Results and Discussion of S-N Data

A total of two air and twelve salt water S-N tests provided useable data. The base data are listed in Table 5 where they are also

TABLE 5  
S-N DATA AND REDUCTION

Spec. #	Time (Hrs.)	Cycles $\times 10^3$	$P_{max}$ (lbs)	Minimum Cross-Sectional Area	$\sigma_{max}$ (ksf)	Environment	Comment
3	120.0	4,500	122	.0213	5.74	Salt Water	Run Out
4	1.4	52	1,220	.0239	50.96	Air	
5	1.2	43.6	840	.0240	35.04	Salt Water	
7	10.7	386.4	472	.0236	19.98	Salt Water	
8	36.8	1,324.8	354	.0248	14.29	"	
9	30.4	1,094.8	363	.0242	14.98	"	
10	19.2	691.2	350	.0232	15.02	"	
11	13.4	660.8	335	.0224	14.98	"	
12	14.5	522.9	300	.0200	15.01	"	
14	14.8	533.7	337	.0224	14.09	"	
15	125.0	4,500	755	.0216	35.00	Air	Run Out
16	12.5	450.3	344	.0229	15.03	Salt Water	
17	2.9	103.2	559	.0224	25.00	"	
18	150.3	5,410	217	.0217	9.94	"	Run Out

reduced according to the method described in Chapter 5. A plot of the S-N data is presented in Figure 50. While there was not enough data generated to statistically determine relationships, two basic observations can be made. The first observation is the obvious degradation of the fatigue life of those specimens tested in salt water. The second observation is that the salt water S-N curve appears to reach runout.

The first observation was expected, however there are two interesting things that should be noted. The first is the severity in the degradation of fatigue life (the approximate endurance limits for lab air and salt water environments are 35 and 10 ksi respectively, while at a stress level of 35 ksi the salt water test failed after 43.6 kilocycles while the lab air test did not fail even after 4,500.0 kilocycles). The second interesting thing to note is that, in light of the observations made concerning the similarity in the fatigue-crack propagation curves, the degradation in the fatigue life can be attributed almost entirely to the initiation stage.

The second observation (an endurance limit in the pitting environment) was not expected. This result might be explained in one of two ways. First it is possible that pit growth did not occur or that it stopped before a large enough pit size was reached to initiate a fatigue crack. The second way this might be explained is that the tests were simply discontinued too early and that failure would have eventually occurred.



### 6.2.2 Results and Discussion of Pit Growth Analysis (Photographic Technique)

The analysis of pit growth was not accomplished because the photographic technique employed failed. The photographic technique failed for two reasons. The first reason was that the reactions at the corrosion pits produced gaseous bubbles which adhered to the specimen's surface and effectively covered the pits from view. Photographs of a specimen surface during testing are shown in Figures 51 and 52. The second reason the photographic technique failed is that the corrosion pits were 'closed corrosion pits'. Closed corrosion pits in this case means that the advancing surface of the pit cannot be seen because of the oxide and other debris which fill and cover the pits. Figure 53 is an SEM photograph illustrating the covering of the pits.

It must be stressed that this technique only failed on this material and only under the specific environmental conditions and specific surface preparation previously described. This technique has been effectively used upon another material (14).

### 6.2.3 Results and Discussion of Fatigue Loaded Pit Geometry

The SEM was used to examine the fracture surfaces of the S-N specimens tested in salt water. One result of this examination was to enable the determination of all pit widths and depths which initiated cracks in each specimen's fracture plane (in some specimens more than one crack was initiated). The measurements made are illustrated in Figures 54 through 56, and are listed along with various values

**Figure 51: Bubbles Obscuring Pits During Testing (16X)**

**Figure 52: Specimen With Corrosion Debris and Bubbles  
Near End of Test (16X)**

**Figure 53: Pit Size Obscured by Corrosion Debris**

**(a) Fracture Plane (150X)**

**(b) Pitted Surface (100X)**

**Figure 54: Example of Pit Dimension Measurements**

**(a) Fracture Plane (400X)**  
**(Pit Depth)**

**(b) Pitted Surface (400X)**  
**(Pit Width)**

Figure 55: Example of Pit Dimension Measurements

- (a) Fracture Plane (003X)  
(Pit Depth)
- (b) Pitted Surface (200X)  
(Pit Width)

Figure 56: Example of Pit Dimension Measurements

- (a) Fracture Plane (500X)  
(Pit Depth)
- (b) Pitted Surface (300X)  
(Pit Width)

calculated from them in Table 6.

The actual pit depths for crack initiation are plotted against the specimen's maximum alternating stress in Figure 57. This plot reveals decreasing pit depths with increasing maximum alternating stress. This would be expected since the stress intensity is directly proportional to both the nominal stress ( $\sigma$ ) and the flaw length ( $a$ ) and therefore theoretically the flaw length will decrease with increasing nominal stress.

Another, and perhaps more interesting result may be found in Figure 58. This figure is a plot of the  $a/2c$  ratio for each pit which initiated a crack against the maximum alternating stress. While there is not enough data to actually say, it does appear that a pit's  $a/2c$  ratio increases with increasing maximum alternating stress. If this relationship is indeed true, it would have a significant impact upon the life prediction of a pitted structure due to the  $a/2c$  effect upon the stress intensity.

#### 6.2.4 Results and Discussion of the Semielliptical Surface Flaw Model of a Pit

Using the pit dimensions measured with the SEM, the data reduction methods described in Chapter 5 were used to calculate 1) the threshold stress intensity for the actual pits and 2) the pit depths and diameters based upon the threshold stress intensity from the FCP curves ( $K_{o_{cp}} = 3.20 \text{ ksi}\sqrt{\text{in}}$ ) and the actual  $a/2c$  ratios. The base data and the reduced data can again be found in Table 6.

Figure 59 relates the calculated threshold stress intensity from

TABLE II

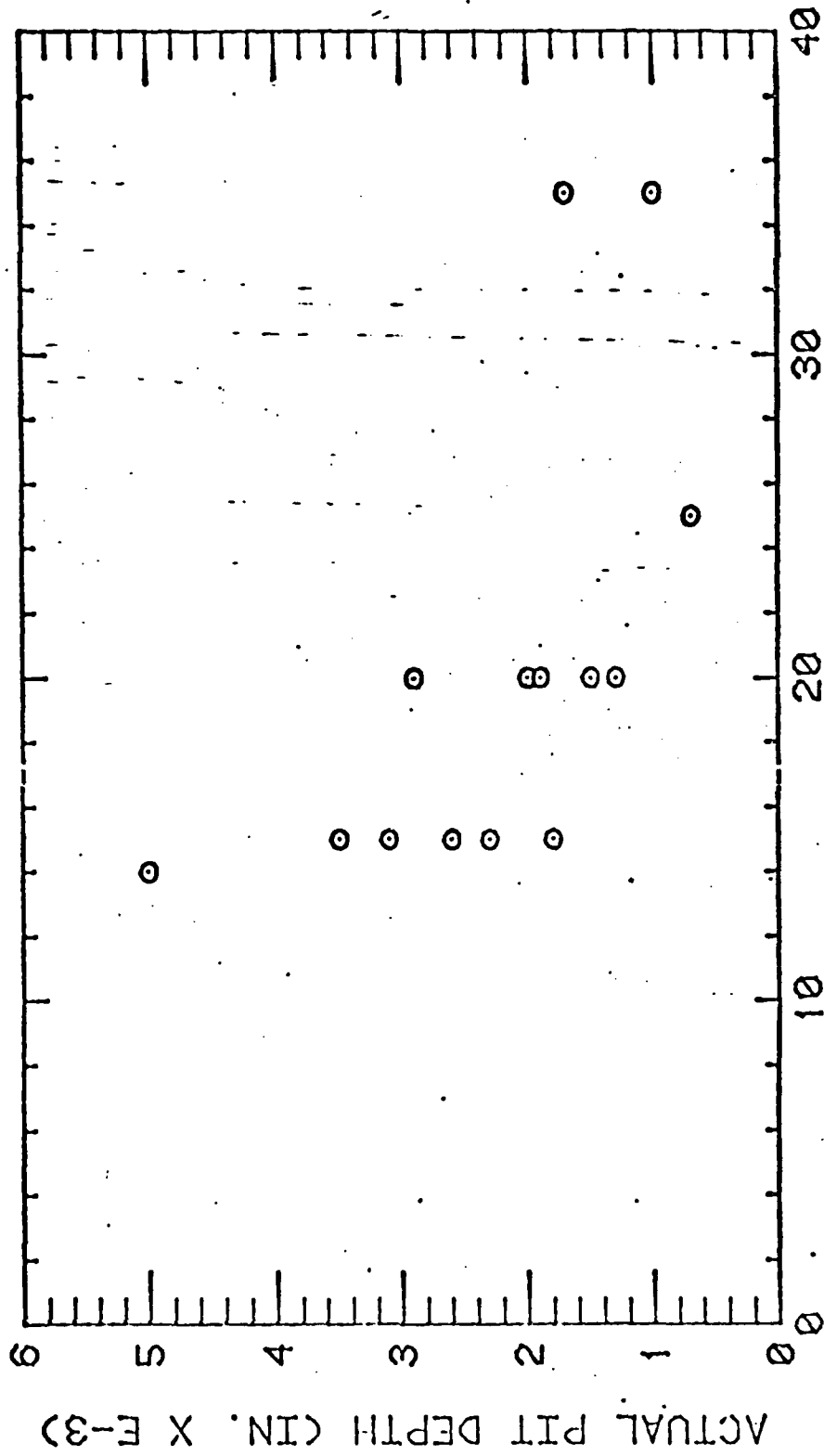
## PIT DIMENSIONS AND CALCULATIONS FOR FATIGUE CRACK INITIATION

Specimen #	Pit #	Actual Pit Depth $a_a$ (in.)	Calculated* Pit Depth $a_c$ (in.)	Actual Pit Dia. $a_a$ (in.)	Calculated* Pit Dia. $2c_c$ (in.)	a/2c	Maximum Stress (ksi)	Calculated* Threshold Stress Intensity (ksi $\sqrt{in}$ )	Pit Depth Actual/Calculated
14	1	.0050	.0203	.0249	.1010	.201	14.0	1.59	.246
9	1	.0031	.0146	.0289	.1364	.107	15.0	1.48	.212
10	1	.0018	.0149	.0153	.1263	.118	15.0	1.11	.121
11	1	.0026	.0195	.0107	.0802	.243	15.0	1.17	.133
12	1	.0035	.0158	.0233	.1053	.150	15.0	1.50	.222
16	1	.0023	.0173	.0120	.0901	.192	15.0	1.17	.133
16	2	.0026	.0164	.0156	.0982	.167	15.0	1.27	.159
7	1	.0029	.0100	.0140	.0483	.207	20.0	1.72	.29
7	2	.0015	.0086	.0109	.0523	.138	20.0	1.33	.174
7	3	.0013	.0035	.0099	.0549	.131	20.0	1.25	.153
7	4	.0020	.0098	.0102	.0500	.196	20.0	1.45	.204
7	5	.0019	.0083	.0162	.0709	.117	20.0	1.53	.230
17	1	.0007	.0050	.0077	.0549	.091	25.0	1.20	.14
5	1	.0017	.0044	.0050	.0129	.340	35.0	2.00	.386
5	2	.0010	.0030	.0056	.0166	.179	35.0	1.86	.333
5	3	.0017	.0035	.0069	.0141	.246	35.0	2.24	.486
5	4	.0010	.0033	.0044	.0146	.227	35.0	1.75	.303

\*Based upon  $K_{0cp} = 3.20$ , which was determined from FCG tests.

+Stress intensity calculated for semielliptical surface flaw using actual dimensions.

ACTUAL PIT DEPTH VS NOMINAL STRESS



MAXIMUM STRESS (KSI)

Figure 57: Pit Depth - Maximum Stress Correlation

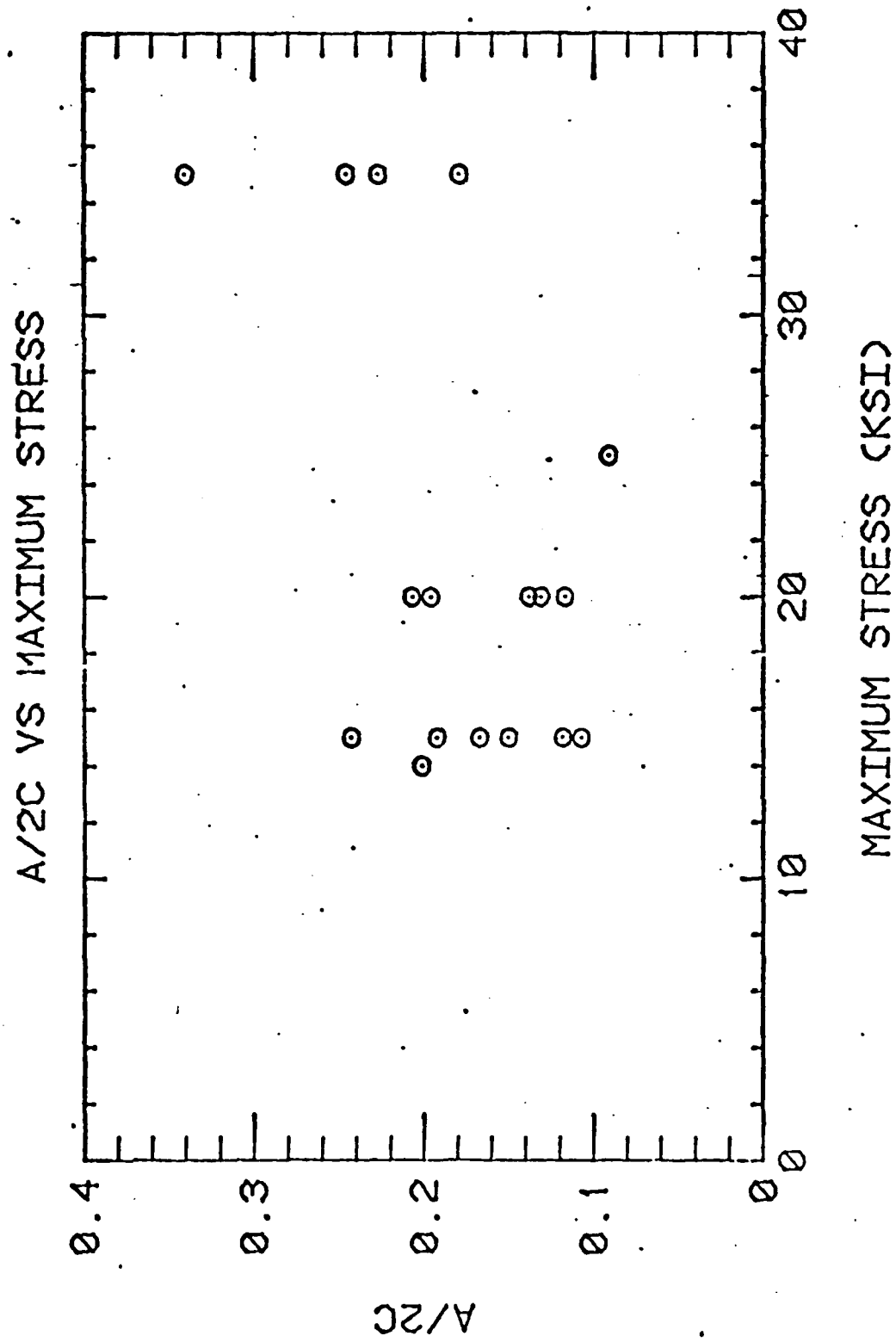


Figure 58: Pit Geometry - Maximum Stress Correlation

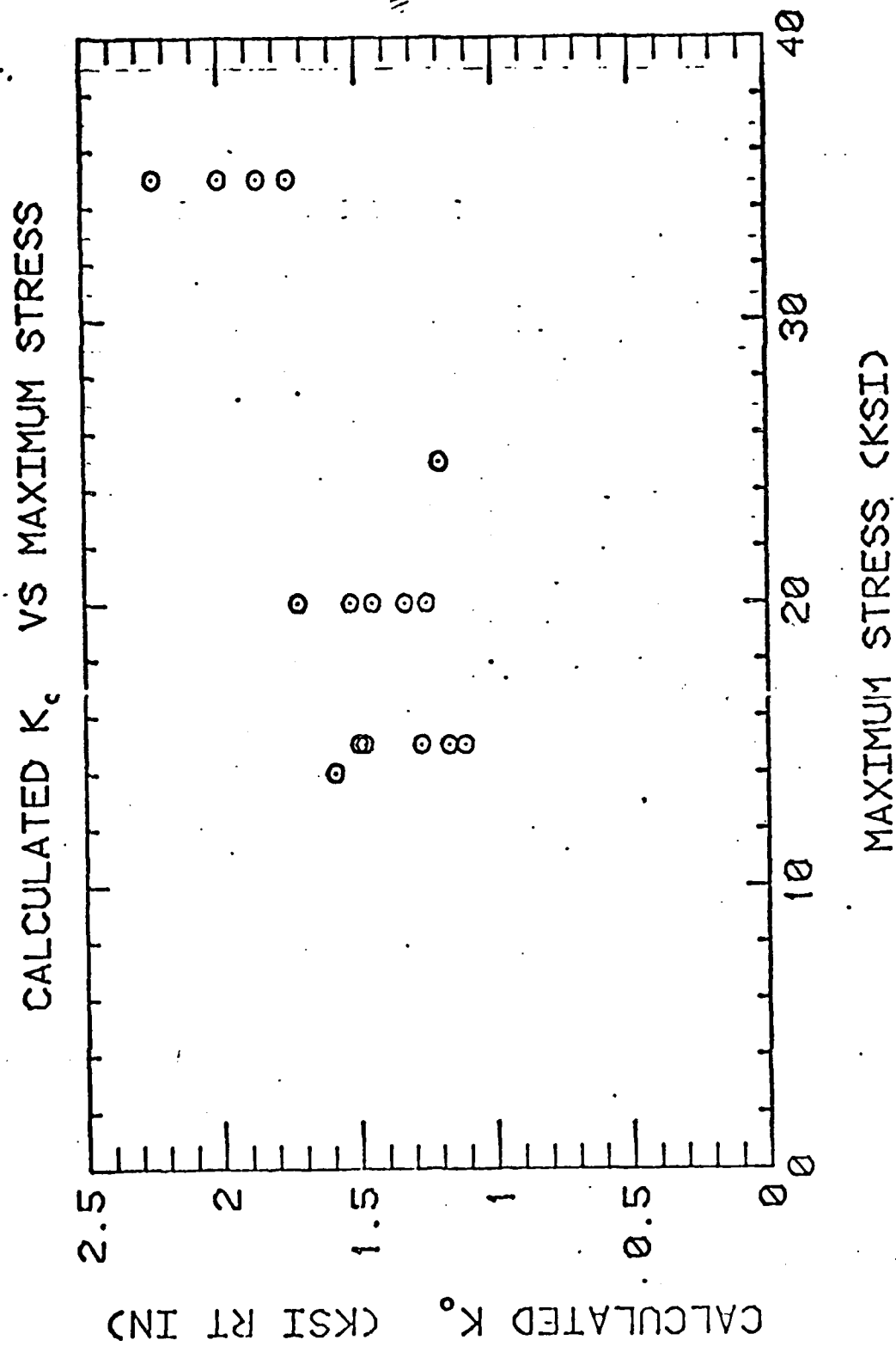


Figure 59: Stress Intensity - Maximum Stress Correlation

actual pit dimensions to the maximum alternating stress. From the figure it may be observed that all of the calculated threshold values fall below the threshold values predicted from the FCP threshold ( $K_{o_{cp}}$ ) of  $3.0 \text{ ksi}\sqrt{\text{in}}$ . However, it may also be observed that as the maximum alternating stress increases, the calculated  $K_o$  increases which in effect reduces difference between calculated  $K_o$  and  $K_{o_{cp}}$ .

Because of the pit's three dimensionality, theory would predict the threshold stress intensity calculated from the actual pits to be greater than or equal to  $K_{o_{cp}}$  (i.e. actual pit dimensions should be greater than those calculated from  $K_{o_{cp}}$ ). Since the exact opposite occurred (actual pit dimensions were less than those calculated from  $K_{o_{cp}}$  (Figures 60 and 61)), the validity of  $K_{o_{cp}}$  comes into serious doubt.  $K_{o_{cp}}$  could be incorrect for two reasons. First there is possibly not enough data to accurately predict it. Secondly  $K_{o_{cp}}$  evaluated by this method may not accurately predict the threshold stress intensity.

### 6.3 Results and Discussion of Fractographic Examination

Fractographic examination of both the crack growth and S-N specimens resulted in the fractographs presented in Figures 62 through 74. The fractographs for the air crack growth specimen (Figures 62 through 65) and the salt water crack growth specimen (Figures 66 through 68) illustrate the changes in fracture mode as  $\Delta K$  increases. As may be observed both specimens show the same transitions in fracture mode as  $\Delta K$  increases. (The salt water specimen's fractographs actually appear

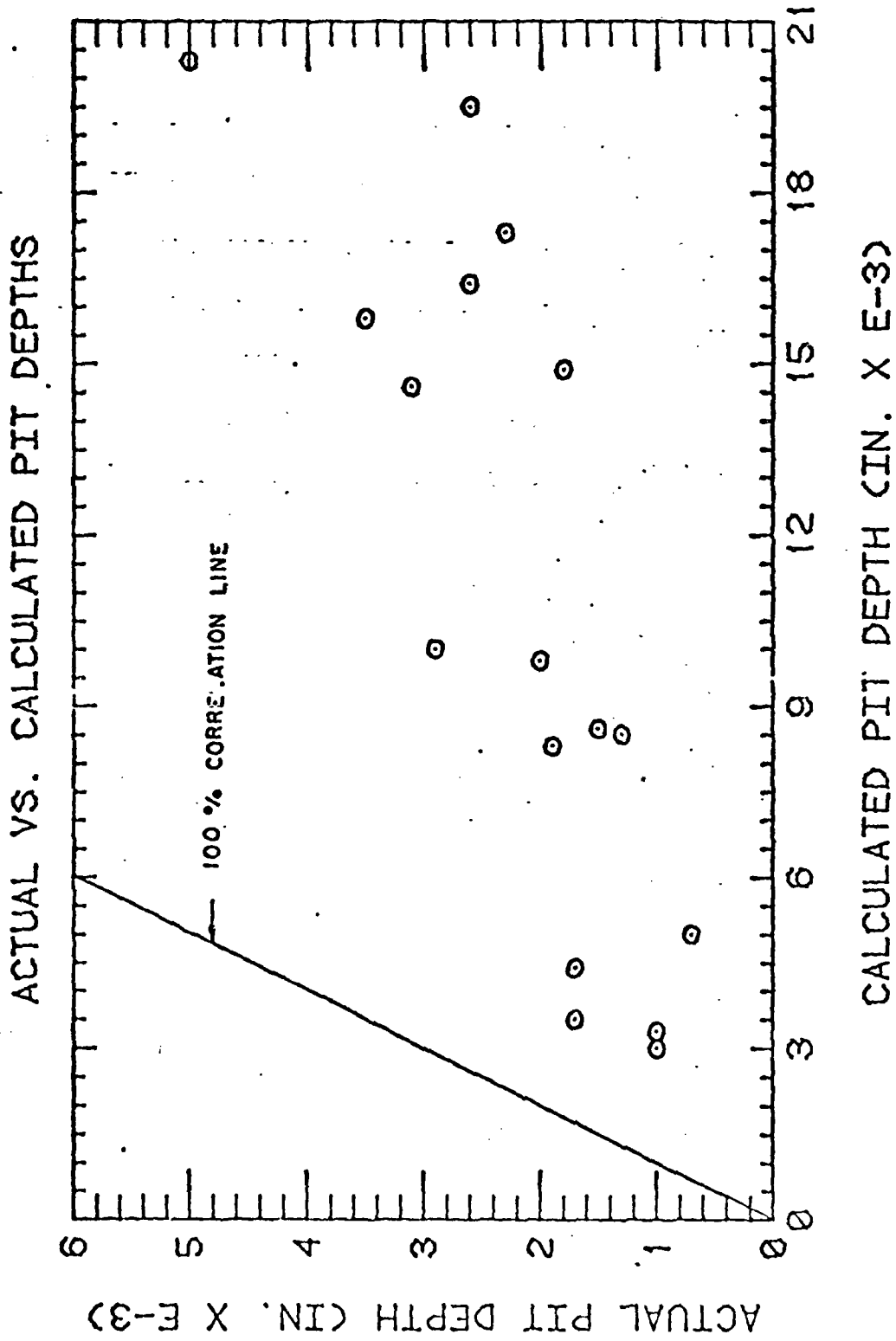


Figure 60: Actual - Calculated Pit Depth Comparison

PIT DEPTH RATIO VS. MAXIMUM STRESS.

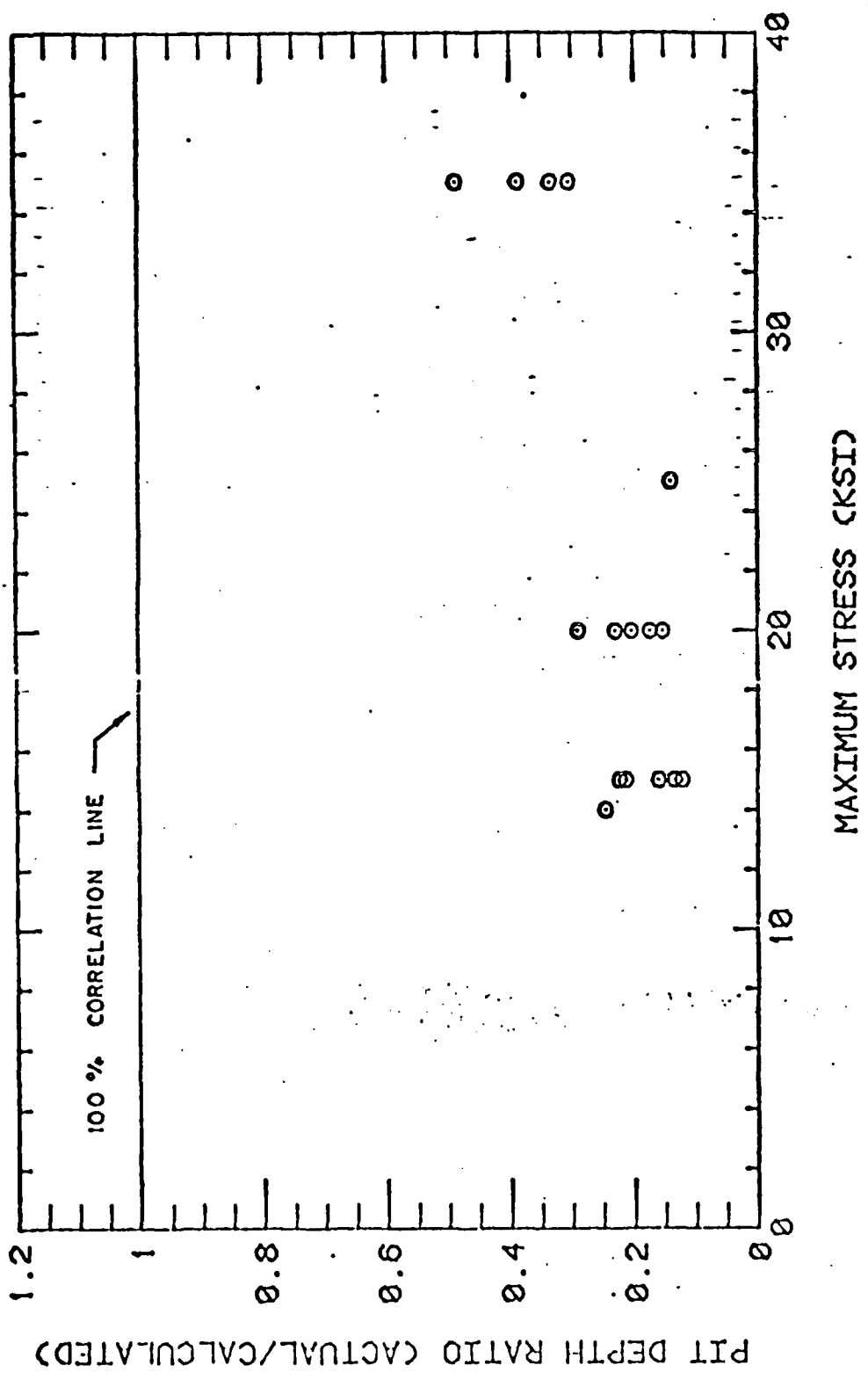


Figure 61: Pit Depth Ratio - Maximum Stress Correlation

**FRACTOGRAPHY**  
**FOR**  
**CRACK PROPAGATION SPECIMEN**  
**AIR TESTS**

**Figure 62:** Typical Fracture Surface In Low  $\Delta K$  Region

$\Delta K$  4 ksi $\sqrt{\text{in}}$

(Flat cleavage with cleavage steps parallel to  
advancing crack front)

200x

(Arrow Indicates Direction of Crack Propagation)

**Figure 63:** Typical Fracture Surface In Lower Intermediate

$\Delta K$  Region

$\Delta K$  7 ksi $\sqrt{\text{in}}$

(Transition between cleavage with steps parallel  
to advancing crack front and cleavage with steps  
perpendicular to advancing crack front)

200x

FRACTOGRAPHY  
FOR  
CRACK PROPAGATION SPECIMEN  
AIR TESTS

Figure 64: Typical Fracture Surface In Intermediate  
 $\Delta K$  Region

$\Delta K$  9.5 ksi $\sqrt{\text{in}}$

(Flat cleavage fracture with cleavage steps  
perpendicular to the advancing crack front)

200x

Figure 65: Typical Fracture Surface In High  $\Delta K$  Region

$\Delta K$  20 ksi $\sqrt{\text{in}}$

(Ductile tearing)

200x

FRAC TOG R A P H Y  
FOR  
CRACK PROPAGATION SPECIMEN  
SALT WATER TESTS

Figure 66: Typical Fracture Surface In Lower Intermediate  
 $\Delta K$  Region  
 $\Delta K$  5.5 ksi $\sqrt{\text{in}}$   
(Transition between cleavage with steps parallel  
to advancing crack front and cleavage with steps  
perpendicular to advancing crack front)  
200x

Figure 67: Typical Fracture Surface In Intermediate  
 $\Delta K$  Region  
 $\Delta K$  10.5 ksi $\sqrt{\text{in}}$   
(Flat cleavage fracture with cleavage steps  
perpendicular to the advancing crack front)  
200x

FRAC~~T~~OGRAPHY  
FOR  
-CRACK-PROPAGATION SPECIMEN  
SALT WATER TESTS

Figure 68: Typical Fracture Surface In High  $\Delta K$  Region

$\Delta K$  24 ksi $\sqrt{\text{in}}$

(Ductile tearing)

200x

FRACTOGRAPHY

FOR

S-N SPECIMEN

AIR TESTS

Figure 69: Fracture Surface Near The Initiation Point

200x

Figure 70: Fracture Surface Away From the Initiation Point

100x

FRACTOGRAPHY  
FOR  
S-N SPECIMEN  
SALT WATER TESTS

Figure 71: Fracture Surface Near The Initiation Point  
200x

Figure 72: Fracture Surface Away From The Initiation Point  
100x

FRACTOGRAPHY

FOR

S-N SPECIMEN

Figure 73: Striations On Air Specimen At Cleavage -  
Ductile Tearing Transition  
Striation Spacing  $9.5 \times 10^{-5}$  in  
1300x

Figure 74: Striations On Salt Water Specimen At  
Cleavage-Ductile Tearing Transition  
Striation Spacing  $1.02 \times 10^{-4}$   
1300x

rougher than those of the air specimen's, however this is attributable to the corrosion of the fracture surface being exposed to the corrosive environment for an extensive period of time and not a difference in fracture mode.) Cleavage fracture with cleavage steps parallel to the advancing crack front was observed at low  $\Delta K$  values. Cleavage fracture with cleavage steps generally perpendicular to the advancing crack front was observed in the intermediate  $\Delta K$  range. Primarily ductile tearing was observed at high  $\Delta K$  levels. Fatigue striations were not observed on any of the crack propagation specimens.

Figures 69 and 70 illustrates typical fracture areas of the air S-N tests while Figures 71 and 72 do the same for the salt water tests. The air and the salt water S-N fracture surfaces were extremely similar to each other. In Figures 73 and 74 are fractographs of two striation areas which were observed. These were found near the cleavage-ductile tearing transition and thus at relatively high  $\Delta K$  levels. The striations spacing indicates  $da/dN$  rates of approximately  $9.6 \times 10^{-5}$ . This  $da/dN$  rate on the crack propagation curves is the approximate transition between Region II and Region III of the fatigue-crack growth curves. This indicates that the change in slope of the  $da/dN$  curve from Region II to Region III is attributable to a fracture mode change.

In comparing the fracture surfaces of the S-N specimens to those from the propagation specimens it was observed that they were surprisingly similar (considering that the stress intensity gradient is much higher for the S-N specimens) with the areas near the crack initiation points (S-N specimens) corresponding to the intermediate  $\Delta K$  ranges

(crack propagation specimens).

## 7.0 CONCLUSIONS

The following conclusions about the test hypothesis can be drawn from the experimental results:

- 1) The fatigue-crack growth rate of 2124-T851 aluminum (under the given test conditions) is essentially unaffected when the environment is changed from lab air to 3.5% sodium chloride solution.
- 2) A 3.5% sodium chloride solution (as opposed to a lab air environment) accelerates the initiation of fatigue cracks in the material investigated by a 'significant' amount. (This 'significant' amount is indicated by a drop in the endurance limit of approximately 40% yield strength.)
- 3) An endurance limit appeared to be reached for the test material when subjected to a 3.5% sodium chloride solution.
- 4) Pit growth in the test material could not be effectively monitored by the photographic technique employed because bubbles and corrosion debris effectively covered them.
- 5) Since the pit growth could not be monitored, empirical pitting rates could not be evaluated.
- 6) Fatigue crack initiation from corrosion pits was poorly predicted by a threshold stress intensity determined from propagation data.

In addition, the following observations resulted from the work presented:

- 1) Pit size at initiation appears to decrease with increasing maximum alternating stress level as would be expected.
- 2) A pit's  $a/2c$  ratio appears to be a function of maximum stress level ( $\sigma_{\max}$ ), with an increase in  $\sigma_{\max}$  resulting in an increase in the  $a/2c$  ratio.

## 8.0 RECOMMENDATIONS

The following is a list of recommendations for further study and experimentation. It is based on the results of this investigation and includes aspects of this investigation that could be improved.

- 1) Conduct more fatigue-crack growth tests to better evaluate the FCP curve, especially  $K_{o_{cp}}$ .
- 2) Determine, by any method, pit growth rates under fatigue loading so that accurate life predictions can be made.
- 3) Pitting upon cyclicly loaded materials should be studied on specimens with a much larger surface area so as to take into account the area dependence of pitting.
- 4) Analysis of pit initiation under cyclic loading should be conducted in the form of more tests and examination of the pitted surfaces.
- 5) Chemical and electrochemical conditions should be closely monitored and controlled in future tests.
- 6) A three dimensional method should be developed for evaluating the stress at a pit.
- 7) The stress- $a/2c$  relationship should be further investigated.

## 9.0 REFERENCES

1. Petit, D.E., Ryder, J.T., Krupp, W.E., and Hoepfner, D.W., "Investigation of the Effects of Stress and Chemical Environments on the Prediction of Fracture in Aircraft Structural Materials," Technical Report AFML-TR-74-183, Air Force Materials Laboratory, Wright-Patterson Air Force Base, Ohio, 1974.
2. Wohler, A., "Zeitschrift für Bauwesen," 10, 1860.
3. Hoepfner, D.W., and Krupp, W.E., "Prediction of Component Life by Application of Fatigue Crack Growth Knowledge," Engineering Fracture Mechanics, Vol. 6, 1974, pp. 47-70.
4. Inglis, C.E., "Stress in a Plate Due to the Presence of Cracks and Sharp Corners," Transactions of the Institution of Naval Architects, Vol. LV, Part 1, London, 1913.
5. Griffith, A.A., "Phenomena of Rupture and Flow in Solids," Philosophical Transactions of the Royal Society (London), Series A221, 1921, pp. 163-198.
6. Grosskruezel, J.C., "Strengthening and Fracture in Fatigue (Approaches For Achieving High Fatigue Strength)," Metallurgical Transactions, Vol. 3, No. 5, May, 1972, pp. 1255-1262.
7. Hoepfner, D.W., "The Initiation of Fatigue In Aluminum Alloys," presented at the Symposium on The Relation Between Heat Treatment, Microstructure and Fatigue in Structural Materials, sponsored by AIME, Atlanta, Georgia, May, 1971.
8. "Tentative Method of Test For Constant-Load-Amplitude Fatigue Crack Growth Rates Above  $10^{-8}$  m/cycle," ASTM Committee E24, ASTM, 1977.
9. Hudak, S.J., Jr., and Saxena, A., "Development of Standard Methods of Testing and Analyzing Fatigue Crack Growth Rate Data (Third Annual Report)," Technical Report AFML F33615-75-C-5064, Air Force Materials Laboratory, Wright-Patterson Air Force Base, Ohio, 1977.
10. Bowie, G.E., and Hoepfner, D.W., "Numerical Modeling of Fatigue and Crack Propagation Test Results," Proceedings of the 1976 International Conference on Computer Simulation for Materials Applications, Nuclear Metallurgy, Vol. 20, Part 2, 1976, pp. 1171-1178.

11. Reeves, R.K., "Microstructural and Environmental Effects on Fretting Fatigue," A Doctoral Dissertation Presented to the Graduate School of the University of Missouri-Columbia, May, 1977.
12. Kondas, K.R., "Influence of Microstructural and Load Wave Form Control on Fatigue-Crack Growth Behavior of Precipitation Hardening Stainless Steel," A Doctoral Dissertation Presented to the Graduate School of the University of Missouri-Columbia, July, 1976.
13. Mueller, L.N., "The Statistical Analysis and Presentation of Fatigue-Crack Growth Rate Data," A Master Thesis Presented to the Graduate School of the University of Missouri-Columbia, May, 1978.
14. Hoepfner, D.W., "Fatigue Crack Initiation Concepts in Solids," Submitted to Journal of Mechanics and Physics of Solids for publication, 1978.
15. Forsyth, P.J.E., "Fatigue Damage and Crack Growth in Aluminum Alloys," Acta Metallurgica, Vol. 11, No. 7, July 1963, pp. 703-717.
16. Sadananda, K., Shahinian, P., "Prediction of Threshold Stress Intensity for Fatigue Crack Growth Using a Dislocation Model," International Journal of Fracture, Vol. 13, No. 5, October, 1977, pp. 585-594.
17. Freudenthal, A.M., The Inelastic Behavior of Engineering Materials and Structures, Wiley & Sons, Inc., New York, 1950.
18. Purcell, A.H., "Dislocations and Fatigue Cracking," Industrial Research, April, 1977, pp. 81-84.
19. Pelloux, R.M., Stoltz, R.E., and Moskovitz, J.A., "Corrosion Fatigue," Materials Science Engineering, 25, 1976, pp. 193-200.
20. Hertzberg, R.W., Deformation and Fracture Mechanics of Engineering Materials, John Wiley & Sons, New York, 1976.
21. Craig, H.L., Jr., Crooker, T.W., and Hoepfner, D.W., editors, Corrosion Fatigue Technology, ASTM Special Technical Publication 642, American Society for Testing and Materials, 1978.
22. Howard, D., and Pyle, T., "Transgranular Stress-Corrosion Cracking," British Corrosion Journal, Vol. 3, No. 6, November, 1968, p. 301-304.

23. Jolliff, J.V., "Lecture Notes on Fatigue and Corrosion Fatigue," 1974.
24. Panhuise, J.A., "The Effect of a Frequency-Environment Synergism on the Fatigue-Crack Growth of SA533B-1: A Nuclear Pressure Vessel Steel," A Masters Thesis presented to the Graduate School of the University of Missouri-Columbia, August, 1976.
25. Poon, C.J., "The Effect of Environment and Frequency on the Fatigue Behavior of Welded Pressure Vessel Steel," A Masters Thesis presented to the Graduate School of the University of Missouri-Columbia, July 1976.
26. Mayfield, M.E., "Corrosion Assisted Fatigue In 2024-T851 Aluminum Alloy," A Masters Thesis presented to the Graduate School of the University of Missouri-Columbia, May 1978.
27. Braun, A.A., "The Effect of Frequency, Environment, and R Ratio on the Fatigue-Crack Growth of a Nuclear Pressure Vessel Steel," A Masters Thesis presented to the Graduate School of the University of Missouri-Columbia, August 1977.
28. Ford, F.P., and Hoar, T.P., "On the Mechanism of Corrosion Fatigue in Aluminum 7 wt% Magnesium," Institute of Metals (London), Monograph and Report Series, No. 36, 1973.
29. Gell, M., and Duquette, D.J., Corrosion Fatigue: Chemistry, Mechanics and Microstructure, NACE, Houston, 1972, p. 366.
30. Latanision, R.M., and Staehle, R.W., "Plastic Deformation of Electrochemically Polarized Nickel Single Crystals," Acta Metallurgica, Vol. 17, No. 3, March 1969, pp. 307-319.
31. Tyson, W.R., and Alfred, L.C.R., Corrosion Fatigue: Chemistry, Mechanics and Microstructure, NACE, Houston, 1972, p. 281.
32. Jacko, R.J., and Duquette, D.J., "Hydrogen Embrittlement of a Cyclically Deformed High Strength Aluminum Alloy," Metallurgical Transactions A, Vol. 8A, November 1977.
33. Nelson, H.G., Tetnol, A.S., and Williams, D.P., "The Kinetics and Dynamic Aspects of Corrosion Fatigue in a Gaseous Hydrogen Environment," International Corrosion Conference Series, Vol. NACE-2, National Association of Corrosion Engineers, Houston, 1972.
34. Raymond, L., editor, Hydrogen Embrittlement Testing, ASTM Special Technical Publication 543, American Society for Testing and Materials, 1974.

35. Reed-Hill, R.E., Physical Metallurgy Principles, D. Van Nostrand Co., New York, 1973.
36. Davidson, D.L., and Lankford, J., "Crack Tip Plasticity Associated with Corrosion Assisted Fatigue," Office of Naval Research, Arlington, Virginia, 1976.
37. Fontana, M.G., and Greene, N.D., Corrosion Engineering, McGraw-Hill, New York, 1967.
38. Shreir, L.L., editor, Corrosion, Volume 1, Newnes-Butterworths, Boston, 1965.
39. Dallek, S. and Foley, R.T., "Mechanisms of Pit Initiation on Aluminum Alloy Type 7075," Journal of the Electrochemical Society, Vol. 123, No. 12, December 1976.
40. De De Micheli, S.M., "The Electrochemical Study of Pitting Corrosion of Aluminum in Chloride Solution," Corrosion Science, Vol. 18, 1978, pp. 605-616.
41. Rowe, L.C., "Measurement and Evaluation of Pitting Corrosion-Field and Laboratory Studies," ASTM-STP 576, American Society for Testing and Materials, 1976, pp. 203-216.
42. Godard, H.P., Canadian Journal of Chemical Engineering, Vol. 38, October 1960, p. 1671.
43. Aziz, P.M., Corrosion, Vol. 12, Oct. 1956, p. 495.
44. Barsom, J.M., and McNicol, R.C., "Effect of Stress Concentration on Fatigue-Crack Initiation in HY-130 Steel," Fracture Toughness and Slow Stable Cracking, ASTM Special Publication 559, American Society for Testing and Materials, 1974, pp. 183-204.
45. Irwin, G.R., "Crack-Extension Force for a Part-Through Crack in a Plate," Journal of Applied Mechanics, December 1962, pp. 651-654.
46. Paris, P.C., and Sih, G.C., "Stress Analysis of Cracks," Fracture Toughness Testing and Its Applications, ASTM Special Technical Publication 381, American Society for Testing and Materials, 1965.
47. Dickson, J.A., "Aluminum Alloy 2124," "Alcoa Green Letter," Aluminum Company of America, New Kensington, PA., 1970.
48. Van Horn, K.R., Aluminum, Vol. I. Properties Physical Metallurgy and Phase Diagrams, American Society for Metals, Metals Park, Ohio, 1967.

49. Source Book on Industrial Alloy and Engineering Data, ASM Engineering Bookshelf, American Society for Metals, USA, 1978.
50. Aluminum Standards and Data, The Aluminum Association, New York, 1968.
51. Lifka, B.W., Sprowls, D.O., and Kaufman, J.G., "Exfoliation and Stress Corrosion Characteristics of High Strength, Heat-Treatable Aluminum Alloy Plate," Alcoa Research Laboratories, New Kensington, PA, 1967.
52. Analysis by: "St. Louis Testing Laboratories, Inc.," 2810 Clark Ave., St. Louis, MO 63103, 1978.
53. 1976 Annual Book of ASTM Standards, Part 7, American Society for Testing and Materials, Philadelphia, 1976.
54. Campbell, J.E., Berry, W.E., and Fedderson, C.E, Damage Tolerant Design Handbook, Metals and Ceramics Information Center, Battelle-Columbus Laboratories, Columbus, Ohio, 1972.
55. Kehl, G.L., Principles of Metallographic Laboratory Practices, McGraw-Hill Book Co., New York, 1949.
56. ASM, Metals Handbook, Vol. 7, 9th edition, American Society for Metals, Metals Park, Ohio, 1974.
57. ASTM, "Standard Method of Test for Plane Strain Fracture Toughness of Metallic Materials," E399-74, Philadelphia, PA, 1974.

Fatigue Crack Growth Reduced Data

Specimen AF4

2124-T851 Aluminum

Sine Wave

Crack Length =  $.5013 + a'$

Frequency = 10 Hz

R = +0.1

3.5% NaCl Solution Environment

$P_{max}$ (lbs.)	$a'$ (in.)	N(kilocycles)	$da/dN$ (in./cycle)	K( $ksi\sqrt{in.}$ )
1200	0.0996	0	0.0	--
1200	0.1109	50	2.260 E-7	4.07
1200	0.1287	100	3.560 E-7	4.11
1200	0.1375	150	1.760 E-7	4.13
1200	0.1505	200	2.600 E-7	4.17
1200	0.1626	250	2.420 E-7	4.20
1200	0.1731	300	2.100 E-7	4.23
1200	0.1963	350	4.640 E-7	4.30
1200	0.2106	400	2.860 E-7	4.34
1200	0.2138	450	6.400 E-8	4.35
1200	0.2455	500	6.340 E-7	4.45
1200	0.2632	550	3.540 E-7	4.51
1200	0.2848	600	4.320 E-7	4.59
1200	0.2958	650	2.200 E-7	4.63
1200	0.3170	700	4.240 E-7	4.71
1200	0.3461	750	5.820 E-7	4.82
1200	0.3761	800	6.000 E-7	4.95
1200	0.3909	850	2.960 E-7	5.01
1200	0.4088	900	3.580 E-7	5.09
1200	0.4436	950	6.960 E-7	5.24
1200	0.4659	1000	4.460 E-7	5.34
1200	0.4795	1050	2.720 E-7	5.40

Fatigue Crack Growth Reduced Data

Specimen AF3

2124-T851 Aluminum

Sine Wave

Crack Length =  $.5021 + a'$

Frequency = 10 Hz

R = +0.1

3.5% NaCl Solution Environment

$P_{max}$ (lbs.)	$a'$ (in.)	N(kilocycles)	$da/dN$ (in./cycle)	K(ksi $\sqrt{in.}$ )
1000	0.1345	0	0.0	--
1000	0.1374	40	7.250 E-8	3.44
1000	0.1412	80	9.499 E-8	3.45
1000	0.1430	120	4.500 E-8	3.46
1000	0.1484	160	1.350 E-7	3.47
1100	0.1683	200	4.975 E-7	3.51
1200	0.1782	240	2.475 E-7	3.89
1200	0.1831	280	1.225 E-7	4.26
1200	0.1949	320	2.950 E-7	4.29
1200	0.2065	360	2.900 E-7	4.33
1200	0.2124	400	1.475 E-7	4.35
1200	0.2285	440	4.025 E-7	4.40
1200	0.2887	540	6.020 E-7	4.61
1200	0.3367	640	4.800 E-7	4.79
1200	0.3740	690	7.460 E-7	4.94
1200	0.4047	740	6.140 E-7	5.07
1200	0.4289	790	4.840 E-7	5.18
1200	0.4796	840	1.014 E-6	5.41
1200	0.5285	890	9.780 E-7	5.65
1200	0.5793	940	1.016 E-6	5.90
1200	0.6320	990	1.054 E-6	6.18
1200	0.7087	1040	1.534 E-6	6.63
1200	0.8373	1090	2.572 E-6	7.54
1200	0.9264	1120	2.970 E-6	8.36
1200	1.0745	1150	4.936 E-6	10.28
1200	1.2078	1160	1.333 E-5	12.94
1200	1.2411	1164	8.324 E-6	13.80
1200	1.2919	1166	2.495 E-5	15.27
1200	1.4971	1167	2.061 E-4	24.28

Specimen AF2 (con't)

$P_{max}$ (lbs.)	$a'$ (in.)	$N$ (kilocycles)	$da/dN$ (in./cycle)	$K$ (ksi/ $\sqrt{In.}$ )
800	1.0598	3620	8.149 E-07	6.63
800	1.0798	3640	1.000 E-06	6.64
800	1.1027	3660	1.144 E-06	7.09
800	1.1327	3680	1.500 E-06	7.46
800	1.1537	3690	2.100 E-06	7.73
800	1.1753	3700	2.160 E-06	8.03
800	1.1901	3705	2.960 E-06	8.25
800	1.2026	3710	2.299 E-6	8.43
800	1.2186	3715	3.400 E-6	8.79
800	1.2332	3720	2.920 E-6	8.95
800	1.2508	3725	3.520 E-6	9.27
800	1.2721	3730	4.260 E-6	9.67
800	1.2999	3735	5.559 E-6	10.24
800	1.3320	3740	6.420 E-6	10.96
800	1.3454	3742	6.700 E-6	11.28
800	1.3589	3744	6.749 E-6	11.61
800	1.3792	3746	1.015 E-5	12.15
800	1.4032	3748	1.100 E-5	12.32
800	1.4305	3750	1.365 E-5	13.64
800	1.4667	3752	1.810 E-5	14.84
800	1.4918	3753	2.509 E-5	15.74
800	1.5216	3754	3.980 E-5	17.31
800	1.5578	3754.5	5.239 E-5	18.44
800	1.5677	3754.7	4.974 E-5	18.89
800	1.5971	3754.9	1.470 E-4	20.29

Fatigue Crack Growth Reduced Data

Specimen AF2

2124-T851 Aluminum

Sine Wave

- Crack Length = .500 + a'

Frequency = 10 Hz

R = +0.1

Lab Air Environment

$P_{max}$ (lbs.)	a' (in.)	N (kilocycles)	da/dN (in./cycle)	K (ksi $\sqrt{in.}$ )
800	0.4317	0	0.0	--
800	0.4345	50	5.600 E-08	3.45
800	0.4379	100	6.799 E-08	3.46
800	0.4450	200	7.100 E-08	3.48
800	0.4538	300	8.800 E-08	3.51
800	0.4619	400	8.100 E-08	3.53
800	0.4691	500	7.200 E-08	3.55
800	0.4803	600	1.120 E-07	3.59
800	0.4904	700	1.010 E-07	3.62
800	0.5015	800	1.110 E-07	3.65
800	0.5095	900	0.000 E-08	3.68
800	0.5184	1000	8.900 E-08	3.71
800	0.5252	1100	6.800 E-08	3.37
800	0.5296	1200	1.440 E-07	3.78
800	0.5486	1300	9.000 E-08	3.81
800	0.5565	1400	7.900 E-08	3.83
800	0.5745	1500	1.800 E-07	3.89
800	0.6004	1600	2.590 E-07	3.98
800	0.6071	1700	6.700 E-08	4.01
800	0.6071	1700	6.700 E-08	4.01
800	0.6225	1800	1.540 E-07	4.06
800	0.6360	1900	1.350 E-07	4.11
800	0.6546	2000	1.860 E-07	4.18
800	0.6714	2100	1.680 E-07	4.24
800	0.6902	2200	1.880 E-07	4.32
800	0.7059	2300	1.570 E-07	4.38
800	0.7201	2400	1.420 E-07	4.44
800	0.7333	2500	1.320 E-07	4.50
800	0.7481	2600	1.480 E-07	4.56
800	0.7636	2700	1.550 E-07	4.63
800	0.7807	2800	1.710 E-07	4.71
800	0.8005	2900	1.980 E-07	4.80
800	0.8233	3000	2.280 E-07	4.92
800	0.8468	3100	2.350 E-07	5.04
800	0.8716	3200	2.480 E-07	5.18
800	0.9047	3300	3.310 E-07	5.38
800	0.9239	3350	3.840 E-07	5.51
800	0.9416	3400	3.540 E-07	5.63

Specimen AF1 (con't)

$P_{max}$ (lbs.)	$a'$ (in.)	$N$ (kilocycles)	$da/dN$ (in./cycle)	$K$ (ksi/ $\sqrt{in.}$ )
1000	1.2234	3895	8.400 E-6	10.89
1000	1.2270	3895.5	7.200 E-6	10.97
1000	1.2325	3896	1.100 E-5	11.03
1000	1.2371	3896.5	9.203 E-6	11.18
1000	1.2407	3897	7.200 E-6	11.26
1000	1.2440	3897.5	6.597 E-6	11.33
1000	1.2486	3898	9.199 E-6	11.43
1000	1.2510	3898.5	4.800 E-6	11.49
1000	1.2554	3899	8.02 E-6	11.59
1000	1.2585	3899.5	6.197 E-6	11.66
1000	1.2703	3900	2.360 E-5	11.94
1000	1.2745	3900.5	3.400 E-6	12.04
1000	1.2834	3901	1.779 E-5	12.26
1000	1.2895	3901.5	1.219 E-5	12.41
1000	1.2950	3902	1.100 E-5	12.55
1000	1.3039	3902.5	1.780 E-5	12.79
1000	1.3114	3903	1.499 E-5	12.99
1000	1.3164	3903.5	1.000 E-5	13.13
1000	1.3234	3904	1.400 E-5	13.31
1000	1.3366	3904.5	2.639 E-5	13.78
1000	1.3434	3905	1.359 E-5	13.90
1000	1.3529	3905.5	1.900 E-5	14.19
1000	1.3667	3906	2.759 E-5	14.63
1000	1.3732	3906.5	1.300 E-5	14.84
1000	1.3796	3907	1.280 E-5	15.05
1000	1.3974	3907.5	3.560 E-5	15.66
1000	1.4165	3908	3.819 E-5	16.35
1000	1.4326	3908.5	3.220 E-5	16.96
1000	1.4507	3909	3.620 E-5	17.69
1000	1.4922	3909.5	8.300 E-5	19.49
1000	1.5401	3910	9.579 E-5	21.85

Specimen AF1 (con't)

$P_{max}$ (lbs.)	$a'$ (in.)	$N$ (kilocycles)	$da/dN$ (in./cycle)	$K$ (ksi $\sqrt{in.}$ )
1000	0.3373	1740	1.51 E-7	3.96
1000	0.3434	1840	5.60 E-8	3.98
1000	0.3642	1940	2.08 E-7	4.05
1000	0.3818	2040	1.76 E-7	4.11
1000	0.3926	2140	1.08 E-7	4.15
1000	0.4082	2240	1.56 E-7	4.20
1000	0.4315	2340	2.33 E-7	4.29
1000	0.4526	2440	2.11 E-7	4.37
1000	0.4873	2540	3.47 E-7	4.50
1000	0.5062	2650	1.89 E-7	4.57
1000	0.5419	2740	3.57 E-7	4.72
1000	0.5720	2840	3.010 E-7	4.64
1000	0.6038	2940	3.180 E-7	4.98
1000	0.6248	3040	2.100 E-7	5.07
1000	0.6310	3090	1.240 E-7	5.10
1000	0.6541	3140	4.620 E-7	5.21
1000	0.6627	3190	1.72 E-7	5.25
1000	0.6895	3290	2.680 E-7	5.38
1000	0.7190	3390	2.950 E-7	5.32
1000	0.7537	3490	3.470 E-7	5.71
1000	0.7940	3590	4.120 E-7	5.95
1000	0.8453	3690	5.040 E-7	6.27
1000	0.8968	3740	1.030 E-6	6.64
1000	0.9176	3760	1.040 E-6	6.80
1000	0.9315	3780	6.950 E-7	6.92
1000	0.9545	3800	1.150 E-6	7.12
1000	0.9773	3820	1.140 E-6	7.33
1000	1.0281	3840	2.539 E-6	7.86
1000	1.0722	3860	2.205 E-6	8.39
1000	1.1072	3870	3.500 E-6	8.87
1000	1.1181	3873	3.632 E-6	9.03
1000	1.1260	3876	2.633 E-6	9.15
1000	1.1392	3879	4.399 E-6	9.36
1000	1.1493	3882	3.367 E-6	9.52
1000	1.1665	3885	5.732 E-6	9.81
1000	1.1844	3888	5.967 E-6	10.13
1000	1.1879	3889	3.500 E-6	10.19
1000	1.1935	2890	5.600 E-6	10.30
1000	1.1978	3891	4.300 E-6	10.38
1000	1.2043	3892	6.500 E-6	10.51
1000	1.2089	3893	4.598 E-6	10.60
1000	1.2162	3894	7.301 E-6	10.74
1000	1.2192	3894.5	5.996 E-6	10.80

Fatigue Crack Growth Reduced Data

Specimen AF1

2124-T851 Aluminum

Sine Wave

Crack Length =  $.496 + a'$

Frequency = 10 Hz

R = +0.1

Lab Air Environment

$P_{max}$ (lbs.)	$a'$ (in.)	N (kilocycles)	$da/dN$ (in./cycle)	K (ksi/ $\sqrt{in.}$ )
1000	0.1269	0	0.0	--
1000	0.1282	20	6.50 E-8	3.40
1000	0.1437	120	1.55 E-7	3.44
1000	0.1502	160	1.62 E-7	3.45
1000	0.1580	200	1.95 E-7	3.47
1000	0.1620	240	9.99 E-8	3.47
1000	0.1675	230	1.37 E-7	3.49
1000	0.1769	320	2.35 E-7	3.51
1000	0.1776	360	1.75 E-8	3.51
1000	0.1801	400	6.25 E-8	3.52
1000	0.1868	440	1.67 E-7	3.53
1000	0.1892	480	6.00 E-8	3.54
1000	0.1917	520	6.25 E-8	3.54
1000	0.1931	560	3.50 E-8	3.55
1000	0.2023	600	2.30 E-7	3.57
1000	0.2045	640	5.75 E-8	3.58
1000	0.2084	680	9.49 E-8	3.58
1000	0.2133	720	1.22 E-7	3.60
1000	0.2175	760	1.05 E-7	3.61
1000	0.2242	800	1.67 E-7	3.63
1000	0.2295	840	1.32 E-7	3.64
1000	0.2349	880	1.35 E-7	3.65
1000	0.2394	920	1.12 E-7	3.67
1000	0.2463	960	1.72 E-7	3.69
1000	0.2508	1000	1.12 E-7	3.70
1000	0.2566	1040	1.45 E-7	3.71
1000	0.2612	1030	1.15 E-7	3.73
1000	0.2652	1120	1.00 E-7	3.74
1000	0.2678	1160	6.50 E-8	3.75
1000	0.2703	1200	6.25 E-8	3.75
1000	0.2777	1240	1.85 E-7	3.78
1000	0.2838	1280	1.52 E-7	3.70
1000	0.2881	1320	1.07 E-7	3.81
1000	0.2906	1360	6.25 E-8	3.81
1000	0.2936	1400	7.50 E-8	3.82
1000	0.2980	1440	1.10 E-7	3.84
1000	0.3120	1540	1.40 E-7	3.88
1000	0.3227	1640	1.07 E-7	3.91